THE UNIVERSITY OF CALGARY

A PREDICTIVE MODEL FOR GAS FUELED SPARK IGNITION ENGINE APPLICATIONS

by

Shiva Om Bade Shrestha

A DISSERTATION
SUBMITTED TO THE FACULTY OF GRADUATE STUDIES
IN PARTIAL FULFILLMENT OF THE REQUIREMENTS FOR THE
DEGREE OF DOCTOR OF PHILOSOPHY

DEPARTMENT OF MECHANICAL AND MANUFACTURING ENGINEERING

CALGARY, ALBERTA

August, 1999

Abstract

A simulative model for establishing the performance parameters of spark ignition engines fueled with a range of gaseous fuels and their mixtures is presented. The incidence of knock and its relative intensity as well as cyclic variations are also accounted for. The two-zone model incorporates a procedure for deriving an estimate of the effective duration of combustion and the associated mass burning rate for various operating conditions and gaseous fuels.

The preignition chemical reaction activity of the unburned end gas zone and its consequences on cylinder pressure development is evaluated while using detailed chemical kinetics. The onset of autoignition and knock is established via a parameter that monitors the incremental pressure increase solely due to the preignition reaction activity per unit of mean effective combustion pressure. This knock parameter corresponds also to the specific energy release within the end gas due to the preignition reaction activity relative to the total energy released by combustion per unit of initial cylinder volume. For normal knock-free combustion the value of this parameter remains throughout the combustion period relatively very low, while for knocking combustion its value exceeds a certain acceptable limit. The more intense the knocking the earlier this value is reached.

It is also shown that this relatively simple model can be used to predict various aspects of engine performance parameters including the incidence of knock, operational limits and the influence of any diluents in the fuel-air mixtures. The prediction of the operational limits was in good agreement with the corresponding experimental values for a wide range of operating conditions (e. g. compression ratios from 6:1

to 16:1 and initial mixture temperatures from 300 to 450 K). Similarly, agreement between the predicted and corresponding experimental values was good for various engine performance parameters, especially for low and moderate concentrations of the diluent in the fuel-diluent mixtures. Furthermore, the knock inhibiting capacity of the diluents carbon dioxide and nitrogen on the onset of knock in a spark ignition engine were also evaluated quantitatively.

The present contribution also describes results of an experimental and analytical investigation where mixtures of hydrogen and oxygen as produced by the electrical dissociation of water were added to the intake of a spark ignition engine operating on commercial methane over a range of operating conditions. The corresponding performance when hydrogen and oxygen were added individually was also considered. It is shown that such additions can produce improvement in engine performance, primarily for relatively lean mixtures and low compression ratios. However, the improvement to the power output is insufficient to meet the energy demand for water electrolysis should the hydrogen be produced on board while using some of the engine power output.

A stochastic approach was also developed to simulate the phenomenon of cyclic variations commonly observed in spark ignition engines. It is shown that the approach developed may be used to account for the variability of the different engine performance parameters, including the probability of onset of knock and to provide more realistic averaged predicted values of output parameters, such as power and efficiency for any given set of operating conditions with their corresponding possible ranges of fluctuation.

Acknowledgements

The author expresses his sincere gratitude and appreciation to his supervisor, Dr. Ghazi A. Karim, for his guidance and support throughout this research work. The author would also like to extend sincere thanks and appreciation to Dr. Ida Wierzba, the author's previous supervisor, for her continuous support and valuable suggestions at different stages of this work. The author's gratitude also goes to Dr. J. A. C. Kentfield for his valuable helping tips and advice.

This dissertation has been possible because of unconditional support and encouragement of the author's parents and family. The author wishes to express profound gratitude to his parents, Dharma Lal and Chandra Devi, and deepest appreciation to his wife, Ramita. Thanks also go to the author's sons, Sayuz and Shirish and daughter, Sharon, for their love, understanding and patience during this hard time. The author also wants to take this opportunity to thank the author's sister, Gita, and brother-in-law, Sukha Sagar Shrestha, for their constant encouragement and support. Similarly, thanks go to the author's brother, Dev Krishna and his family for their help.

It has been a pleasure to work with fellow graduate students, Alireza A. Attar, Bhakta B. Ale, Emad B. F. Khalil, Ramsey Bunama, Viktor Kilchyk and others in the Department of Mechanical and Manufacturing Engineering. Also, the contribution of the ex-graduate students, Drs. Al-Alousi, Al-Himyary, Gao and Attar, to this work is gratefully acknowledged.

The author acknowledges the co-operation of the technical staff especially Mr. R. Gustafson and secretarial staff including Cecile Calverley, Lynn Banach and Valintina

Kouznetsova.

Finally, the author likes to gratefully acknowledge the financial support provided by the Department of Mechanical and Manufacturing Engineering, Natural Sciences and Engineering Research Council of Canada (NSERC), EA-RTH Systems Inc. and Province of Alberta Graduate Fellowship.

Dedication

To My Beloved Parents

Dharma Lal and Chandra Devi Bade Shrestha

and My Wife Ramita and Children

Sayuz, Sharon and Shirish

Table of Contents

List of Tables

List of Figures

List of Symbols

A, B	Constants
a	Crank Radius
ATDC, ATC	After Top Dead Centre
ABDC	After Bottom Dead Centre
AVG	Average Value
BDC	Bottom Dead Centre
BTDC, BTC	Before Top Dead Centre
C, c	Constant, Concentration
C', $C"$,C_1, C_2	Constants
CA	Crank Angle
CFD	Computational Fluid Dynamics
CFR	Co-operative Fuel Research Engine
CNG	Compressed Natural Gas
COV	Coefficient of Variation
Cp	Specific Heat at Constant Pressure
$\overline{Cp}$	Average Specific Heat at Constant Pressure
Cv	Specific Heat at Constant Volume
CR	Compression Ratio
D	Cylinder Bore Diameter
d_c	Effective Flame Propagation Distance

Degr.,deg.	Crank Angle in Degree
E_{jf} and E_{jb}	Forward and Backward Activation Energies of the j^{th} Reaction
ER	Equivalence Ratio
EGR	Exhaust Gas Recirculation
F	Function, F-Distribution Test Function
G	Cochran's Test Function
g	Gradient Vector
H_u	Energy Released Due to End-Gas Preignition Reactions
H_o	Total Energy Released Due to Normal Combustion
h	Specific Enthalpy
$imep$	Indicated Mean Effective Pressure
K	Dimensionless Knock Parameter
K_{jf} and K_{jb}	Forward and Backward Rate Constants for the j^{th} Reaction
K_{p1} to K_{p9}	Equilibrium Constants
L	Length of The Connecting Rod
L_i	Flammability Limit of a Specie "i"
L_{mix}	Flammability Limit of the Mixture
LPG	Liquefied Petroleum Gas
MBT	Minimum Timing for Best Torque
M	Molecular Weight
m	Mass
m_o	Mass of Fresh Charge
N	Number of Cycle

$\overline{N}_{C/O}$	Carbon to Oxygen Atomic Ratio
$\overline{N}_{H/O}$	Hydrogen to Oxygen Atomic Ratio
$\overline{N}_{N/O}$	Nitrogen to Oxygen Atomic Ratio
$\overline{N}_{I/O}$	Inert to Oxygen Atomic Ratio
n_r	Number of Mole of Residuals
n_θ	Polytropic Index
P	Absolute Pressure
P_o	Gas Pressure in the Motored Engine
Q	Heat Transfer
R	Gas Constant
$\overline{R}$	Universal Gas Constant
R_{jf} and R_{jb}	Forward and Backward Reaction Rates of the j^{th} reaction
rev./min.	Revolution Per Minute
RMS	Root Mean Square
RON	Research Octane Number
RPM, rpm	Revolution Per Minute
RR	Reaction Rate
ΔR	Residual Error
$\overline{\Delta R}$	Mean Residual Error
S	Stroke
S_f	Flame Speed
S_p	Average Piston Speed
S_u	Laminar Flame Speed

$S.I., SI$	Spark Ignition
T	Temperature (K)
T_o	Intake Temperature (K)
TDC	Top Dead Centre
t	Time
U	Internal Energy
u	Specific Internal Energy
V	Volume
V_c	Clearance Volume
V_d	Swept Volume
v	Specific Volume
W	Power Output
X_i	Chemical Specie Formula
x	Set of Design Variables or Operational Parameters
y	Fuel Molar Fraction
Z'	Constant

Greek

σ	Root Mean Square
σ_m	Multiplier Function for Mass Burning Rate
λ	Heat Transfer Coefficient
θ	Crank Angle (Degree)

$\theta_{e.i.}$	Crank Angle at the End of Ignition Lag (Degree)
$\theta_{e.c.}$	Crank Angle at the End of Combustion Duration (Degree)
α_{ijf} and α_{ijb}	Stoichiometric Coefficients
ρ	Mixture Density
ρ_c	Correlation Coefficient
$\rho_{o,i}$	Inlet Mixture Density
ϕ	Fuel Equivalence Ratio
η	Efficiency of Simulation
η_v	Volumetric Efficiency
$\Delta\theta$c	Combustion Duration
$\Delta\theta$c, m	Combustion Duration for a Mixture
$\Delta\theta$ig	Ignition Lag

Subscripts

av	Average
b	Burned
c	Combustion, End of Combustion
e	Exhaust, Experimental Value
F, f	Fuel
i	Species, Initial
j	Cycle
jf	Forward Reaction

jb	Backward Reaction
l	Lean Limit
m	Mean Value, Mixture
max	Maximum
min	Minimum
o	Initial Conditions
p	Products
r	Rich Limit, Reactants
s	Simulated Value
st	Spark Timing
t	Time
u	Unburned
w	Wall

Chapter 1

INTRODUCTION

1.1 Background

The introduction of ever stringent emission requirements for combustion devices all around the world has given serious challenges for researchers, designers and engineers to overcome. The problem is not only to design and operate these devices within the ultra-low emission standards but also they are to be more efficient, reliable and cost effective. At the present time, most of the energy produced for world consumption is from fossil fuels. The main contribution comes from crude petroleum followed by coal and natural gas. Moreover, about 97% of the current world transport fuel energy consumption is based on crude/petroleum oil based products and the transport sector is the most oil-dependent of the all the major energy sectors in the economy [1]. These considerations have been translated into ever deteriorating air quality of many cities around the world and vehicular emissions have become the major urban air pollution problem in this century.

Furthermore, the substantial increase in the concentration of carbon dioxide in the atmosphere, has created a huge environmental concern. Environmentalists, researchers and scientists have pointed out that the global warming caused by the green house gases may substantially change the world climate pattern and increase the sea level with a potential danger to submerge many cities around the world. Nobody is sure about the end effect of such a global warming which might be devastating.

These serious concerns have led the international community to come up with the Kyoto agreement which aims to limit green house gas production and its release into the environment. Within the developed world, Canada has promised not only to freeze the production of green house gases, including carbon dioxide, at the level of 1990 but also to reduce their production by 6% below the 1990 level by the year 2013.

These challenges have demanded not only more efficient and ultra-low emissions but also lesser green house gases producing combustion devices. Accordingly, the present state of the heavy reliance of the transportation sector on petroleum based products which produce substantial amounts of green house gases per unit energy output has been a great concern. In these situations, naturally, the use of renewable energy would be the best solution to zero green house effect. Unfortunately, this solution for the transportation sector is a very long term proposition, due to the serious problems associated with its generation and portability at the present time.

Attention has been drawn to alternative fuels, such as liquefied petroleum gas (LPG), compressed natural gas (CNG) and methanol as a more environmentally friendly fuels in recent years. In fact, the combustion of LPG does produce marginally less carbon dioxide emissions than an equivalent amount of gasoline. This beneficial effect will remain marginal, because LPG supplies from indigenous sources are only sufficient to replace 4-5% of total gasoline usage [2]. However, due to the more abundant availability and relatively uniform distribution of natural gas sources among the regions of the world in comparison to liquid fuels [3], compressed natural gas (CNG) has become one of the most promising alternative fuels which can be directly used in suitably modified vehicles. Both CNG and methanol-powered

vehicles produce roughly one third less greenhouse gas emissions than equivalent gasoline-powered vehicles, with CNG being the superior fuel.

1.2 Natural Gas as a Vehicular Fuel

Due to the superior technical qualities of natural gas in comparison to other alternative and conventional liquid fuels, it has considerable potential as a clean fuel for the motor vehicles of the future. The advantages of natural gas include a high research octane number (RON) of 120 [4], the highest of any commonly used fuel, should permit the use of high compression ratios which increases engine efficiency. Among other advantages of natural gas are its extremely low photochemical reactivity, zero evaporative emissions, reduced cold start and low temperature emissions due to the elimination of cold mixture enrichment and its compatibility with fuel efficient lean-burn technology.

Natural gas is also safer than gasoline because natural gas is lighter than air and dissipates quickly when accidentally released. Its ignition temperature ($\simeq 650°C$) is far higher than that of gasoline ($\simeq 320°C$) [5]. It also has a relatively narrow range of flammable concentrations in air and when below about 5 percent and above 15 percent, natural gas will not burn. The combination of high ignition temperature and limited flammability make accidental combustion of natural gas less likely than gasoline and other common fuels. Moreover, studies conducted in the late 1970s could not identify a single instance when a CNG cylinder failed in a collision in contrast to the records of collision-caused fuel leakage and fires in gasoline and LPG fuelled vehicles [6].

Natural gas which mainly consists of methane, has a low carbon to hydrogen ratio and has the ability to mix more thoroughly with air eliminating local regions of rich and/or lean mixtures which result in lower levels of pollution in general. Moreover, its low lean operational limit and the absence of higher hydrocarbons makes it suitable for optimised ultra-low pollution engines.

These advantages in operating vehicles on natural gas have significantly increased the conversion and/or manufacturing of gas fueled engines in recent years. This is being largely motivated not only by the environmental concerns but also by its relatively cheaper cost and abundant availability. At present, most of the developed countries including Canada, U. S., Italy, Australia, New Zealand, the Netherlands have a variety of promotional programs to use more clean transport alternative fuels, particularly natural gas [2]. Other countries such as Mexico has also developed comprehensive programs to convert existing transport fleets into natural gas usage.

The operation of a vehicle on natural gas is not without disadvantages, problems and penalties. For example, natural gas is carried on vehicles as a compressed gas in high pressure cylinders which are built to rigorous and high quality standards. Nevertheless, for equal volume of storage tank, the energy content of CNG at 20 MPa (3000 psig) and ambient temperature is about one-fifth that of diesel fuel and one-fourth that of gasoline. This low thermal storage capacity of CNG poses a significant problem in some applications, such as in passenger cars. However, the recent developments on high-strength composite materials have made it possible to reduce the weight of CNG cylinders substantially and enable it to carry more fuel without any substantial sacrifice in load.

Direct conversion of a diesel or spark ignition engine to operate on fumigated

natural gas will normally result in a loss of power about 10-15% at full throttle. This loss is mainly the result of displacement of air by the gaseous fuel. Other contributing factors include a low burning velocity, low energy content and high ignition temperature [5]. Hence, in order to maintain its original performance, a spark ignition or a diesel engine when converted to operate on natural gas, should undergo changes such as having its compression ratio adjusted to a more optimal value. The higher efficiency due to the increased compression ratio results in more work output for each unit of mixture inducted, thus offsetting the reduced power.

The laminar flame speed of natural gas is lower than that of other hydrocarbons mainly because of its relatively high effective activation energy. This effect is most significant under lean mixture conditions, which can lead to misfiring and increased hydrocarbon emissions in engine applications. The unburned hydrocarbons are mainly composed of methane, which has low reactivity to form ozone and photochemical smog in an urban environment, which would contribute to the green house effect. Lean operation with natural gas has been always attractive due to the reasons of high thermal efficiency, low likelihood of knock, reduced exhaust emissions especially NOx and the capacity to use higher compression ratios while reducing heat transfer in a spark ignition engine. However, the low burning velocity, low combustion rate and the tendency to misfire at these leaner mixtures have been an obstacle. To overcome this, various measures have been tried such as increasing the ignition energy [7], stratifying the mixture, intensifying the level of turbulence, modifications made to the design of the combustion chamber, intake ducts and piston shape and others [8, 9, 10, 11]. Another recent attempt to increase the burning velocity and combustion rate of such lean mixtures has been the addition of a small quantity of

hydrogen, a fuel having a much cleaner and faster rates of burning, into the main fuel methane [12, 13, 14].

Natural gas, which is mainly methane, may contain a number of other higher hydrocarbons such as propane, ethane and butane and diluents such as nitrogen, carbon dioxide and water vapour in different proportions depending upon its origin and mode of production. In some cases the contents of carbon dioxide and other diluents in natural gas may be as much as 35% or even higher [2]. Such variations in the composition of natural gas can significantly alter the performance of combustion devices and substantially increase the emissions.

Cyclic combustion variations have been recognised as limiting the performance of internal combustion engines particularly at fuel-lean conditions and with large exhaust gas recirculation [15]. Generally, cyclic variations are at a minimum at equivalence ratios close to the stoichiometric. Investigations of the role of engine operating and design parameters on cyclic variations have been carried out extensively. A comprehensive review of such early research was presented by Young [16]. However, the reason for cyclic variations are not entirely clear. It is expected that if cyclic combustion variations were to be eliminated or reduced, then substantial improvements in engine performance, fuel consumption and noxious emissions reduction may be obtained.

1.3 Objectives

The major objectives of the research were as follows:

- to develop further and validate a comprehensive model of a spark ignition en-

gine including knock modeling while operating on methane and its blend with other gaseous fuels such as hydrogen, propane and ethane.

- to investigate and develop a simple prediction method for determining the operational limits of a spark ignition engine.

- to evaluate and develop a predictive method of the effects of the presence of some diluents with the main fuel methane on the performance of a spark ignition engine.

- to establish the effectiveness of hydrogen as an additive to methane for engine applications and evaluate the prospect for the production of the needed hydrogen on board the engine.

- to examine, develop and validate a comprehensive model for the cyclic variations in a spark ignition engine that is capable of simulating adequately the cyclic variations phenomenon commonly observed in engines.

1.4 Outline of Dissertation

In the current chapter, the background and importance of this research in the development of natural gas spark ignition engines are discussed. In Chapter 2, a literature review of the work relating to the modeling of combustion, knock and cyclic variations in the internal combustion engines will be presented.

Chapter 3 is devoted to the description of a comprehensive model of simulation of the performance and knock intensity of a spark ignition engine while operating on methane, hydrogen, propane, ethane and their mixtures.

Chapter 4 describes the experimental set-ups of a CFR engine, which was used to

obtain the required experimental data to support the model developed. It includes the testing procedure and calibration of equipment.

Chapter 5 deals with the operational limits of a spark ignition engine and effects of various operating and design parameters on the limits. It includes two proposed predictive methods for determining the operational limits of a spark ignition engine fueled with gaseous fuels.

Chapter 6 describes and validates an approach that predicts the effects of the presence of diluents with the main fuel methane on the various performance characteristics of the engine.

Chapter 7 evaluates the effectiveness of the addition of a relatively small quantity of hydrogen to the methane and the viability of the production of the hydrogen in-situ on board of the engine.

Chapter 8 presents a stochastic model developed to simulate and investigate the cyclic variations of various performance parameters including the probability of the onset of knock in a spark ignition engine.

Chapter 9 concludes with brief general summary and conclusions of the work and suggests areas for further research.

A list of references and appendixes are attached at the end of this work.

Chapter 2

LITERATURE SURVEY

2.1 Combustion Modeling

The modeling of the complex combustion processes of the internal combustion engine has been a major area of research and development for many years. Recent development of digital computers with high capabilities and reasonable cost has increased the interest to develop a comprehensive, yet relatively simple simulation models of internal combustion engine phenomena. This was aided by the need to obtain high fuel economy and low emissions which made the optimization of engine performance via wholly experimental approaches a lengthy and expensive process. Broadly, many kinds of numerical simulation models have been developed over the years and according to their functions, they can be divided into two general categories: diagnostic and predictive models. The diagnostic models which are usually based on engine experimental data, mainly the pressure-time history, attempt to analyze and provide needed information about the various processes in the engine. However, the predictive models, under given operating conditions, simulate the engine combustion processes and produce key engine combustion parameters such as pressure-time and mean temperature-time histories.

Combustion engine models may also be classified into three broad categories according to whether they are: zero-dimensional, quasi-dimensional or multi-dimensional models.

A zero-dimensional model assumes usually that the mixture throughout the cylinder remains homogeneous and of uniform properties as time is varied independently. The combustion processes are often simplified by being treated as a heat addition or heat release phenomenon established usually on the basis of analysis of the first law of thermodynamics and experimental data. In its simple form, the heat release rate is usually taken as the product of the mass burning rate of the fuel and its effective heating value. When correlations of the variations of the heat release rate with time are derived empirically and used in the zero-dimensional model, they can produce calculated results of reasonable accuracy.

The quasi-dimensional model can provide sufficient data for the variations of in-cylinder pressure, temperature and concentration. This type of model employs some conceptualizing of the various individual processes occurring in the engine cycle, such as mixture formation of air, fuel and residual gas, change in concentrations, heat release and heat transfer. All these individual processes together with the equations of mass and energy conservation within each zone provide the detailed data necessary for calculating the performance of an internal combustion engine. Generally, in these models, the rate of burning is derived from a physical sub-model of the turbulent combustion processes.

Multi-dimensional computational fluid dynamics (CFD) models are based on the numerical solution of mass, momentum, energy and species conservation equations in either one, two or three dimensions to follow the propagation of the flame or combustion front through the entire engine combustion chamber. A detailed CFD model can provide a formidable amount of predicted detailed data of the flow field for an operating engine. But its validity is still limited by how accurate is the understanding

of the associated combustion phenomena such as turbulent flow, reaction rates, heat transfer and how accurate boundary conditions can be set. Meanwhile, these models require a significant amount of computer power even for the prediction of turbulent fluid flow with a simplistic description of the complex chemical reactions which take place during combustion. As a result, the use of a multi-dimensional zone model with full chemistry as part of a routine cycle simulation program remains effectively not feasible at present. Accordingly, most of the combustion models being used tend to be either of the zero-dimensional or quasi-dimensional types.

The earliest models used in the internal combustion engine were the air standard cycle models [17] where unlike the real process, the models consider neither combustion nor time with property changes in the working fluid accomplished by heat or work transfer. In spite of the obvious lack of correspondence with the real processes in engines, these models were used originally to predict some useful general trends of a qualitative nature, such as the effects of changes in compression ratio, initial temperature and pressure on engine work output and efficiency.

To improve the modeling effort, the fuel-air cycle and subsequently the single zone combustion models were introduced. The earlier work of Withrow and Rassweiler [18] correlated the pressure rise due to combustion in the cylinder with the fraction of the mass burned and enabled it to be directly determined from the pressure-time diagram. Their approach was used subsequently in many models over the years.

For many years, single-zone models were the main approach available for modeling the performance of internal combustion engines. For example, Gatowski and Heywood [8] used a single zone model to represent the cylinder charge to research the blow-by gases in crevice flow and their effects on engine operation. This model

relies on the pressure-time history of the engine through a heat release analysis that includes the effects of heat transfer, crevice flows and spark ignition. Heat transfer coefficients were calculated on the basis of a formulation similar to Woschni's [19]. Such a model demonstrated that complicated combustion phenomena in engine operation could be examined with simple experimental set-ups and moderate computing requirements.

The application of single-zone models can often be found in the simulation of combustion processes in motored engines. The whole charge in the motored engine can be treated as the end gas being compressed and sensitized to autoignition condition in a single zone model to research the effects of the chemical and physical processes on the autoignition characteristics of the charge. Various researchers (e. g. [20, 21, 22, 23, 24]) have used motored engine techniques to develop detailed chemical kinetic mechanism of hydrocarbon oxidation which provides a fundamental understanding of autoignition chemistry and other combustion problems involving commercial hydrocarbon fuels.

Krieger and Borman [25] presented a diagnostic thermodynamic model for spark ignition engine heat release calculations. In their model, the combustion chamber was divided into two-zones, burned zone and unburned zone. The flame front was assumed to be infinitesimally thin. The mass burning rate was estimated from pressure-time experimental data. Heat transfer was also considered. Peters and Borman [26], using a similar model examined the effects of various parameters on cyclic variations in the engine.

Patterson et. al. [27] and Benson et. al. [28] developed a similar two-zone model for the spark ignition engine that included the intake and exhaust systems. Generally

a laminar flame speed correlation is used to simulate empirically turbulent flame propagation without a clear indication of the basis for this determination. The models were employed to simulate the whole power cycle, estimate the performance of the engine and predict NOx emissions in some cases.

Hong [29] used an empirical Weibe-type mathematical function to represent the fuel burning rate and examined single-zone and two-zone models. The ignition lag and combustion duration were determined by curve-fitting. Based on this approach, he claimed that the effects of choosing different combustion models, single-zone or two-zone models, on the development of the pressure-time diagram were small.

Al-Alousi [30] and Al-Himyary [31] at the University of Calgary carried out an extensive experimental work on a CFR engine using common gaseous fuels and their mixtures such as methane, hydrogen and propane and diluents such as carbon dioxide and nitrogen. They used the measured pressure variations with time in single and two-zone models to calculate the corresponding duration for flame initiation (ignition lag) and propagation (combustion duration). They compiled much information about the variations of these periods and the effective heat release rate with common operating parameters and fuel composition.

Gao [32], later on, developed a two-zone model and used Al-Himyary's [31] data to validate the predicted performance of a spark ignition engine using methane as a fuel. He used a triangular type function for the mass burning rate to estimate the variations of pressure and mean temperature in the burned and unburned zones. He also incorporated a chemical kinetic scheme of 32 elementary reactions and 14 reactive species in his model to consider the reaction activity within the unburned zone and the possibility of autoignition and knock. He defined an energy based

knock criterion to estimate whether knock is to take place and its intensity when it occurs. The model was further enhanced by Attar [13] incorporating a more detailed chemical kinetic scheme. He was able to estimate well the various parameters of the engine performance including the borderline condition for knock and developed analytically optimization procedures while using fuels such as methane, hydrogen and their mixtures.

Turbulent flame modeling is an important aspect in engine combustion research. Some models simulated turbulent flame propagation by a laminar flame propagation speed correlation multiplied by a turbulent factor, such as Benson et. al. [28]. Sirignano [33] applied the principles of conservation of mass, energy, momentum and chemical species to simulate the combustion and flow process in an engine with the turbulent flame speed assumed controlled by the turbulent motion heat transfer rate to the unburned mixture ahead of the flame. However, no verification of the results was presented. Hires et. al. [34] developed correlations for ignition delay and combustion duration in a spark ignition engine by using a turbulent eddy entrainment concept of Tabaczynski [35]. They assumed that the turbulent integral scale is proportional to the instantaneous chamber height prior to flame initiation, and the turbulent intensity scales proportional to the mean piston speed. Blumberg and Kummer's conic function of mass burning rate [36] was used to produce the correlation. In order to give the necessary parameter values at the point of 50% mass burned, a relationship between burned volume and burned mass must be assumed. However, some references such as Al-Himyary's [31] showed that this relationship is not always valid for all operating conditions.

The k-ϵ turbulent model has been employed where the turbulent kinetic energy

is integrated over the whole combustion chamber to provide spatially average turbulence predictions and the dissipation rate, ϵ, is related to the integral length scale. The advantage of such models is that they are relatively straight forward computationally, but the ad hoc nature of turbulence assumed is plausible but arbitrary [37, 38].

2.2 Knock Modeling

Knock which has been one of the key factors limiting engine performance and efficiency from the very beginning is defined as the abnormal combustion of part of the end-gas ahead of the arrival of the turbulent flame front following spark ignition. The sudden and rapid heat release due to this abnormal combustion leads to a rapid pressure rise followed by pressure fluctuations within the chamber, objectionable noise and excessive local heat loss to the walls. Knock is acknowledged to be caused by the autoignition of this unburned mixture. In order to model and predict the incidence of knock, the variations in the unburned gas state parameters and preignition reaction activities in the unburned mixture need to be analyzed and appropriately estimated. Generally, during knock the normal development of combustion, characterized by a smooth rise in pressure, ceases when the pressure rises suddenly and high-frequency pressure fluctuations can be observed. These frequencies are governed by the size and shape of the combustion chamber, the velocity of sound in the charge and the engine operating conditions. The knock phenomenon varies substantially from one cycle to another, and does not necessarily occur every cycle especially at the borderline of knock.

The studies, in general, of knock in the spark ignition engine may be divided into three major groups: knock detection, knock rating and knock modeling. A wide range of approaches have been employed for the detection of the onset of knock and for categorizing its intensity. These involved various experimental investigations of knock phenomena. Some detection methods were developed based on these observations [39, 40, 41].

From the outset of internal combustion engine development, it was clear that the onset of knock and the knock rating are strongly related to the nature and composition of the fuel [42, 43]. Lovell [44] found that the tendency to knock and its intensity are related to the molecular structure of that fuel. Individual hydrocarbon compounds vary enormously in their ability to resist knock, depending on their molecular size and structure. Hydrocarbon fuels are grouped generally into three families of Paraffins, Olefins and Napthenes-Aromatics. Increasing the length of the carbon chain in Paraffins increases the knock intensity while it decreases generally when the fuel is changed from Paraffins to Olefins and Aromatics. Napthenes have significantly greater knocking tendency than the corresponding size aromatics. The use of isomers and the addition of some additives to the fuel can reduce the knock intensity of hydrocarbon fuels. The discovery of the antiknock properties of tetraethyl lead additives [45] was one of the most important findings of early research into fuels and knock.

Karim and Klat [43] established the knock limits for different common gaseous fuels including methane, propane, ethylene, hydrogen and their mixtures. They presented experimental results obtained in the CFR engine showing the effects of mixture strength, compression ratio and intake temperature on the knock limits.

Another contribution is that due to Annand and Sulaiman [46] who presented experimental results in terms of the critical spark ignition timing for borderline knock at constant compression ratio.

To consider the knock resistance of a gaseous fuel in spark ignition engines, an analogy to the octane number rating had been proposed involving the methane number. It is defined as the percentage by volume of methane in a binary mixture with hydrogen that exactly matches the knock intensity of the unknown fuel sample under specified operating conditions in a CFR engine. Leiker et. al. [47] and Ryan et. al. [48] who studied this experimentally under a specified set of test conditions, suggested that the methane number can be used as a practical indication of the knock resistance qualities of gaseous fuels.

Over the years, a number of theories have been put forward to explain the basis for the onset of knock. Broadly, these theories may be catagorized into three groups: detonation wave theory, flame acceleration theory and autoignition theory. However, in recent years, it is accepted that the incidence of knock is due to autoignition in the end gas. The older suggestion that knock may be due to the acceleration of the normal flame front to supersonic speeds (detonation) has been essentially ruled out. Numerous recent high speed schlieren and shadow graph photographic studies support the autoignition theory [49, 50, 51]. They show that autoignition commonly occurs in one or more discrete locations within the end gas and then propagates to the other parts of the charge inside the cylinder. This end gas autoignition has also been detected by optical fiber techniques and correlated with schlieren methods [52, 53, 54]. In some of these studies the flame front from the end-gas autoignition sites was found to propagate at slightly supersonic speeds (developing detonation). It has

been argued that the rapid release of energy occurs because of the acceleration of the advancing flame front to sonic velocity which in typical engine conditions would be of the order of 700 m/s. However, high speed film studies of knock have shown no evidence of flame front speeds approaching sonic velocity before knock [51, 54, 55]. Hence, it is now widely accepted that knock originates from the spontaneous autoignition of one or more local regions in the end gas. Additional regions then ignite till the whole end-gas is fully reacted. The rate of spread of these autoignited combustion centres can vary significantly. Under some conditions, this spread could be sufficiently slow for no pressure oscillations to be detected, thus autoignition does not necessarily lead to knock [49, 51]. Under heavy knock conditions, the spread of the auto-ignited region and hence the energy release is extremely rapid and high-amplitude pressure fluctuations may result.

In order to predict the onset of knock in engines, it is necessary to model and predict the unburned gas state parameter variations and the unburned gas preignition reaction activity. Therefore, there is a need to build up a combustion model to estimate unburned gas state parameters such as pressure and temperature, and an appropriate chemical reaction mechanism for modeling the unburned gas preignition reactions.

Karim [56] developed a simple analytical approach to predict knock in spark ignition engines. A criterion for knock based on a gross chemical reaction of the fuel-air mixture in the end gas was used to predict the onset of knock. After adjusting some rate constants in the reaction mechanism, the calculated model gave a good agreement between predicted and experimental results. He suggested that more reaction steps are needed to be added to the kinetic scheme to predict a wider range

of knocking conditions observed experimentally.

Livengood and Wu [57] developed a simple model for engine knock, using the pressure and temperature data of a fired engine. Good agreement was obtained in predicting the results for n-heptane and a blend of n-heptane and iso-octane.

Trumpy et. al. [58] numerically simulated ethane oxidation mechanism by 75 steps reaction model in the end gas using a simple energy equation without consideration of heat transfer to the wall and mass changes due to flame propagation. Their work stated that it is possible to predict knock from simulating preignition chemical reactions in the end gas.

Westbrook and his colleagues [21, 22, 23, 59] developed comprehensive mechanisms for the combustion reactions of different common fuels and attempted to use them in the modeling of knock and self-ignition of some hydrocarbons. They reported relatively good agreement with their experimental results in estimating the ignition delay times under relatively simple situations such as a constant volume reactor.

Dimpelfeld and Foster [60] used the chemical kinetic mechanism of Westbrook to simulate knock in spark ignition engines with the assumption that the end gas is adiabatically compressed, and the end gas temperature is only a function of cylinder pressure. Leppard [61] predicted ethane air mixture knock mechanism by using Westbrook, Dryer and co-workers detailed chemical kinetics mechanism. Their predicted results showed good agreement with the corresponding experimental values.

Chun et. al. [62] predicted knock in a spark ignition engine using a simple chemical kinetics model obtained from Hu and Keck [63] and assuming the end gas to be adiabatically compressed. Their results showed good agreement for some fuels

such as isooctane while for others some reaction activation energy constants needed to be adjusted.

Karim and co-workers [64, 65] were able to develop a comprehensive detailed chemical kinetic scheme, including 155 reaction steps and 39 species to predict the autoignition of common gaseous fuels such as methane, propane, hydrogen and their mixtures. Karim and Gao [32, 66] applied this scheme and simulated the onset of knock in a CFR engine for methane operation. The scheme was further applied by Attar [13] to model the borderline of knock and to optimize operating conditions in the CFR engine while operating on methane, hydrogen and their mixtures. They defined a criterion for the onset of knock based on the specific volumetric energy release due to auto-ignition reactions relative to the total energy release to be expected from the combustion of the fuel. They developed a two-zone model to estimate the variations of pressure and temperature within the burned and unburned zones and used an empirical correlation for the corresponding combustion duration and heat release rate due to flame propagation profile.

In contrast to these approaches, some researchers have been trying to combine a very simplified and limited chemical kinetic representation with CFD codes such as those of KIVA to simulate the knock phenomena [67, 68, 69] as well as the associated pressure oscillations [70]. These models tend so far to benefit from the detailed fluid mechanics calculations and to consider the variations of temperature and pressure within the volume of cylinder, but suffer from long computation times and gross inadequacy of the chemical representation with the required scales for engine modeling. That is why, normally, the chemical kinetic schemes in these models remain insufficiently comprehensive in comparison to the multi-zone models.

2.3 Cyclic Variation Modeling

The problem of cyclic variations in engine operation has long been recognized as the fundamental problem of variations in the combustion process from one cycle to the next and manifests itself as variations in pressure development and engine output. These variations can be one of the factors limiting the performance of internal combustion engine particularly for fuel lean operation and when employing large exhaust gas recirculation. The earlier studies of cyclic combustion variations were focused on determining the effects of engine and operating variables on cyclic variations in combustion and pressure development in general. Later studies, generally concentrated on specific aspects of the problem such as the effect of in-cylinder flows and non-homogeneity in cyclic variations. Results from previous investigations about the effects of engine and operating variables on cyclic variation were complied and comprehensively summarized by Young [16].

The studies of cyclic variations, broadly, may be divided into three main categories: effects of operating and design engine variables on cyclic variation, origin of cyclic variation and cyclic variational modeling.

The studies of the effects of operating and design engine variables on cyclic variations were mainly aimed at understanding the contributions of each variable to combustion and pressure development. The procedure used in most of these studies was a systematic change of one variable at a time. Cylinder pressure, size and shape of early flame kernel and/or flame arrivals at several locations in the cylinder were generally monitored over many cycles. Parameters used to characterize the cyclic variations ranged from flame arrival times and sizes and shapes of the early flame

kernel development at definite time or location to maximum rates of pressure rise, peak pressures and their crank angle occurrences, to such integral parameters as indicated mean effective pressure and the area under the pressure-crank angle curve.

One of the strong influencing factors on cyclic combustion variations was found to be the equivalence ratio of the mixture. A number of researchers [71, 72, 73, 74, 75] studied the effects of the overall equivalence ratio of the mixtures on the cyclic variation in a spark ignition engine and concluded that minimum cyclic variations, generally, occur at a slightly rich equivalence ratio of 1.10 to 1.25, corresponding to the fastest flame speed and approximately to the mixture strength for maximum power. Studies of the influence of charge dilution whether with exhaust residuals or with other diluent gases, were found generally to result in increased cyclic variations [71, 72, 76, 73, 77]. This is due to several adverse effects associated with the diluted mixtures such as lower laminar flame speed resulting in slow flame development and burning rates [78], lower energy density leading to lower expansion velocity [79] and increase in charge non-homogeneity [80]. Moreover, Karim [71] observed higher cyclic variability with the diluent carbon dioxide due to its higher heat capacity than for nitrogen, otherwise for the same operating conditions. Nakanishi et. al. [77] in their studies of the exhaust gas recirculation (EGR) concluded that with a mixture diluted with EGR, both the initial and later flame propagation processes became slower and dispersed. This tendency became greater with the increased percentage of EGR.

Another factor that influences the cyclic variations was the ignition system. Several ignition characteristics such as spark energy, spark duration, spark plug gap, spark location, number of spark plugs and electrode shape have been investigated.

Results from early investigations [72, 71, 73] pointed out that a few characteristics of the ignition system e.g. spark location and number of ignition points had a measurable effect on cyclic combustion variations. The other characteristics contributed only little to cyclic variations. In general, any change which decreased the maximum flame travel distance or increased the rate of mass burning, and thus decreased flame travel time, resulted in lowered cyclic variations [16]. Thus, any attempt to increase the burning rate or decrease flame travel distance will reduce the cyclic variations, for example using multiple ignition points [76, 81] or locating the spark plug suitably to different combustion chamber shapes [82, 83] to increase the burning rate. Another aspect that affects cyclic variations is the spark timing. Minimum cyclic variations are observed at best torque (MBT) timings [71, 75]. However, Karim [71] and Hirao and Kim [82] found that the effect of spark timing was influenced by both mixture strength and spark plug location.

Engine speed is another factor that would affect cyclic variations. Generally, an increase in engine speed increases the cyclic variations [74, 84, 85, 86]. This is attributed to the associated increase in turbulence and reduction in absolute combustion time. But at the same time the increase in turbulence would increase the flame speed, which in turn could reduce the cyclic variations. However, Karim [71] found that the effect of engine speed on cyclic pressure variations depended on the equivalence ratio. At lean mixtures, lower cyclic variations were observed as engine speed was increased, probably because increased flame speeds resulted in the main heat release occurring nearer top dead centre. At the best-power mixture strengths, little benefits of increased speed were noticed. At richer mixtures, an adverse effect resulted as the engine speed was increased, possibly because of stratification caused

by the inadequate mixing of fuel and air.

The effect of compression ratio on cyclic variations appears to be weak [87, 72, 88, 84, 78]. Generally, higher compression ratios, because of the associated lower residuals and higher temperatures, resulted in lower relative variations in peak pressure; other factors being equal. The shape of the combustion chamber has a direct effect on the flame propagation period by confining a flame front propagation from ignition site to the chamber walls. For this reason, the best chamber shape, from the cyclic dispersion point of view, would allow the greatest amount of cylinder volume to be engulfed per unit of travel of flame front, propagating from the spark plug [89, 90, 91]. Such a chamber would have the shortest combustion duration period and consequently, the lowest cycle-to-cycle variations of engine output [92].

Pundir et. al. [80] studied the influence of charge non-homogeneity on cyclic variations using two fuels i.e. gasoline and propane in a CFR engine. Results indicated that charge non-homogeneity increased as the mixture became leaner or richer. The mixture of propane and air was found much more homogeneous than that of gasoline and air at the range of equivalence ratios used. The effect of swirl motion did not improve homogeneity of the charge significantly but the mixing process in the carburettor and intake manifold was found to be more important. It was noted that cyclic variations increased with mixture non-homogeneity. When a shrouded valve was introduced cyclic variations were found to be much lower compared to the non-shrouded valve case because of the resulting improvement in turbulence augmented flame propagation rates.

Matekunas [93] investigated the effects of intake configurations and spark plug locations in an engine fuelled with propane using flame photography. The three con-

figurations used were: a conventional valve with an ordinary port, a conventional valve with a swirl and a shrouded valve with an ordinary port. With this combination of intake configuration and spark plug location, several degrees of mixture motion and different burning rates were produced and examined. He observed that combustion variations appeared to be classified into two regimes. In one regime with the operation near the lean limit, the initiation period becomes a significant source of variations and the flow conditions at the spark plug is the important factor. The second regime, for the operation away from the incipient of misfire, is dependent on the overall cylinder flow pattern, but is not strongly dependent on flow conditions at the spark plug.

A number of researchers [94, 16, 95, 96] agreed that the major cause of cyclic combustion variations originated from the first period of combustion process i. e. the fluctuations in the flame kernel development and growth which subsequently affected the later flame propagation process. Any factor that influenced this period of combustion contributed in one way or another to cyclic variation. For example, the variations in the gas motion and the mixture strength near the spark plug location at the time of ignition have been found to have important effect on cyclic variation [73, 97, 98].

Patterson [73] investigated cyclic combustion variation in both single and multi-cylinder engines with geometrically identical cylinder sizes. Various operating conditions were examined including the effect of increasing mixture motion by using a shrouded inlet valve. With a large sample size of 2000 cycles of cylinder pressure-time data and using a maximum rate of pressure rise to quantify cyclic variation, he postulated that the major cause of cyclic variations was the cyclic variation of mixture

motion within the cylinder near the spark plug at the time of ignition. Namazian et. al. [94] studied the flame kernel formation in a single cylinder square cross-section transparent engine using schlieren photography. They found the influence of the interaction of the flame kernel with the combustion chamber walls on the flame propagation process and cycle peak pressure. This could be explained by the fact that the increased flame front area promoted a faster entrainment of fresh mixture across the flame front which resulted in increasing burning rate. Faster combustion with a short flame travel distance gave a more rapid rate of pressure rise for these cycles and a higher peak pressure.

Hansel [99] while deducing the amount of cyclic variations due to turbulence, indicated that when the flame kernel emerges from the spark plug gap, it is affected by turbulence and local equivalence ratio. The transition from the kernel to the established flame front will be fast or slow depending upon the conditions and their variations at the ignition site. Because the local equivalence ratio and turbulence in the vicinity of spark plug can vary from cycle to cycle due to the non-uniform mixing of air and fuel and/or due to erratic vaporization of liquid fuel, cyclic dispersion is observed. An example of such a situation occurs in engines when in-cylinder fuel injection or with fuels such as methanol with high heat of vaporization are used. Karim [71], Patterson [73], Hansel [99] and Quader [100] have shown significant reduction in cyclic variations when liquid fuel was replaced by a gaseous fuel.

However, the studies by Matthes et. al [101] and Peters et. al. [102] have shown that if the mixture strength is varying spatially, lower cyclic variations can be achieved, than with the well mixed homogeneous mixture. In situations where burning rates are faster, which are achieved through charge stratification by in-

cylinder injection, the cyclic variations were observed to be lower. However, a more recent study by Lee and Foster [103] using Rayleigh scattering measurements could not confirm the variation in mixture composition in the vicinity of the spark plug gap as a major contributor to cycle-to-cycle variations in combustion for the homogeneous mixture cases. But, they observed that the variation in mixture concentration at the vicinity of the spark plug for very lean mixtures with port injection correlated with cyclic variation.

Due to the complex nature of the problem, several empirical and semi-empirical models of the cyclic combustion variations have been proposed. Most of these models were developed to relate combustion and pressure variations to velocity variations (e.g. [16, 104, 105, 106, 99, 88]). The basis for most of the models developed was that the cycle to cycle velocity variations early in the combustion period in the spark gap vicinity were mainly responsible for combustion variations.

Most workers divide the effects of chemistry and flow fields into two separate flame regimes, laminar and turbulent [107, 108, 109, 110]. In turn, the laminar flame speed, for example, has been found to be affected by: equivalence ratio, temperature, pressure, inert gas concentration and others. The flow field effect is generally expressed as a flame speed increase from the laminar case. The ratio of turbulent to laminar flame speed is in common use. The parameters often used to describe this enhancement are: turbulence intensity, turbulence length scale and flame size. Apart from these parameters the mean velocity in the vicinity of the spark plug , heat loss to walls and spark plug electrodes are used in models which describe the very early flame development [111, 112].

Since cyclic variations in a spark ignition engine is complex and depends upon

a number of independent parameters, it has been considered by some researchers [15, 71, 113, 114, 115, 116] as a stochastic process of random nature on the basis of their experimental findings (e.g. [71, 117, 118]).

This preceding review of research on combustion, knock and cyclic variations in spark ignition engines illustrates the complexity of the engine processes and the lack of their full understanding particularly at the fundamental level. Most of the models developed which remain insufficiently comprehensive and incomplete, have their own advantages and disadvantages. There is still much room for further progress in this field of research activity. For example, there is a need to develop an effective model that predicts engine performance including the operational limits, the effects of diluents present in the main fuel while accounting for cyclic variations and estimating the probability of occurrence of knock in an engine. The present work attempts to contribute to these aspects of spark ignition engine performance while using gaseous fuels.

Chapter 3

SIMULATION MODEL OF A SPARK IGNITION ENGINE

3.1 Brief Description of the Model

The present simulation model based on the model developed by Karim and co-workers at the University of Calgary [31, 119, 32] is a two zone quasi-dimensional model capable of predicting the performance of a gas fueled spark ignition engine including the prediction of the onset of knock and its intensity and the simulation of cyclic variations of the combustion process of the engine. In this model, the homogeneous charge of the cylinder is assumed during the combustion period to be divided into two zones: burned products and unburned reactants that comprise the end gas region. The composition of the unburned reactants is usually known at all times up to the time of spark ignition, since the fuel and air flow rates were closely metered and the presence of residual gases accounted for.

An appropriate combustion energy release rate pattern [32, 120] is employed. This is based on formulations obtained following examination of a large number of experimental data for a variety of operating conditions that were shown to be capable of producing the pressure time development with reasonable accuracy. Several types of functions have been considered for such energy release rates in the literature [4] such as triangular, sine or Wiebe functions. Purely to maintain a simplicity of

approach, a triangular type function consistent with that obtained earlier by Karim et. al. [32, 120] was adopted in the present modeling. It is assumed that the combustion energy release would take place over a certain "combustion duration" that would start just beyond the spark ignition timing after a short "ignition lag period" when a significant amount of energy begins to be released due to flame kernel development and growth and would end as a result of the termination of turbulent flame propagation.

Formulations for the combustion duration variations with some of the key operating parameters were obtained from the mass of experimental data in a CFR engine operating on methane as well as binary mixtures of methane with hydrogen, ethane and propane [31, 32, 13]. The resulting energy release rate diagram whose base is the combustion duration would have its area represent the known total effective energy released during the cycle by combustion. This approach was shown to give engine pressure temporal development and hence performance, that is in good agreement with experiment. This approach also avoids attempting to predict unnecessarily the detailed features of turbulent flame propagation which remain at present of questionable practical value due not only to their complexity but also to their uncertainty [121, 34].

In order to monitor during the modeling exercise of spark ignition engine performance for the likelihood of the onset of knock, the reactivity of the end gas region of the charge needs to be evaluated throughout employing sufficiently detailed description of the reaction kinetics of the charge. The formation and growth with time of the associated reactive species need to be considered together with the energetic consequences of such reactions [119]. Accordingly, a detailed kinetic scheme was

employed in the present analysis and was based largely on that described in references [122, 123]. This scheme can describe well the preignition and combustion reactions of common gaseous fuels such as propane, ethane, methane and hydrogen and their mixtures for conditions relevant to those normally encountered within the operating range of engines that involve lean mixtures and relatively high temperatures and pressures. The scheme employed listed in Appendix (B), consisted of 155 elementary reaction steps and the following 39 chemical species:

CH, CHCO, CH2, CH2CO, CH2O, CH3, CH3CHO, CH3CO, CH3O, CH3O2, CH4, C2H, C2H2 C2H3, C2H4, C2H5, C2H6, C3H4, C3H5, C3H6, IC3H7, NC3H7, C3H8, CO, CO2, H, H2, H2O, H2O2, HCO, HO2, N2, O, O2, OH, N2O, NO, N, NO2.

The corresponding thermo-chemical data were obtained mainly from JANAF tables [124]. The scheme, when necessary, could include additional reactions and species accounting for the detailed reactions of nitrogen and/or fuel mixtures that may contain more fuel components.

A knock parameter, K, is incorporated in the model to establish whether knock may take place or not. It is based on the variations with time of the calculated accumulated amount of energy released within the transient size of the end gas due to the preignition reactions while employing the full kinetic scheme per unit of the instantaneous cylinder volume, relative to the total energy expected to be released normally through flame propagation over the whole cycle per unit of cylinder swept volume [125, 126, 13]. As the preignition reaction activity of the end gas becomes significantly intense to produce autoignition and hence knock, the value of the parameter increases despite the continued reduction in the size of the end gas

beyond a critical value that was found experimentally to be associated with the onset of mild knocking.

The composition of the products of flame propagation is calculated at the prevailing temperature while accounting for thermodynamic dissociation [127] as listed in Appendix (A). Heat transfer from the two combustion zones to the outside engine walls is accounted for, while using experimentally based formulations such as those due to Woschni [19].

The solution of the set of relevant simultaneous equations employing numerical methods yields values of the main properties of the two combustion zones and their variations with time. From the knowledge of the calculated cylinder pressure variation with time and volume changes, the corresponding indicated power output and efficiency could be evaluated. Moreover, the net rates of production and consumption of each species in the reactive end gas charge could be established. These are functions of the rates of all the simultaneous reaction steps involved [122, 123, 128] in the detailed chemical kinetic scheme for the oxidation of the fuel mixture.

The model developed was shown to be capable of predicting engine performance parameters such as the temporal variations in cylinder pressure and the mean temperatures of the two zones for different speeds, intake temperatures, intake pressures and spark timings as well as accounting for the effects of changes in some design parameters such as compression ratio, engine size and valves timing [13, 126]. Good agreement between the simulated and corresponding experimental data was found. The model, as will be shown, could also predict satisfactorily the onset of autoignition of the end gas which is responsible for engine knock as well as simulating cyclic variations of the engine.

3.2 General Description of the Model

3.2.1 Major Assumptions

As mentioned earlier in this model, the cylinder charge is assumed during the combustion process to be divided into two zones: burned products and unburned reactants which comprise the end gas region, as shown in Figure 3.1. The composition of the

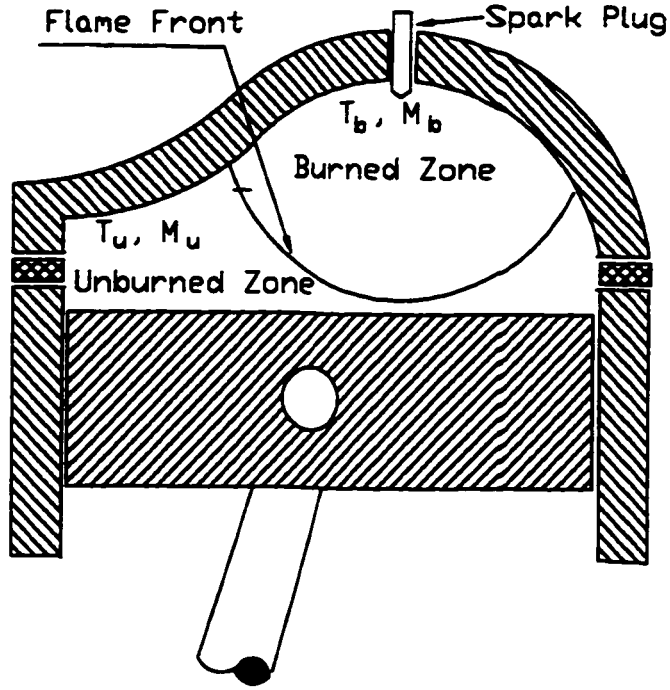

Figure 3.1: Schematic Diagram of the Two-Zones Model.

mixture of the unburned reactants is assumed to be known at all times up to the instant of spark ignition, since the fuel and air flow rates into the engine are closely metered and the presence of residual gases accounted for. However, when considering the reactivity of the end gas, detailed reaction rates and the associated reactive species are accounted for, together with the energetic consequences of such reactions [66]. The composition of the burnt products is calculated using a dissociation scheme

[127], while the transient composition of the unburned zone is established throughout using the chemical kinetic calculations. The following are the main assumptions in the model:

- The systems of burnt and unburned zones are considered to be homogenous and have uniform properties at all times.
- The pressure at any time is uniform throughout the cylinder.
- Flame thickness is negligible.
- Gases behave as ideal.
- Leakage from the cylinder is negligible.

Equation of State:

$$PV = mRT, \qquad dh_i = c_{p_i} dT, \qquad du_i = c_{v_i} dT \tag{3.1}$$

where m is the total mass of the charge, V is the cylinder volume determined from the dimensions of the engine and its movement, T is mean temperature, h_i, u_i, c_{p_i} and c_{v_i} are specific enthalpy, internal energy, heat capacity at constant pressure and at constant volume, respectively for a species "i".

Mass Conservation:

$$m = m_u + m_b \qquad \Rightarrow \frac{dm_u}{d\theta} = -\frac{dm_b}{d\theta} \tag{3.2}$$

where subscript u indicates unburned mixture and subscript b is for the burned mixture. θ is crank angle.

Volume Conservation:

$$V = V_u + V_b \Rightarrow \frac{dV}{d\theta} = \frac{dV_u}{d\theta} + \frac{dV_b}{d\theta} \tag{3.3}$$

The total volume of the engine cylinder and the rate of its change can be expressed respectively as:

$$V = \frac{1}{2}S(\frac{\pi D^2}{4})[\frac{2}{CR-1} + 1 - \cos\theta + \frac{a}{4L}(1 - cos2\theta)] \tag{3.4}$$

and

$$\frac{dV}{d\theta} = \frac{1}{2}S(\frac{\pi D^2}{4})(\sin\theta + \frac{a}{2L}\sin 2\theta) \tag{3.5}$$

where

- D= Internal diameter of the cylinder
- S= Stroke
- CR= Compression ratio
- a= Crank Radius
- L= Length of the connecting rod

Indicated Work of the Engine: The incremental work done by the whole charge considered to be the system can be further expressed by the mean cylinder pressure

and the corresponding change of the system volume.

$$\frac{dW}{d\theta} = P\frac{dV}{d\theta} \tag{3.6}$$

Energy Conservation: The energy equation for the whole charge at any instant time, corresponding to a crank angle, θ, is:

$$\frac{dQ}{d\theta} = \frac{dU}{d\theta} + \frac{dW}{d\theta} \tag{3.7}$$

where

$$U = m_u u_u + m_b u_b \Rightarrow \frac{dU}{d\theta} = m_u\frac{du_u}{d\theta} + u_u\frac{dm_u}{d\theta} + m_b\frac{du_b}{d\theta} + u_b\frac{dm_b}{d\theta} \tag{3.8}$$

and

- $dQ/d\theta$= the rate of heat transfer of the charge.
- $dW/d\theta$= the rate of work done by the charge.
- $dU/d\theta$= the rate of change in internal energy of the charge due to the change in temperature and chemical reaction of the mixture.

Calculating the amount of residual gas: At the end of the exhaust stroke residual gas fills the whole clearance volume at the exhaust pressure and temperature. The amount of residual gas is given as:

$$n_r = \frac{P_e V_c}{\bar{R} T_e} \tag{3.9}$$

where n_r is the number of moles of residuals, $\overline{R}$ is the universal gas constant, V_c is clearance volume, P_e and T_e are exhaust temperature and pressure, respectively.

Intake stroke: At the beginning of the intake stroke, the residual gas is assumed to expand from the exhaust pressure to the intake pressure, isentropically. If number of moles of residuals, n_r, exhaust and intake pressures, etc. are known, then the cylinder volume at which the fresh charge begins to enter the cylinder can be estimated since at the beginning of the intake stroke the pressure of the residuals is normally higher than that of the intake manifold and the fresh charge would not enter into the cylinder until the pressure inside the cylinder is dropped sufficiently through expansion following the piston outward movement.

The fresh charge when enters the cylinder is assumed to mix homogeneously with the residual gas. The resulting charge temperature and the amount of fresh charge can be estimated by applying the First Law and the conservation of mass equation. Since the intake valve does not close exactly at bottom dead centre nor open at top dead centre and because of the pressure loss through the intake valve and scavenging process, a correction factor is incorporated into the volumetric efficiency. It is defined as the mass flow rate of fresh fuel-air mixture divided by the rate that could have ideally been introduced via the volume displaced by the cylinder.

$$\eta_v = \frac{m_o}{\rho_{o,i} V_d} \tag{3.10}$$

where m_o is the mass of fresh charge into the cylinder per cycle, $\rho_{o,i}$ is the mixture density and V_d is the swept volume.

Compression and Expansion Strokes: The compression process is assumed to start at the bottom dead centre(BDC) just after the charge mass has reached its final value. For simplicity during compression involving relatively low temperature values, the gaseous fuels reactions were neglected. Otherwise, they would have been accounted for, when deemed necessary. Combustion of the charge is then initiated by a spark discharged normally well before top dead centre(TDC) position.

The first law of thermodynamics when applied to the charge as a single zone during compression before flame initiation and expansion following the completion of flame propagation results:

$$\frac{dQ}{d\theta} = mc_v\frac{dT}{d\theta} + P\frac{dV}{d\theta} \tag{3.11}$$

A combination of Equations 3.1 and 3.11 after rearrangement gives:

$$\frac{dP}{d\theta} = [-(1+\frac{R}{c_v})P\frac{dV}{d\theta} + (\frac{R}{c_v})\frac{dQ}{d\theta}]/V \tag{3.12}$$

$$\frac{dT}{d\theta} = T(\frac{1}{V}\frac{dV}{d\theta} + \frac{1}{P}\frac{dP}{d\theta}) \tag{3.13}$$

Combustion Period: During flame propagation, when the volume charge is assumed to be divided into two zones, burned and unburned zone, the energy equation can be written as:

$$(u_b - u_u)\frac{dm_b}{d\theta} + m_u c_{v_u}\frac{dT_u}{d\theta} + m_b c_{v_b}\frac{dT_b}{d\theta} + P\frac{dV}{d\theta} - \frac{dQ}{d\theta} = 0 \tag{3.14}$$

Differentiating the equation of state , $PV = mRT$, with respect to crank angle θ:

$$\frac{dV}{d\theta} = (\frac{V_b}{m_b} - \frac{V_u}{m_u})\frac{dm_b}{d\theta} + \frac{m_u R_u}{P}\frac{dT_u}{d\theta} + \frac{m_b R_b}{P}\frac{dT_b}{d\theta} - \frac{V}{P}\frac{dP}{d\theta} \tag{3.15}$$

Applying the first law to a unit of mass of m_u:

$$\frac{du_u}{d\theta} = \frac{1}{m_u}\frac{dQ_u}{d\theta} - P\frac{dv_u}{d\theta} \tag{3.16}$$

where Q_u is heat transfer to the unburned mixture and v_u is the specific volume of the unburned mixture. Equation 3.16 can be rewritten as:

$$c_{v_u}\frac{dT_u}{d\theta} = \frac{1}{m_u}\frac{dQ_u}{d\theta} - Pv_u(\frac{1}{T_u}\frac{dT_u}{d\theta} - \frac{1}{P}\frac{dP}{d\theta}) \tag{3.17}$$

Using $Pv = RT$ and $R = c_p - c_v$, the above equation can be reduced to:

$$m_u c_{p_u}\frac{dT_u}{d\theta} = V_u\frac{dP}{d\theta} + \frac{dQ_u}{d\theta} \tag{3.18}$$

From Equations 3.14, 3.15 and 3.18, the equations for $dT_u/d\theta$, $dT_b/d\theta$ and $dP/d\theta$ are:

$$\frac{dT_u}{d\theta} = \frac{V_u}{m_u c_{p_u}}\frac{dP}{d\theta} + \frac{1}{m_u c_{p_u}}\frac{dQ_u}{d\theta} \tag{3.19}$$

$$\frac{dT_b}{d\theta} = \frac{P}{m_b R_b}[\frac{dV}{d\theta} - \frac{(R_b T_b - R_u T_u)}{P}\frac{dm_b}{d\theta} - \frac{R_u V_u}{P c_{p_u}}\frac{dP}{d\theta} - \frac{R_u}{P c_{p_u}}\frac{dQ_u}{d\theta} + \frac{V}{P}\frac{dP}{d\theta}] \tag{3.20}$$

$$-\frac{dP}{d\theta}\left(\frac{c_{v_u}}{c_{p_u}}V_u - \frac{c_{v_b}R_u}{R_b c_{p_u}}V_u + \frac{c_{v_b}}{R_b}V\right) = \left(1+\frac{c_{v_b}}{R_b}\right)P\frac{dV}{d\theta} - \frac{dQ}{d\theta} \tag{3.21}$$

$$+\left[(u_b - u_u) - c_{v_b}\left(T_b - \frac{R_u}{R_b}T_u\right)\right]\frac{dm_b}{d\theta} + \left(\frac{c_{v_u}}{c_{p_u}} - \frac{c_{v_b}}{R_b}\frac{R_u}{c_{p_u}}\right)\frac{dQ_u}{d\theta}$$

As stated earlier, in this work the heat transfer from the two zones to the outside wall was estimated, using formulations recommended by Woschni [19]. Alternative formulations of course could be equally used if necessary.

$$\frac{dQ}{dt} = \lambda A(T - T_w) \tag{3.22}$$

where T_w is the cylinder wall temperature, assumed to be in this statement constant and T is the mean temperature of the charge, estimated by the following equation:

$$T = \frac{m_u\overline{c_{p_u}}T_u + m_b\overline{c_{p_b}}T_b}{m_u\overline{c_{p_u}} + m_b\overline{c_{p_b}}} \tag{3.23}$$

and λ is the heat transfer coefficient:

$$\lambda = 3.26D^{-0.2}P^{0.8}T^{-0.55}\left[C_1 S_p + C_2\frac{VT_1}{P_1V_1}(P - P_o)\right]^{0.8} \tag{3.24}$$

A is the area of the cylinder wall. In accordance with the recommendation of Woschni, in this equation C_1 equals to 6.18 applied to the scavenging period while for compression and expansion strokes it is equal to 2.28. C_2 is 3.24×10^{-3} (m/sK) for the whole cycle. D is the cylinder diameter in (m). V_1, T_1 and P_1 represent the known state of the working gas related to the inlet valve closure. P_o is the gas

pressure in the cylinder of the corresponding motored engine in the absence of combustion. V, T and P represent the instantaneous known state of working gas in the real engine in m^3, K and kPa, respectively. S_p is the average linear piston speed in m/s.

The total heat transfer through the whole cylinder walls equals to the sum of the heat transfers from the burned and unburned zones.

$$\frac{dQ}{dt} = \frac{dQ_u}{dt} + \frac{dQ_b}{dt} \tag{3.25}$$

This equation may be written as follows:

$$\lambda A(T - T_w) = \lambda_u A_u(T_u - T_w) + \lambda_b A_b(T_b - T_w) \tag{3.26}$$

where

$$A = A_u + A_b \tag{3.27}$$

Combining Equations 3.26 and 3.27, burned and unburned zone heat transfer areas, A_b and A_u, may be found.

$$A_b = \frac{A[\lambda(T - T_w) - \lambda_u(T_u - T_w)]}{\lambda_b(T_b - T_w) - \lambda_u(T_u - T_w)} \tag{3.28}$$

$$A_u = \frac{A[\lambda(T - T_w) - \lambda_b(T_b - T_w)]}{\lambda_u(T_u - T_w) - \lambda_b(T_b - T_w)} \tag{3.29}$$

Thus, the heat transfer through the burned and unburned zones are:

$$\frac{dQ_b}{dt} = \lambda_b A_b (T_b - T_w) \tag{3.30}$$

$$\frac{dQ_u}{dt} = \lambda_u A_u (T_u - T_w) \tag{3.31}$$

3.2.2 Energy Release Pattern

The combustion energy release rate due to the burning of the fuel can be obtained from an assumed energy release pattern derived on the basis of an analysis of the mass of experimental data with methane as a fuel. This effective formulation for the mass burning rate is shown to be adequate for modeling pressure-time development, knock and other performance parameters of interest [31].

The combustion energy release is assumed to take place over a certain combustion duration $\Delta\theta_c$ that starts just beyond the instant of passing the spark after an ignition lag time when energy just begins to be released detectably due to flame kernel development and ends as a result of the end of flame propagation having consumed the entire mixture. The area enclosed by the resulting energy release rate diagram with time would represent the total effective energy released by combustion. The examination of a very large number of such diagrams for a wide range of operating conditions indicated that the shape of these diagrams tends to be essentially similar [126, 31]. A simple approach may consider such rate diagrams to approximate to triangles with a base that corresponds to the combustion duration and the area is the known total energy release. Alternative variations on such an assumed shape can of course be made but will contribute very little to changing the pressure development with time.

Combustion Duration

The combustion duration in a spark ignition engine can be estimated using a simple experimentally based approach. The variations of combustion duration with equivalence ratio is found to have a similar trend to that shown typically in Figure 3.2, which is consistent with the typical variations of the turbulent flame speed with equivalence ratio, since the duration is proportional to the inverse of the averaged flame speed [13].

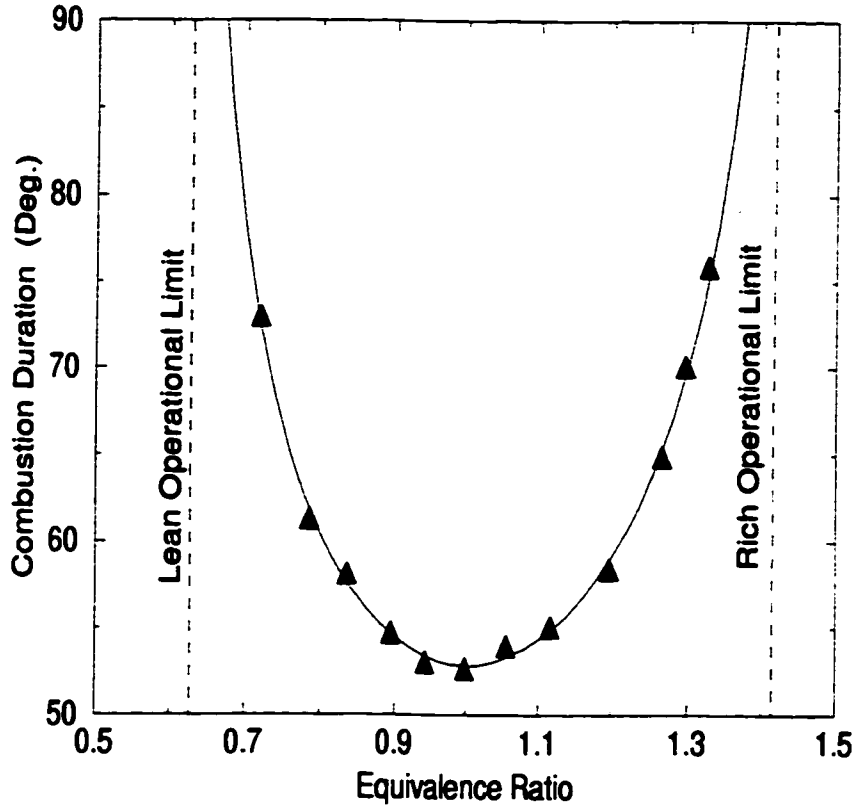

Figure 3.2: Typical Variations of Experimentally Derived Combustion Duration Versus Equivalence Ratio in a CFR Spark Ignition Engine with Methane at 900 rev./min., $\theta_{st} = 10$ BTDC, CR =8.5:1, $T_o = 300$ K and $P_o = 87$ kPa.

Moreover, the operational equivalence ratio limits correspond to the combustion failure limits, as encountered in a typical spark ignition engine, which are associated with extremely long combustion duration. These limits have been established experimentally and methods for their estimation for any specific engine has been successfully proposed [129, 130]. The minimum combustion duration occurs around the stoichiometric ratio and can either be estimated or measured experimentally [66]. Therefore, an appropriate combustion duration correlation can be formulated for any engine operating condition. As an example, the following empirical formula was used:

$$\Delta\theta_c = Ae^z + Be^z \tag{3.32}$$

where

$$z = -(\phi_{min} - \phi)/\sqrt{(\phi_r - \phi)} \tag{3.33}$$

and

$$x = (\phi_{min} - \phi)/\sqrt{(\phi - \phi_l)} \tag{3.34}$$

$\Delta\theta_c$ is the combustion duration in degrees for an equivalence ratio of ϕ. The lean and rich operational limits equivalence ratios are ϕ_l and ϕ_r, respectively. The equivalence ratio for minimum combustion duration is ϕ_{min} which is usually around the stoichiometric. A and B are constants that can be derived for the engine and set

up employed. ϕ_l and ϕ_r can be found or estimated for any operating conditions. Karim et. al. [43, 129] measured the apparent lean and rich operational limits for several fuels in a CFR spark ignition engine for different operating conditions. The lean limit, for methane, was found to be approximately a linear function of the mean mixture temperature at the moment of spark discharge by Karim and Wierzba [130]. The lean operational limit can then be represented by:

$$\phi_l = A_1 T_{st} + B_1 \tag{3.35}$$

where A_1 and B_1 are constants, which were found to be $-1/50000$ and 0.071 , by fitting the relevant experimental data in a CFR engine. T_{st} is the average calculated mixture temperature (K) at the moment of spark discharge.

Karim and Wierzba [130] also found that the rich flammability limit is a linear function of the difference of the mixture temperature at the moment of spark discharge (T_{st}) and the mixture temperature at intake conditions (T_o).

$$\phi_r = A_2(T_{st} - T_o) + B_2 \tag{3.36}$$

where A_2 and B_2 are constants. These were found from fitting the relevant experimental data in a CFR engine to be 1/10000 and 0.1, respectively.

Most hydrocarbons tend to have a similar flame propagation characteristics in a spark ignition engine [131], especially within the same group, for example paraffins. Thus , the combustion duration calculation method can be extended to other fuels such as propane and ethane. The values of the constants of Equations 3.35 and 3.36

for these fuels then can be estimated from relevant experimental data. In the present work the values of constants, A_1, B_1, A_2 and B_2 for ethane are derived from experimental observation as -1/50000, 0.05, 1/10000 and 0.08 respectively [131], while for propane these values are -1/50000, 0.04, 1/10000 and 0.0566 respectively [130].

The lean and rich flammability limits for hydrogen in air, at atmospheric temperature and pressure, are 4% and 75% by volume, respectively [127]. These values will be modified at higher temperatures and pressures such as those existing in the cylinder at the time of spark passage [13].

Since the minimum value of the combustion duration occurs around the stoichiometric mixture, then the following simplification can establish the values of A and B in terms of the known ϕ_l, ϕ_r, ϕ_{min} and $\Delta\theta_{c,min}$ by taking $d\Delta\theta_c/d\phi|_{\phi_{min}} = 0$:

$$A = \Delta\theta_{c,min}\left[\frac{\sqrt{(\phi_{min}-\phi_l)/(\phi_r-\phi_{min})}}{1+\sqrt{(\phi_{min}-\phi_l)/(\phi_r-\phi_{min})}}\right] \tag{3.37}$$

$$B = \frac{\Delta\theta_{c,min}}{1+\sqrt{(\phi_{min}-\phi_l)/(\phi_r-\phi_{min})}} \tag{3.38}$$

where $\Delta\theta_{c,min}$ is the minimum combustion duration.

There are basically two main factors affecting the combustion duration in a spark ignition engine. The first factor is the cylinder geometry and size, which decide the effective flame propagation distance, d_c. The other factor is the effective flame propagation speed, S_f:

$$\Delta\theta_{c,min} = f(d_c, S_f) \tag{3.39}$$

In a spark ignition engine, due to the motion of the piston and the changing with time of temperature and pressure, both d_c and S_f vary during combustion. Various simplifications may be introduced to find a correlation for estimating the minimum combustion duration for a certain engine and operating condition particularly when lean mixture operation is involved. For example, assuming that the flame propagation distance d_c is proportional to $V_{st}^{1/3}$ is a reasonable approximation during combustion, where V_{st} is the combustion chamber volume at the time of spark discharge and depends on the spark timing and the compression ratio. This way an advanced spark timing and a low compression ratio will lead to a longer flame propagation path. Correlating the corresponding experimental data obtained from a CFR engine led to the following equation [132]:

$$\Delta\theta_{c,min} = C\frac{V_{st}^{1/3}}{CR^{(1/2)}}f(S_f) \tag{3.40}$$

The apparent flame propagation speed, S_f, is the other important factor influencing the value of the combustion duration which for any equivalence ratio and engine speed would depend on mixture temperature and pressure. Since the flow in a spark ignition engine is strongly turbulent, the flame propagation is also turbulent and it is affected by the engine speed and nature of the turbulence intensity and scale. Numerous research investigations have been carried out of premixed laminar flame propagation in constant volume cells. Some correlations for laminar flame propagation have been developed. However, these correlations cannot be applied directly to the engine modeling mainly because of the variable geometry of the combustion chamber and the intense turbulent nature of the flow in a running engine. A general approach that

proved to be effective is to use the correlations for laminar flame propagation after incorporating some appropriate corrections to fit the observed experimental engine data [28, 31].

Al-Himyary [31] developed a generalized expression for the maximum flame propagation speed for methane based on extensive experimental data obtained by others under different operating conditions. He found that the maximum burning speed occurs at an equivalence ratio of around 1.036, corresponding to the minimum combustion duration, and that:

$$S_{f,max} = P^{-0.457} \exp(-746.8/T + 6.193) \tag{3.41}$$

where P and T are instantaneous mixture pressure (atm) and temperature (K), respectively, and $S_{f,max}$ is the maximum flame propagation speed.

For a fixed engine speed, it is reasonable to assume that the maximum apparent flame propagation rate is proportional to the $S_{f,max}$. Thus, with the maximum burning speed according to Equation 3.41, the minimum combustion duration of Equation 3.40 may be expressed as:

$$\Delta\theta_{c,min} \propto \frac{d_c}{S_{f,max}} \propto \frac{V_{st}^{1/3}}{C R^{(1/2)}} P^{0.457} e^{(764.8/T)} \tag{3.42}$$

In this formula, P and T are the instantaneous mean pressure and temperature of the mixture during combustion. They are unknown before the combustion process calculation in a predictive model. But, what is known are the P and T values at the moment of spark discharge. Thus, some correction is needed to make this

formula usable for predicting the combustion duration which was found for methane operation as:

$$\Delta\theta_{c,min} = C\frac{V_{st}^{1/3}}{CR^{(1/2)}}P^{0.457}e^{(764.8/T)} \tag{3.43}$$

The effects of turbulence on the combustion duration are still to be discussed. It was known that the turbulent characteristic velocity is usually a function of the mean piston linear speed S_p [4] and it can be used to represent turbulence effects. Hirst et. al. [133] found that:

$$\Delta\theta_{c,min} \propto {S_p}^{1/3} \tag{3.44}$$

Utilizing this simple relationship will yield the following expression for the final form of minimum combustion duration correlation.

$$\Delta\theta_{c,min} = C'\frac{V_{st}^{1/3}}{CR^{(1/2)}}P^{0.457}e^{(764.8/T)}{S_p}^{1/3} \tag{3.45}$$

where C' is a constant which depends on the cylinder geometry and the spark plug location and S_p is piston speed. No doubt, other correlative approaches of experimentally observed data can be derived. For example a simpler method to calculate the value of $\Delta\theta_{c,min}$ will be discussed later in this chapter. In any case, the value of $\Delta\theta_{c,min}$ in the key relationship of Equation 3.37 does not need to be known necessarily highly accurately. Moreover, for lean operation even an assumed negligibly small value for $\Delta\theta_{c,min}$ at the stoichiometric equivalence ratio can produce reasonably workable approximation for the value of $\Delta\theta_c$ as a function of ϕ.

For any given set of operating conditions, from the computations during the compression stroke, the mean values of pressure and temperature at the moment of spark discharge are known. Equation 3.45 gives the value of the minimum combustion duration, while the lean and rich operational limits can be found using the procedure described earlier. The constants A and B then can be calculated. By substituting these into Equation 3.32, the combustion duration can be predicted. This method for estimating the combustion duration may be applied for various operating conditions. Only one constant C' needs to be determined by measuring the combustion duration once for the engine of interest. A typical comparison between the estimated combustion duration values calculated in accordance with this procedure and the corresponding experimental values obtained in a CFR engine operating on methane and air is shown in Figure 3.3. It can be seen, from these typical cases, that the combustion duration estimated according to the proposed predictive model produces good agreement with experimentally derived data.

Ignition Lag

The combustion process in a spark ignition engine can be conceived to progress over two primary stages, the ignition lag and the effective combustion duration. When the spark is discharged, no significant combustion energy release appears immediately since time is needed to initiate the nucleous of a propagating flame kernel. The period of the ignition lag is conceived to start at the moment of spark discharge and ends at the time when a significant flame development takes place involving a certain detectable amount of burned mass and energy are released. The description of this delay in energy release as ignition lag in spark ignition engines is to distinguish it

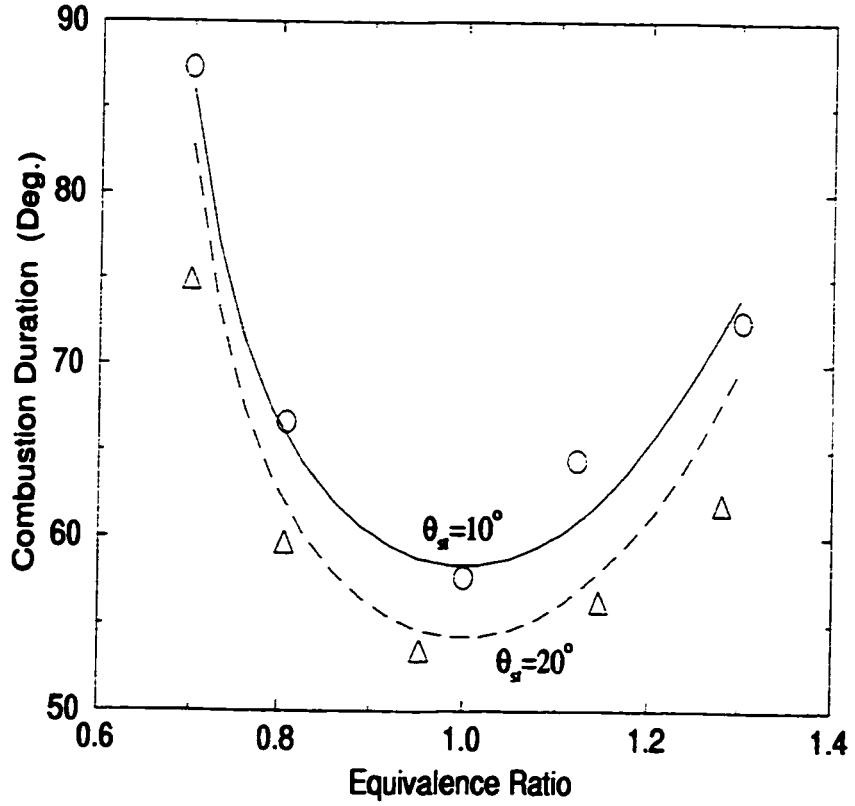

Figure 3.3: A Comparison Between Estimated Combustion Duration Versus Equivalence Ratio and Experimental Data from a CFR Spark Ignition Engine with Methane at 900 rev./min., CR =8.5:1 and T_o = 294 K for Two Spark Timings.

from that of the ignition delay in diesel engines and it is somewhat arbitrary. Usually, the amount of the burned gas mass during the ignition lag is taken for convenience as the criterion for the ignition lag length. The amount has been considered ranges from 1% to 5% of the total charge. Hires [34] took 1% of total mass as the end of the ignition lag, while Hong [29] considered 2% at the end point. Al-Himyary [31] suggested 5% mass consumption at the end of ignition lag. In the present work, Al-Himyary's criterion for ignition lag is used so that the model predictive results

can be compared with the mass of his diagnostic results.

In a spark ignition engine, the length of the ignition lag is governed mainly by the chemical reaction activity and the diffusive transport processes. Although most of the details concerning the chemistry and fluid mechanics of the initial flame kernel growth in a spark ignition engine are not fully clear, the effects of several operational parameters on the ignition lag have been investigated [31, 60, 111]. It was found, among the many important operational parameters influencing ignition lag length are the equivalence ratio, piston speed, mixture temperature and pressure. To find a correlation for the variation of the ignition lag with operating conditions, a similar procedure as that used for estimating the combustion duration was adopted. Figure 3.4 shows a typical plot of experimentally derived values of the ignition lag with equivalence ratio [30] displaying excessively long lags at the lean and rich limits. There is also a minimum ignition lag that corresponds with the fastest flame propagation for any operational conditions. Accordingly, the variations of the ignition lag with equivalence ratio can also be represented by a similar exponential function as that of Equation 3.32 obtained for the combustion duration:

$$\Delta\theta_{ig} = A_{ig} \exp\left(\frac{\phi_{min} - \phi}{\sqrt{\phi - \phi_l}}\right) + B_{ig} \exp\left(\frac{\phi - \phi_{min}}{\sqrt{\phi_r - \phi}}\right) \tag{3.46}$$

where

- $\Delta\theta_{ig}$ ignition lag length, crank angle (Degrees).
- ϕ equivalence ratio.
- ϕ_{min} equivalence ratio where the combustion duration is the shortest.

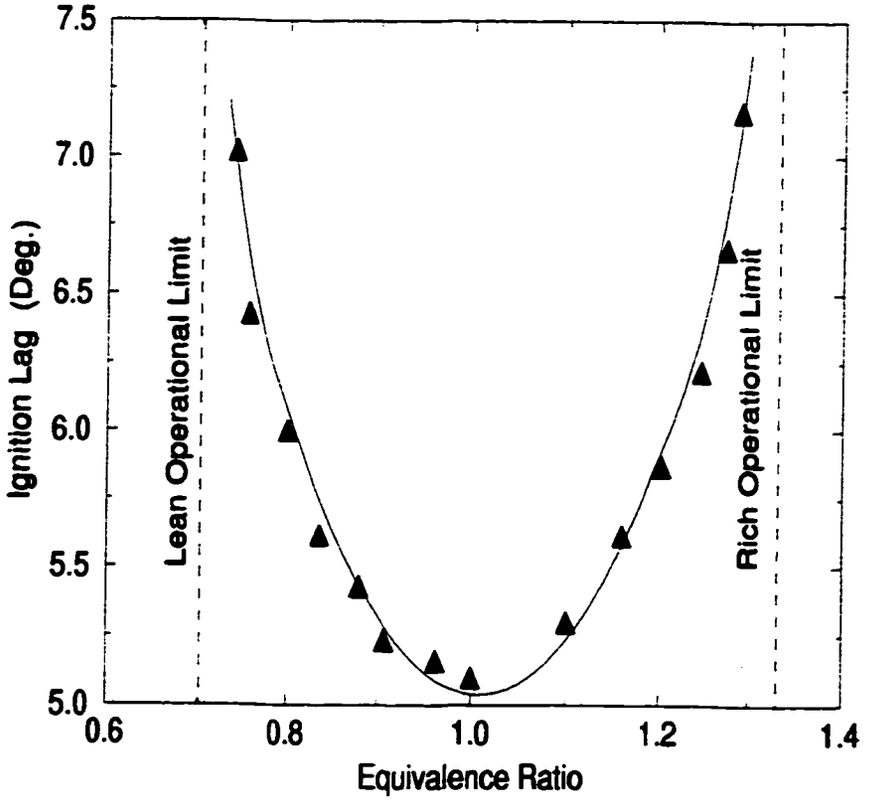

Figure 3.4: Typical Variations of Experimentally Derived Ignition Lag with Equivalence Ratio in a CFR Spark Ignition Engine with Methane at 900 rev./min., $CR = 8.5 : 1$, $P_o = 87$ kPa and $T_o = 300$ K.

- ϕ_l lean operational limit.
- ϕ_r rich operational limit.
- A_{ig}, B_{ig} constants.

and similar to the model for combustion period:

$$A_{ig} = \Delta\theta_{ig,min}\left[\frac{\sqrt{(\phi_{min} - \phi_l)/(\phi_r - \phi_{min})}}{1 + \sqrt{(\phi_{min} - \phi_l)/(\phi_r - \phi_{min})}}\right] \tag{3.47}$$

and

$$B_{ig} = \frac{\Delta\theta_{ig,min}}{1 + \sqrt{(\phi_{min} - \phi_l)/(\phi_r - \phi_{min})}} \tag{3.48}$$

The value of the minimum ignition lag, $\Delta\theta_{ig,min}$, can be found also by fitting experimental data to the following expression to produce acceptable agreement with the corresponding experimental observations.

$$\Delta\theta_{ig,min} = C'' \frac{T_{st}^{(1/2)} S_p^{1/3}}{CR^{(1/2)}} \tag{3.49}$$

where $\Delta\theta_{ig,min}$ is the minimum ignition delay and C'' is a constant. A_{ig} and B_{ig} may be estimated from Equations 3.47 and 3.48. Hence, the ignition lag can be found using Equation 3.46. Figure 3.5 is a typical comparison between the estimated ignition lag using the approach described and the corresponding results of experimental analysis [30]. It is to be remembered that since the value of the ignition lag tends to be always quite small relative to the length of the combustion duration, a less precise estimate of the length of the ignition lag would not produce significant errors in estimating engine output parameters.

Combustion Duration and Ignition Lag for Fuel Mixtures

Many researchers investigated the effect of the addition of common gaseous fuels such as hydrogen, ethane or propane to methane on the effective flame burning speed and performance of an engine [30, 14, 134]. Generally, there appears to be no reliable model capable of predicting the burning velocity of fuel mixtures within a wide range of temperature, pressure and composition, especially in relation to the spark

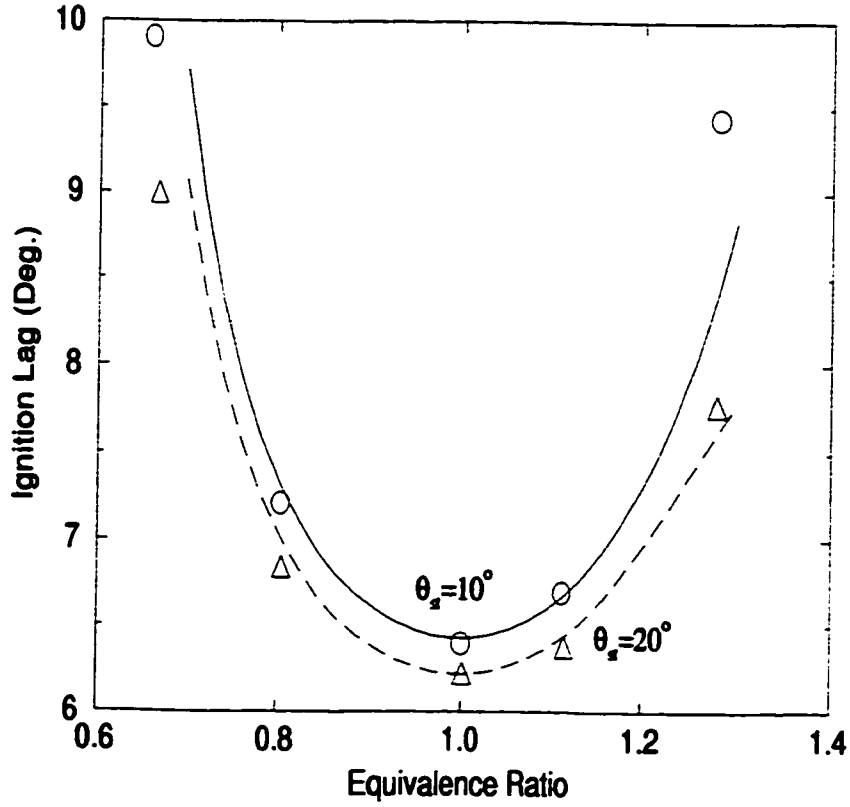

Figure 3.5: A Comparison Between the Estimated Ignition Lag and Experimental Data from a CFR Spark Ignited Engine for Methane Operation at 900 rev./min., CR =8.5:1, T_o = 300 K and P_o = 87 kPa for Two Spark Timings.

ignition engine, where fully turbulent conditions prevail throughout. Hence, any correlation for the combustion duration and ignition delay, for methane-hydrogen, methane-ethane and methane-propane mixtures have to be based on experimental data obtained directly from the measurement of the combustion duration and ignition lag in the engine. Consequently, an expression for the combustion duration of a fuel mixture based on experimental observations we made in a CFR engine can be given

approximately as:

$$\frac{1}{\Delta\theta_{c,m}} = \frac{y_1}{\Delta\theta_{c1}} + \frac{y_2}{\Delta\theta_{c2}} + \frac{y_3}{\Delta\theta_{c3}} + \ldots \tag{3.50}$$

where y_i is the molar fraction of the fuel,"i", in the fuel mixture and $\Delta\theta_{ci}$ is the corresponding combustion duration or ignition lag for the engine when operating with the fuel component "i" on its own under the same conditions. $\Delta\theta_{c,m}$ is the combustion duration or ignition lag for the mixture.

To estimate the corresponding operational limits of a mixture of fuels the Le'Chatelier's rule was applied [127] using the values of the known limits of the individual fuel components under the same operating condition, i. e.:

$$\frac{1}{L_{\text{mix}}} = \sum \frac{c_i}{L_i} \tag{3.51}$$

where c_i is the fractional molar concentration of the specie "i" in the fuel mixture, L_i is the flammability limit of that specie at that specified temperature and pressure and L_{mix} is the flammability limit of the mixture.

A typical comparison between such estimated combustion duration or ignition lag with experimentally derived data [13] for mixtures of hydrogen and methane in the CFR engine are shown in Figures 3.6 and 3.7. Similarly, in Figures 3.8 and 3.9 the estimated combustion durations and ignition lags for propane-methane and ethane-methane mixtures are presented along with their corresponding experimental data.

Thus, the full model developed to estimate the mean effective combustion dura-

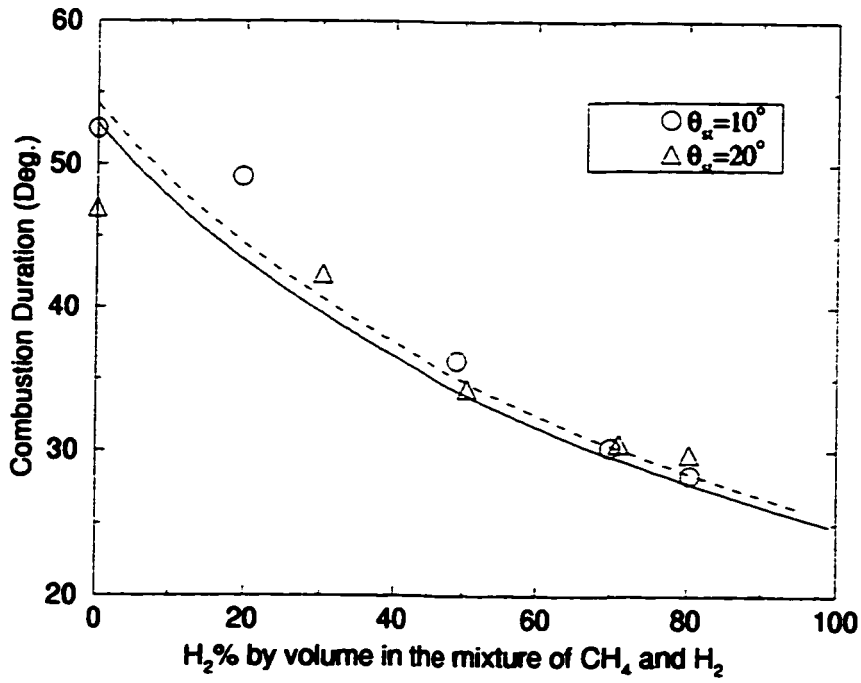

Figure 3.6: Calculated Combustion Duration Variations for Mixtures of CH_4 and H_2 at 900 rev./min., CR =8.5:1, $\phi = 1.0$, $P_o = 87$ kPa, $T_o = 300$ K.

tion and ignition lag for methane operation can be extended for applications involving other gaseous fuels and their mixtures. Due to the nature of the strong turbulent flow encountered within a running spark ignition engines and the associated cyclic variations, the real value of the combustion duration tends to be necessarily fluctuating and statistical in nature. Hence, the accurate prediction of the combustion duration in a theoretical model is difficult, if not unavailable at present and it will be shown in any case as strictly unnecessary for measures to predict engine performance parameters with gaseous fuels.

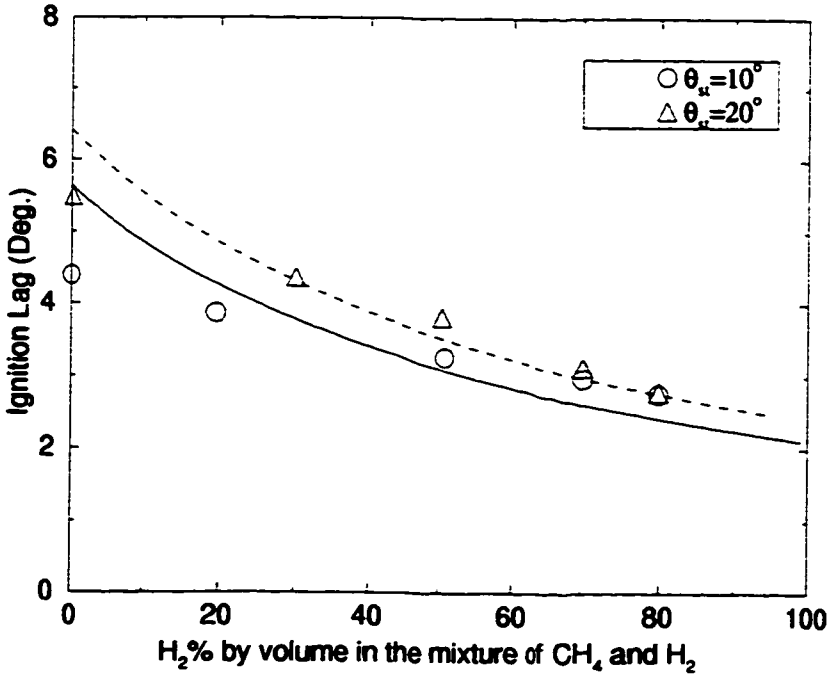

Figure 3.7: Comparison of the Calculated Ignition Lag with Experimental Data for Mixtures of CH_4 and H_2 at 900 rev./min., CR =8.5:1, ϕ = 1.0, P_o = 87 kPa, T_o = 300 K.

Mass Burning Rate Profile

Several functions have been suggested in the literature to represent the mass burning rate in spark ignition engines. For example, triangular, sine and Weibe type functions have been used [4]. The mass of data obtained experimentally when methane is the fuel over a very wide range of operating conditions, as shown typically in Figure 3.10, can be viewed for simplicity to approximately follow a triangular format [126, 31] for the mass burning rate. Therefore, it can be represented by:

$$\Delta m = \frac{2m_o}{\Delta\theta_c}\sigma_m \tag{3.52}$$

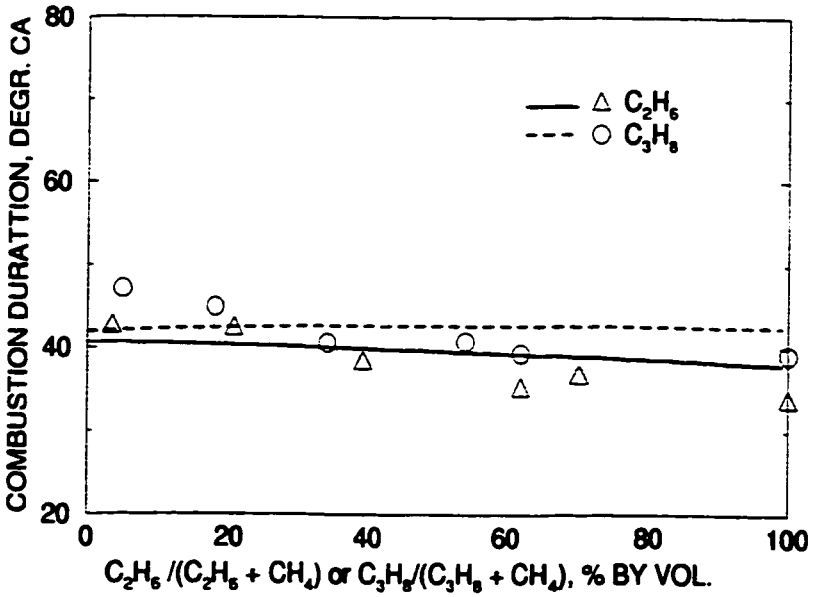

Figure 3.8: Calculated Combustion Duration Variations for Mixtures of Ethane-Methane or Propane-Methane at 900 rev./min., CR =8.5:1, $\phi = 1.0$, $P_o = 87$ kPa, $T_o = 300$ K and $\theta_{st} = 15$ BTC for Ethane-Methane Mixtures and $\theta_{st} = 10$ BTC for Propane-Methane Mixtures. Our Own Experimental Points are Shown.

where

$$\sigma_m = \frac{\theta - \theta_{e.i.}}{\theta_{max} - \theta_{e.i.}} \qquad \text{when} \qquad \theta_{e.i.} \leq \theta \leq \theta_{max} \tag{3.53}$$

$$\sigma_m = \frac{\theta_{e.c.} - \theta}{\theta_{e.c.} - \theta_{max}} \qquad \text{when} \qquad \theta_{max} \leq \theta \leq \theta_{e.c.} \tag{3.54}$$

where $\theta_{e.i.}$, $\theta_{e.c.}$ and θ_{max} are the crank angles at the end of ignition lag, the end of combustion duration and at a location associated with maximum mass burning rate. This latter may be assumed to be at around 2/3 of the combustion duration as obtained for the CFR engine at much of the specified operating conditions. Other

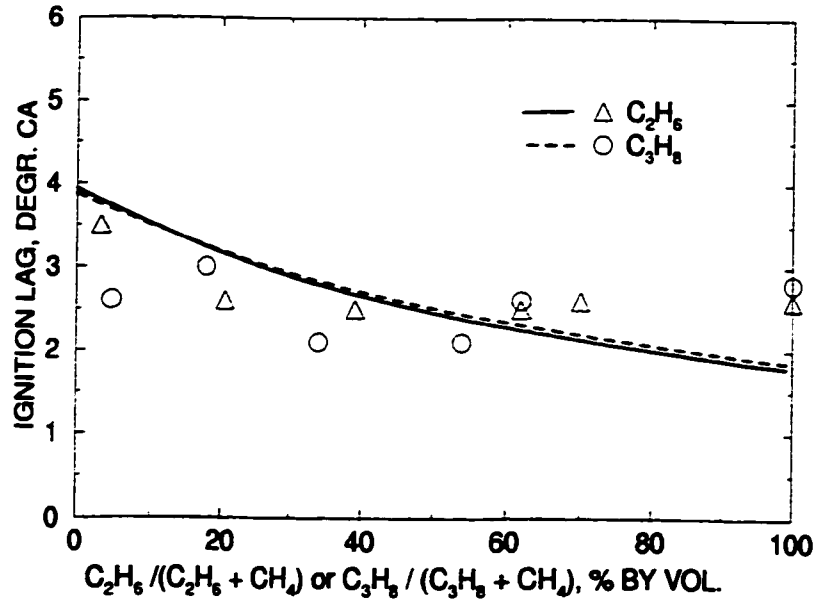

Figure 3.9: Comparison of the Calculated Ignition Lag with Experimental Data for Mixtures of Ethane-Methane or Propane-Methane at 900 rev./min., CR =8.5:1, ϕ = 1.0, P_o = 87 kPa, T_o = 300 K and θ_{st} = 15 BTC for Ethane-Methane and θ_{st} = 10 BTC for Propane-Methane Mixtures.

viable distribution can be easily used also whenever necessary.

The solution of the set of the relevant simultaneous equations employing numerical methods yields values of the main properties of the two-zones and their variations with time. From a knowledge of the calculated cylinder pressure variation with volume changes, the corresponding indicated power output and thermal efficiency could be evaluated by a simple integration of the PdV term over the whole working cycle. With this quasi empirical thermodynamics approach no reliable estimates however can be made at this stage of the nature and extent of emissions.

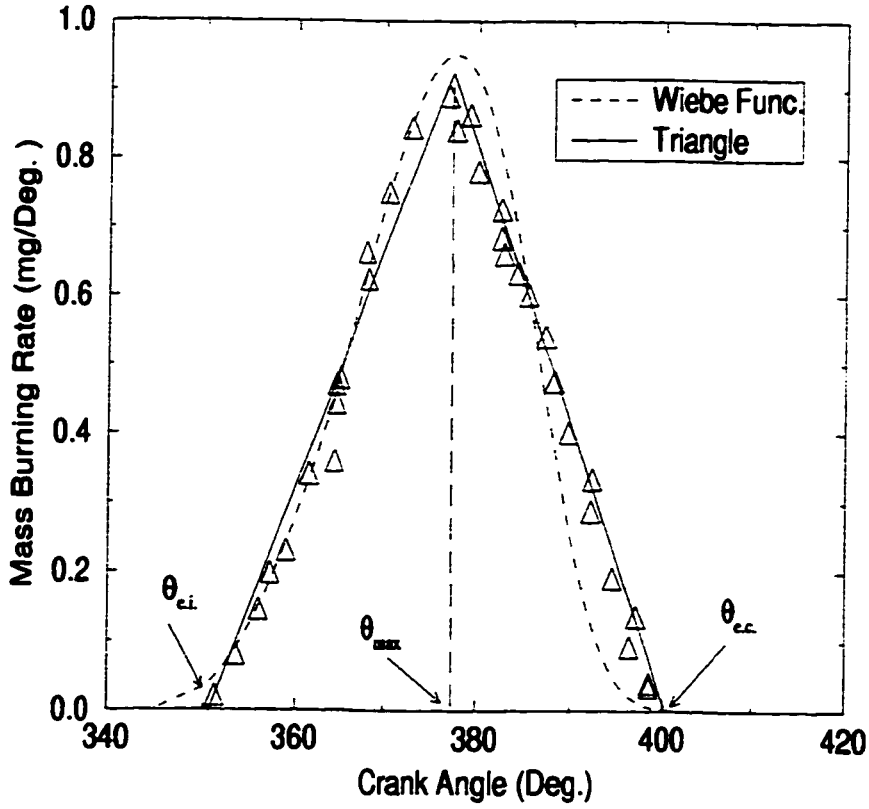

Figure 3.10: Comparison Between Calculated and Experimentally Derived Mass Burning Rates. Operating Parameters 900 rev./min., CR =8.5:1, θ_{st} = 15 BTDC, $\phi = 1.0$, $T_o = 300$ K.

A Simplified Alternative Method for Calculating Combustion Duration

As mentioned earlier, simplified methods for the estimation of the combustion duration can be also used specially in the case where much of the experimental information was not available, since the small changes in the value of the combustion duration will not effect considerably the performance parameters of the spark ignition engine. Moreover, as stated earlier the combustion duration in a spark ignition engine tends to be necessarily fluctuating and statistical in nature.

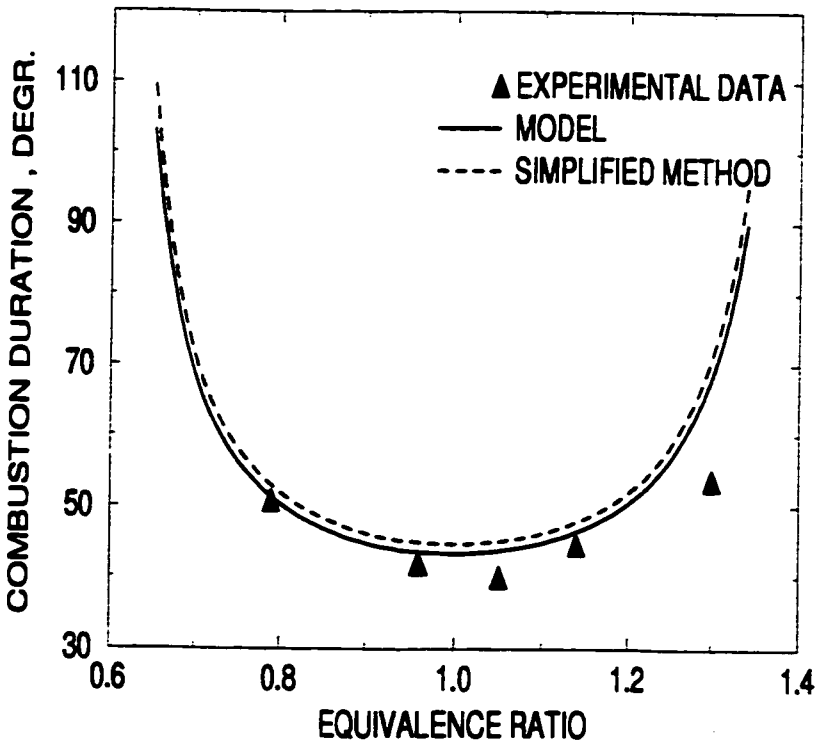

Figure 3.11: Comparison of the Calculated Combustion Duration Using the Model and the Simplified Method for Various Equivalence Ratios at CR =8.5:1, ϕ = 1.0, P_o = 87 kPa, T_o = 294 K and θ_{st} = 27.5 BTC. The Corresponding Experimental Values are also Shown.

For example, the fastest burning rate or the minimum combustion duration in a spark ignition engine occurs around the stoichiometric equivalence ratio at MBT timing [13, 30, 4]. For these best operating conditions, generally the maximum pressure occurs just after the top dead centre producing the maximum power output and efficiency. The position of the crank angle at the maximum pressure can also be viewed as the location where the pressure rise due to the combustion of the fuel and the pressure changes due to the volume changes in the cylinder are equal. Accordingly, the first term of the right hand side of Equation 3.21 which represents the pressure change due to the volume change in the cylinder must be equal to

the rest of the terms which is basically the pressure changes due to the effective combustion of the fuel so that the derivative of the pressure is zero which corresponds to the maximum pressure. This information can be used to calculate the combustion duration at the operating conditions using the mass burning rate profile described in the previous section. This combustion duration will be the minimum combustion duration, $\Delta\theta_{c,min}$, at that operating conditions. Once, the $\Delta\theta_{c,min}$ is found, it can be substituted in Equation 3.37 to calculate subsequently the combustion duration at other operating conditions.

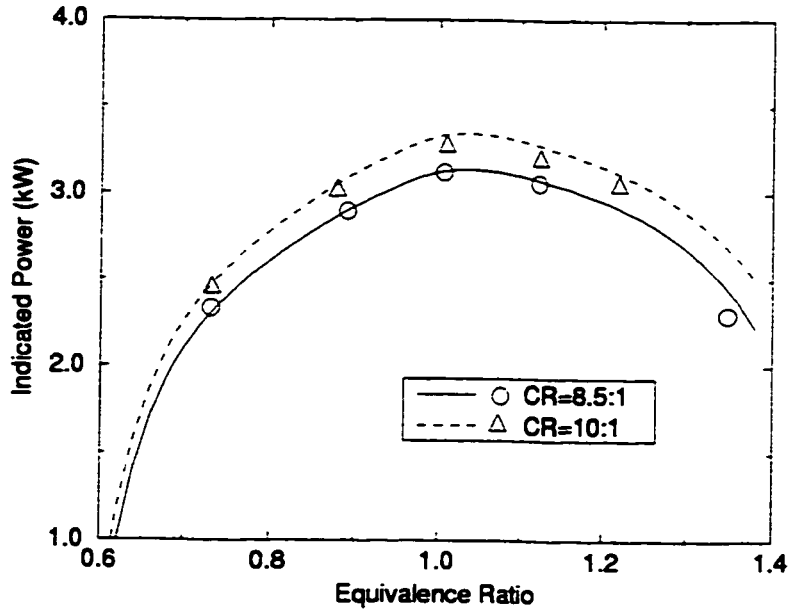

Figure 3.12: A Typical Variations of Indicated Power Output with Equivalence Ratio for Different Compression Ratios While Operating on Methane at 900 rev./min., Spark Timing of 15 degrees BTC and Initial Temperature of 294 K. Experimental Points are also Shown.

As a typical example, the crank angle at the maximum pressure for the best power output with MBT of 27.5 degrees BTC at the operating condition of 8.5:1 compres-

sion ratio, initial room temperature and atmospheric pressure in a spark ignition CFR engine with the fuel methane was found around 10 degrees ATC [30, 135]. Accordingly, the calculation of the combustion durations using this simplified method and the model were carried out and the results were presented along with the corresponding experimental values [30, 135] in Figure 3.11. In these calculations the values of ignition lag period were neglected, since these values tend to be very small relative to the values of the corresponding combustion duration at these best operating conditions. As it can be seen that the difference between the combustion durations calculated from the model and the simplified method was small and less than 3%. Hence, both methods produced good agreement with the corresponding experimental values with an error less than 9% for the model and 13% for the simplified method, except for the very lean and rich limit operations.

For an example, a comparison of some of the typical results of the calculations with our corresponding experimental data is presented. The indicated power output versus the equivalence ratio for two different compression ratios is shown in Figure 3.12 while operating on methane. Very good agreement can be seen between the predicted and the corresponding experimental values. Similarly, in Figure 3.13, a typical comparison is presented for fuel mixtures such as methane-propane and methane-ethane. It can be seen that the increasing addition of ethane or propane to methane resulted in only relatively small improvement in the indicated power output at constant spark timing. This was expected because of both ethane and propane provide somewhat faster combustion rates and higher heating values on volume basis than those for methane. Moreover, the addition of propane tends to produce slightly higher output than the corresponding values for ethane addition for

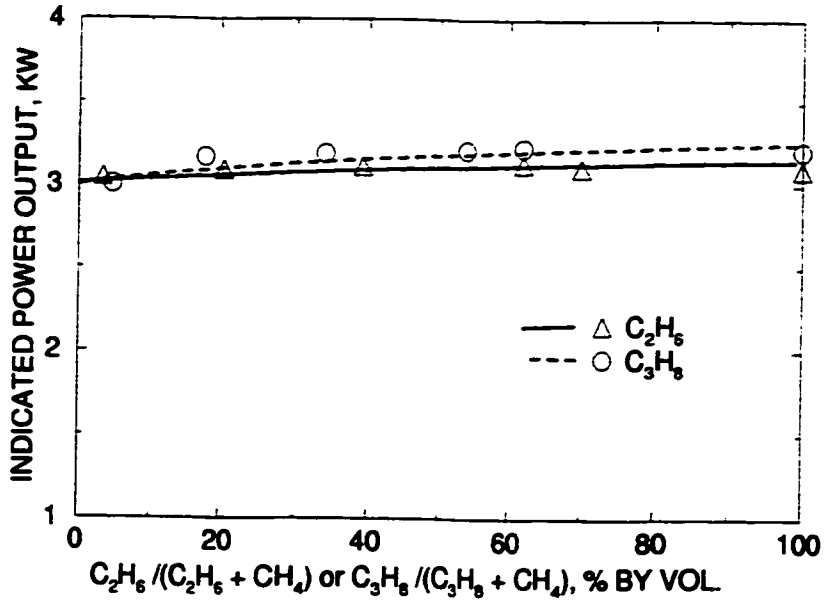

Figure 3.13: The Indicated Power Output Variations When Operating on Methane-Ethane and Methane-Propane Mixtures for a Compression Ratio of 8.5:1, Equivalence Ratio of 1.0, Spark Timing of 15 degrees BTC for Methane-Ethane Mixtures and 10 degrees BTC for Methane-Propane Mixtures and Initial Mixture Temperature of 298K at 900 rev./min. The Corresponding Experimental Data are also Shown.

the same mixtures and operating conditions, since propane tends to have slightly faster combustion rates and has a higher heating value on volume basis than ethane. These trends are also consistent with those reported experimentally by others (e.g. [30]). As evident from these figures, the agreement between the simulated engine parameters by the model and the corresponding experimental data appears to be very good.

3.2.3 Knock Modeling

The current model described considers knock to take place when the energy released due to preignition reaction activity within the end gas becomes sufficiently significant and intense that results in autoignition of a portion of the mixture yet to be consumed by the propagating flame. The knock criterion developed by Karim et al [126, 13] was used. It is based on the calculated accumulated amount of energy release that is due solely to end gas preignition reactions activity per unit of the instantaneous charge volume, relative to the total energy to be released normally through flame propagation over the whole cycle per unit of cylinder swept volume, i.e.

$$Knock \quad Criterion(K) = \frac{\frac{Energy \quad Released \quad by \quad End \quad Gas \quad Reactions}{Volume}|_t}{\frac{Energy \quad Released \quad By \quad Combustion}{Volume}|_{t0}} \tag{3.55}$$

The energy released by the self reactions of the end gas is defined as:

$$H_{u_t} = \int_{t_{st}}^{t} dE_u = (h_{st} - h_t)m_u \tag{3.56}$$

where h is the enthalpy of the mixture per unit of mass ($h = \sum c_i h_i$) and m_u is the instantaneous end-gas mass. Subscripts t_{st} and t indicate the values at the spark discharge and at any instant of time, respectively.

The energy released due to normal combustion can be simplified as:

$$H_o = h_o m_o \tag{3.57}$$

where h_o is the effective heating value of the charge and m_o is the initial or total

mass of the charge. Consequently, Equation 3.55 may be simplified as:

$$K = \frac{(h_{st} - h_t)m_u/V_t}{h_o m_o/V_o} \tag{3.58}$$

In order to predict the energy release by end gas reactions, a detailed chemical kinetics model including 155 reaction steps and 39 species is used. A chemical reaction scheme involving i species and j reaction steps can be represented by the following set of reaction equations:

$$\sum_{i=1}^{n} \alpha_{ijf} X_i \underset{K_{jb}}{\overset{K_{jf}}{\rightleftharpoons}} \sum_{i=1}^{n} \alpha_{ijb} X_i \qquad j = 1, 2, ..., n \tag{3.59}$$

where α_{ijf} and α_{ijb} are stoichiometric coefficients of the i^{th} species appearing in the reactants and products of the j^{th} reaction , respectively. X_i is the formula for a species i taking part in the reaction.

The net rate of production and consumption of each species (i) of a reactive end gas charge depends on the rates of all the reaction steps involved [136, 128] in the detailed chemical kinetic scheme for the oxidation of fuel. Therefore, the change of chemical species concentration over a certain element of time can be calculated from the following set of equations:

$$\frac{dc_i}{dt} = \frac{1}{\rho} \sum_{j=1}^{n} (R_{jb} - R_{jf}) \tag{3.60}$$

where c_i is the concentration of i^{th} species, ρ is the mixture density, R_{jf} and R_{jb} are the forward and backward reaction rates of the j^{th} reaction, respectively, which can be calculated by:

$$R_{jf} = K_{jf} \prod_{I=1}^{n} (\rho c_i)^{\alpha_{ijf}}$$
$$R_{jb} = K_{jb} \prod_{I=1}^{n} (\rho c_i)^{\alpha_{ijb}} \tag{3.61}$$

K_{jf} and K_{jb} are the forward and backward rate constants for the j^{th} reaction and can be calculated according to the following:

$$\begin{aligned} K_{jf} &= A_{jf} T^{B_{jf}} \exp(-\frac{E_{jf}}{RT}) \\ K_{jb} &= A_{jb} T^{B_{jb}} \exp(-\frac{E_{jb}}{RT}) \\ or \qquad K_{jb} &= \frac{K_{jf}}{K_{jc}} \end{aligned} \tag{3.62}$$

K_{jc} is the corresponding equilibrium constant of the reaction step and A_{jf}, A_{jb}, B_{jf} and B_{jb} are constants for the forward and backward rate constants of the j^{th} reaction equation. E_{jf} and E_{jb} are the activation energies of the forward and backward reactions of the j^{th} reaction equation, respectively. K_{jf} and K_{jb} are related through the corresponding equilibrium constant. K_{jc} is the equilibrium constant based on the concentrations for the j^{th} reaction equation.

When the above set of simultaneous equations is solved numerically, the concentration of each species in the unburned zone at any instant of time can be found. The physical properties of the species, the reaction scheme used and its corresponding

constants for methane, propane and hydrogen are listed in Appendix (B).

The knock modeling thus proceeds to monitor the reaction activity and the changes in the concentrations of each of the reacting species using the above group of equations right from the time of spark discharge, or even earlier when necessary. This is carried out for each time increment while accounting for the local temperature, pressure and volume of the end gas throughout, right up to the point of the total consumption of the unburned charge by the propagating flame at the end of the combustion period. When the end gas chemical reaction activity is sufficiently intense, the associated energy release may also cause some further temperature and pressure rise.

Normally the effects of any reaction activity within the unburned gas on the total cylinder pressure is relatively small compared with that due to normal combustion, prior to the onset of knocking when no autoignition takes place. However, the situation for the unburned zone temperature may be different. The effect of the end gas reaction on temperature is assumed to be limited to the end gas zone itself. Since the end gas reaction rate is very sensitive to temperature, the effect of the end gas reaction on the end gas temperature should be accounted for. These influences, clearly, cannot be predicted from the thermodynamic two-zones combustion model alone. Accordingly, a modified procedure was employed to consider the effects of the thermal contribution of the end gas reactions. At each time interval, the reaction rates of the end gas were calculated at the predicted T_{ub} and P from the two-zones model. Then, the resulting temperature change dT'_{ub} of the end gas zone due to these reactions over the short time interval was evaluated at constant cylinder pressure. If the resulting calculated temperature change dT'_{ub} is detectably larger than the

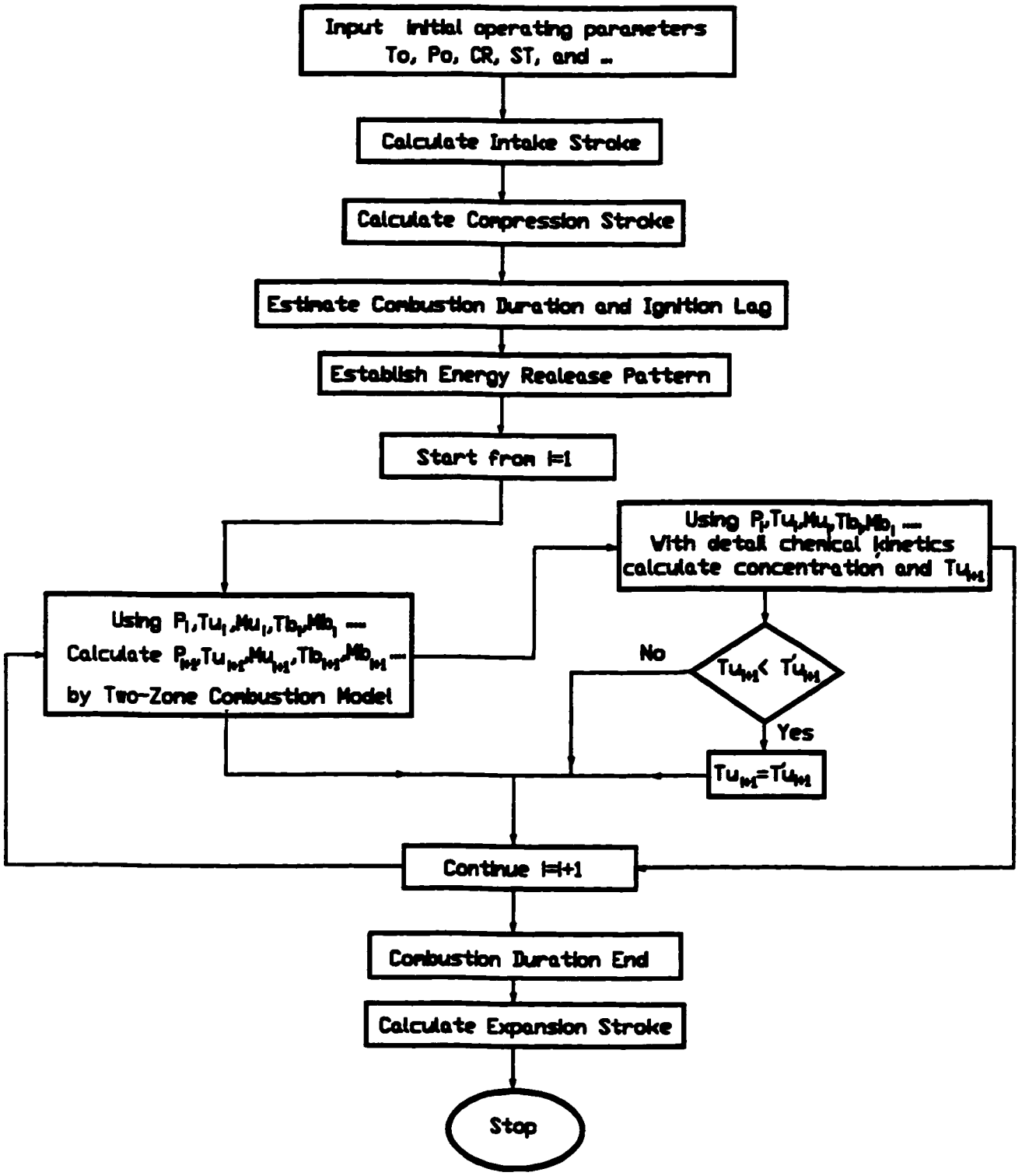

Figure 3.14: Flow-Chart of Two-Zone Knock modeling.

temperature change dT_{ub}, due to only flame propagation, then it was used as the new dT_{ub} for the next interval of considering the chemical reaction rate instead of the value derived from the two-zones combustion progression model. The procedure followed in the knock modeling is shown schematically in Figure 3.14.

Figure 3.15 compares the variations of the calculated unburned gas mean cylinder charge temperature with crank angle for methane operation based on the normal flame propagation model and the reactive end gas model for a typical knocking operating condition. Since the combustion process in the engine involves a significant end gas reactions activity, T_{ub} increases quickly, which speeds up the preignition reactions and causes advanced autoignition with greater intensity. The effect of the end gas reaction on the unburned zone temperature is made through the addition of the temperature rise due to end gas reaction to the normal unburned zone temperature obtained from the two zone combustion model. This modified unburned zone temperature is used to estimate the end gas chemical reactivity. If operating conditions were far from those producing knock, the changes in the T_{ub} due to reaction activity were negligible and the unburned zone temperature obtained from the modified model, including the effect of the chemical reaction, were the same as the two-zone progression model.

The model described has been shown to be capable of being used to predict engine performance parameters such as the temporal variations in cylinder pressure and the two zone temperatures for different speed, intake temperature, intake pressure and spark timing, as well as the effects of changes in some design parameters such as bore diameter and compression ratio [126, 13]. The model appears to be capable also of predicting satisfactorily the onset of autoignition which is responsible for

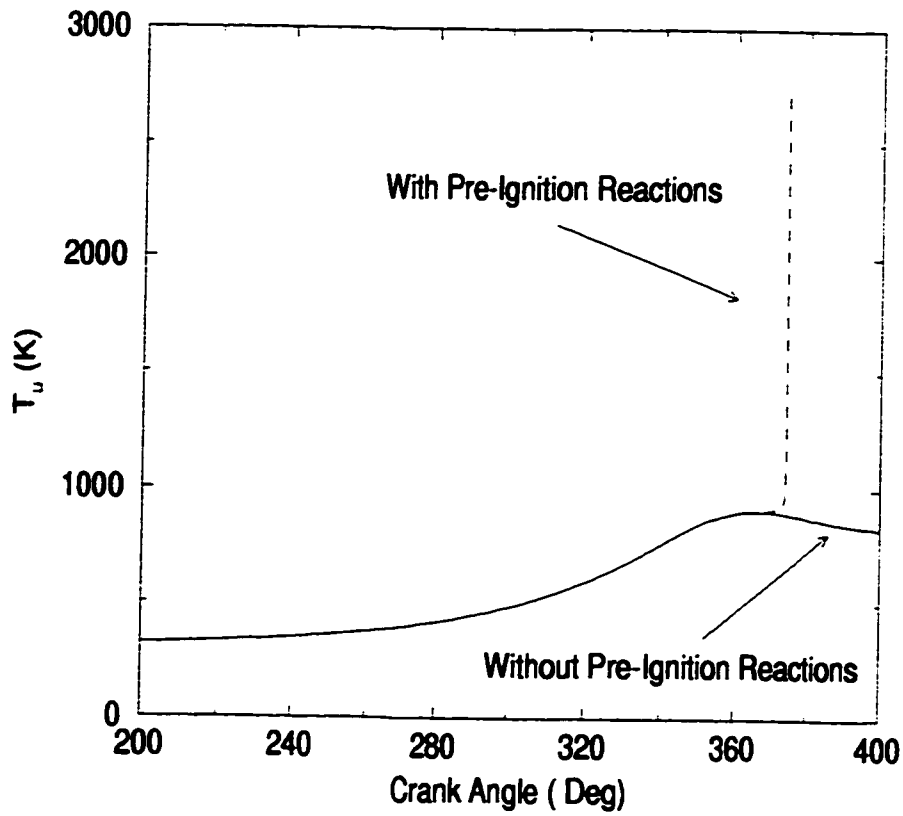

Figure 3.15: Variations of the Calculated Unburned Temperature Versus Crank Angle for Methane Operation at 900 rev./min., $CR = 16$, $\phi = 0.88$, $\theta_{st} = 10$ BTC and $T_o = 311$ K at Experimentally Knocking State for a CFR Engine.

engine knock. An important feature of the approach followed is that the model can be used without requiring direct cylinder pressure-time data beforehand, correlations for the level of turbulence of the charge nor for direct modeling of flame propagation.

The knock criterion of Equation 3.58 developed can be used to test for the onset of knock and to represent effectively engine knock intensity in gas fueled spark ignition engines. Since the spark timing is set so that most combustion takes place around top dead centre to produce the largest power output from the engine, V_o/V_t

is approximately equal to $(CR-1)$. Hence, Equation 3.58 may be simplified as:

$$K = (\frac{h_{st} - h_t}{h_o})\frac{m_u}{m_o}(CR-1) \tag{3.63}$$

Figures 3.16 and 3.17 show two typical variations with time of end-gas relative energy release, dimensionless mass and knock criterion K for a knock free and a borderline knock operation. At the beginning of the combustion process in the

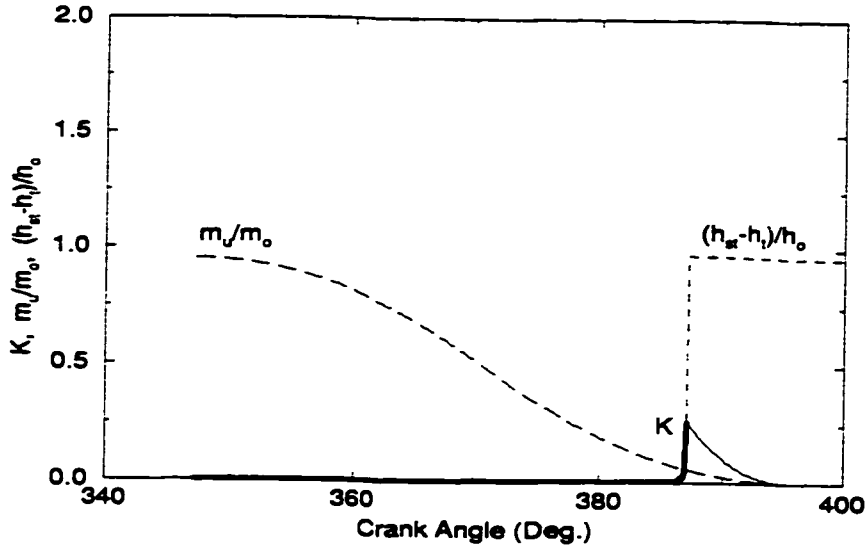

Figure 3.16: Typical Variations of K, m_u/m_o and $(h_{st} - h_t)/h_o$ with Crank Angle for an Effectively Knock Free Operation with Methane at 900 rev./min., $CR = 11$, $\theta_{st} = 18$ BTC, $\phi = 1.0$, $P_o = 87$ kPa, $T_o = 308$ K. The Thick Line Shows the Variations of K Before Autoignition of the End-Gas.

engine, since the reaction rate of the end gas is very slow, K values tend to be small. As the combustion process progresses, the end-gas temperature and pressure are increased, causing an increase in the reactivity of the end gas and therefore end gas energy release due to autoignition. On the other hand, the consumption of the charge by flame propagation decreases the ratio of m_u/m_o according to the mass burning

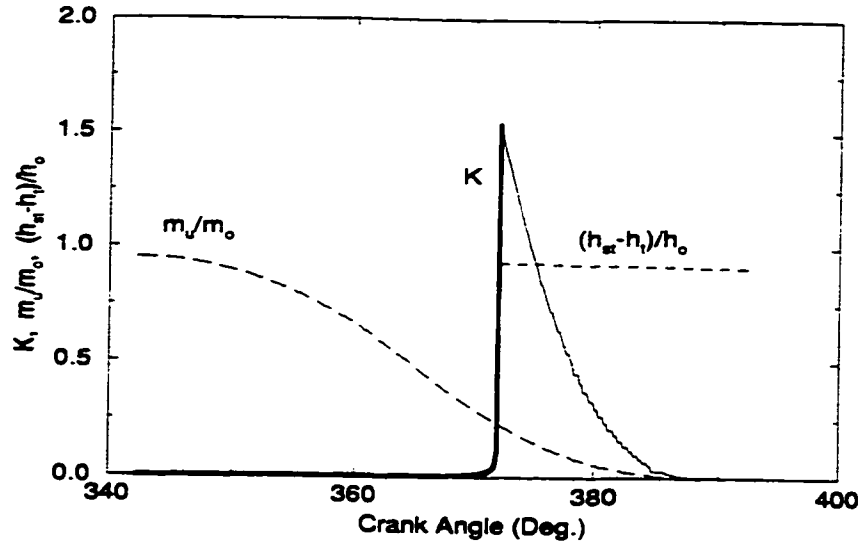

Figure 3.17: Typical Variations of K, m_u/m_o and $(h_{st} - h_t)/h_o$ with Crank Angle for Borderline Knock Operation with Methane at 900 rev./min., $CR = 11$, $\theta_{st} = 23$ BTC, $\phi = 1.0$, $P_o = 87$ kPa, $T_o = 308$ K. The Thick Line Shows the Variations of K Before Autoignition of the End-Gas.

rate function of Equation 3.52. As a result, the K value increases to a maximum and then drops to zero as the end gas is consumed by the flame propagation. A rapid rise in the value of K is associated with the onset of autoignition in the mixture. The maximum value of K depends on the amount of self reacted energy released, which is a function of the size of the end gas at the time of autoignition. If autoignition takes place at virtually the end of the combustion duration, the amount of energy released will be too small and cannot produce a detectable knock. But, if under more severe operating conditions a large portion of the charge participated in the autoignition well ahead of flame arrival, a detectable knock can be observed (see Figures 3.16 and 3.17).

Through comparison with experimental data, it was found that whenever the

value of the knock criterion exceeded a certain threshold value, then the operating conditions will be associated with a knocking behaviour. The bigger the difference, the greater is the intensity of knock, as shown typically in Figure 3.18. For knock free operation, the value of this criterion remains throughout below the threshold value. It appears to work well enough to establish whether knock is to be encountered and

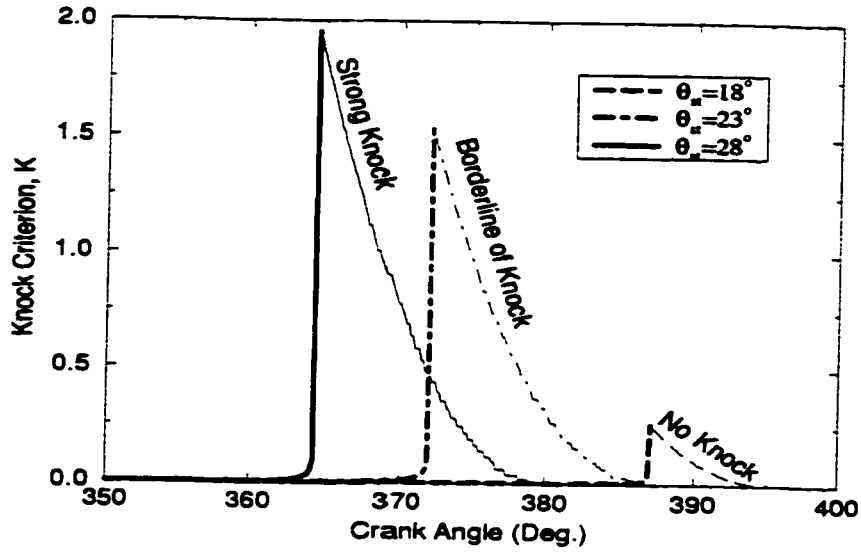

Figure 3.18: Variations of the Knock Criterion K with Crank Angle for Methane Operation at 900 rev./min., $CR = 11$, $\phi = 1.0$, $T_o = 308$ K, and $P_o = 87$ kPa at Three Experimentally Conditions Showing no Knock, Borderline Knock and Strong Knock Operations. The Thick Lines Indicate the Variations Before Autoignition of the End-Gas.

its relative intensity for any set of operating conditions.

The model was applied to some operating conditions (that were established experimentally to produce light knock in a CFR engine in our lab) to investigate the threshold value for knock criterion at borderline knock. The variations of K values with crank angle for some of these typical examples, for methane-hydrogen operation at 900 rev./min., are shown in Figure 3.19. The maximum values of the

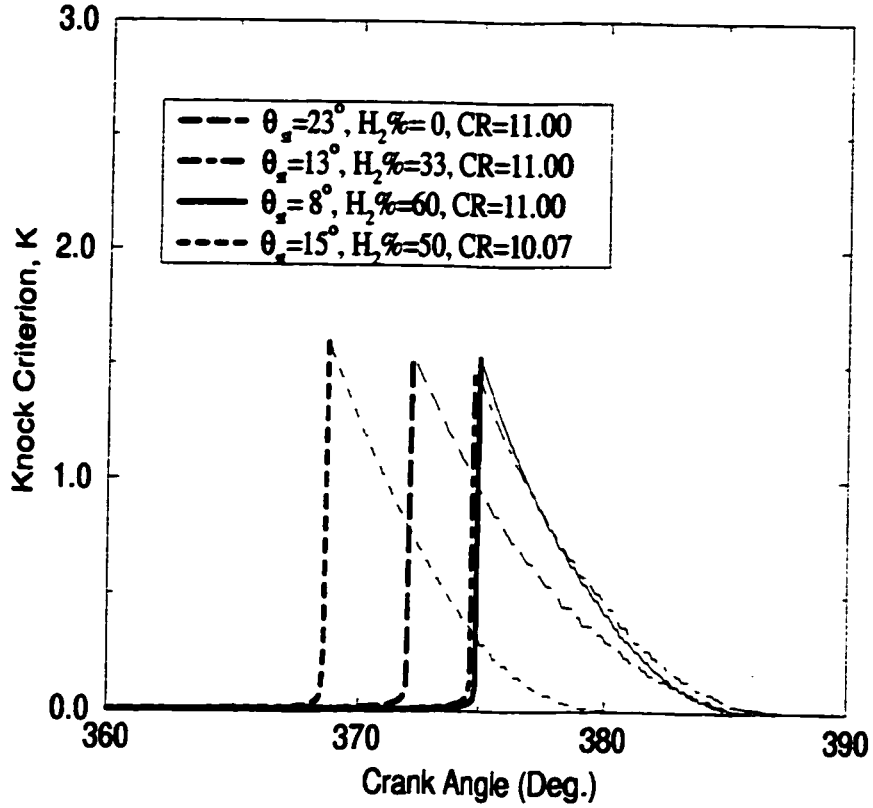

Figure 3.19: Variations of the Calculated K with Crank Angle for Some Operating Conditions Associated with Knock Limit Operations in a CFR Engine Using Methane-Hydrogen Mixtures at 900 rev./min., $\phi = 1.0$, $P_o = 87$ kPa, $T_o = 305$ K. The Thick Lines Show the Variations of K Before Autoignition of the End-Gas.

knock criterion was found to be approximately 1.50 for these borderline knock operations [126, 13]. These typical examples and other similar results show that the operating condition for the knock limit may be determined theoretically by assuming a value of 1.5 for maximum knock criterion at borderline knock operation.

The origin of the size of this critical value is uncertain, but probably represents a slight excess (of 50%) of energy release due to autoignition at knock relative to the normal total energy release that can be released in the swept volume which the

engine can cope with adequately. Furthermore, K represents a pressure ratio of the pressure increase due to preignition reactions in the end gas relative to the mean effective combustion pressure rise over the whole cycle.

Chapter 4

EXPERIMENTAL SETUP

The quasi two-zone model developed in Chapter 3 needs a reliable measurement of the cylinder pressure-time histories in order to validate the correlations developed for the combustion duration, ignition lag, volumetric efficiency and the knock phenomenon. The corresponding crank angle-time records had to be also measured for calculation of the cylinder volume at every point in the cycle. The accuracy of the experimental data is even more vital especially for the modeling of cyclic variations in the spark ignition engine in Chapter 8. The model needs to be applied to a variety of engine operating conditions. Therefore, it was necessary that the effects of variations in key operating parameters such as equivalence ratio, fuel compositions, spark timing, mixture intake temperatures and compression ratio be investigated experimentally.

This chapter describes the experimental set up and the procedure for collecting and analysing the data needed.

4.1 Apparatus

4.1.1 Engine

The well known CFR research engine was used. It is a single cylinder, four stroke, spark ignition engine of continuously variable compression ratio (from 4.46:1 to 16:1) and spark timing (up to 40° before top dead centre). The engine has the following

dimensions as specified for model CFR-48 by the relevant ASTM manual [137]:

- Pancake shape combustion chamber
- Crankshaft Radius = 57.15 mm
- Stroke = 114.3 mm
- Connecting Rod Length = 254.0 mm
- Cylinder Bore = 82.55 mm
- Displacement = 611.73 cm^3
- Shrouded Intake Valve opens at 10° ATDC and closes at 34° ABDC.
- Plain Exhaust Valve opens at 40° BTDC and closes at 15° ATDC.
- Cylinder Water Jacket temperature maintained constant at 373 K.

The engine was coupled to an induction motor dynamometer that maintains a constant engine speed of 900 rev./min. The intake system was modified to allow operation on gaseous fuels and to provide control and metering of the fuel/air ratio. Furthermore, modifications, as will be explained later, were made to accommodate the instrumentation needed for continuous recording of the pressure-crank angle data. Figure 4.1 shows a schematic diagram of the experimental set-up.

The instrumentation available can be categorized into two systems, Engine Instrumentation, and a Data Acquisitions System. The former is intimately associated with the running of the engine while the latter is primarily intended for actual data collection and storage activities.

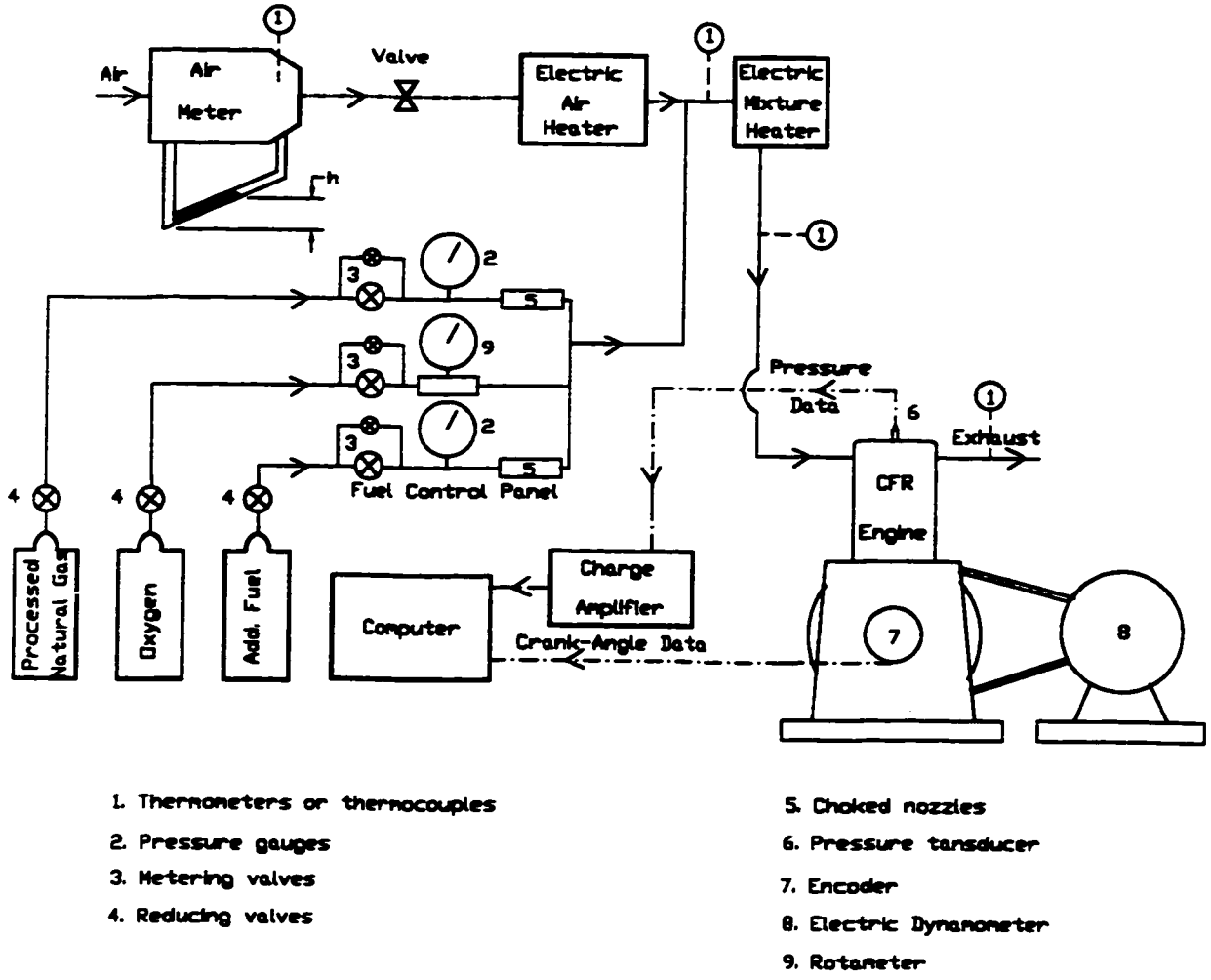

Figure 4.1: Schematic Diagram of Experimental Set-up.

4.1.2 Engine Instrumentation

The engine tested had been modified from the standard ASTM setup to include air and fuel metering systems. The spark timing control system and the mechanisms for varying the compression ratio were part of the engine as supplied by the manufacturer. Spark timing can be varied from -40 to +40 degrees from top dead centre, while the compression ratio can be changed from 4.46:1 to 16:1.

Gaseous Fuels, as shown in Figure 4.1, were drawn from high pressure bottles.

The composition of samples of the processed natural gas and other fuels used during the work appear in Appendix (D). The dissociated products of water were simulated by being made from individually supplied metered gases that were homogeneously mixed with the incoming fuel-air mixture at constant intake ambient temperature and pressure. The gaseous fuels were supplied in different combinations through precalibrated choked metering nozzle systems while the required amount of oxygen was introduced through a calibrated rotameter. The air mass flow rate was measured by a laminar viscous flow meter. The system provides the capability to measure and control the fuel composition accurately for a wide range of Air/Fuel ratios. The details of air and fuel metering systems and the procedure for their calibration plus the final calibration graphs are discussed in Appendix (C).

4.1.3 Data Acquisition System

A water cooled piezoelectric *Kistler* pressure transducer (model 609 with sensitivity of $41.334 \mu C/kPa$) was mounted flush with the cylinder surface through an opening in the top of the pancake shaped cylinder head for pressure measurement such that the axis of the transducer was parallel to the cylinder axis. The transducer was connected to a *Kistler* charge amplifier and the resultant signal was routed to the data acquisition system computer for sampling.

The other instrumentation system is the crank angle and real time measurement system which is an electric encoder fitted to the end of the crank shaft that can recognize 1000 points in each 360°, with the first one at TDC. The timing system and the corresponding time data (2000 points for each thermodynamic cycle) were then written to a binary file on the hard disk of the computer.

4.1.4 Main Computer for Data Processing

The instrumentation systems listed above provide timing and pressure data in binary form for a chosen number of cycles. These data had to be processed and converted to decimal values before further processing could be undertaken. This operation was carried out on the same computer system on which the program for the diagnostic model was run. The mainframe computer used was IBM 486 and a Sun Computer System. Both supported a graphics package that was extensively used in all stages of data manipulation and processing. A detailed description of the use of the graphics capabilities of the system will be included in the section on experimental procedure. Final plots were produced on a laser printer attached to a Sun Computer System.

4.2 Experimental Procedure

The experimental scheme was designed to obtain data such that the effects of changes to the main operational parameters of the engine could be examined with minor modification and adjustment to the engine setup.

Generally, a set of operating conditions was chosen and the data from the engine collected and stored for later processing. The following are the different parameters that were varied and the values chosen for them.

Most of the data were collected with spark timings of 5, 10, 15, 20 and 30 degrees of crank angle before top dead centre except when either misfiring or knock occurred.

Three values of compression ratio were used , namely 8.5:1, 10:1 and 11:1. There were also cases when it was not possible to use all these values of compression ratios due to the onset of knock. Some tests for compression ratios of up to 16:1 were also

carried out.

The equivalence ratio could be varied very widely but the range employed in testing varied from 0.65 to 1.20 approximately with all other operating conditions kept constant. This range was repeated for each change in spark timing and compression ratio for a constant intake mixture temperature. Data were also collected for conditions when it was possible to run the engine at a leaner equivalence ratio when no misfire could be detected. The calculation of the equivalence ratio was based on the volumetric composition of the fuels as described in Appendix (D).

The effects of the addition of hydrogen, propane or ethane to the mixtures of methane and air were investigated. These additives were added to the processed natural gas from 0% to 100% by volume of the resulting fuel mixture. The intake mixture temperature was maintained constant at around 21° C for all the experiments carried out.

4.3 Data Collection and Processing Procedure

A three hour warming up period was provided for the stabilization of the charge amplifier of the pressure transducer. The data acquisition system would then be prepared for data collection by feeding in the necessary program. The engine was then started and allowed to run until the water coolant jacket reached the steady state temperature of 373 K. After all the operating conditions were established, the data collection would begin. The pressure signal was frequently affected by the excessive magnetic field generated by the spark as well as the spark system capacitor recharged cycle. This could not be avoided, and sometimes it resulted in very steep pressure

trace spikes appearing at spark time. It was decided to deal with this problem at the data processing stage.

When operating with fuel mixtures a computer program was used to determine the settings on the additive control panel such that the percentage of additive with respect to the fuel was kept constant even as the fuel-air ratio was varied. The supply of the additional fuel such as hydrogen, propane or ethane via choked nozzles would not affect the mass flow of another fuel being supplied such as methane but it affected obviously the mass flow rate of air intake to the cylinder.

Generally, each run consisted of collecting data for 20 consecutive cycles at a sampling rate of 66.7 microseconds (which corresponds to 0.36° at the 900 rev./min. used). However, for the modeling of the cyclic variation process each run consisted of collecting data for 100 consecutive cycles. This produced 2000 pressure-time sample points per thermodynamic cycle. At the same time the crank angle was sampled from the encoder to produce a pressure-crank angle data on a computer file. The processing of the data file was carried out by a computer program which performed the following operations.

4.3.1 Conversion

All of the pressure data were converted to the decimal system from the binary numbers provided by the A/D system. The range as well as the gain factor settings of the A/D were taken into consideration while doing this conversion.

4.3.2 Establishing a Reference Point

The voltages generated by the pressure transducer were not indicative of the associated absolute values of pressure. It was therefore important that a fixed absolute value of pressure was associated with one point of the cycle such that a correlation between voltage and pressure could be established for each cycle. The absolute value of the cylinder pressure at the first sampled point of each cycle (TDC of the intake stroke) was assumed to have a value similar to the local atmospheric value. This assumption allowed the processing of the data to yield a pressure-time record for each cycle.

4.3.3 Data Examination

The data collected was first examined to check for any irregularities caused by the magnetic fields generated when the spark was passed. The affected points were smoothed by the program and a corrected data file would be recorded.

4.3.4 Correction for Spark-Inducted "Spikes"

When the spark-inducted "spikes" occurred, they typically involved a single sample point that was affected by the spark passage to register a high value of voltage. The magnitude of spikes varied between prominent values where the rate of pressure rise was thousands of times higher than expected to that where it was twice the expected rate. They were all characterized by a rise then drop in pressure value. The computer graphics capabilities were utilized to plot each cycle in a run separately for visual inspection, as well as to calculate and examine the rate of change of pressure around spark time. Corrections were made by adjusting the value of the affected sample

point such that it would lie on the straight line through the two points on either side of this spike.

4.3.5 Average Cycle Data Calculation

Arithmetic averaging of the pressure-time data of 20 and/or 100 cycles for each run was carried out after all of the above corrections to the recorded data had been made. This record contained 2000 points of associated average cylinder pressure and corresponding crank angle of that run. The data resulting from the above treatment was used by the program embodying the model for calculating power output, combustion duration, ignition lag, cyclic variations of different parameters, etc. without further modification.

4.4 Determination of Combustion Duration and Ignition Lag

The thermodynamic processes during the compression and expansion strokes may be approximated by a polytropic process. The polytropic index, n_θ, changes significantly during flame propagation and may be considered to be approximately constant during compression of the fresh charge and expansion of the products. Hence, the evaluation of the ignition lag and combustion duration for spark ignition engine, as was developed by Al-Alousi et. al.[30, 135], is simplified merely by evaluating the instantaneous polytropic index n_θ for both compression and expansion for the observed values of pressure and the corresponding cylinder volume, i.e.:

$$PV^{n_\theta} = Constant \tag{4.1}$$

Differentiating and re-arranging for polytropic index n_θ:

$$n_\theta P V^{n_\theta - 1} dV + V^{n_\theta} dP = 0 \Rightarrow n_\theta = -\frac{V dP}{P dV} \tag{4.2}$$

where V and P are the instantaneous cylinder volume and pressure. For discrete pressure and volume readings, Equation 4.2 can be reduced to:

$$n_\theta = -\frac{V_m(P_j - P_{j-1})}{P_m(V_j - V_{j-1})} \tag{4.3}$$

where

$$\begin{aligned} V_m &= \frac{V_j - V_{j-1}}{2} \\ P_m &= \frac{P_j - P_{j-1}}{2} \end{aligned} \tag{4.4}$$

$j-1$ and j represent the initial and final conditions of each sampling time.

For any operating condition, the crank angle at which the spark takes place is fixed at a constant value of θ_{st}. Usually the spark causes only a small kink in the apparent value of n_θ. Moreover, this crank angle, θ_{st}, indicates the beginning of the ignition lag, while its end ($\theta_{e.i.}$) is associated with a rapid increase in the value of the index n_θ (see Figure 4.2). $\theta_{e.i.}$ also indicates at the same time the start of the significant energy release and the beginning of combustion, i.e.:

$$Ignition\ Lag,\ \Delta\theta_{ig}, = \theta_{e.i.} - \theta_{st} \tag{4.5}$$

The end of energy release by combustion will be associated with the first occasion

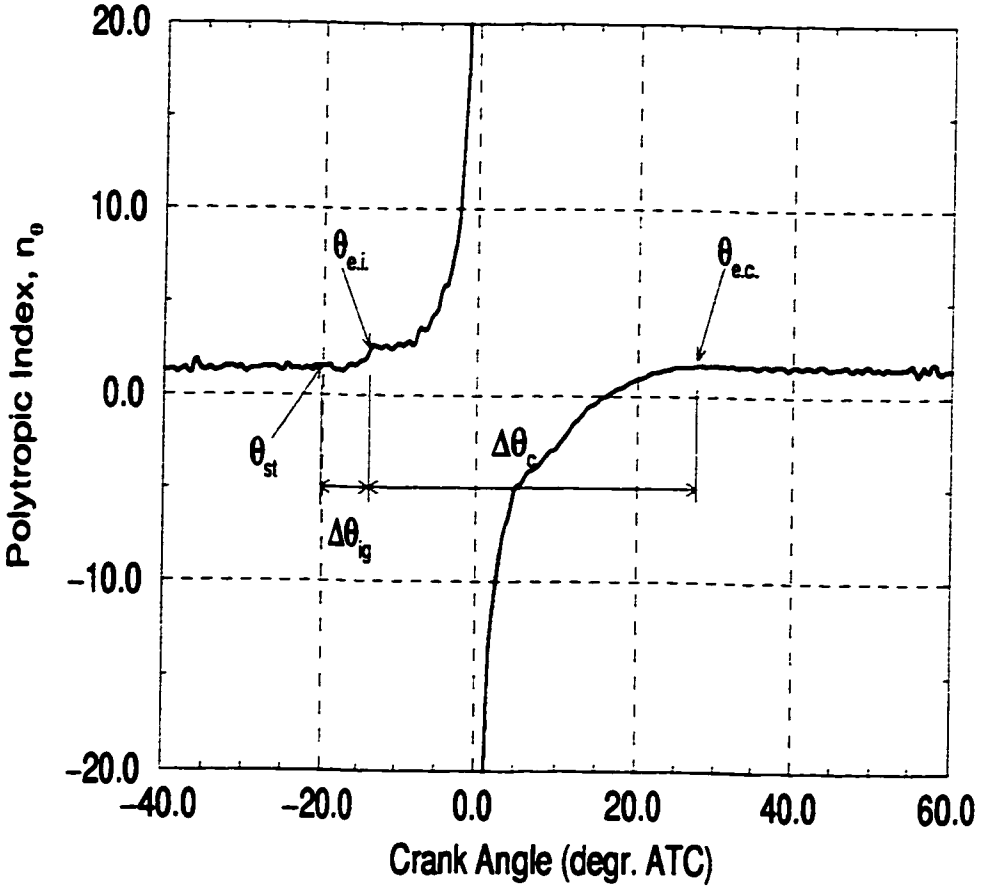

Figure 4.2: The Typical Variation of Polytropic Index with Crank Angle.

of the effective polytropic index n_θ approaching a relative constant value that of polytropic expansion index involving the products of combustion (see Figure 4.2). This crank angle will be called $\theta_{e.c.}$, i.e.:

$$\textit{Combustion Duration}, \quad \Delta\theta_c, = \theta_{e.c.} - \theta_{e.i} \tag{4.6}$$

Chapter 5

OPERATIONAL LIMITS IN A SPARK IGNITION ENGINE

5.1 Introduction

The operation of combustion devices on gaseous fuels especially when using lean mixtures is attractive and economically worthwhile since in principle it can offer improved efficiency, reduced exhaust emissions and longer operational life. However, lean operation is associated with significant reductions in the reaction rates leading to low burning and energy release rates. Normally, this trend is made more serious with the low overall temperatures associated with the combustion of lean mixtures. Moreover, very lean mixture operation can produce increased emissions of unburned hydrocarbons and cyclic variations that lead to erratic combustion and performance. Accordingly, there are distinct operational mixture limits beyond which acceptable engine performance cannot be maintained. These limits vary in value depending on numerous factors that would include the type of fuel used and various operational and design parameters.

Some efforts have been made in the past to examine the operational limits of lean burn engines in general and ignition failure in particular [138, 139, 135, 130, 129]. Nevertheless, there is still a need to investigate further not only the operational and combustion limits in homogeneously charged spark ignition engines, but also whether

simple procedures can be developed for their prediction and how lean operation can be enhanced further in general. With the emphasis on the reduction of exhaust emissions and superior fuel economy, the operational limits of rich mixtures in contrast to the lean limits are of little practical value.

Accordingly, the present contribution as an example of the possible extension of application of the predictive model described in Chapter 3, examines the operational limits of a spark ignition engine fueled with the gaseous fuel methane , propane and hydrogen for a range of conditions. The predicted results then are compared with the corresponding experimental values obtained on the single cylinder CFR engine.

5.2 The Approach

In a spark ignition engine, the time taken for the initiation of a flame kernel and for a detectable amount of exothermic energy release following the passage of an electric spark increases rapidly as the mixture is made leaner or richer than stoichiometric [30, 31]. Moreover, the combustion period, associated with the time needed for subsequent turbulent flame propagation throughout the whole charge increases also rapidly as the mixture is leaned or enriched. The associated cyclic variations in the values of these periods also increase to an extent that in some cycles some combustion may be still proceeding at the time of exhaust valve opening or the flame propagation is interrupted due to quenching by expansion before the charge is fully consumed. Further leaning of the mixture (or enriching it for the rich limit) would lead to the flame failing to propagate and/or the flame kernel to establish itself bringing eventually regular engine operation to a halt. The mixture that would just bring

about such a halt to regular combustion is defined to be the lean or rich operational limit of the engine. This was sometimes described somewhat loosely as the lean/rich ignition limit under the specific conditions.

These operational limits were established experimentally simply when any gradual leaning (or enriching) of the mixture brought about a sudden loss of all power, combined with a rapid and abrupt drop in the exhaust gas temperature. A number of different approaches can be employed to describe operational limits. For example, they can be based on the equivalence ratio at which first engine misfire occurs [140], selected frequency of total misfires [100], selected frequency of cylinder peak pressure [141], specific amounts of hydrocarbon or carbon monoxide in the exhaust gases, number of audible misfires counted over a period of time, variation of the area under the measured cylinder P - V diagram [106] and variations in the mean effective pressure [88]. It can be seen these definitions vary substantially and their choice was prompted often largely by the specific needs of the investigation.

For example, in spark ignition engine experiments involving typically homogeneous mixtures of methane or propane and air and a variable compression ratio CFR engine running at a constant speed, and using spark timing that depends on the compression ratio (e.g. as shown in Figure 5.3), both the lean and rich operational limits associated with combustion failure and power loss, were established [43]. The lean limit observed then, unlike the rich limit, was affected only little by changes in the compression ratios (6.5:1 to 16:1). However, an increase in the intake charge temperature from 311 K to 429 K produced a marked extension of the lean limit. The effect on the lean ignition limit of higher compression temperatures, due to the greater compression ratio, was probably offset by other operational factors. For

example, smaller spark advances are normally associated with higher compression ratios. Moreover, other factors may include increased heat transfer, lower temperatures at the start of compression resulting from smaller quantities of trapped hot residual gases mixing with the fresh inducted charge and the associated changes in the level and intensity of turbulent flow of the mixture at the time of ignition.

It would be useful to correlate the roles of various operating parameters such as intake temperature, compression ratio, spark timing , engine speed and others on the observed lean operational limits. For example, it is important to find out whether some of the concepts that have been developed for the flammability limits under quiescent conditions may be applicable with modification to the observed engine limits, particularly in relation to changes in pressure which has no significant effect on the lean flammability limits, but considerable effect on the corresponding rich limits [142].

It has been shown that the established lean flammability limits of quiescent homogeneous common gaseous fuels and air at various initial mixture temperatures appear to correspond to the mixtures that produce on combustion approximately the same adiabatic flame temperature [143, 144]. However, Karim and Wierzba [130] found that the observed operational lean limit mixtures in the engine at constant compression ratio (from 6.5:1 to 16:1) but variable intake temperature (311 to 429 K), whether for methane or propane operation, do not show such a tendency. Instead these limiting mixtures tend to be associated with variable and higher values of calculated flame temperature. It indicates that the operational limit corresponds to a richer/leaner limit than the recognized flammability limit for the same temperature and pressure. For any compression ratio by increasing the intake temperature,

the observed lean operational limit for the engine would correspond to operational mixtures having higher calculated flame temperatures. This trend is most likely a reflection of the consequences of increased heat transfer to the cylinder walls associated with higher temperatures and the changes in the turbulence intensity when higher compression ratios and/or intake temperatures are employed. Similar observations were also noted for the observed rich operational limit in the engine where this temperature concept does not hold [130].

The operational limits of an engine, hence, depend upon a number of factors that influence not only the flame initiation and propagation processes but also the heat transfer to cylinder wall and/or mechanical losses if any. Nevertheless, the operational limits in an engine can be viewed to occur when the rate of energy release due to the chemical reactions within the flame front cannot keep pace with the demands for transporting sufficient energy to adjoining layers of the fresh mixtures, overcoming external thermal losses to the surrounding cylinder walls and mechanical and motoring losses due to friction etc. Therefore, to predict the operational limits in an engine it can be considered to be associated with a certain threshold of energy released rate. Once this threshold rate for an engine is evaluated, then the operational limits of the engine may be calculated for other operating conditions. Moreover, our experimental results in the variable compression ratio CFR engine operating at constant speed showed that such threshold value of the energy released rate at the operational limits corresponded to a certain value of the indicated power output of the engine. This arises from the fact that mechanical losses remain relatively unchanged at constant speed.

Therefore, the indicated power output of the engine is considered to represent this

critical threshold value which can be calculated by the model described in Chapter 3 for a known experimental operational limit of the engine. This value is then assumed to remain essentially the same for other operating conditions of the engine and fuels at the same speed.

5.2.1 Results and Discussion

The lean and rich operational limits of an engine are calculated for different operating conditions by means of the approach described in the previous section. These calculated values were compared with the corresponding experimental values obtained by others as well as our own experimental results. A typical set of our experimental results from a variable compression ratio CFR engine at constant speed, is shown in Figure 5.1, where the operational limit was defined as the condition associated with the first detection of a misfire at various compression ratios. The corresponding calculated values are also shown as thick lines. The threshold values of the indicated power output for the lean and rich operational limits were calculated for the referenced experimental lean and rich limits at equivalence ratios of 0.62 and 1.28 respectively, at a compression ratio of 8.5:1, spark timing of 20 BTC, initial mixture temperature of 294 K and an engine speed of 900 rev./min. The agreement between the experimental and calculated values of these operational limits was very good and well within the experimental uncertainties.

This approach, as mentioned earlier, was also tested against some other experimental data available in the open literature. For example, the predicted lean and rich operational limits for a variable compression ratio CFR engine fueled with methane were shown in Figure 5.2 along with the corresponding experimental data using a

varying spark timing with compression ratio as used in the Motor Method [43]. For these cases, the threshold value of the indicated power output for the operational limits with methane was calculated for the referenced experimental lean and rich limits of equivalence ratios of 0.62 and 1.36 respectively, at a compression ratio of 6:1, spark timing of 21.5 degrees BTC and initial charge temperature of 311 K [43]. The agreement of the predicted lean operational limits for various compression ratios with their experimental counterparts appears to be very good and within 3.1 percent for the range of compression ratio considered. The corresponding deviation for the rich limit is less than 3.4 percent. The operational limits due to the incidence of knock at higher compression ratios are also shown in the figure. The border line of knock was calculated according to the procedure described in the previous chapter.

In Figure 5.3, the lean operational limit of the CFR engine while operating on methane, propane and hydrogen are shown for a range of compression ratios at variable spark timing. It can be seen that these limits vary widely among the three fuels but change only little over the whole compression range considered. The decrease in spark advance employed as the compression ratio is increased, is an important factor that tended to offset the effects of other factors such as increased temperature at the time of spark passage, changes in turbulence level, a reduced mass of trapped residual gases, increased heat transfer and others associated with increasing the compression ratio. The slight reduction in the lean limit observed with propane is probably a reflection of the relatively higher reactivity of propane and air mixtures during compression. As shown in the figure, the agreement between the predicted lean operational limits and the corresponding experimental data [129] for methane and propane was very good. However, the predicted lean operational

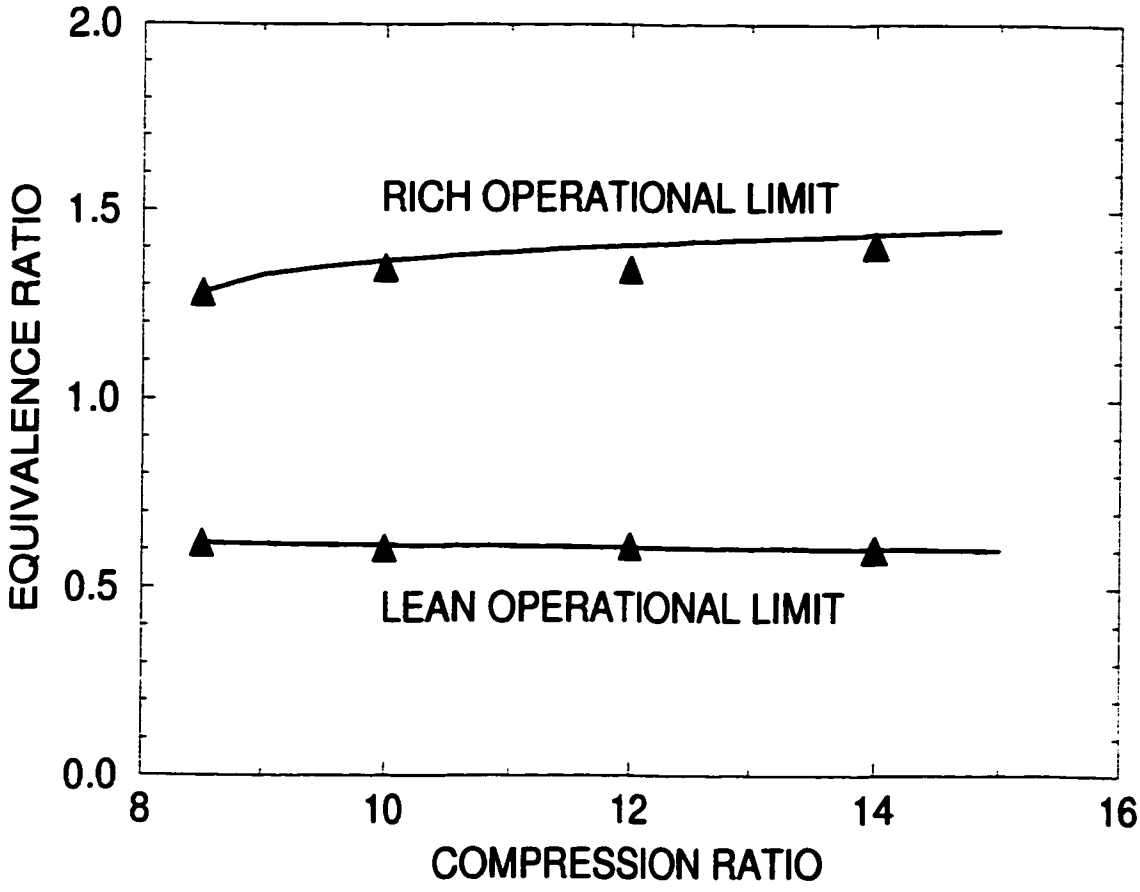

Figure 5.1: The Predicted and Experimental Operational Limits of a CFR Engine Fueled with Methane for Various Compression Ratios at Spark Timing of 20 BTC, Intake Charge Temperature of 294 K, Engine Speed of 900 rev./min. and Atmospheric Pressure.

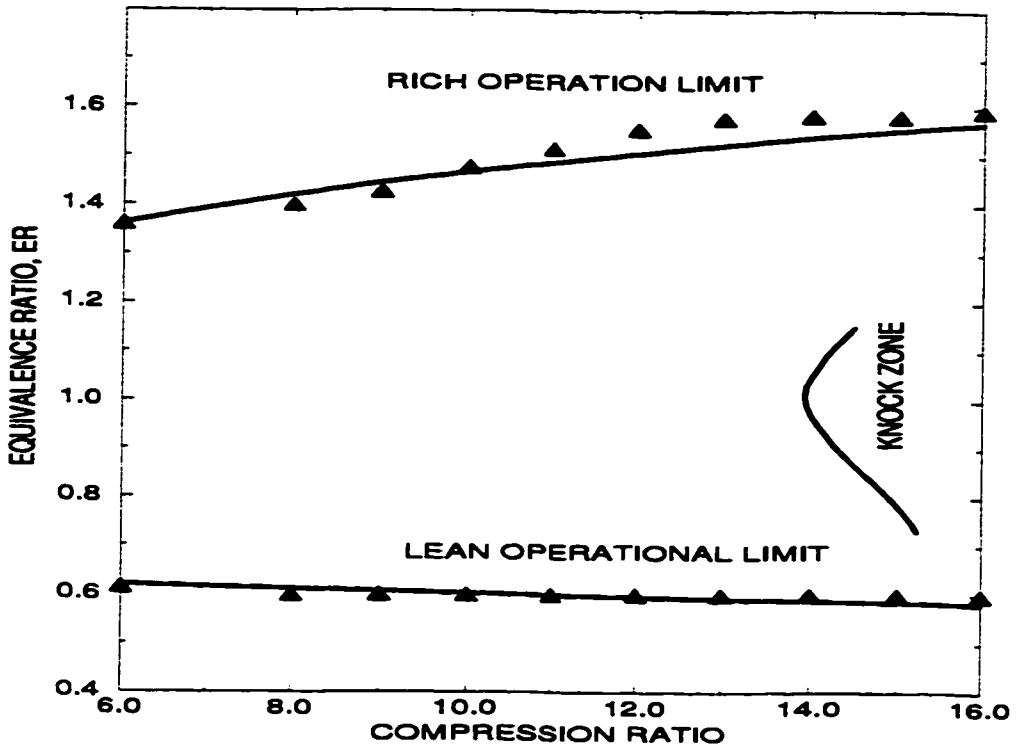

Figure 5.2: The Predicted and Experimental Operational Limits of a CFR Engine Fueled with Methane for Different Compression Ratios at Atmospheric Pressure and Intake Charge Temperature of 311 K at 900 rev./min.

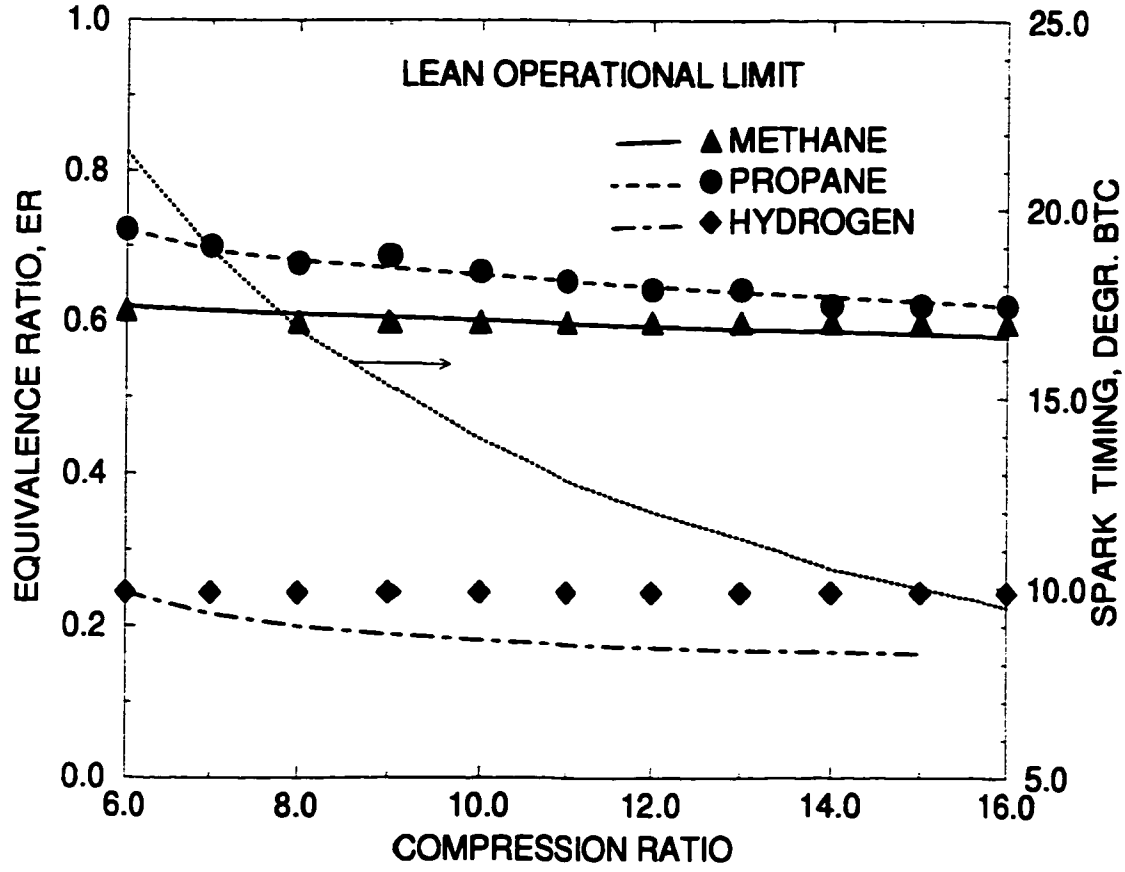

Figure 5.3: The Variations of Predicted and Experimental Values of Lean Operational Limits with Compression Ratio for Different Gaseous Fuels at Atmospheric Pressure and Intake Temperature of 311 K at 900 rev./min.

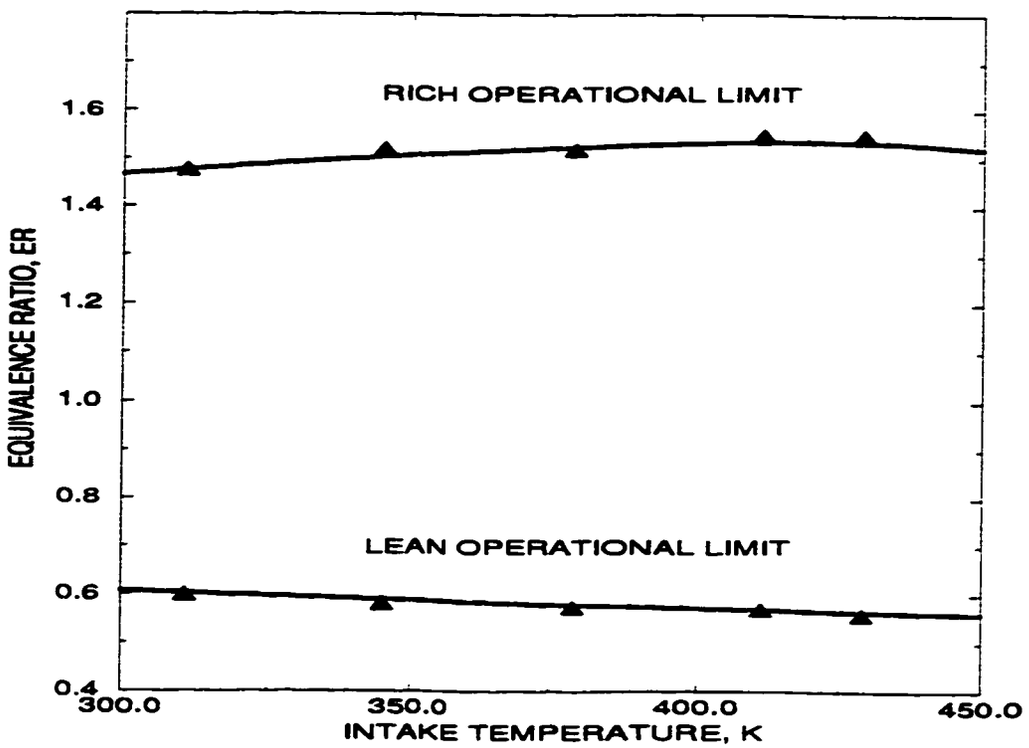

Figure 5.4: The Variation of Experimental and Predicted Operational Limits in a CFR Engine with Changes in Mixture Temperature for Fuel Methane at a Compression Ratio of 10:1, Spark Timing of 13.9 degrees. BTC and Engine Speed of 900 rev/min.

limits for hydrogen were wider than the corresponding experimental values [129].

The operational limits of the CFR engine with methane for different initial temperatures at a compression ratio of 10:1, spark timing of 13.9 degrees BTC and atmospheric intake pressure, are presented in Figure 5.4. It is shown that the predicted lean operational limits excellently match the corresponding experimental values [129, 43] with a deviation of under 1 percent. Similarly, the predicted rich operational limits were also in good agreement with their experimental counterparts to within 1.2 percent. Therefore, the proposed prediction method for the operational limits of a spark ignition engine using the model developed appears to work satisfactorily for the engine and operating condition considered in this contribution. However, it is evident that the accuracy of the information used to calculate the threshold value of energy release of the engine is important and heavily affects the success of the prediction of the lean and rich operational limits of the engine.

5.3 An Alternative Approach

In principle, an approximate simplified approach, similar to the one described in Section 3.2.2 to estimate the combustion duration, can be used to predict the operational limits of a spark ignition engine when much of the experimental information is absent and an approximate value of the limit is needed to be made. Moreover, the combustion process at these limiting conditions tends to be essentially highly fluctuating with considerably large cyclic variations.

For example, as the fuel mixture becomes leaner or richer than stoichiometric, flame propagation rates would become increasingly slow, producing very long com-

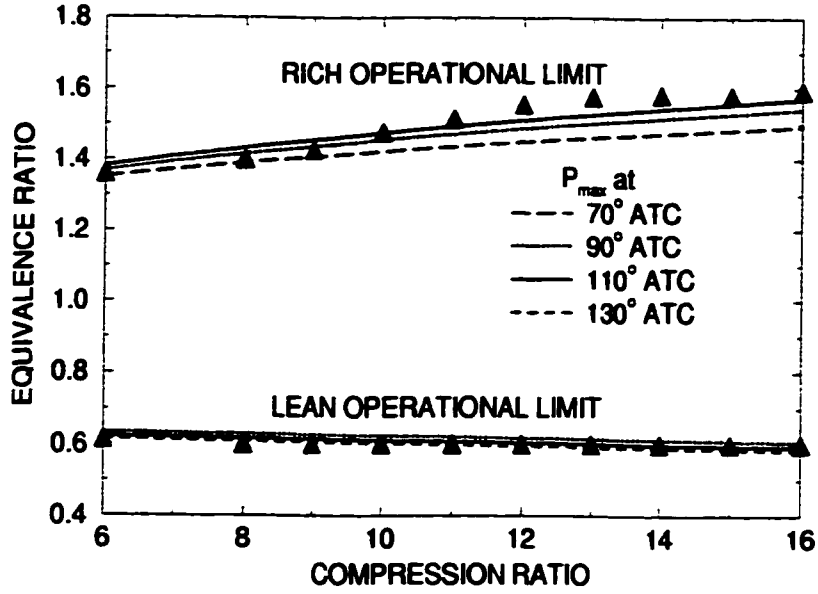

Figure 5.5: The Calculated Operational Limits (Using the Alternative Approach) in a CFR Engine Fueled with Methane for Different Compression Ratios at Atmospheric Pressure and Intake Charge Temperature of 311 K at 900 rev./min. The Corresponding Experimental Data are also Shown.

bustion durations at the operational limits. It would be expected for these limiting fuel mixtures that the value of maximum cylinder pressure would be small as well as the crank angle of its occurrence would shift considerably away from TDC down the expansion stroke. On this basis, the crank angle for maximum cylinder pressure is the location where the pressure rise due to the combustion of the fuel and heat transfer is equal to that due to cylinder volume changes. A number of estimations of the operational limits using the model described in Chapter 3 were made for operating conditions similar to those encountered in the CFR engine where corresponding experimental data are available.

Some of the typical results of such an approximate approach are presented in Figure 5.5 for the rich and lean operational limits for the variable compression ratio

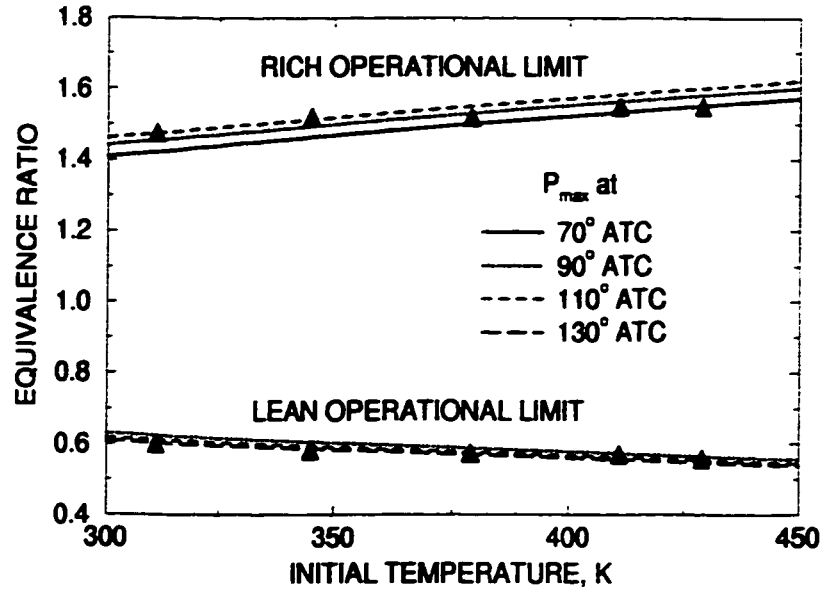

Figure 5.6: The Variation of Calculated Operational Limits (Using the Alternative Approach) in a CFR Engine Fueled with Methane for Different Initial Mixture Temperatures at a Compression Ratio of 10:1, Spark Timing of 13.9 degrees. BTC and 900 rev./min. The Corresponding Experimental Values are Shown.

CFR engine fueled with methane using a variable spark timing with compression ratio, as used in the Motor Method [43] for a number of cases involving different assumed values of crank angle for the achievement of a maximum in cylinder pressure. Similarly, Figure 5.6 shows the operational limits for different initial temperatures at compression ratio of 10:1 and spark timing of 13.9 degrees BTC. The corresponding experimental values are also shown.

It can be seen in these figures that the prediction for the lean operational limit made by assuming that P_{max} occurs at the crank angle 110 degrees ATC produced good agreement with experimental results for the cases considered. Similarly, the values of the rich operational limits predicted by assuming that P_{max} takes place at around 90 degrees ATC were in good agreement with their corresponding experi-

mental values reflecting somewhat different level of combustion activities at the two types of operational limits. The corresponding evaluated errors then are within 4% and 5% for the lean and rich operational limits, respectively. It may also be seen that the prediction of lean operational limits was relatively less affected by the assumed value of crank angle at the P_{max} in comparison to the rich limit cases.

Chapter 6

THE EFFECTS OF THE PRESENCE OF DILUENTS IN GAS FUELED S. I. ENGINES

6.1 Introduction

The presence of diluents can be encountered with methane in numerous situations in practice. For example, carbon dioxide may be present with methane in natural gases, biogases produced through the fermentation of organic waste materials, in the by-products of gasification and reforming of heavy oil or coal, in waste gases of the petrochemical industry and in landfills, coal beds and sewage gases. The composition of such fuel mixtures, which may also contain the diluents nitrogen and water vapour, can vary very widely depending upon their origin and the mode of their production. Moreover, the increased practice of resorting to some exhaust gas recirculation in methane fueled combustion devices, primarily for emissions control, will result in the fuel utilized in association with some carbon dioxide and other diluents. The presence of these diluents can bring about significant changes to the combustion characteristics of the methane and may undermine its effective utilization in conventional combustion devices. There is a need to understand fully the origin and nature of the limitations of their combustion in air so as to effect ultimately more efficient, reliable and environmentally acceptable utilization.

The present investigation, as another example of the possible extension of applic-

ation of the predictive model described earlier in Chapter 3, accounts for the effects of the presence of the diluents carbon dioxide and nitrogen with methane and its effect on the performance of a methane fueled SI engine over a range of operating conditions. The results of such prediction then are compared with some experimental data obtained on the single cylinder CFR engine.

6.2 Some Thermodynamic Considerations

The presence of a diluent with methane reduces the effective heating value of the fuel mixture with the energy released by the oxidation reactions of the fuel component becomes shared with the diluent. This will result in a net reduction in the flame temperature achieved and the associated flame propagation rate. Therefore, the resulting combustion duration, described earlier, will be longer than for the same conditions with the pure fuel and will depend on the type and extent of diluent used. For example, the energy released by combustion taken by the carbon dioxide component will increase significantly as the temperature is increased since the specific heat of carbon dioxide increases with temperature at a rate much greater than those for nitrogen or air. The carbon dioxide will also tend to undergo increasingly endothermic dissociation reactions that increase rapidly in intensity as high combustion temperatures are approached. These will also tend to modify significantly and somewhat adversely the composition of the final products of combustion. The net effect is the substantial reduction of the flame temperature and the flame propagation rates with the presence of carbon dioxide with the methane [145]. On this basis it would be expected that the effect of the presence of carbon dioxide on the combustion

duration will be more pronounced than with nitrogen addition.

The amount of reduction in flame temperature is especially significant for the near stoichiometric mixtures where the energy release and consequently the resulting temperature is highest [146, 147]. With lean and rich mixtures containing substantial concentrations of diluents, calculated temperatures will be so low that they may not permit flame propagation to proceed even on the application of a significant ignition energy source [31].

High initial mixture temperature will result in high calculated adiabatic flame temperature. It has been shown that the concentration of carbon dioxide in the products of combustion decreases virtually linearly with the increase in initial mixture temperature since dissociation effects increase in their intensity [145, 147]. At relatively low initial preheat mixture temperatures and particularly with high carbon dioxide concentration in the fuel, much of the carbon dioxide remains undissociated to act largely as a diluent.

The reaction rate of mixtures of methane and air under isothermal conditions will be little affected by the presence of diluent [146]. It is the energy released by the reaction and hence the consequent resulting temperature when permitted to change with time, that will be affected and reduced very significantly by the increased presence of the diluent in the mixture. These factors are mainly responsible for bringing about the substantial reduction normally observed in the oxidation rates in combustion processes such as under constant pressure or volume conditions. The slowing down of the overall conversion rate of the fuel and the associated energy release will depend on the diluent involved, the temperature level and equivalence ratio.

It is shown [147] through the application of detailed chemical kinetics that the course of the oxidation reactions can be followed computationally over a wide range of initial composition, temperature and pressure. Such kinetic modeling showed that the presence of a diluent such as carbon dioxide with methane reduces the reaction rates for the same operating conditions and would extend the time needed for accelerating the reaction rate to ignition, as well as the time needed to complete combustion and achieve near equilibrium conditions.

6.3 The Approach

A simple analytical approach is suggested based on the assumption that the presence of a diluent with the fuel in a spark ignition engine may be simulated by being considered as a heat sink at the flame front that reduces the flame temperature substantially. This reduction in temperature will reduce drastically the chemical reaction and energy release rates since they are exponentially dependent on temperature and consequently will lead to a considerable increase in the combustion and ignition lag periods for otherwise the same initial operating conditions.

The detailed chemical kinetic modeling by Zhou [122] and Karim et. al. [147] for methane oxidation in the presence of the diluents nitrogen and carbon dioxide showed that when an apparent single step reaction is fitted to the fuel conversion rate, RR, then it can be of the following form:

$$RR = k[CH_4]^a[O_2]^b[D]^c exp(-\frac{E_A}{RT}) \tag{6.1}$$

They showed over the temperature and pressure ranges encountered in engine ap-

plication, the index "c" of the diluent, D, tends to be much smaller than one. This would indicate that under isothermal conditions the reaction rate with a diluent will not be significantly dissimilar in magnitude from that involving pure fuel. Furthermore, the thermal diffusivity of the fuel-air mixture, as our calculations showed, is not affected substantially at the same level of temperature by changes in the concentrations of diluents, especially since the diffusivity term appears under a square root in the flame propagation calculations. The length of the combustion duration in an engine is governed by the turbulent flame propagation rate which, for simplicity, may be considered a function of the corresponding laminar flame speed at the prevailing operating conditions. Thus, the simple relationship advocated by Zeldovich, Frank-Kamenetskii and Semenov [148, 149] in terms of the thermal diffusivity and the mean chemical reaction rate of the mixture, may suggest that the flame propagation rate and the corresponding combustion duration for a mixture will be mainly governed by the prevailing flame temperature level and somewhat less dependent on the diluent concentrations.

Therefore, as an approximate approach, it will be assumed that the overall combustion characteristics will be essentially similar at the same temperature whether fuel-diluent-air or pure fuel-air mixtures are employed for the same operating conditions. For simplicity, the combustion temperature may be based on the corresponding calculated adiabatic value under constant volume conditions for initial mixture conditions that correspond to those prevailing at spark timing. Any diluent present in the mixture can be viewed to be associated with either the air or the fuel. In the present approach it was assumed to have been associated with the fuel. This is an approach similar to that used quite successfully in predicting the role of changes in

the diluent concentration on establishing the flammability limits [143, 150, 144]

The adiabatic temperature of the products of combustion of a fuel-diluent-air mixture for a given equivalence ratio and operating conditions was evaluated from the energy equation:

$$(\sum_i U_{r_i,m})_{T_{st}} = (\sum_i U_{p_i,m})_{T_f} \tag{6.2}$$

where $(U_{r_i,m})$ and $(U_{p_i,m})$ are the internal energies of the various components of the reactants and products at the temperature of the spark timing, T_{st} and final temperature T_f, respectively for the fuel-diluent-air mixtures. This final temperature T_f can then be used to determine an apparent equivalence ratio for a mixture of pure fuel and air that yields a similar flame temperature under the same operating conditions, i. e.:

$$(\sum_i U_{r_i,F})_{T_{st}} = (\sum_i U_{p_i,F})_{T_f} \tag{6.3}$$

where $U_{r_i,F}$ and $U_{p_i,F}$ are the internal energies of the various components of reactants and products of the pure fuel-air mixture at the same initial operating conditions and with the same final temperature. Once, such an apparent equivalence ratio of an equivalent pure fuel-air mixture has been found, the corresponding combustion duration and ignition lag can be calculated using the submodels of the combustion duration for the pure fuel described in Chapter 3. Accordingly, this approximation means that combustion duration which is inversely dependent on the flame propagation rate in the engine is dependent only on the corresponding initial and

final combustion temperatures.

The equivalent apparent equivalence ratios calculated according to the procedure described earlier are shown against the actual equivalence ratio of the fuel mixtures containing diluents in Figures 6.1 for methane-nitrogen mixtures and in Figures 6.2 for methane-carbon dioxide mixtures, respectively. It is shown the increased presence of a diluent produced a greater relative change in the apparent equivalence ratio values with mixtures that are close to the stoichiometric values. This is a reflection of the fact that the drop in the combustion temperature due to the presence of a diluent is significantly larger for mixtures with high equivalence ratios than for lean mixtures [145, 147]. It is also evident that as the amount of diluent in the fuel-diluent mixture is increased, the flame temperature will drop sharply, producing the higher drop seen in the calculated apparent equivalence ratio of the mixtures. The effects of the presence of carbon dioxide in the fuel are more significant than those for nitrogen under similar operating conditions reflecting the higher heat capacity and transport properties of carbon dioxide in comparison to nitrogen or air.

The typical values of combustion duration and associated ignition lag when evaluated according to the procedure described, are shown in Figures 6.3 and 6.4 for a normally aspirated unthrottled CFR engine operating on different methane-nitrogen and methane-carbon dioxide mixtures, respectively. The corresponding values based on experimental are also shown [30, 135]. It can be seen that the agreement between the two values deteriorates as the concentration of the diluent is increased in the fuel mixture and as leaner mixtures are employed. Nevertheless, when accounting for the extent of cyclic variation, as described in Chapter 8 and seen in Figure 6.5, these approximate predicted values of the combustion duration are useful for applications to

mixtures around the stoichiometric value. Their values are within the uncertainties encountered experimentally, especially for relatively small concentrations (well below 50%) for both diluents in the fuel. Of course, although only the consideration of lean mixtures is of practical interest, predicted values for rich fuel-diluent-air mixtures showed in general a similar degree of agreement with experimental values.

Similarly, Figures 6.6 and 6.7 show the corresponding predicted values of the ignition lag period together with the corresponding experimental values [30, 135]. The agreement between the two sets of values deteriorates as the mixtures are made leaner or more diluted. Nevertheless, in view of the usual experimental uncertainties, the extent of deviation may be considered acceptable for the small concentrations of both diluents and when the equivalence ratio is kept close to the stoichiometric value.

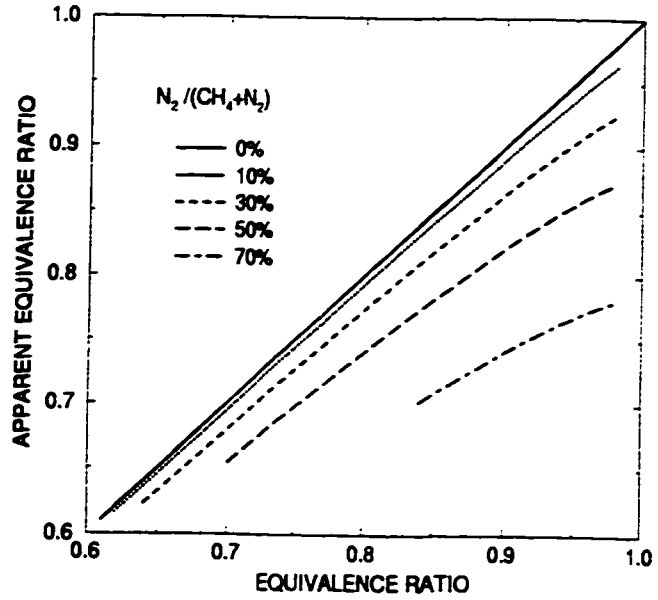

Figure 6.1: The Apparent Equivalence Ratio Variations of a S.I. Engine Fueled with Various Methane-Nitrogen Mixtures for Different Equivalence Ratios at a Compression Ratio of 8.5:1, Spark Timing of 20° BTC, Intake Charge Temperature of 294 K and Atmospheric Pressure.

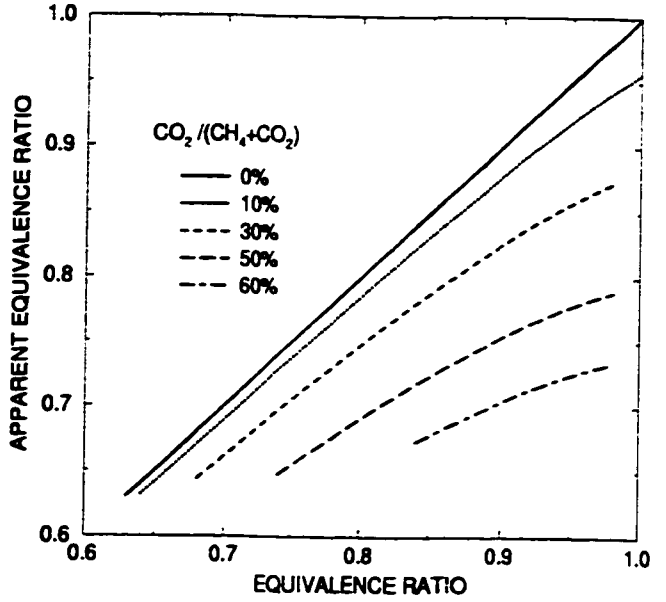

Figure 6.2: The Apparent Equivalence Ratio Variations of a S.I. Engine Fueled with Various Methane-Carbon Dioxide Mixtures for Different Equivalence Ratios at a Compression Ratio of 8.5:1, Spark Timing of 20° BTC, Intake Charge Temperature of 294 K and Atmospheric Pressure.

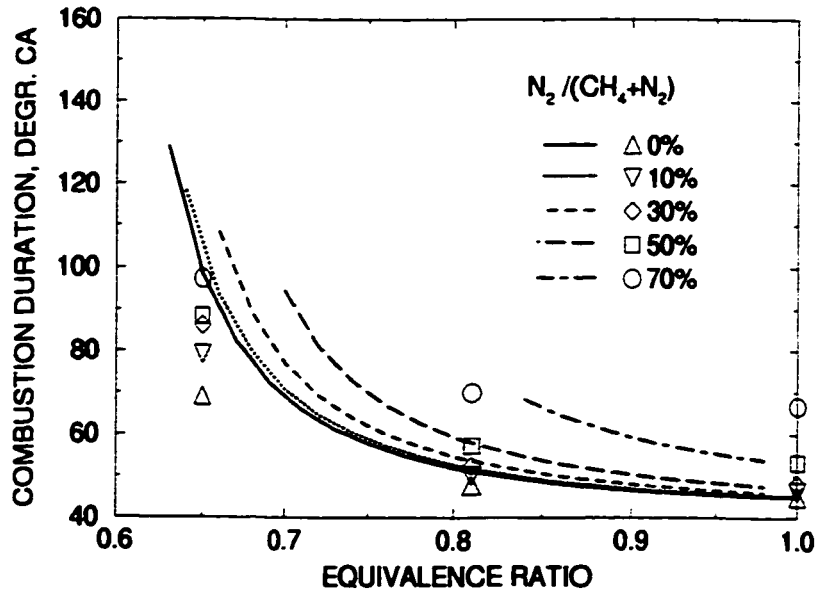

Figure 6.3: The Variation of Combustion Duration in a CFR Engine Fueled with Methane-Nitrogen Mixtures for Different Equivalence Ratios at a Compression Ratio of 8.5:1, Spark Timing of 20° BTC, Intake Charge Temperature of 294 K and Atmospheric Pressure. The Corresponding Experimental Data are also Shown.

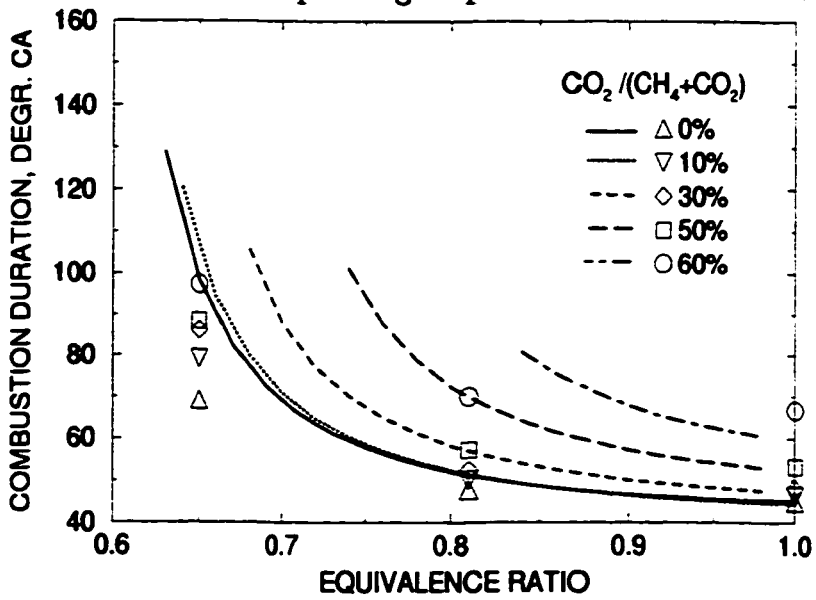

Figure 6.4: The Variation of Combustion Duration in a CFR Engine Fueled with Methane-Carbon Dioxide Mixtures for Different Equivalence Ratios at a Compression Ratio of 8.5:1, Spark Timing of 20° BTC, Intake Charge Temperature of 294 K and Atmospheric Pressure. The Corresponding Experimental Data are also Shown.

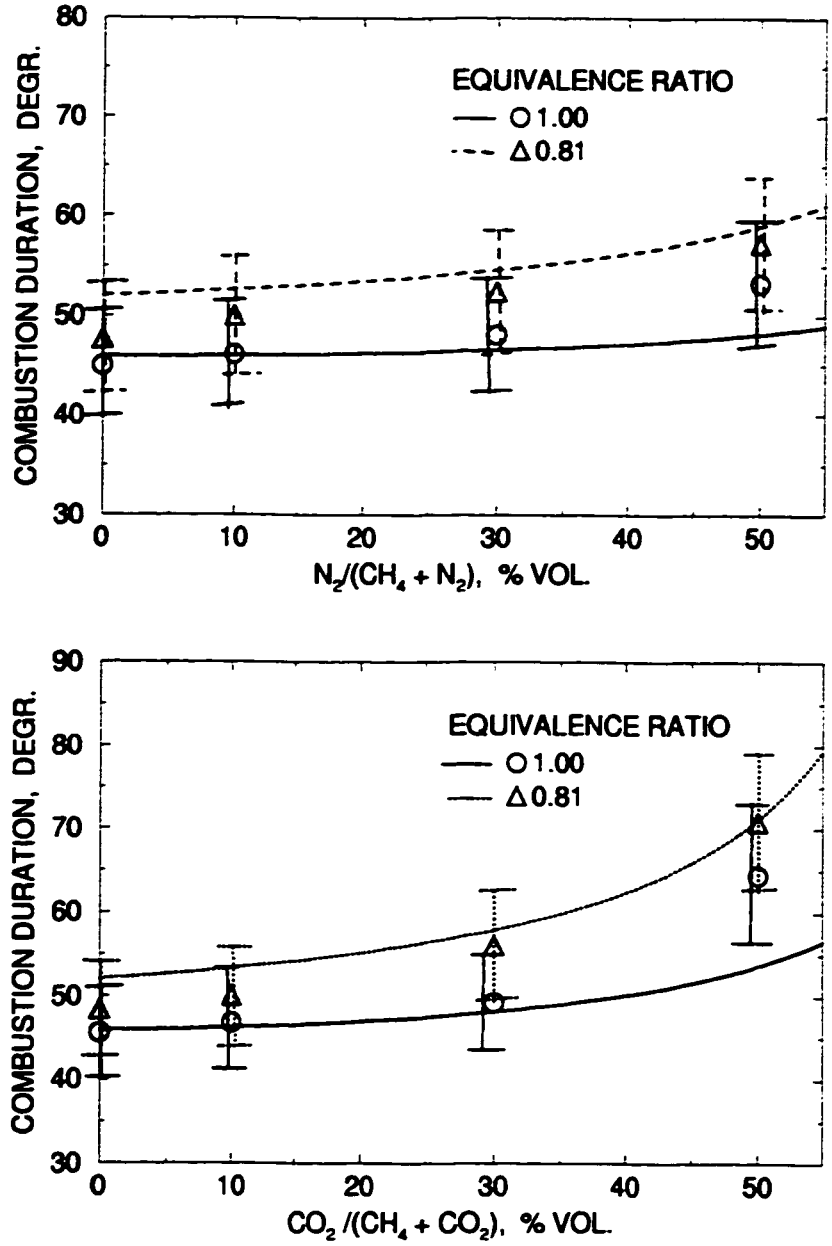

Figure 6.5: The Variation of Calculated Combustion Duration with Concentration of Diluent in Fuel Mixtures for Different Equivalence Ratios at a Compression Ratio of 8.5:1, Spark Timing of 20° BTC, Intake Charge Temperature of 294 K and Atmospheric Pressure. The Corresponding Experimental Data with Their Extent of Cyclic Variation are also Shown.

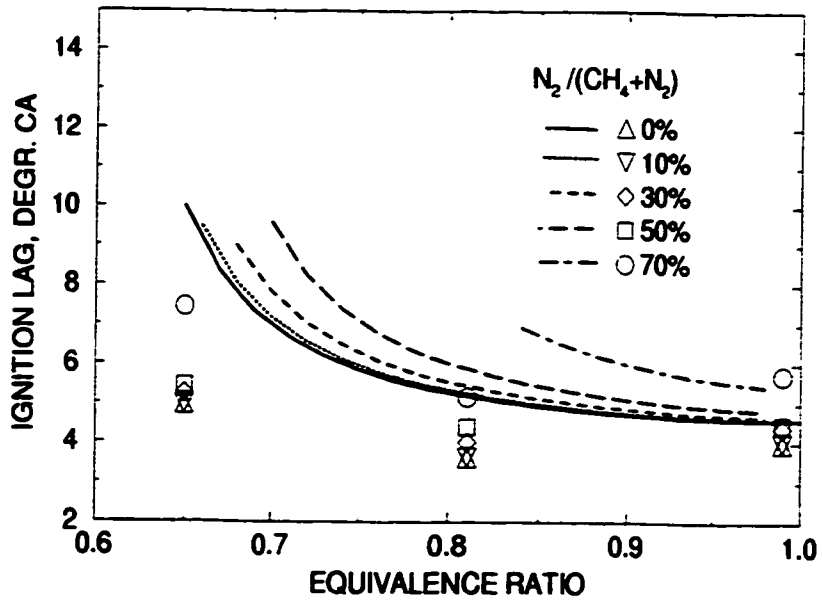

Figure 6.6: The Variation of Ignition Lag Period in a CFR Engine Fueled with Methane-Nitrogen Mixtures for Different Equivalence Ratios at a Compression Ratio of 8.5:1, Spark Timing of 20° BTC, Intake Charge Temperature of 294 K and Atmospheric Pressure. The Corresponding Experimental Data are also Shown.

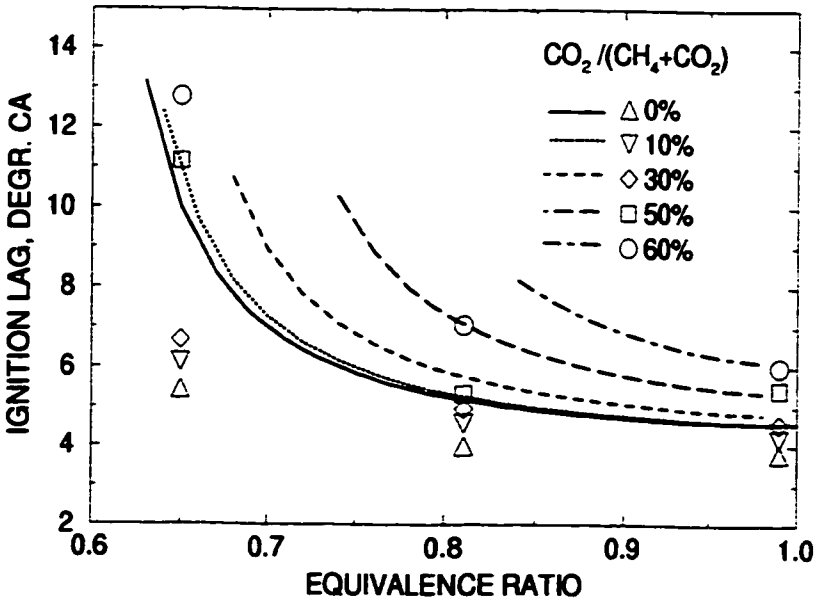

Figure 6.7: The Variation of Ignition Lag Period in a CFR Engine Fueled with Methane-Carbon Dioxide Mixtures for Different Equivalence Ratios at a Compression Ratio of 8.5:1, Spark Timing of 20° BTC, Intake Charge Temperature of 294 K and Atmospheric Pressure. The Corresponding Experimental Data are also Shown.

6.4 An Alternative Simplified Method

An alternative simplified approach may be suggested for estimating the combustion duration in cases where fuel mixtures containing diluents are used in spark ignition engines. This approach is particularly suited to cases where sufficient experimental data are absent.

It was indicated earlier that the value of the combustion duration is fluctuating in nature and relatively small deviations in its value will not affect substantially the predicted average values of engine output. Moreover, as shown in Section 3.2.2 the length of the combustion period, $\Delta\theta_c$, can be predicted once the values of minimum combustion duration, $\Delta\theta_{min}$, and operational limits ϕ_l and ϕ_r are known.

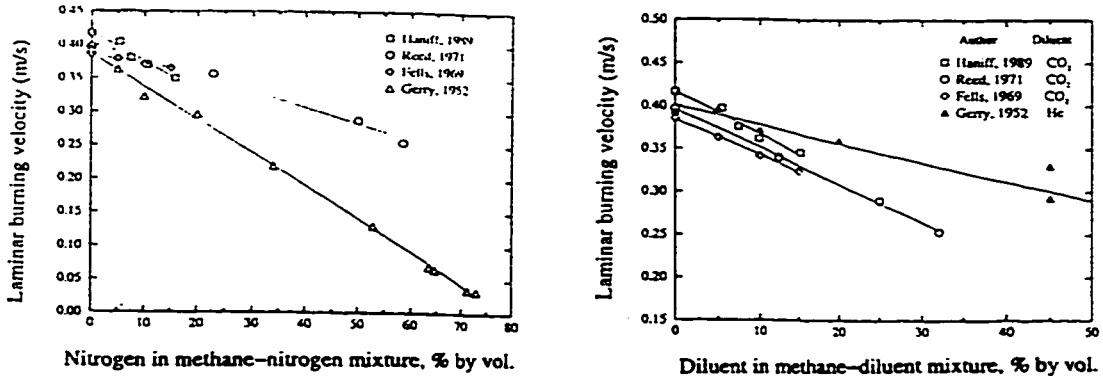

Figure 6.8: Stoichiometric Laminar Burning Velocities of Methane-Diluent Mixtures as Function of Diluent Concentration.

It is observed experimentally that the operational limiting equivalence ratios in an engine, ϕ_l or ϕ_r, are related to the flammability limit values of the fuel in air when calculated for temperature values at the conditions corresponding to those existing at the time of the spark passage [130]. Moreover, the value of the operational lean

limiting equivalence ratio increases approximately linearly as the amount of diluent in the fuel mixture is increased. On this basis, it would be expected that the maximum increase in the amount of diluent, D_{max}, which can be accommodated in the fuel mixture, for any set of operating conditions, will be associated with an operational limiting mixture that is stoichiometric. Thus, an operational limiting equivalence ratio, $\phi_{l,D}$ for an amount of diluent, D, in fuel mixture may be evaluated as:

$$\phi_{l,D} = \frac{D}{D_{max}}(1 - \phi_{l,F}) + \phi_{l,F} \tag{6.4}$$

where $\phi_{l,F}$ is the corresponding equivalence ratio at the operational limit of the pure fuel on its own at the same operating conditions.

Similarly, as indicated earlier, the combustion duration can be viewed to be inversely dependent on the flame propagation rate which, for simplicity as stated earlier, may be considered a function of the corresponding laminar flame speed at the prevailing operating conditions. It has been observed experimentally [151, 152] that the maximum laminar flame speed decreases approximately linearly with the amount of diluent concentration in the fuel mixture as shown typically in Figure 6.8 [151]. The maximum possible amount of diluent concentration in a fuel mixture that can be tolerated operationally will be associated with fuel-diluent-air mixtures that are of stoichiometric equivalence ratio. The flame propagation rates in these mixtures would be very slow leading to a very long combustion duration. Hence, the corresponding minimum combustion duration, $\Delta\theta_{min,D}$, for any fuel mixture containing diluent, D, may be estimated according to the following approximate

relationship:

$$\frac{1}{\Delta\theta_{min,D}} = \frac{1}{\Delta\theta_{min,F}}(1 - \frac{D}{D_{max}}) \tag{6.5}$$

where $\Delta\theta_{min,F}$ is the corresponding minimum combustion duration of the pure fuel mixture on its own at the same operating conditions and D_{max} is the maximum operational concentration of the diluent in the fuel which may be either estimated or determined experimentally for the engine and operating conditions.

Typical results obtained while using such a simplified method with the values for maximum diluent concentration in the fuel for carbon dioxide and nitrogen arbitrarily as 70% and 80% are compared with those relating to the approach described earlier are shown in Figure 6.9 together with the corresponding experimental values. It can be seen that the inverse of combustion duration is approximately linearly proportional to the amount of diluent present in the fuel-diluent mixture. However, the results obtained when using the more simplified approach deviates considerably as the amount of diluent in the mixture is increased. Nevertheless, such a simplified method can produce reasonably approximate results for a small concentration of diluent in a fuel-diluent mixture (up to about 10 - 15%) and may be used to calculate for the initial approximation specially when the experimental information is scarce.

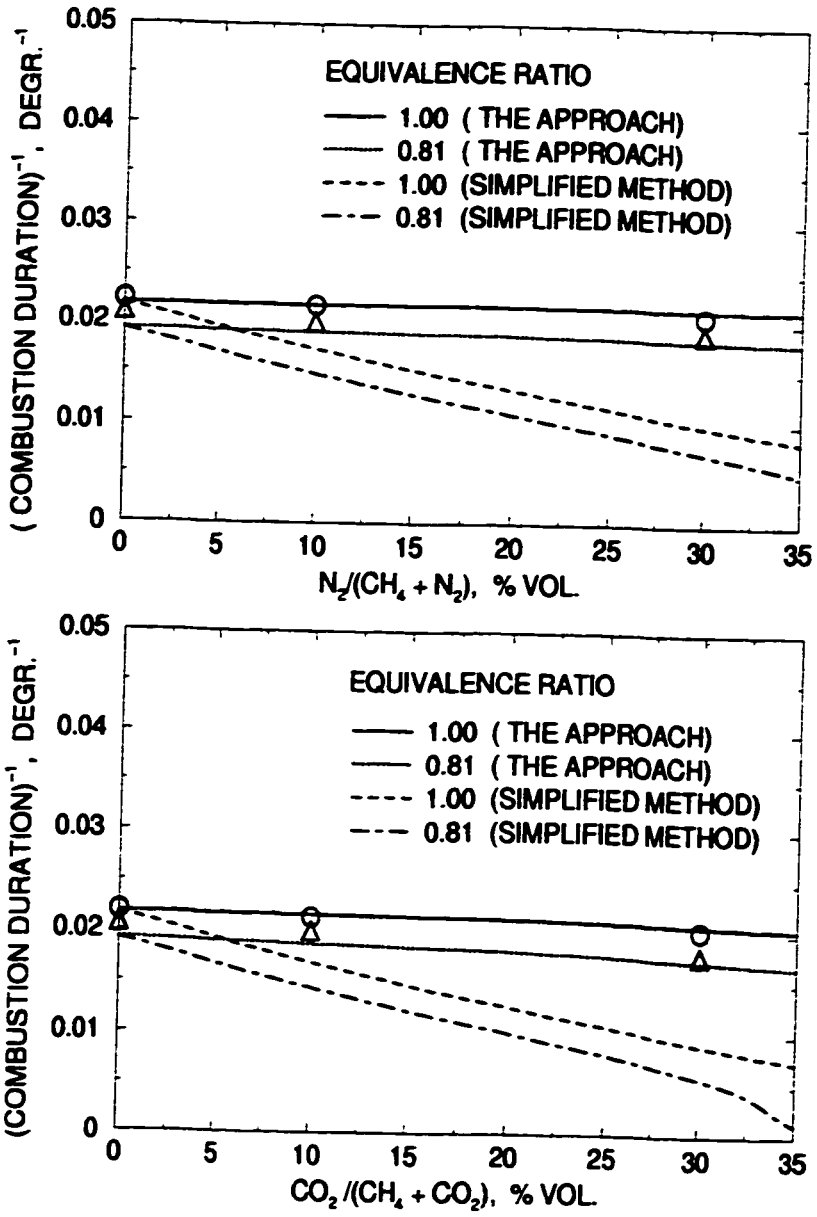

Figure 6.9: The Inverse of Combustion Duration Versus the Concentration of Diluent Present in Fuel Mixture for Different Equivalence Ratios at a Compression Ratio of 8.5:1, Spark Timing of 20° BTC, Intake Charge Temperature of 294 K and Atmospheric Pressure. The Corresponding Experimental Data are also Shown.

6.5 Results and Discussion

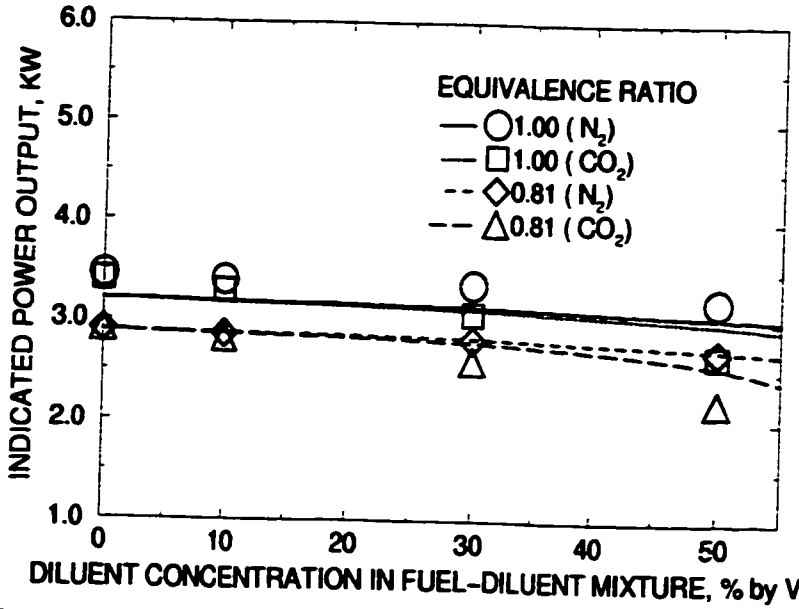

Figure 6.10: The Variation of Indicated Power Output Versus the Concentration of Diluent in Methane-Diluent Mixtures for Two Equivalence Ratios at a Compression Ratio of 8.5:1, Spark Timing of 20° BTC, Intake Charge Temperature of 294 K and Atmospheric Pressure. The Corresponding Experimental Data are also Shown.

Some typical results obtained using the approach described earlier, with methane-nitrogen and methane-carbon dioxide mixtures as fuels were presented over a range of operating conditions consistent with those of the CFR engine. Figure 6.10 shows the calculated indicated power output versus the amount of diluent concentration in the fuel-diluent mixture for two equivalence ratios with the corresponding experimental values [30, 135]. Similarly, in Figures 6.11 and 6.12 the calculated indicated power outputs are presented against the equivalence ratio for various methane-nitrogen and methane-carbon dioxide mixtures, respectively. The corresponding experimental data [30, 135] are also shown. It can be seen in these figures that good agreement exists between the calculated and corresponding experimental power outputs when

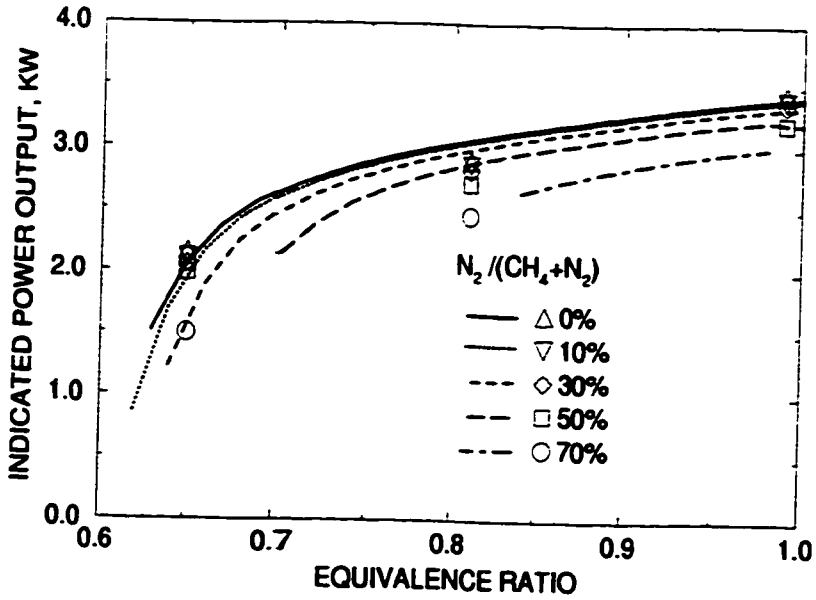

Figure 6.11: The Variation of Indicated Power Output of a CFR Engine Fueled with Various Methane-Nitrogen Mixtures for Different Equivalence Ratios at a Compression Ratio of 8.5:1, Spark Timing of 20° BTC, Intake Charge Temperature of 294 K and Atmospheric Pressure. The Corresponding Experimental Data are also Shown.

the amount of diluent concentration in the fuel-diluent mixtures is not too excessive (e. g. well below 50%).

Similarly, a typical comparison of the power output when calculated using the main approach with that obtained while using the much simplified approach, as described in the previous section is shown in Figure 6.13 for a methane-carbon dioxide mixture. The corresponding experimental data are also shown. It can be seen that the simplified method produces reasonably accurate results when the concentration of the diluent in the fuel mixture is relatively low. The deviation becomes quickly excessive as the concentration of the diluent increases beyond around 15%.

Figure 6.14 shows the calculated indicated power output for different equivalence ratios with the concentration of the diluents nitrogen and carbon dioxide in methane.

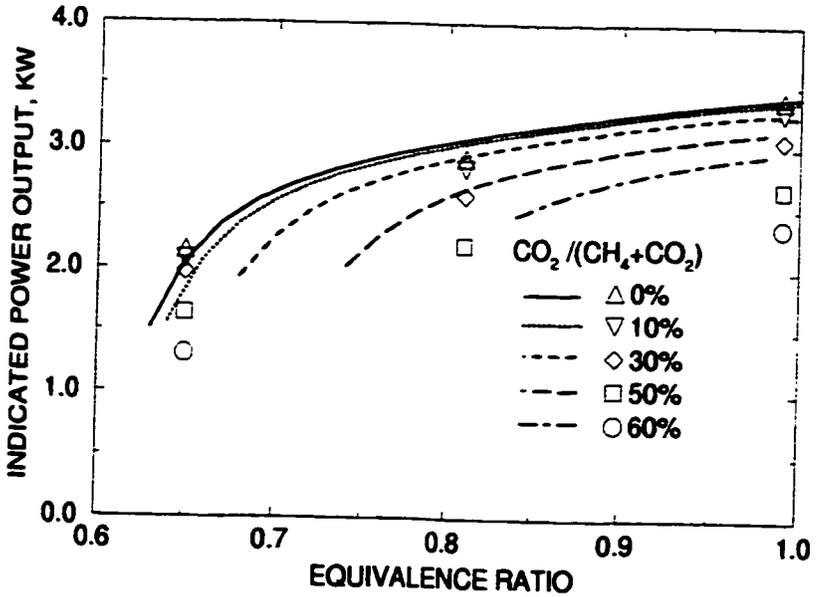

Figure 6.12: The Variation of Indicated Power Output of a CFR Engine Fueled with Various Methane-Carbon Dioxide Mixtures for Different Equivalence Ratios at a Compression Ratio of 8.5:1, Spark Timing of 20° BTC, Intake Charge Temperature of 294 K and Atmospheric Pressure. The Corresponding Experimental Data are also Shown.

It can be seen that the increased presence of the diluent in the fuel-diluent mixtures initially affects only little the indicated power output. However, the presence of a diluent beyond about 50% in the fuel-diluent mixtures, the drop in the indicated power output of the engine is sharp and considerable. In Figure 6.15, the influence of the presence of a diluent for the various compression ratios on the indicated power output are presented. It appears that the increased presence of the diluent in fuel-diluent mixtures starts gradually to decrease the indicated power output of the engine, especially for lower compression ratios. Similarly, Figure 6.16 shows the effect of various diluents on power output for different initial mixture temperatures. It can be seen that the drop in power output is higher for lower initial mixture temperatures and for carbon dioxide than nitrogen as expected.

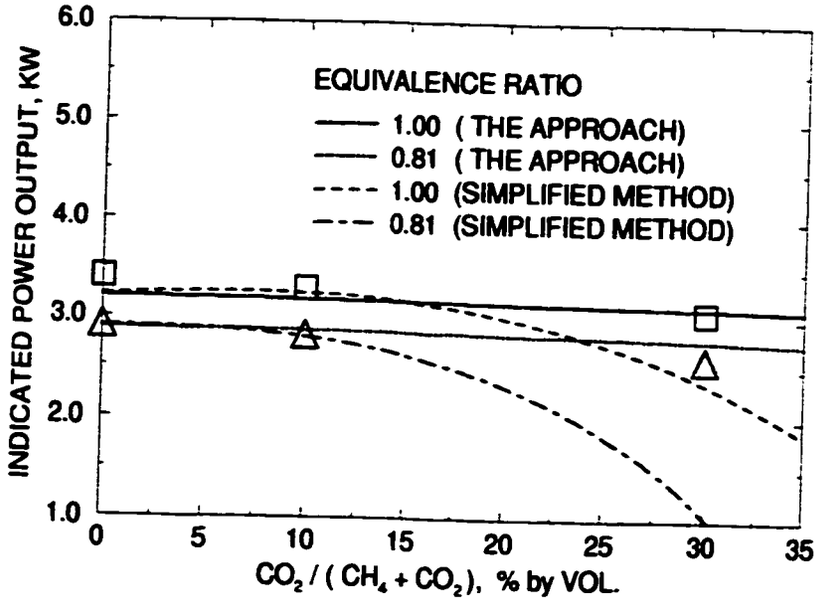

Figure 6.13: The Calculated Indicated Power Output Versus the Concentration of Carbon Dioxide in Methane for Two Equivalence Ratios at a Compression Ratio of 8.5:1, Spark Timing of 20° BTC, Intake Charge Temperature of 294 K and Atmospheric Pressure. The Corresponding Experimental Data are also Shown.

The influence of the amount of diluents in the fuel-diluent mixtures for various spark timing are illustrated in Figure 6.17 for methane-nitrogen and methane-carbon dioxide mixtures. The spark timing, as seen in the figure, needed to be advanced as the amount of the diluent is increased to improve the power output especially in the case of the higher concentration of the diluent in fuel-diluent mixtures. This is even more critical for the diluent carbon dioxide than for nitrogen.

The effects of the presence of a diluent in fuel-diluent mixtures on the incidence of knock were considered analytically using the model described earlier. As mentioned earlier, the model considers knock to take place when the energy released due to the preignition reaction activity of the end gas ahead of the propagating flame becomes sufficiently intense to produce autoignition. For example, at the equivalence ratio of

0.90 and two compression ratios, as shown in Figure 6.18, the preignition reaction activity of the end gas region is inhibited by the increased presence of the diluent in the fuel-diluent mixtures indicating a lower tendency to knock than for the pure-fuel mixture for otherwise the same operating conditions. It is also shown that the inhibition characteristic of carbon dioxide is much greater than for nitrogen. As an example, at the compression ratio of 15:1, the presence of more than 23% of carbon dioxide or 56% of nitrogen with methane would eliminate the knock for the operating conditions shown. However for a slightly lower compression ratio of 14.5:1, only 12% or more of carbon dioxide or 39% or more of nitrogen is needed. These points are also shown in Figure 6.15 by arrows.

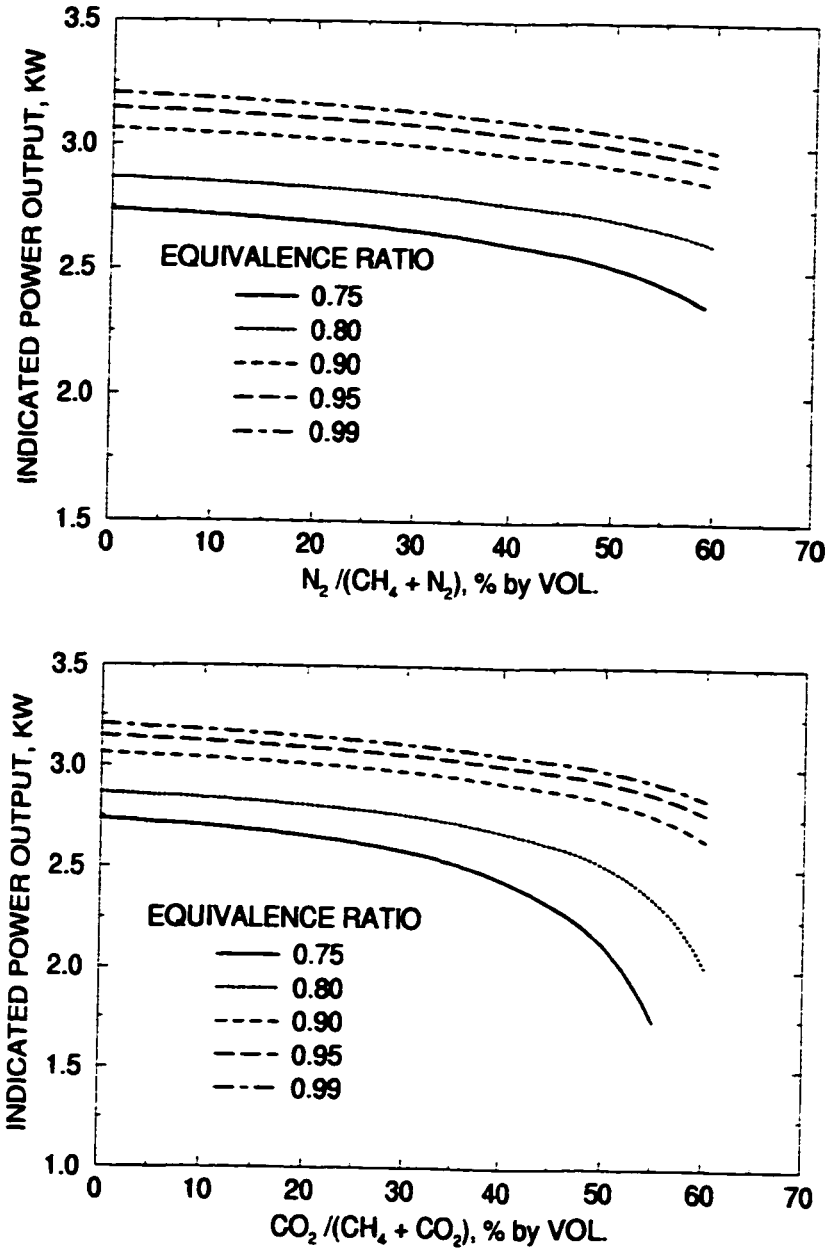

Figure 6.14: The Indicated Power Output Variations of S. I. Engine Versus Concentration of Various Diluents in Fuel Mixtures for Different Equivalence Ratios at a Compression Ratio of 8.5:1, Spark Timing of 20° BTC, Intake Charge Temperature of 294 K and Atmospheric Pressure.

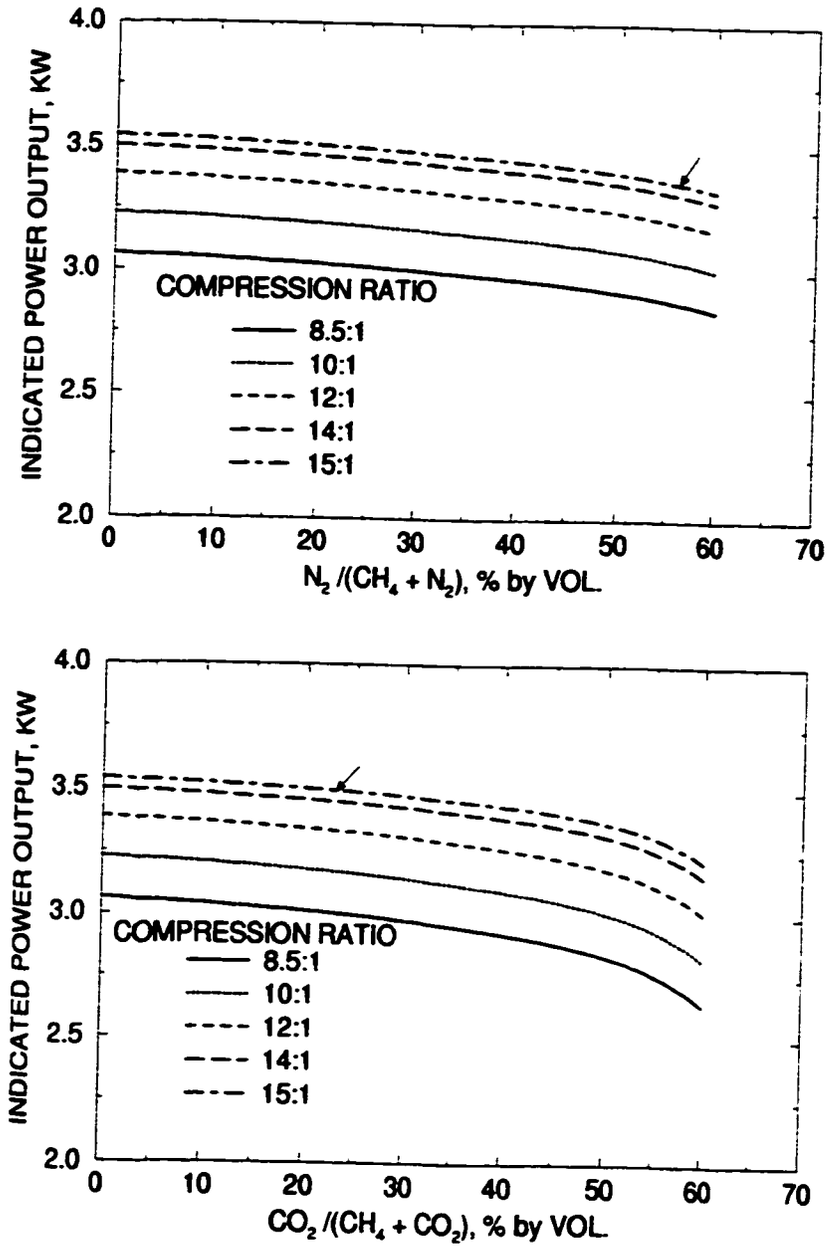

Figure 6.15: The Indicated Power Output Variations of S. I. Engine Versus Concentration of Various Diluents in Fuel Mixtures for Different Compression Ratios at an Equivalence Ratio of 0.90, Spark Timing of 20° BTC, Intake Charge Temperature of 294 K and Atmospheric Pressure. Arrows Indicate the Boarder Line Conditions for Knock.

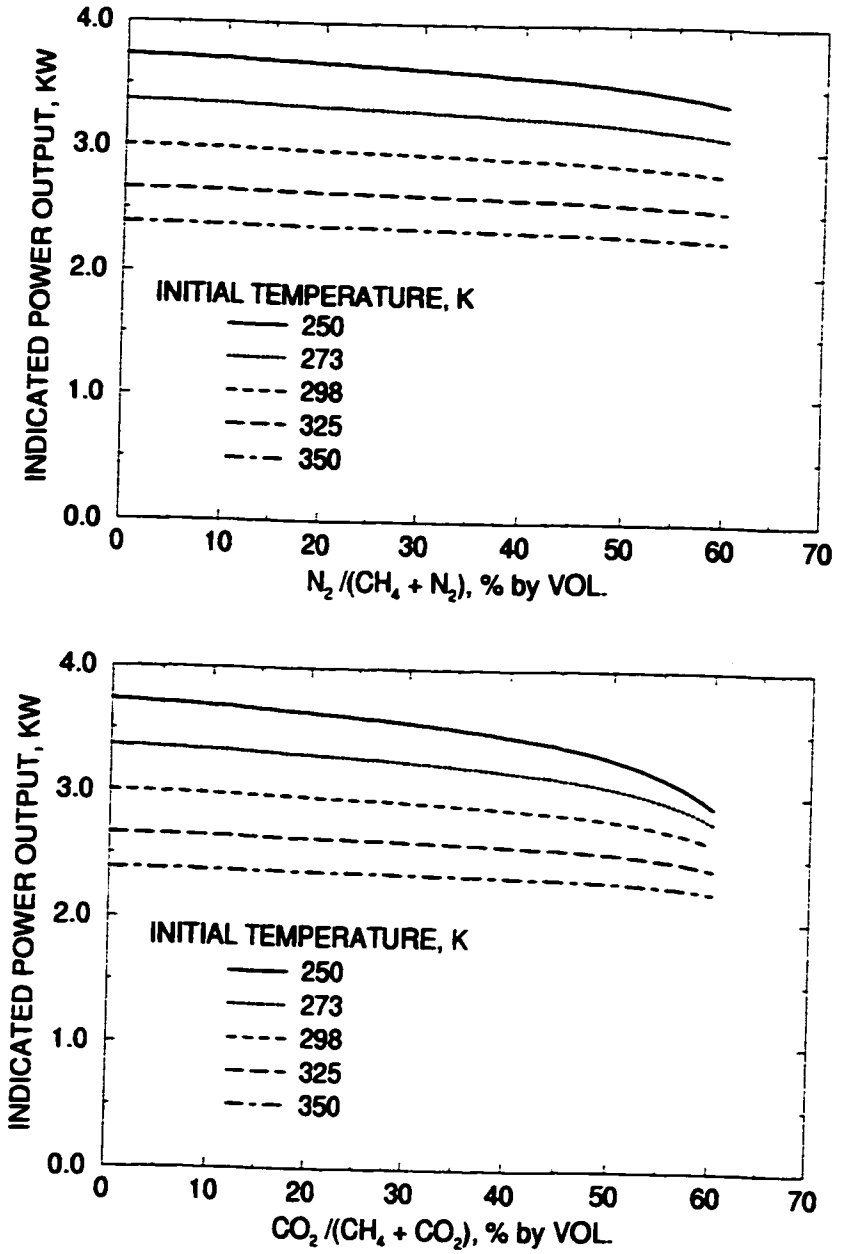

Figure 6.16: The Indicated Power Output Variations of S. I. Engine Versus Concentration of Various Diluents in Fuel Mixtures for Different Intake Charge Temperatures at an Equivalence Ratio of 0.90, Compression Ratio of 8.5:1, Spark Timing of 20° BTC and Atmospheric Pressure.

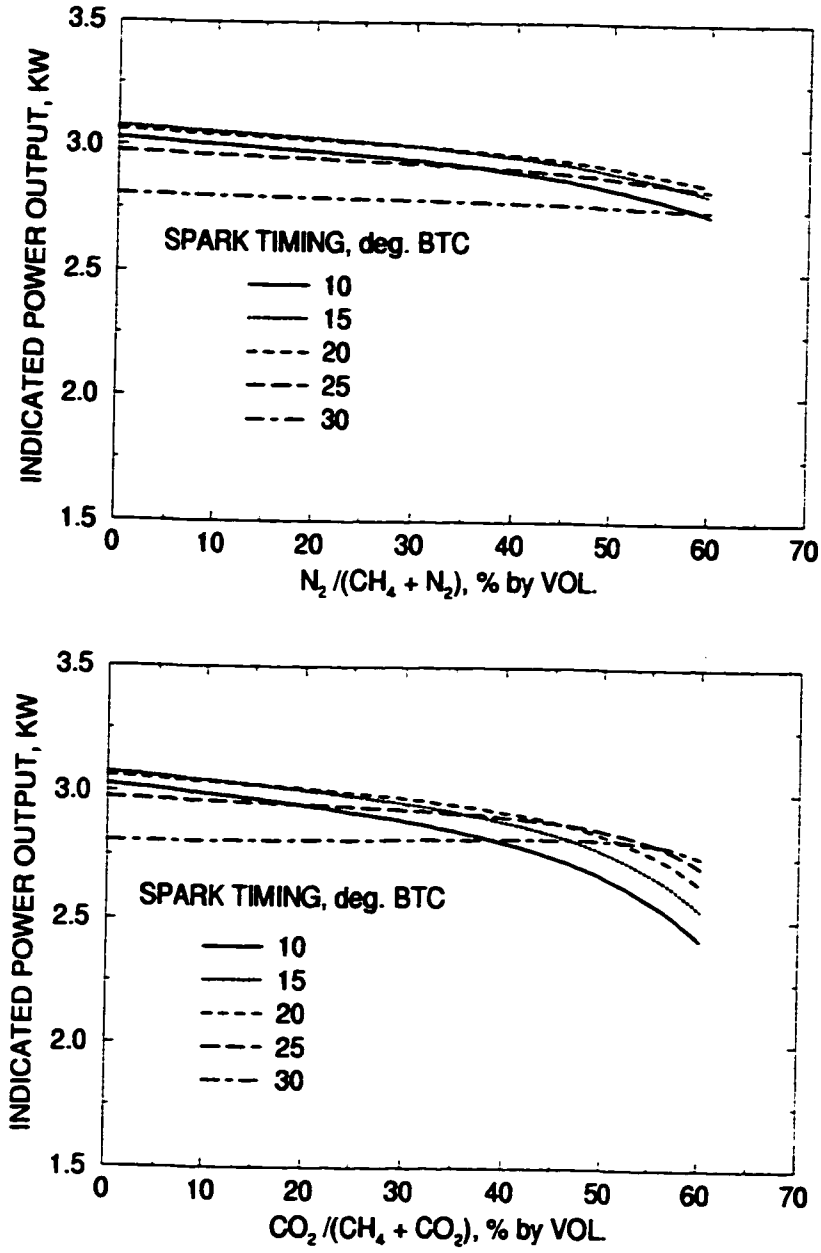

Figure 6.17: The Indicated Power Output Variations of S. I. Engine Versus Concentration of Various Diluents in Fuel Mixtures for Different Spark Timing at an Equivalence Ratio of 0.90, Compression Ratio of 8.5:1, Intake Charge Temperature of 294 K and Atmospheric Pressure.

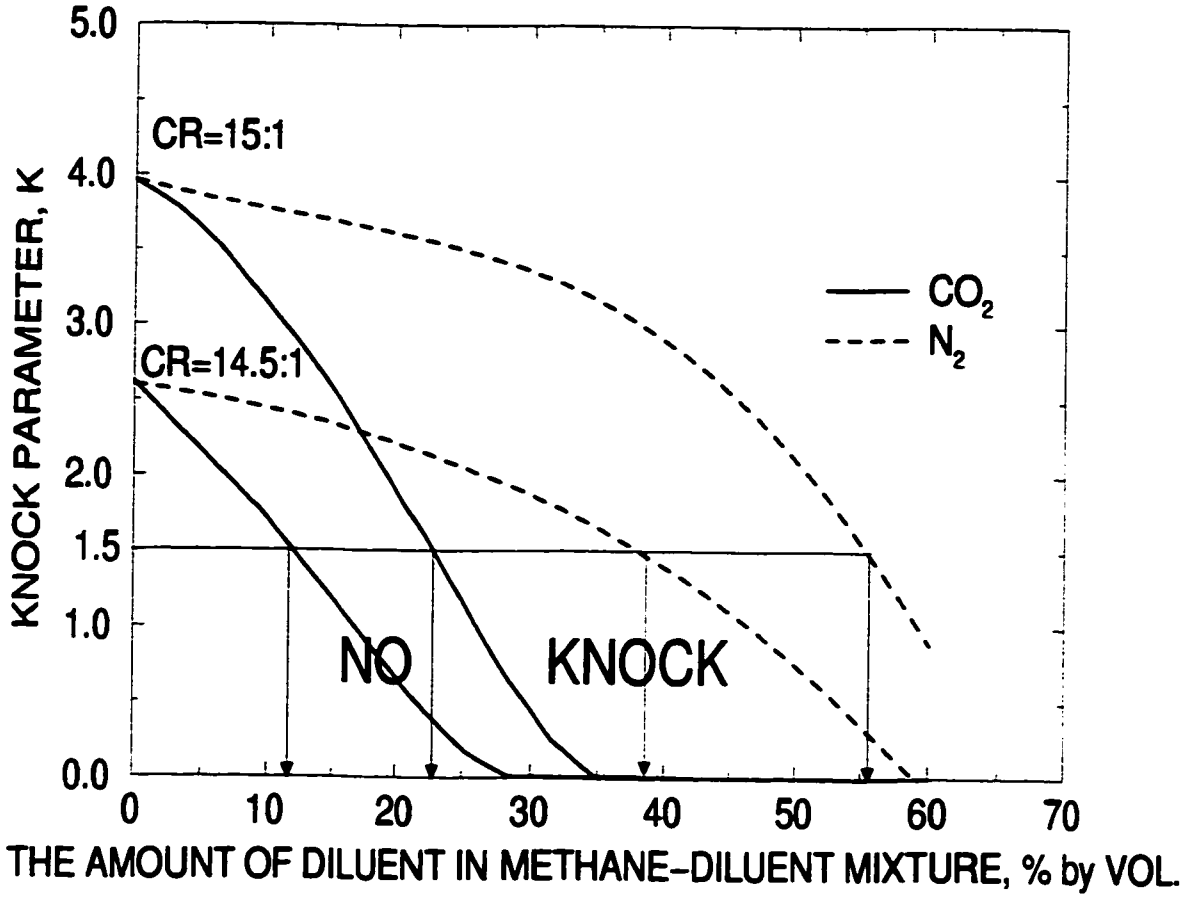

Figure 6.18: The Variation of Knock Parameter, K, Versus Concentration of Various Diluents in Fuel and Diluent Mixtures for Different Compression Ratios at an Equivalence Ratio of 0.90, Spark Timing of 20° BTC, Intake Charge Temperature of 294 K and Atmospheric Pressure.

Chapter 7

HYDROGEN AS AN ADDITIVE TO METHANE FOR SPARK IGNITION ENGINE APPLICATIONS

7.1 Introduction

There is ever increasing interest in operating internal combustion engines on alternative gaseous fuels motivated largely by the demand for cleaner exhaust emissions combined with improvements in efficiency. This is aided by the relatively cheaper cost of gaseous fuels and their abundant availability in comparison to conventional liquid fuels [3]. Moreover, the operation of engines on gaseous fuels such as natural gas, containing mostly methane, has distinct potential operational benefits while retaining excellence in reliability and durability [153].

The operation of engines on lean fuel mixtures has a number of positive features. It can, in principle, provide high thermal efficiency, low likelihood of knock, reduced emissions especially NOx and permits using higher compression ratios while reducing heat transfer. It may permit dispensing with exhaust catalytic treatment and the need for precise control of the mixture quality as usually is the case with stoichiometric operation. However, there are a number of difficulties associated with lean burn operation. These arise primarily from the associated slower flame propagation, less complete combustion, increased cyclic variations and even the occasional flame fail-

ure. These contribute to poor engine power output and excessive emissions that may be encountered with lean operation [154].

An important difficulty in the operation of engines, whether of the spark ignition or compression ignition types, on lean mixtures of methane and air is the associated low flame propagation velocity. Some improvement in the burning rate in spark ignition engines is usually obtained through measures such as the employment of optimum spark timing, improved chamber design and increased turbulence. The extent of increase in the level of turbulence in engines is usually limited and there are penalties associated with the use of excessive turbulence that include excessive heat transfer and higher peak temperatures and hence higher NOx emissions in optimum chamber geometry. Hence, there is a need to enhance the combustion process without bringing about some of these disadvantages. One approach is through the addition to the methane of a small amount of hydrogen, a fuel having a much cleaner and faster rates of burning than methane. The contribution of the hydrogen addition to increased preignition reaction activity is usually relatively small. This procedure is especially attractive since, due to economic and technical reasons, the operation of engines on pure hydrogen fuel remains largely a long term proposition. On the other hand, the use of hydrogen as an additive to methane, especially for engine applications, may be an attractive solution, both at present and in the near future for a reduction of the effects of some of the operational problems associated with engines fueled with methane.

The present contribution describes the results of an experimental and analytical investigation for a spark ignition engine where the addition of some hydrogen to the methane produces notable improvements in performance. It is shown while

employing analytical modeling approaches that if the needed hydrogen is produced in situ on board the engine by the electrolysis of water and the energy required for hydrogen production is accounted for, then the viable range of operation of such an engine is very narrow and economically unattractive.

7.2 The Approach

In order to investigate the effect of the addition of a small amount of hydrogen and hydrogen-oxygen, in their proportion in water, to the main fuel methane on the performance of a spark ignition engine over wide range of operating and design conditions, the predictive analytical model developed in Chapter 3 was employed. When a mixture of common gaseous fuels with methane was used in a spark ignition engine, the expression developed in Chapter 3, Section 3.2.2 for the combustion duration was employed to fit our own experimental observations made in a single cylinder variable compression ratio CFR engine. This empirically based relationship, as mentioned earlier, essentially relates the flame propagation rates of the different component fuels to the observed rate of the fuel mixture according to the molar composition of the fuel mixture under the same engine operating conditions. The evaluation of knock due to presence of hydrogen in the main fuel methane in the spark ignition engine was carried out according to the procedures described in Chapter 3, Section 3.2.3. As mentioned earlier, as the preignition reaction activity of the end gas becomes significantly intense to produce autoignition and hence knock, the value of the knock parameter, K, increases beyond a critical value that was found experimentally to be associated with the onset of mild knocking.

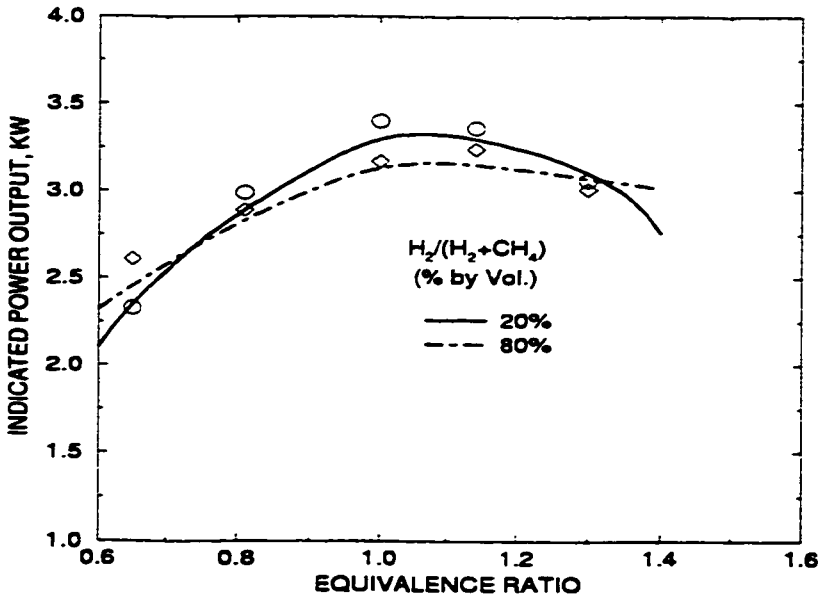

Figure 7.1: The Indicated Power Output Variations with Equivalence Ratio When Operating on Methane-Hydrogen Mixtures for a Compression Ratio of 8.5:1, Spark Timing of 20 degrees BTC and Initial Mixture Temperature of 298K at 900 rev./min. The Corresponding Experimental Data are also Shown.

The present experimental investigation was carried out in a variable compression ratio, single cylinder spark ignited CFR engine. As mentioned in Chapter 4, the dissociated products of water were simulated by being made from individually supplied metered gases that were homogeneously mixed with the incoming fuel-air mixture at constant intake ambient temperature and pressure. The gaseous fuels, methane and hydrogen were supplied in different combinations through precalibrated choked nozzles metering systems while the required amount of oxygen was introduced through a calibrated rotameter. As a typical example, Figure 7.1 shows the level of agreement between the predicted power output and the corresponding experimental data while operating on methane-hydrogen fuel mixtures.

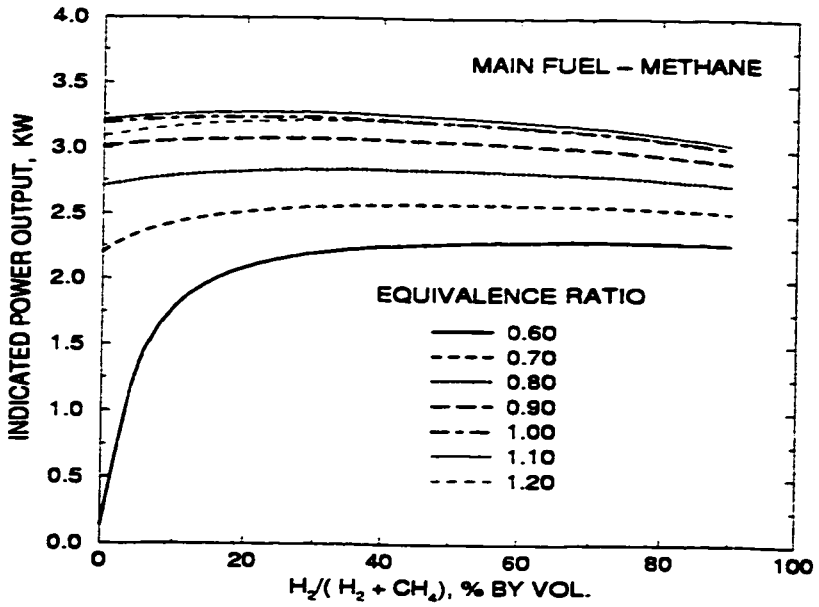

Figure 7.2: The Indicated Power Output Variations with Concentration of Hydrogen in a Fuel Mixture of Methane and Hydrogen for Various Equivalence Ratios at a Compression Ratio of 8.5:1, Spark Timing of 20 degrees BTC and Initial Mixture Temperature of 298K.

7.3 Results and Discussions

The approach was applied to consider the performance of a S. I. Engine over a range of operating conditions in the CFR engine. Some of the calculated results for hydrogen-methane mixtures are shown in Figure 7.2. The addition of hydrogen to methane improves the power output of the engine especially for lean mixtures having low values of equivalence ratios. This is mainly because with low equivalence ratios, the flame speed of the main fuel methane is usually quite low and the presence of the hydrogen with its superior burning rate characteristics enhances the overall burning rates of the mixture significantly. This brings with it a reduction in the cyclic variations that is especially severe at these low equivalence ratios [155]. As the equivalence ratio is increased towards the stoichiometric ratio the relative beneficial

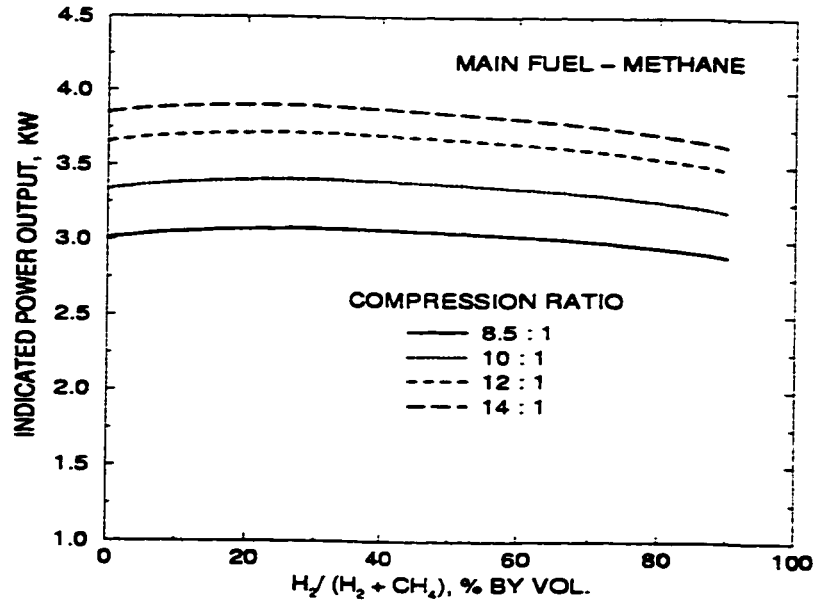

Figure 7.3: The Variations of Indicated Power Versus Concentration of Hydrogen in Fuel Mixtures of Methane and Hydrogen for Different Compression Ratios at Equivalence Ratio of 0.90, Spark Timing of 20 degrees BTC and Initial Temperature of 298 K.

effects of the addition of hydrogen to the methane are diminished, since the burning rates of both fuel components are enhanced significantly. Accordingly, the increased presence of hydrogen at these equivalence ratios makes a lesser relative contribution. Furthermore, the increased presence of hydrogen in the main fuel starts to affect increasingly the power output adversely due to the lower heating value of the hydrogen on molar basis in comparison to that of methane. This is consistent with what is usually observed experimentally [30].

The effects of the increased presence of hydrogen with the methane on the calculated indicated power output for the range of the values of different compression ratios and initial mixture temperatures are shown in Figures 7.3 and 7.4. There is little change in the power output with hydrogen addition to methane for all the

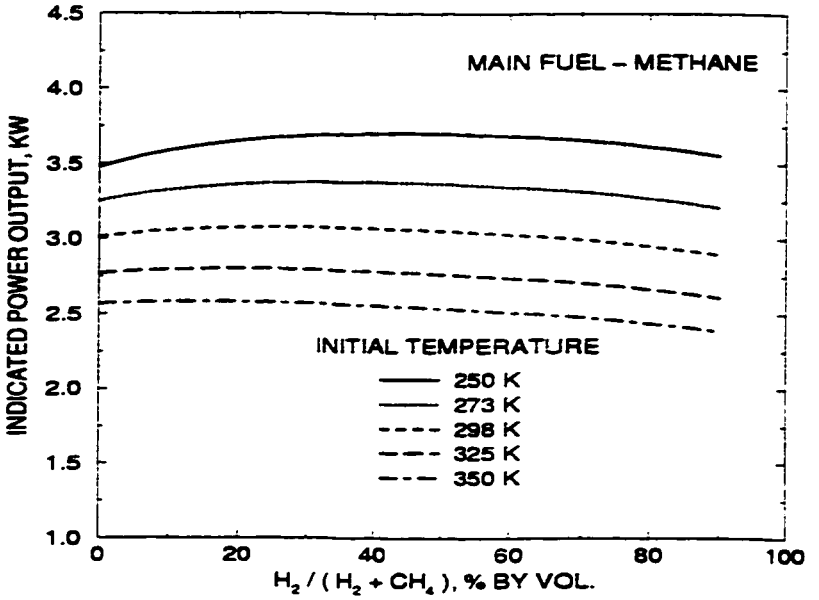

Figure 7.4: The Variations of Indicated Power Output Versus Concentration of Hydrogen in Fuel Mixture of Methane and Hydrogen for Various Initial Temperatures at a Compression Ratio of 8.5:1, Spark Timing of 20 degrees BTC and Equivalence Ratio of 0.90.

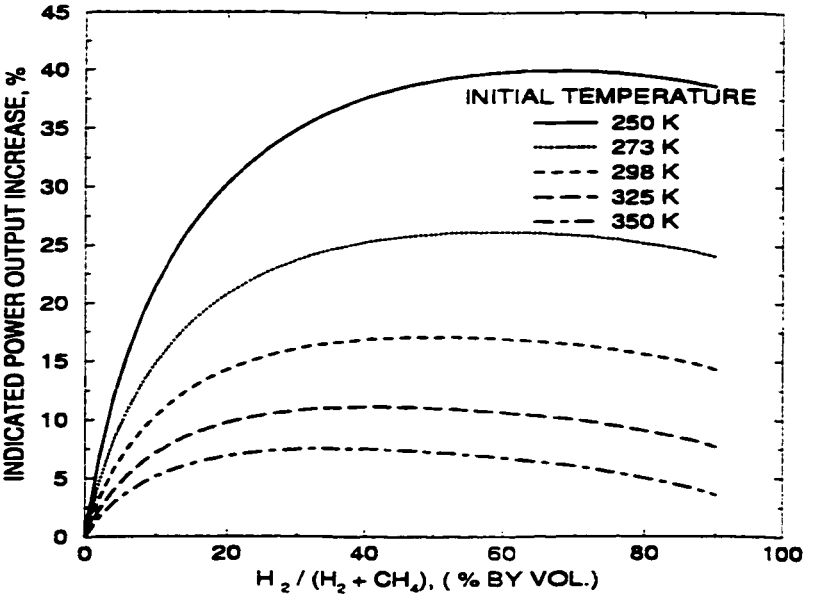

Figure 7.5: The Variations of Indicated Power Output Increase Versus Concentration of Hydrogen in Fuel Mixture of Methane and Hydrogen for Various Initial Temperatures at a Compression Ratio of 8.5:1, Spark Timing of 20 degrees BTC and Equivalence Ratio of 0.70.

compression ratios as shown. However, the presence of hydrogen in the fuel mixture beyond around 20 percent by volume tends to affect adversely the power output due to the lower heating value of hydrogen in comparison to that of methane for all the compression ratios. Similarly, as shown in Figure 7.4, the effects of increased concentration of hydrogen in the fuel mixture on the power output becomes much less pronounced as the mixture initial temperature is increased. This is a reflection of the increased burning rates and reduced total energy released with increasing the intake mixture temperature for non-knocking operation. As an example, for a relatively low intake temperature of 250 K with an equivalence ratio of 0.90, an increase in power of about 7 percent can be achieved from that with methane when 50 percent hydrogen is in the fuel mixture for the operating condition considered. This increase in power output becomes significantly bigger as the equivalence ratio is lowered (e.g. with an equivalence ratio of 0.70, an increase in power of 40 percent can be achieved for the same operating conditions as shown in Figure 7.5).

Some of our typical experimental results when hydrogen-methane mixtures were employed as a fuel in the CFR engine for two compression ratios are presented in Figures 7.6 and 7.7. It can be seen that the observed trends are in general consistent with the analytical results discussed earlier.

An experimental investigation of the effects of the addition of a small amount of oxygen on its own to the main fuel methane was carried out. Figure 7.8 shows typically the indicated power output of the engine for different equivalence ratios at a compression ratio of 8.5:1, spark timing of 20 degree BTC and initial mixture temperature of 294 K. It can be seen that the addition of a small quantity of oxygen to the methane-air mixture does not produce a significant change in performance since

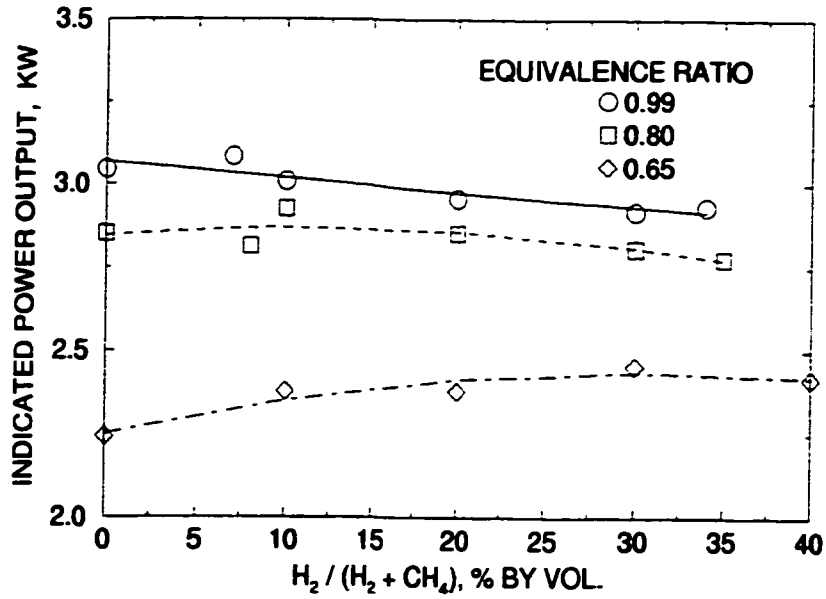

Figure 7.6: The Experimental Indicated Power Output Variations with Concentration of Hydrogen in a Fuel Mixture of Methane and Hydrogen for Various Equivalence Ratios at a Compression Ratio of 8.5:1, Spark Timing of 15 BTC and Initial Mixture Temperature of 295K in CFR Engine at 900 rev./min.

such an addition to a mixture that already contains sufficient oxygen for combustion, especially for the lean mixtures, will have negligible effect.

One of the major limitations associated with the use of hydrogen as an engine fuel is its generation and portability. Hence, the suggestion is made that the small amount of hydrogen that needs to be added to the main fuel methane may be produced continuously in situ on board the engine by the electrolysis of water using the engine output as the source for the necessary energy needed. It has been thought that the enhancement to the power production capacity with hydrogen addition may be sufficiently high to pay for the energy demand for water electrolysis. An evaluation of this proposition needs to be made. Accordingly, using the simulation model described earlier it was shown that the presence of some oxygen produced with the hydrogen

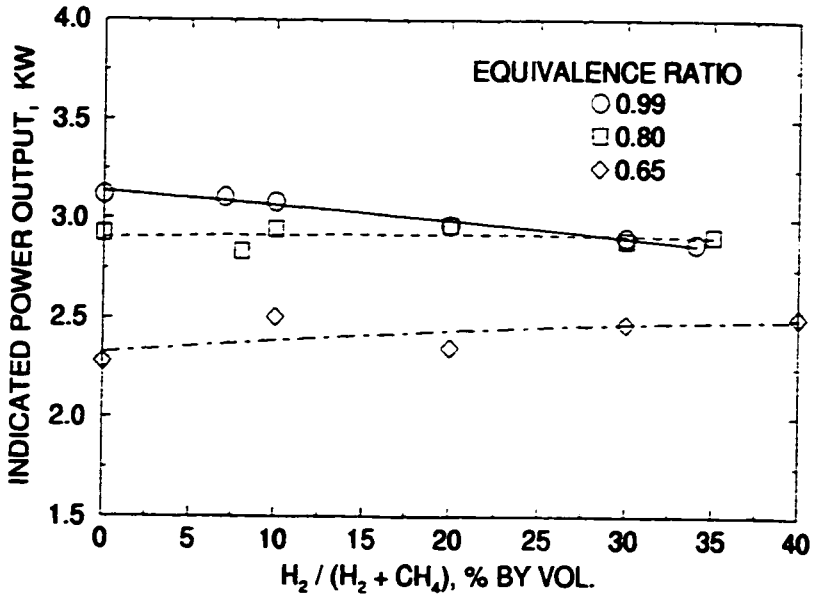

Figure 7.7: The Experimental Indicated Power Output Variations with Concentration of Hydrogen in a Fuel Mixture of Methane and Hydrogen for Various Equivalence Ratios at a Compression ratio of 10:1, Spark Timing of 15 BTC and Initial Mixture Temperature of 295K in CFR Engine at 900 rev./min.

in the electrolysis process in general, enhances the performance of the spark ignition engine further. The slightly oxygen rich intake mixture relative to common air tends to increase the burning rates while affecting only very marginally the total energy input of the mixture. Thus, the increased presence of the products of electrolysis of water further augmented the power output of the engine, as shown in Figures 7.9 to 7.11 for different equivalence ratios, compression ratios and initial mixture temperatures respectively. The increased presence of hydrogen and oxygen in the mixture, not only replaces methane by hydrogen but also some air is replaced by oxygen. In this approach, it has been assumed throughout that only hydrogen and oxygen are the products of water electrolysis and at the low temperatures involved no radicals are able to survive to the engine intake charge stage.

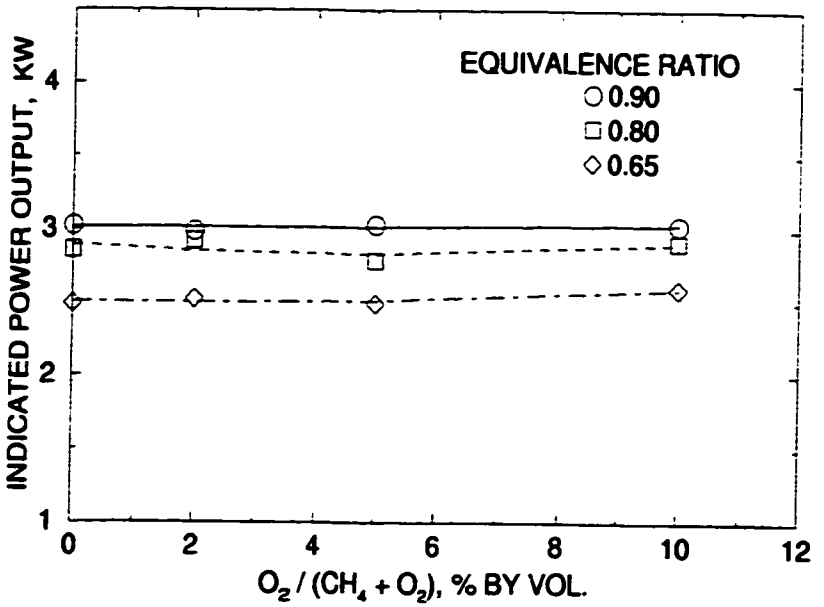

Figure 7.8: The Experimental Indicated Power Output Variations with Concentration of Oxygen in a Fuel Mixture of Methane and Oxygen for Various Equivalence Ratios at a Compression Ratio of 8.5:1, Spark Timing of 20 BTC and Initial Mixture Temperature of 294K in CFR Engine at 900 rev./min.

Similar trends to those of the analytical results can be seen experimentally when various combinations of hydrogen-oxygen mixtures, in their proportion in water, are added to a methane fueled engine as shown for two different compression ratios in Figure 7.12 and 7.13.

The effects of the presence of the hydrogen or hydrogen and oxygen in their proportion in water on the incidence of knock were considered analytically using the approach described earlier. The model considers knock to take place when the energy released due to the preignition reaction activity of the end gas ahead of the propagating flame becomes sufficiently intense to produce autoignition. For example, at a compression ratio of 10:1 and an equivalence ratio of 0.90, as shown in Figure 7.14, the preignition reaction activity of the end gas region becomes enhanced by the

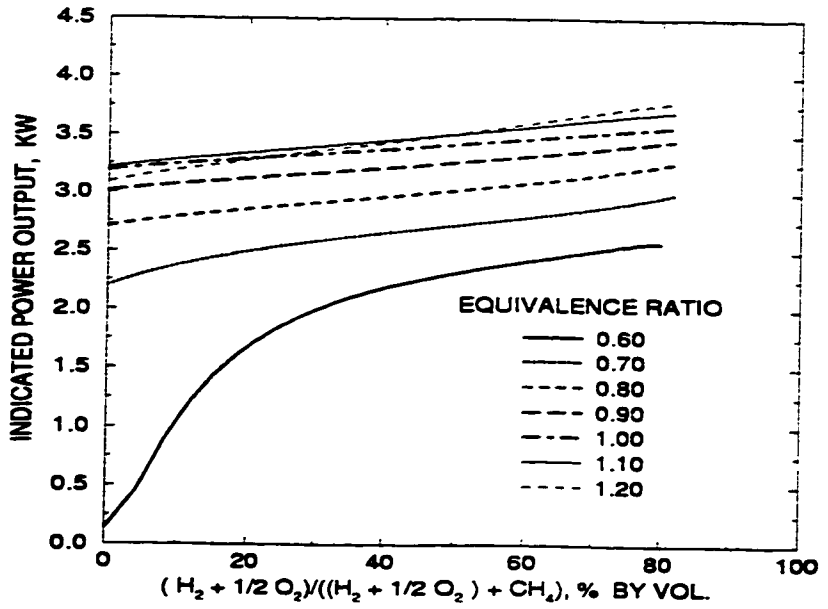

Figure 7.9: The Variations of Indicated Power Output Versus Concentration of Hydrogen and Oxygen in Their Proportions in Water in Fuel Mixtures for Various Equivalence Ratios at a Compression Ratio of 8.5:1, Spark Timing of 20 degrees BTC and Initial Temperature of 298 K.

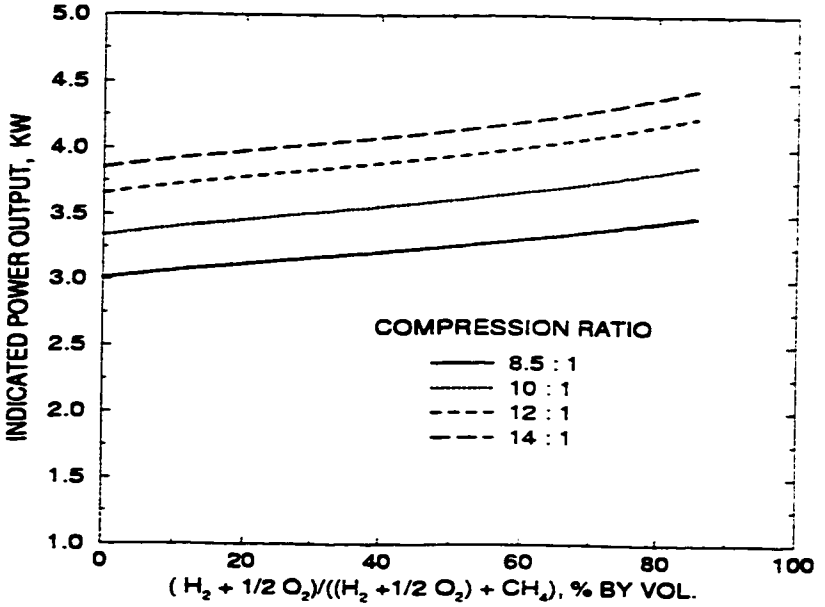

Figure 7.10: The Variations of Indicated Power Output Versus Concentration of Hydrogen and Oxygen in Their Proportions in Water in Fuel Mixtures for Different Compression Ratios at Equivalence Ratio of 0.90, Spark Timing of 20 degrees BTC and Initial Temperature of 298 K.

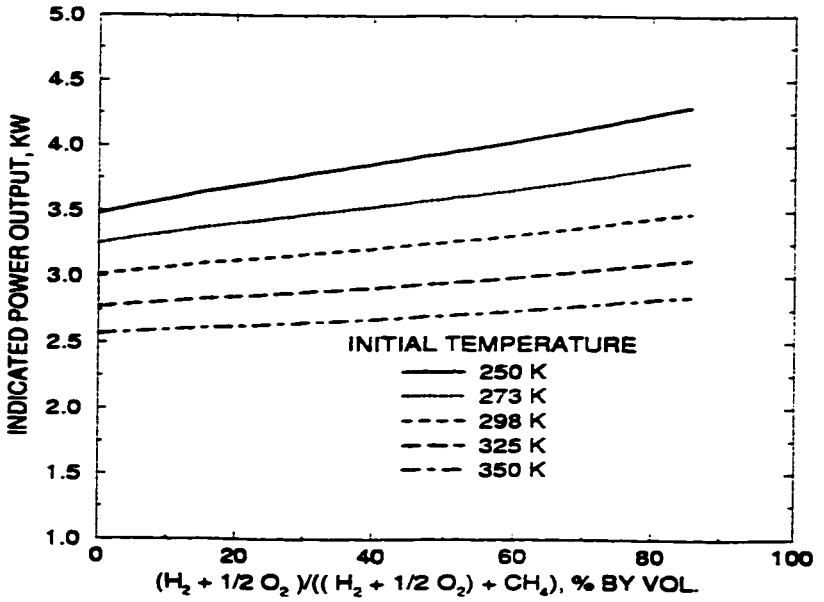

Figure 7.11: The Variations of Indicated Power Output Versus Concentration of Hydrogen and Oxygen in Their Proportions in Water in Fuel Mixtures for Different Initial Temperatures at a Compression Ratio of 8.5:1, Equivalence Ratio of 0.90 and Spark Timing of 20 degrees BTC.

increased presence of hydrogen or hydrogen and oxygen in their proportion in water indicating a greater tendency to knock than with methane for otherwise the same operating conditions.

It is essential whenever the question of hydrogen production on board is put forward that the energetic consequences of this production on the net engine power output must be fully and realistically accounted for. In Figure 7.15, the net energy enhancement due to the addition of hydrogen to the main fuel methane is compared with the energy required to produce the same amount of hydrogen in situ by electrolysis of water. This production energy was based on a 70 percent effectiveness of the electrolysis [156] and an overall electric generation and mechanical efficiency of 30 percent. The viable range of the operating conditions of the engine, as shown for

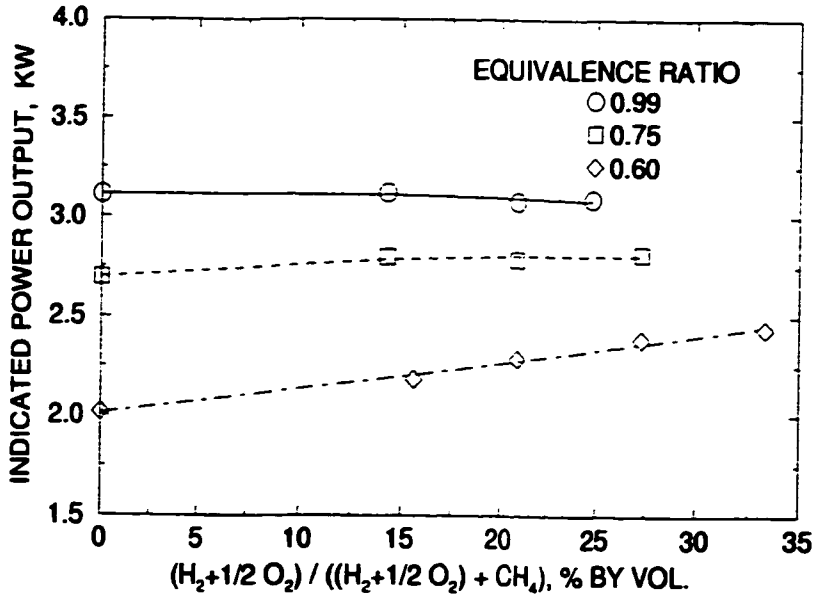

Figure 7.12: The Experimental Indicated Power Output Variations with Concentration of Hydrogen and Oxygen (as the Products of Electrical Dissociation of Water) to Methane for Various Equivalence Ratios at a Compression Ratio of 8.5:1, Spark Timing of 15 BTC and Initial Mixture Temperature of 294K.

a typical case, throughout is very narrow and limited. This would indicate, based on the work and conditions considered in this investigation that it is inadvisable to have the hydrogen produced by electrolysis despite the fact that the presence of the hydrogen with methane in moderate volumetric proportions (20 - 25 %) is certainly operationally attractive.

7.4 Conclusions

- The addition of the hydrogen with methane in moderate volumetric proportions (up to 20 %) can be operationally attractive.

- However, the addition of a small amount of oxygen to the main fuel methane did not produce a noticeable change in engine performance especially for lean

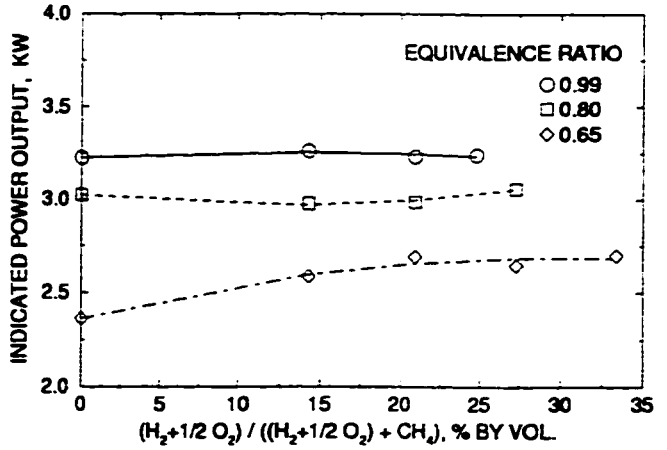

Figure 7.13: The Experimental Indicated Power Output Variations with Concentration of Hydrogen and Oxygen (as the Products of Electrical Dissociation of Water) to Methane for Various Equivalence Ratios at a Compression Ratio of 10:1, Spark Timing of 15 BTC and Initial Mixture Temperature of 294K.

operations.

- The effect of the addition of a small quantity of the products of electrical dissociation of water to a S. I. Engine operating on methane was found both analytically and experimentally to enhance the performance, particularly when operating on relatively lean equivalence ratio mixtures.

- The overall effect of the production of the required amount of hydrogen and oxygen on board the engine through the electrolysis of water while consuming some of the engine output was found energetically to be not viable over much of the engine operating range.

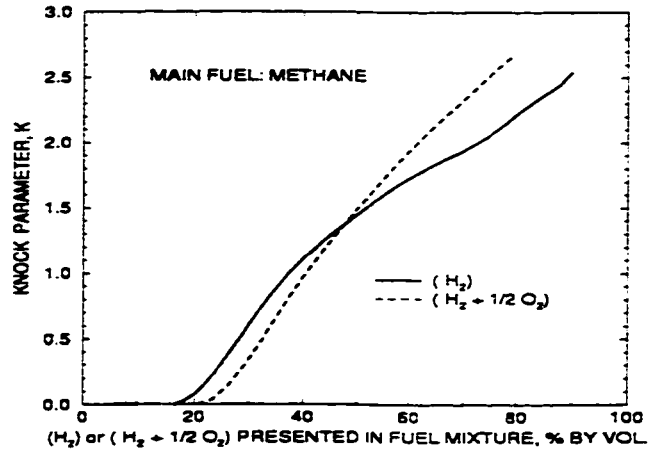

Figure 7.14: The Variations of Knock Parameter, K, Versus Concentration of Hydrogen and Oxygen in Their Proportions in Water in Fuel Mixtures for a Compression Ratio of 10:1, Spark Timing of 20 degrees BTC, Equivalence Ratio of 0.90 and Initial Temperature of 298 K.

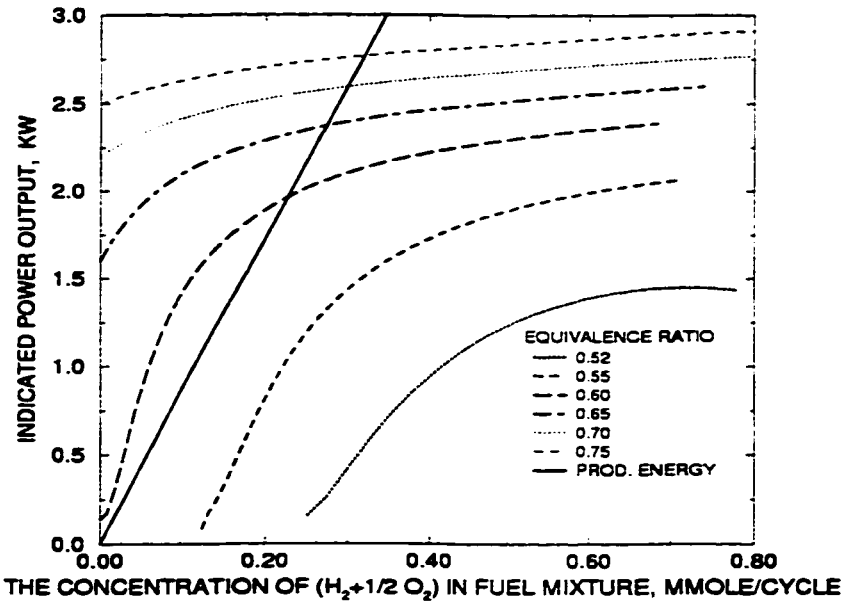

Figure 7.15: The Variations of Indicated Power Output Versus Concentration of Hydrogen and Oxygen in Their Proportions in Water in Fuel Mixtures for Various Equivalence Ratios at a Compression Ratio of 8.5:1, Spark Timing of 20 degrees BTC and Initial Temperature of 298 K. The Predicted Energy Consumption for the Electrolysis is also Shown.

Chapter 8

CYCLIC VARIATIONS IN S. I. ENGINE - A STOCHASTIC APPROACH

8.1 Introduction

Cycle to cycle variations in the combustion process in engines are particularly important for two reasons. First, the spark timing is usually set optimally for the average cycles. Thus, faster-than-average cycles would have effectively an over advanced timing while slower-than-average cycles would have an over retarded timing, which lead to losses in power and efficiency and may lead to increased levels of emissions. Second, it is the extremes in the cyclic variations that often limit engine operation since the cycles with the over advanced spark timing are the first most likely to knock. Thus, they would determine the fuel Octane Number requirements of the engine and limit the compression ratio that can be used and hence engine efficiency. The cycles with a spark timing retarded relative to the optimum value are most likely not to burn completely and would set the practical lean operational limit of the engine. They would also limit the amount of exhaust gas recycling which is used chiefly for NO emissions control, that can be tolerated by the engine.

As discussed earlier cyclic variation in engines is a complex phenomenon and depends upon a number of operating and design factors. Some of these, for example, include the cyclic variations in the gas motion during combustion, variations in the

amounts of fuel, air and exhaust gas supplied to any given cylinder and variations in mixture composition within the cylinder, especially near the spark plug. Some of the design factors include the shape and size of combustion chamber, location and number of spark plugs used and the shape and type of valves employed (e.g. [4, 16, 71, 92, 76, 75, 157, 158]).

Traditionally, the cylinder pressure has been used to indicate the extent of cyclic fluctuations. This has led to the use of pressure related parameters to quantify the fluctuation intensity. The maximum value of cylinder pressure, P_{max}, and its crank angle location are the frequently used parameters [4, 71]. The variation in the indicated mean effective pressure, *imep*, produced is also an often-used parameter although as an integrated parameter it is less sensitive to combustion variations than for example, the maximum pressure. Other parameters generally used to characterize the cycle to cycle variations are flame arrival times at several locations in the cylinder [159, 160, 161, 82], maximum rate of pressure rise and its crank angle location and integrated parameters such as the indicated power output. The standard deviation is usually normalized by the mean value to give a coefficient of variation (e. g. $COV_{P_{max}}$ or COV_{imep}, [71]). The COV_{imep} can also indicate how much torque fluctuations the transmission etc. can tolerate which makes it a good parameter to use for transmission design and to serve as a general indicator of engine behaviour and vehicle driveability [104].

One of the main drawbacks with using traditional parameters such as P_{max} and *imep* derived from the direct measurement of pressure for quantifying the consequences of cyclic variations is the corresponding lack of knowledge of the ongoing processes. It is reasonable to assume that changes in the pressure from cycle to cycle

are mainly due to variations in the combustion process. Sarpal [118] and Soriano [162] found experimentally that when key operational parameters such as equivalence ratio, spark timing and initial temperature were closely controlled, the cyclic pressure variations were mainly due to the variations in the combustion process. Hence, measured pressure values may be used in a heat release model and then to analyze the resulting variations in the heat release function instead of the pressure trace. Another drawback with the traditional approach that uses a small sample of characteristic point values, such as P_{max} or the crank angle at P_{max} (e.g. [93, 113]), is that much of the information contained in the measurement is discarded. Thus, subsequent analysis depends critically on the implicit assumption that these simple statistics do indeed accurately characterize the entire set of time histories.

In this chapter an approach, based on the stochastic modeling of cyclic pressure variations is introduced. In this approach, rather than simply quantifying cyclic variations partially through some point values, a stochastic model for the cycle by cycle variations of the entire pressure/time development over the whole cycle, including the combustion period, is established. Such a model not only provides a more complete representation of the cyclic variations but also enables realistic, cyclically varying pressure-time histories to be generated through simulation.

In the present approach, the bulk of the cycle by cycle pressure variations is encapsulated in a sequence of cyclically varying parameters, whose distribution and correlation comprise a description of the stochastic process model. In many cases these can be approximated by a set of correlated random variables, providing a basis for generating sets of pressure traces with very similar statistical properties to the original data. The stochastic model, therefore, could be used to derive other related

parameters of interest, such as the variations in the *imep*, maximum pressure or crank angle of 50% burn. Moreover, the approach could be adopted to estimate the probability of the incidence of knock in a spark ignition engine at given operating conditions and can suggest ways to improve the efficiency of the engine through, for example, increasing the compression ratio such that the probability of the incidence of knock is kept within an allowable range. Thus, this approach demonstrates that it is possible to characterize the entire time history of cyclic pressure variations through the statistics of a small set of model parameters, providing a much more complete quantification of the phenomena than previously available and a basis for simulating statistically identical pressure time traces.

8.2 The Approach

In principle, the cycle to cycle variations in the combustion process can be attributed to the cyclic variations in any of the parameters known to affect the course of combustion. Several empirical and semi-empirical models have been developed to relate variations in combustion and pressure development to variations in the velocity of the charge (e.g. [16, 104, 105, 106, 99, 88]) and most of the models developed were based on the assumption that cyclic variations in velocity early in the combustion period in the vicinity of the spark gap were mainly responsible for the combustion variations.

Since cyclic variations in the spark ignition engine, as mentioned earlier, is a complex phenomenon that depends upon a number of independent parameters, some researchers [15, 71, 113, 114, 115] considered the cyclic variational process as a

stochastic process of random nature, which is generally consistent with experiment (e.g. [71, 117, 118]). The present approach also uses the stochastic modeling of cyclic variations while using the deterministic model described in Chapter 3 which avoids the prediction of the detailed features of turbulent flame propagation. Once the characteristics of the stochastic model parameters were established, cyclic varying processes could be simulated for any given operating condition. This could eliminate or reduce the need for a large number of observations to analyse cyclic variations in engines saving time and resources.

8.2.1 Experimental Data Collection

The experimental data were collected in the variable compression ratio spark ignition CFR engine according to the experimental set up described in Chapter 4. For each operating condition, the temporal pressure development data were collected for consecutive 500 engine cycles and the first 100 of them, as suggested by Karim [71] and Curry [160], were selected for further analysis in order to save computational time and resources. All the experiments presented here were conducted with the gaseous fuel methane at a constant speed of 900 rev./min. and atmospheric pressure. The typical data collected were for the ten different operating conditions presented in Table 8.1.

As a typical example, the extent of variation in pressure development with time for the experimental data is shown in Figure 8.1 along with their experimental average. The simulated pressure time diagrams for the corresponding operating conditions using the deterministic model as described in Chapter 3 is also shown. These diagrams indicate clearly that the most severe variations in pressure development

Table 8.1: Different Operating Conditions for Experimental Data Collection in CFR Engine Fueled with Methane

Data Set No.	Equivalence Ratio	Compression Ratio	Spark Timing degrees BTC	Initial Temp--erature, K
1	0.66	8.5	20	294
2	0.80	8.5	20	294
3	0.99	8.5	20	294
4	1.10	8.5	20	294
5	0.99	8.5	15	294
6	0.99	8.5	30	294
7	0.65	10.0	20	294
8	0.80	10.0	20	294
9	0.99	10.0	20	294
10	0.99	11.0	20	294

occur during the combustion period reflecting that the variation in engine operation is fundamentally related to the variations in combustion from one cycle to the next.

One of the important factors influencing the cyclic variation of combustion and the subsequent pressure development in the engine was found to be the equivalence ratio of the fuel-air mixture. Generally, minimum cyclic variations were found to occur at a slightly rich equivalence ratio corresponding approximately to the maximum power fuel-air ratio [71, 72, 74, 75, 73]. As the mixture of fuel and air becomes much leaner or richer, the combustion variation starts to increase. It can be also seen in Figure 8.2 where the dependence of the coefficients of variation of the maximum pressure, P_{max}, and the crank angle of its occurrence, $\theta_{P_{max}}$ as well as the intregated parameter such as the indicated mean effective pressure, P_{imep}, is shown. These results indicate that the cyclic variation is a minimum at the equivalence ratios where the burning rates are maximum corresponding to the shortest combustion durations and the best power values, as expected.

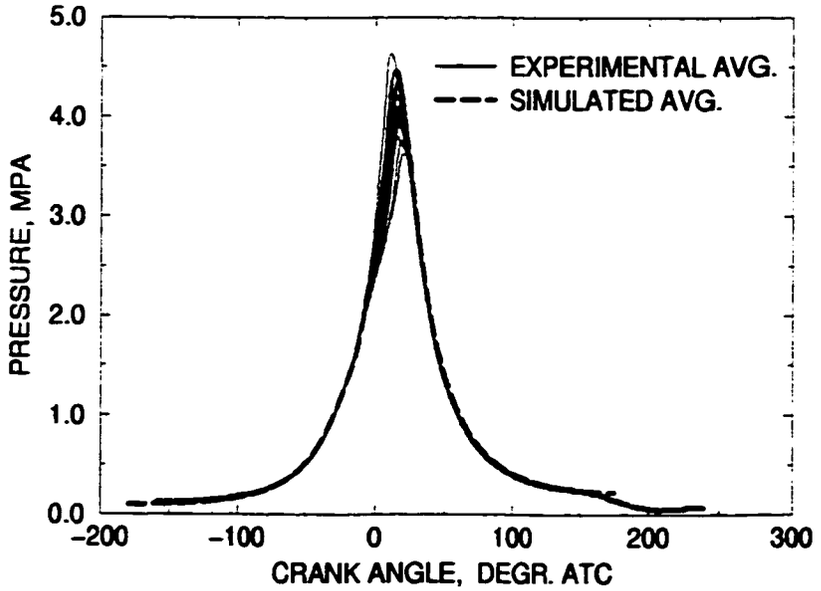

Figure 8.1: A Typical Cyclic Variations of Pressure-Time Histories at Equivalence Ratio of 0.99, Compression Ratio of 8.5:1, Spark Timing of 20 degrees BTC and Initial Temperature of 294 K (Experimental Data Set No. 3). The Corresponding Experimental Average and Simulated Base/Average from the Model are also Shown.

The phasing of the combustion process relative to the cylinder volume changes plays an important role in determining the character of the pressure and engine output variations. For a given variation of burning rate for example, the pressure variations are not as severe for faster burning charges as for slower ones. For the fast-burning cases, a large fraction of the energy release occurs near top dead centre, when the combustion chamber volume is changing relatively very slowly. As a result, the pressure variations are due mainly to the combustion variations. With slower burning, where a large part of the energy release occurs later in the cycle, the variations in pressure due to the combustion variation is augmented considerably by the changes in pressure due to the rapidly varying cylinder volume during this part of the cycle. As a typical example, the character of the maximum pressure variations

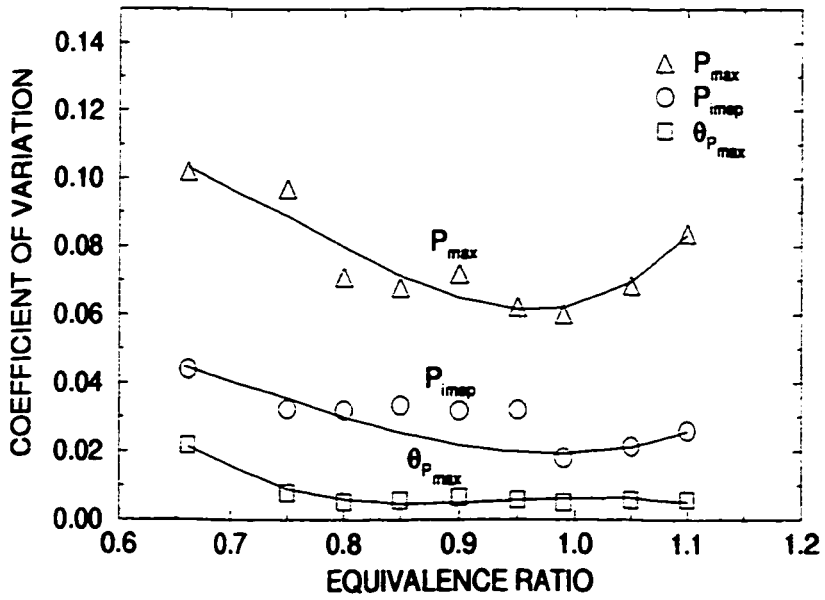

Figure 8.2: The Coefficient of Variations of Various Parameters for Different Equivalence Ratios at a Compression Ratio of 8.5:1, Spark Timing of 20 degrees BTC and Initial Temperature of 294 K.

is illustrated in Figure 8.3 for two mixtures of near stoichiometric and lean equivalence ratios. For the faster burning mixture of an equivalence ratio of 0.99, the histogram of the maximum pressure variations is somewhat close to normal distribution. However, for the lean equivalence ratio mixture with much slower burning rate and longer combustion duration, the histogram of the maximum pressure variations appears clearly to be skewed to the right [71, 30, 105, 114, 115] reflecting the predominant influence of the rapid changes in cylinder volume during combustion [71]. Due to the lower sensitivity of the indicated mean effective pressure to cyclic variations, such characteristics, as shown in Figure 8.4, tend to be less pronounced in comparison to the variation in the previous more marked case. Similarly, the histograms of the crank angle for the occurrence of maximum pressure, for both equivalence ratios 0.99 and 0.66 as shown in Figures 8.5, tend to show the frequency of distributions for

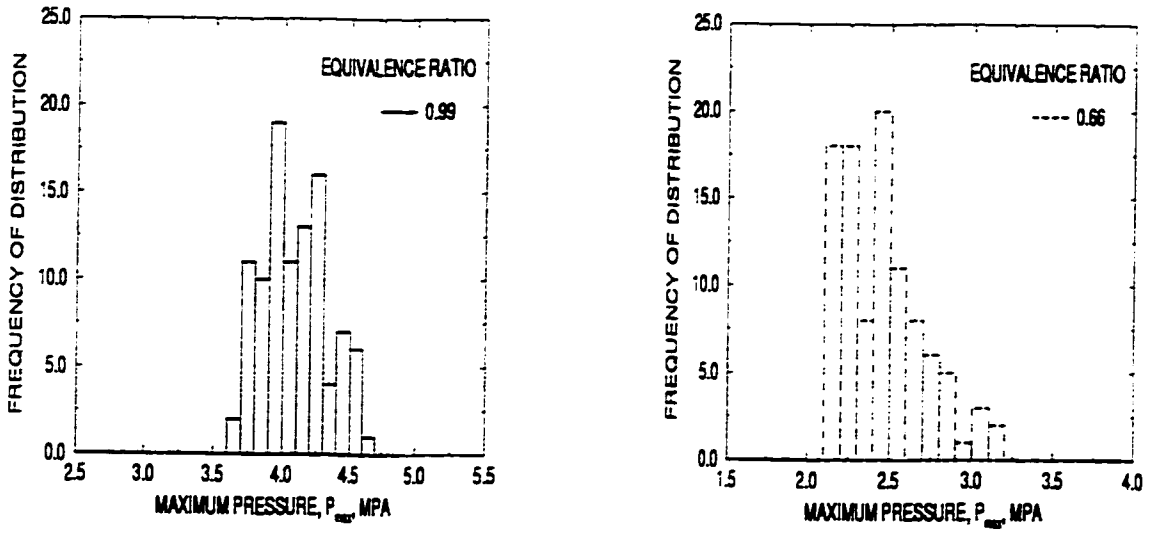

Figure 8.3: The Frequency of Distributions of Maximum Pressures for Different Equivalence Ratios at a Compression Ratio of 8.5:1, Spark Timing of 20 degrees BTC and Initial Temperature of 294 K.

the near stoichiometric mixture appears closer to being normal, while, for the lean mixture case the distribution appears to be more random and widely spread. The histograms of the combustion duration and the crank angle at maximum burning rate which is normalized to the corresponding combustion duration, as shown for different equivalence ratios in Figures 8.6 and 8.7, appear to be near normal for the stoichiometric case but the corresponding data for the very lean mixture, are spread more widely especially for the crank angle at maximum burning rate, θ_{max}.

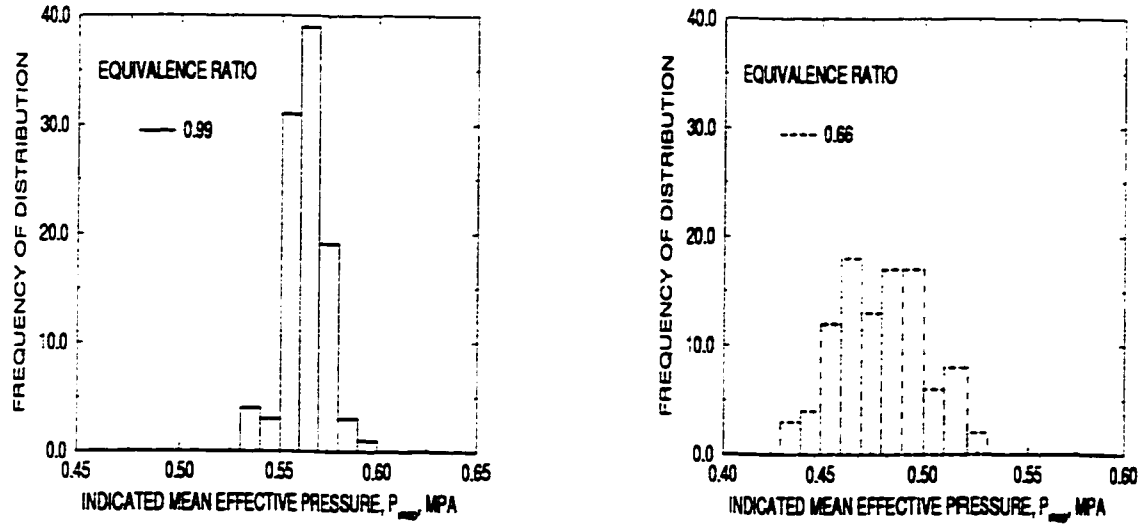

Figure 8.4: The Frequency of Distribution of Indicated Mean Effective Pressure for Different Equivalence Ratios at a Compression Ratio of 8.5:1, Spark Timing of 20 degrees BTC and Initial Temperature of 294 K.

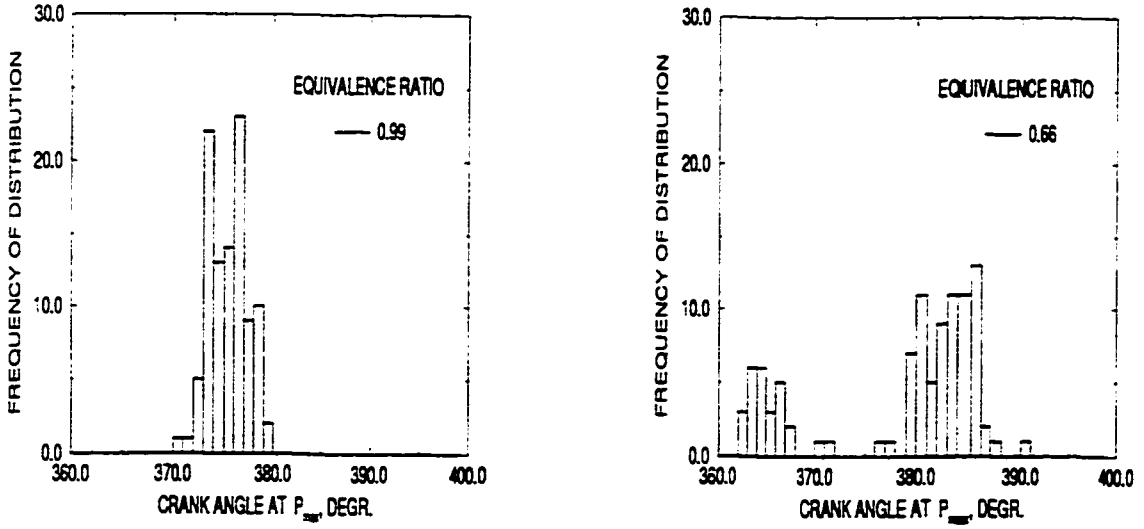

Figure 8.5: The Frequency of Distribution of Crank Angle at P_{max} for Different Equivalence Ratios at a Compression Ratio of 8.5:1, Spark Timing of 20 degrees BTC and Initial Temperature of 294 K.

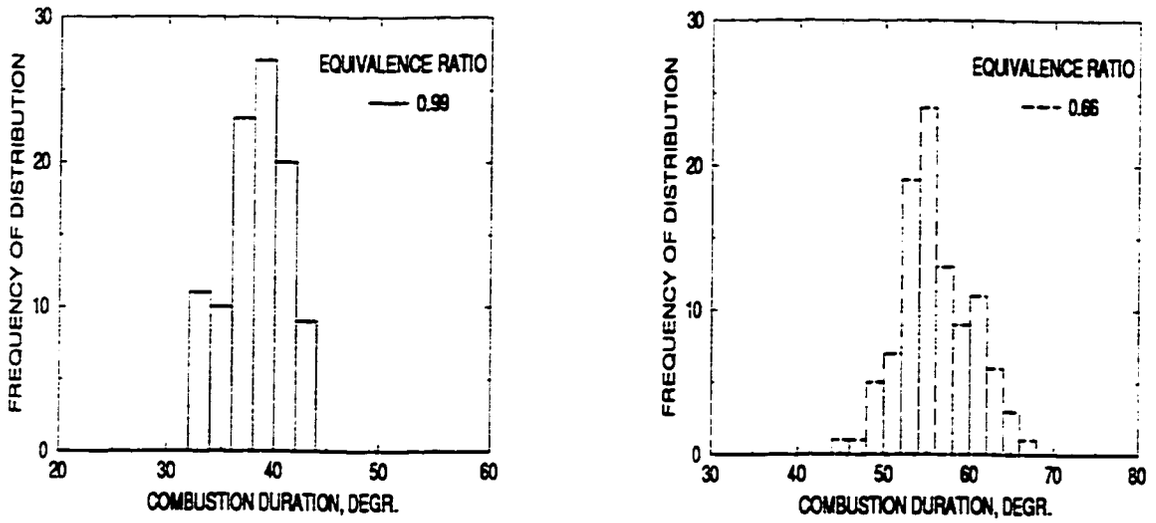

Figure 8.6: The Frequency of Distribution of Combustion Duration, $\Delta\theta_c$, for Different Equivalence Ratios at a Compression Ratio of 8.5:1, Spark Timing of 20 degrees BTC and Initial Temperature of 294 K.

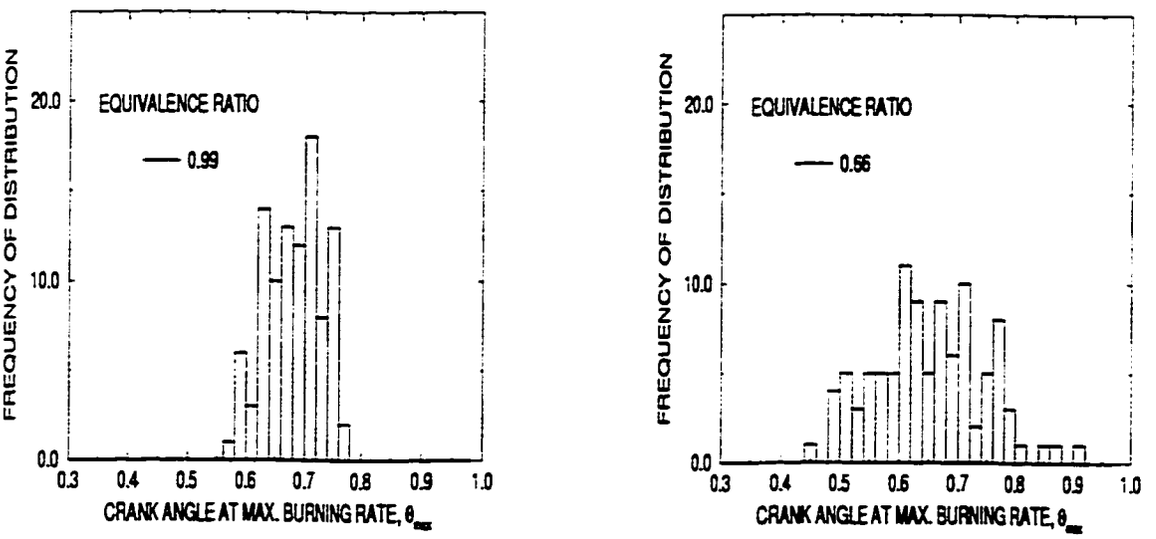

Figure 8.7: The Frequency of Distribution of Normalized Crank Angle at Maximum Burning Rate, θ_{max} for Different Equivalence Ratios at a Compression Ratio of 8.5:1, Spark Timing of 20 degrees BTC and Initial Temperature of 294 K.

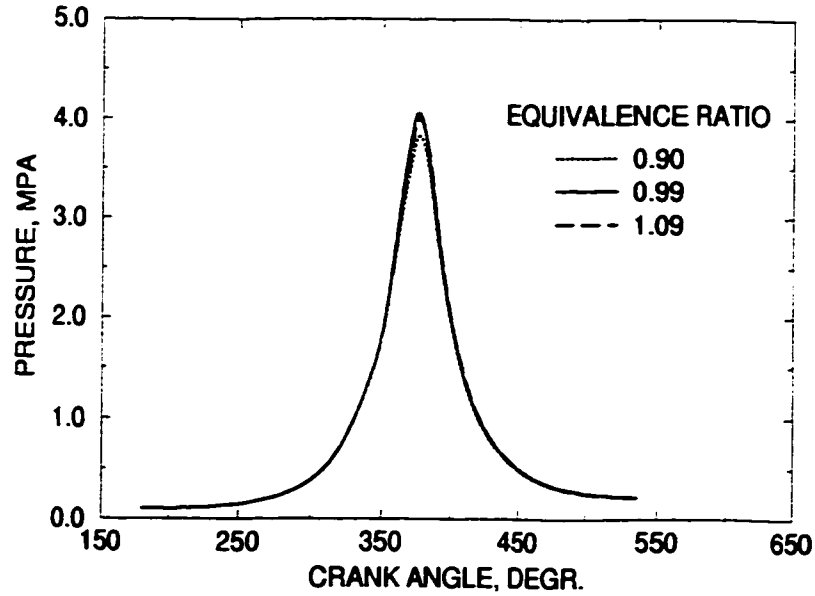

Figure 8.8: The Typical Variations of Cyclic Pressure in the Cylinder for 10% Changes in Equivalence Ratio at a Compression Ratio of 8.5:1, Spark Timing of 20 degrees BTC and Initial Temperature of 294 K.

8.2.2 Parametric Study

The effect of the perturbations of each operating parameter on engine performance were investigated analytically. As shown in Figure 8.8, it appears that a perturbation of 10% in the equivalence ratio could not match the extent of variations in pressure observed (e. g. in Figure 8.1). A similar perturbation in turn in the values of spark timing, initial mixture temperature and pressure, as shown in Figures 8.9 to 8.11, also did not influence very significantly the variations in cylinder pressure [126]. Moreover, in our experimental testing, where all operating parameters were closely monitored and controlled, a level of 10% cyclic variation in any of the operating parameter was unlikely. However, the impact of changes in compression ratio which can be seen in Figure 8.12 to be pronounced, is a minor consequence since such a

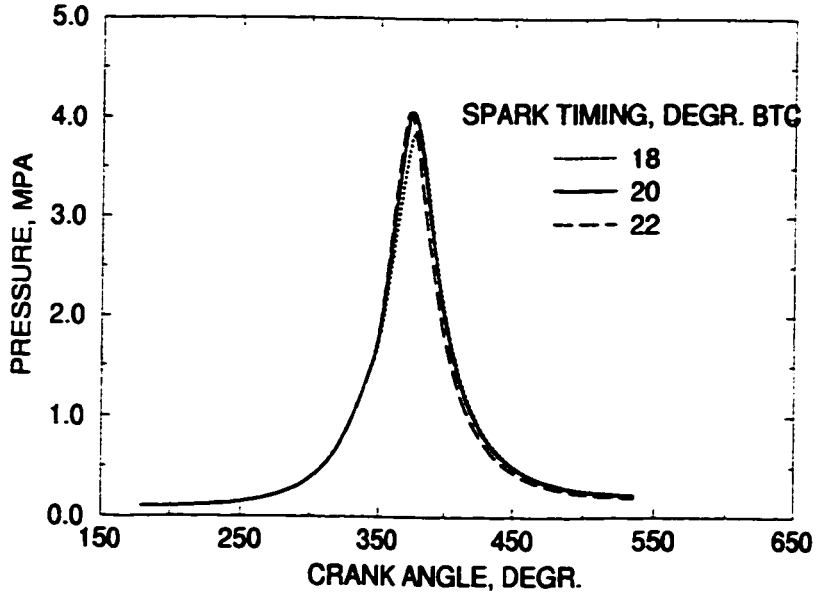

Figure 8.9: The Typical Variations of Cyclic Pressure in the Cylinder for 10% Changes in Spark Timing at Equivalence Ratio of 0.99, Compression Ratio of 8.5:1 and Initial Temperature of 294 K.

variation in practice is normally highly unlikely.

As was indicated earlier, the cyclic variations in the cylinder pressure are mainly due to variations in the combustion process. Thus, it would be reasonable to consider the variations in the energy/heat release rate function as a consequence of the variations in the combustion process contribute mainly to the observed variations in cylinder pressure. Moreover, as demonstrated in the previous section, the analysis of the experimental data showed that the variations in these energy release function parameters, namely the combustion duration, $\Delta\theta_c$, and the crank angle at which maximum burning rate, θ_{max}, takes place were more severe than any other operating parameter considered.

Figure 8.13 shows a typical example when various perturbations in the location of $\theta_{\max}$ produced substantial changes to the cylinder pressure development with

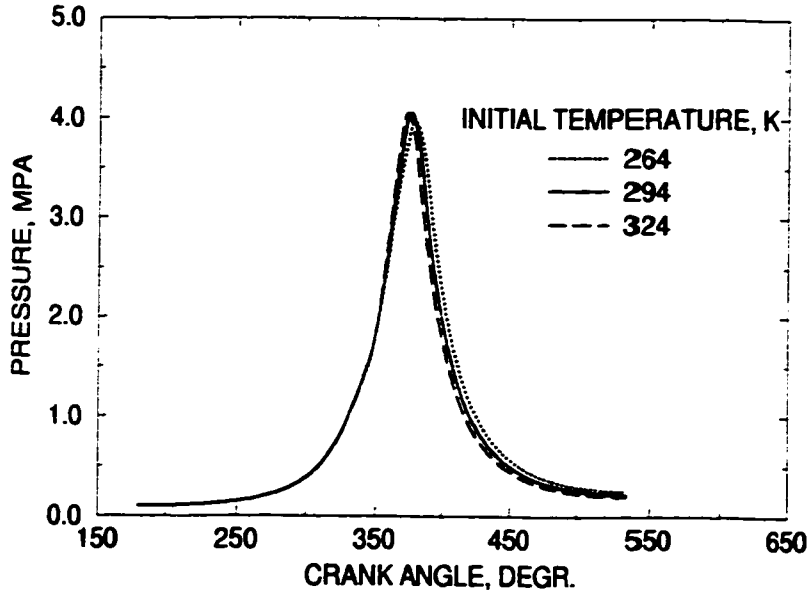

Figure 8.10: The Typical Variations of Cyclic Pressure in the Cylinder for 10% Changes in Initial Temperature at Equivalence Ratio of 0.99, Compression Ratio of 8.5:1 and Spark Timing of 20 degrees BTC.

time. Moreover, the experimentally observed extent of variation in θ_{max}, as shown in Figure 8.7, was generally much higher than 10%. The corresponding effect of small variations (e. g. 10%) in the length of the combustion duration is shown in Figure 8.14. The experimentally observed cyclic variations in the combustion durations (for example, as shown for the experimental data sets No. 1 and 3 in Figure 8.6) had much higher values than 10%, depending upon the operating conditions.

In principle, any set of parameters that can influence the extent of cyclic variation in S. I. Engines can be considered as a set of the stochastic model parameters for the simulation. However, some parameters have a stronger influence than others as illustrated earlier. Therefore, to keep the model as simple as possible, the number of the independent variables to be considered needs to be reduced to a minimum as far as possible. Furthermore, the examination of the real physical possibilities of the

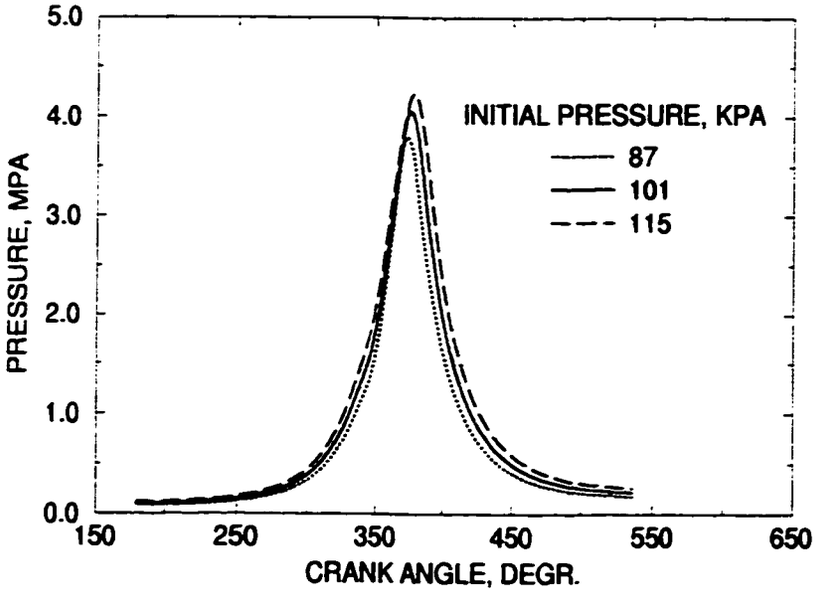

Figure 8.11: The Typical Variations of Cyclic Pressure in the Cylinder for 10% Changes in Initial Pressure at Spark Timing of 20 degrees BTC, Equivalence Ratio of 0.99, Compression Ratio of 8.5:1 and Initial Temperature of 294 K.

extent of cyclic variations in the values of selected independent variables needs to be considered for the given operating conditions and set-up.

Accordingly, because of the severe cyclic variations in combustion parameters in comparison to other parameters and merely to keep the model as simple as possible the energy release parameters of the deterministic model of Chapter 3 namely, the crank angle of the maximum heat release, θ_{max} and the combustion duration $\Delta\theta_c$ were considered as the stochastic model parameters for the simulation. However, any other set of parameters can also be included easily if found necessary, which is very much less likely.

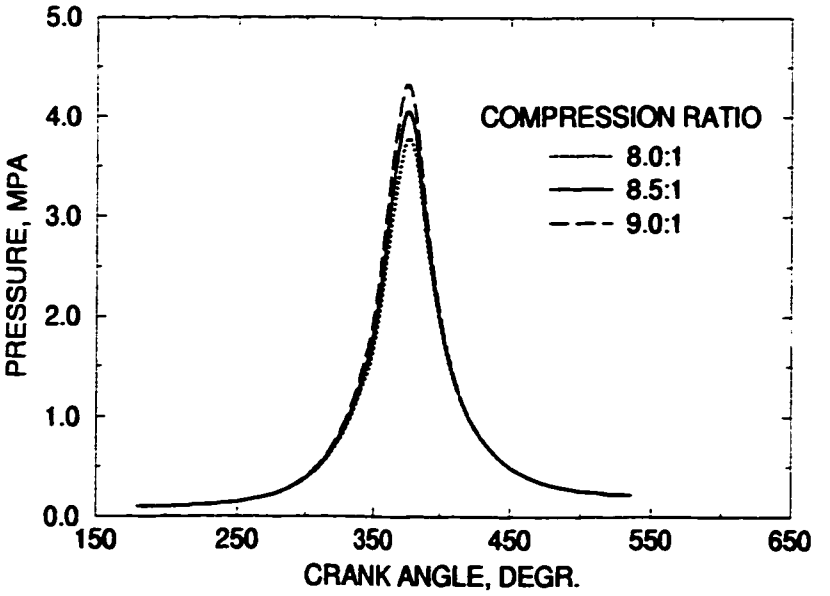

Figure 8.12: The Typical Variations of Cyclic Pressure in the Cylinder for Changes in Compression Ratio at Equivalence Ratio of 0.99, Spark Timing of 20 degrees BTC and Initial Temperature of 294 K.

8.2.3 Simulation of Experimental Cycles

The simulation of 100 cycles for each data sets of Table 8.1 were generated using the deterministic model described in Chapter 3 as a base (or simulated mean) at the corresponding operating conditions. The values of the identified stochastic parameters in previous section of the model can be found by fitting the simulated model to the corresponding experimental data on a cycle by cycle basis. The aim is to reduce the residual error, as far as possible, between the simulated and corresponding experimental cylinder pressures at the same crank angle, i.e. :

$$\Delta R_j = \sum_i (P_{e,i} - P_{s,i})^2 \tag{8.1}$$

- where, ΔR_j is the residual error of the "j"th cycle,

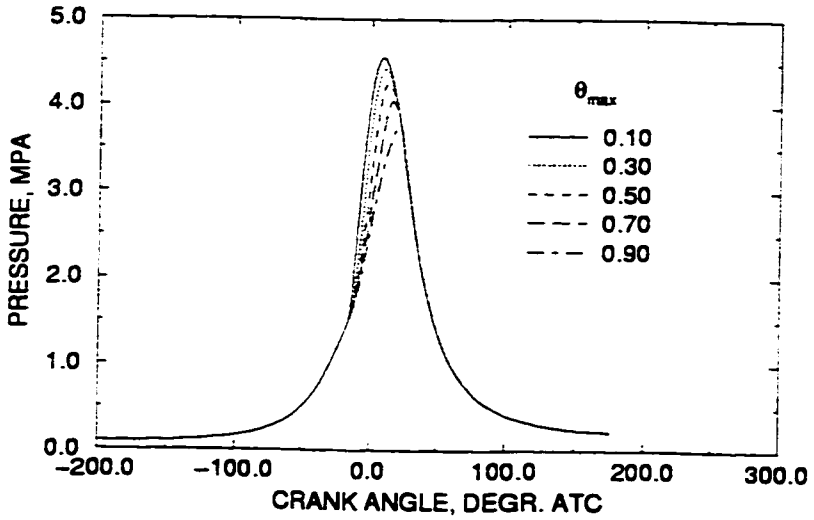

Figure 8.13: The Typical Variations of Cyclic Pressure in the Cylinder for Various Changes in the Normalized Crank Angle of Maximum Burning Rate, θ_{max}, in Fraction of Combustion Duration at Equivalence Ratio of 0.99, Compression Ratio of 8.5:1, Spark Timing of 20 degrees BTC and Initial Temperature of 294 K.

- $P_{e,i}$ is the measured pressure at the crank angle "i" and
- $P_{s,i}$ is the simulated pressure at the corresponding crank angle.

The residual error is calculated as a sum of the square of the errors in order to reflect the phase as well as the magnitude of pressure differences between the simulated and corresponding experimental values. Since the major pressure variations occur during the combustion period and to economize in computational time, the residual error was evaluated over the combustion duration only [114, 115].

In principle, different numerical methods can be adopted to minimize the residual error function of Equation 8.1, e.g. the least square minimization method and gradient method. The multi variable gradient method [163] was adopted in this

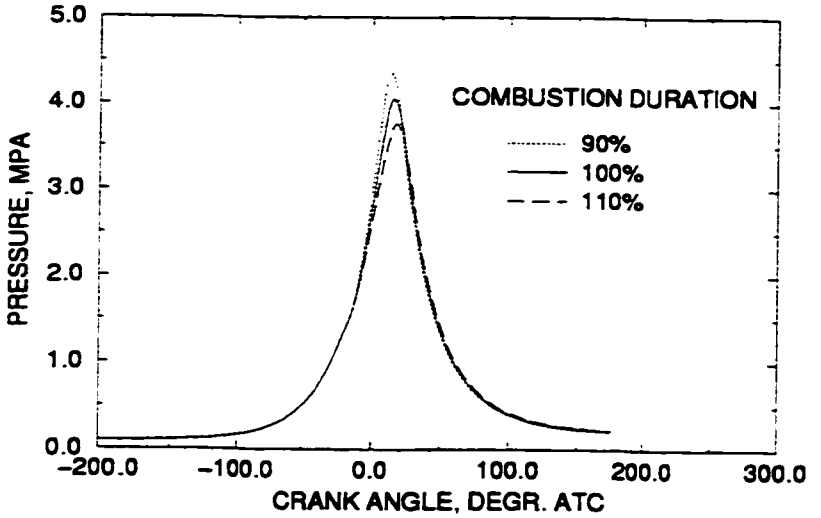

Figure 8.14: The Typical Variations of Cyclic Pressure in the Cylinder for 10% Changes in Combustion Duration at Spark Timing of 20 degrees BTC, Equivalence Ratio of 0.99, Compression Ratio of 8.5:1 and Initial Temperature of 294 K.

approach, i.e.:

$$P_{s,i} = F(x_k) \tag{8.2}$$

the gradient vector is evaluated as:

$$g_i = g(x_k) = \nabla F(x_k) = (\frac{\delta F}{x_1}, \frac{\delta F}{x_2} \ldots\ldots\ldots \frac{\delta F}{x_k}) \tag{8.3}$$

Accordingly, the experimental cycles were regenerated cycle by cycle using the simulation model. As a typical example Figures 8.15 shows the level of agreement (e. g. for the data set No. 3) between the simulated and the corresponding experimental values of the cylinder pressure for five arbitrarily selected engine cycles out of 100. The corresponding values of the stochastic parameters; the crank angle

at the maximum burning rate, θ_{max} (in the fraction of combustion duration), the combustion duration, $\Delta\theta_c$, and the residual errors following the fitting of all engine cycles for each data set were evaluated.

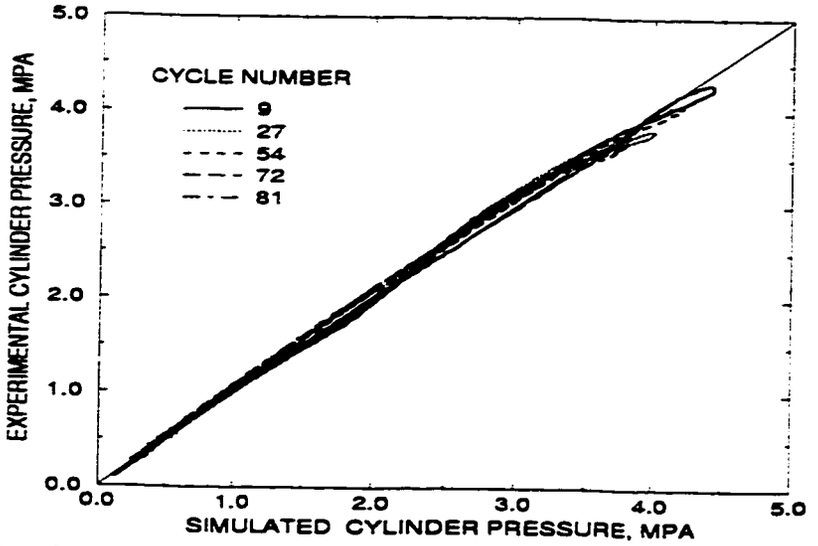

Figure 8.15: The Comparison Between the Experimental and Simulated Variations in Cylinder Pressure for Different Engine Cycles at Equivalence Ratio of 0.99, Compression Ratio of 8.5:1, Spark Timing of 20 degrees BTC and Initial Temperature of 294 K (Data Set No. 3).

Although these graphs (e. g. Figure 8.15) provide a useful visual impression of the ability of the model to characterize cyclic pressure variations, it is also useful to develop some quantitative measures with which to compare the results of different data sets and even the performance of a different model, if any. A simple and common measure is given by the mean residual error taken over all cycles and crank angles, i.e.

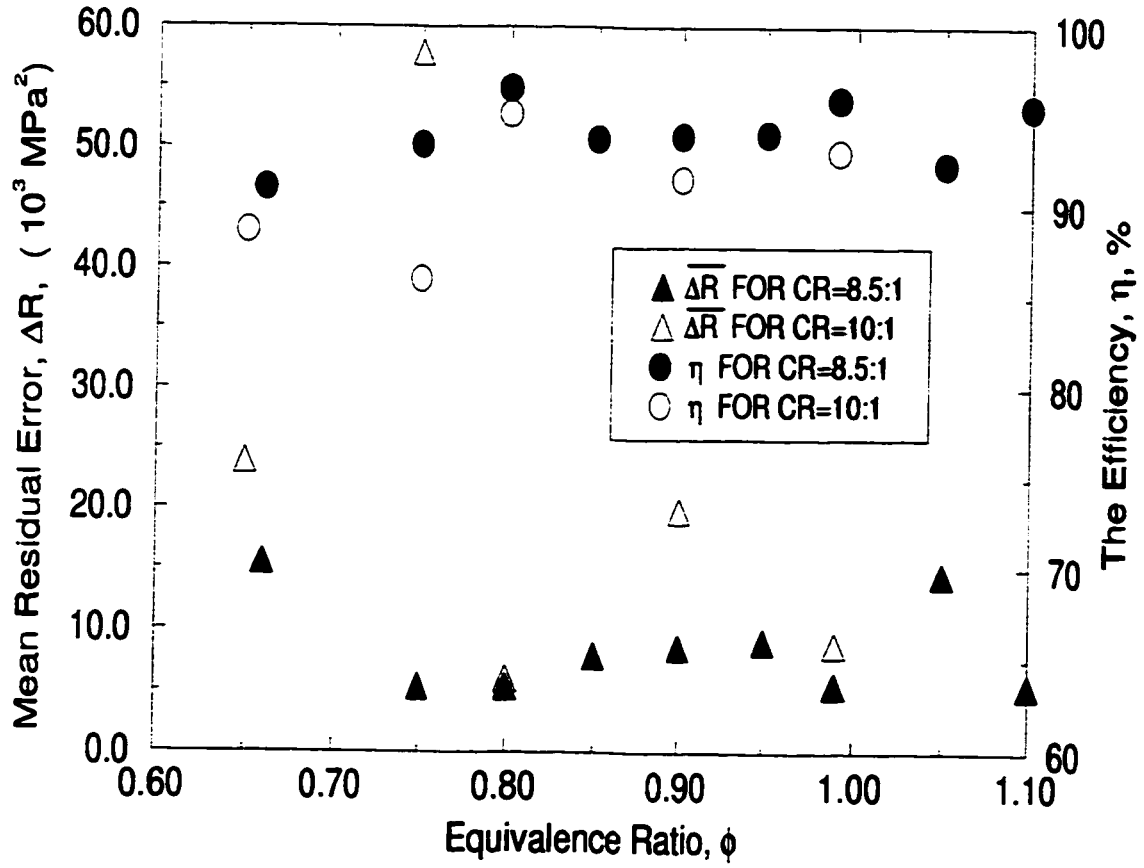

Figure 8.16: The Value of Mean Residual Error and the Efficiency of Simulation Versus Equivalence Ratio for Different Compression Ratios at Spark Timing of 20 degrees BTC and Initial Temperature of 294 K.

$$\overline{\Delta R} = \frac{1}{N_j}\sum_j \overline{\Delta R_j} = \frac{1}{N_i N_j}\sum_i \sum_j (P_{e,i} - P_{s,i})_j^2 \qquad (8.4)$$

Another useful measure to define the level of fitness of the simulated cycles is a non-dimensional parameter, which we can describe as the "efficiency of simulation", η . It is defined as:

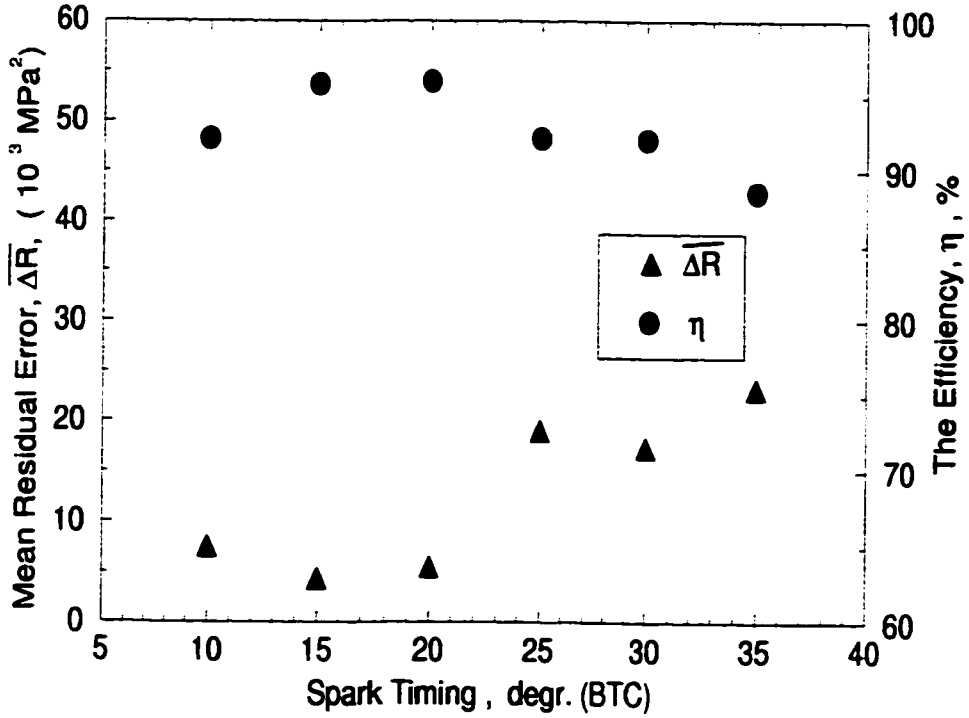

Figure 8.17: The Value of Mean Residual Error and the Efficiency of Simulation Versus Spark Timing at Equivalence Ratio of 0.99, Compression Ratio of 8.5:1 and Initial Temperature of 294 K.

$$\eta = 1 - \sqrt{\frac{1}{N_i N_j} \sum_i \sum_j \left(1 - \frac{P_{s,i}}{P_{e,i}}\right)^2_j} \tag{8.5}$$

An efficiency of simulation of one (i. e. $\eta = 1$), for example, would indicate that the cyclic pressure variations had been perfectly modeled, whilst an efficiency of $\eta = 0$ would indicate that nothing was known about the cyclic variations and mean pressure ensembles.

The efficiencies and mean residual error have been evaluated for a number of data sets including those in Table 8.1 and shown as a typical example in Figure 8.16

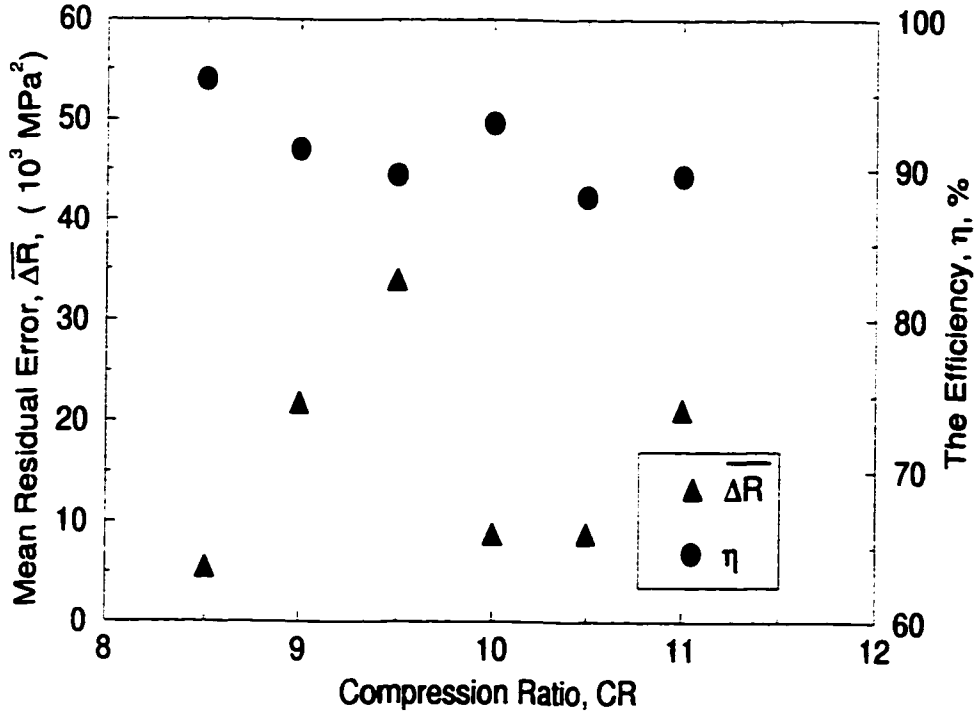

Figure 8.18: The Value of Mean Residual Error and the Efficiency of Simulation Versus Compression Ratio at Spark Timing of 20 degrees BTC, Equivalence Ratio of 0.99 and Initial Temperature of 294 K.

to 8.18 against equivalence ratio, spark timing and compression ratio, respectively. As it can be seen from these figures the agreement between the simulated and the corresponding experimental engine cycles were very good since the mean residual errors were small, except as expected for the very lean operating conditions. The efficiency of the simulation was about 90% or more for the simulation conducted.

8.2.4 The Statistical Analysis of Stochastic Parameters

The combustion model used is not in itself a stochastic model of the cylinder pressure development unless the statics of the model parameter are also defined. The typical probability/frequency distributions of the identified model parameters, the crank

angle of maximum burning rate, θ_{max}, and the combustion duration, $\Delta\theta_c$, for each data sets were evaluated. A typical example for the data set No. 2 is shown in Figures 8.19 and 8.20 respectively while more examples are included in Appendix (E). The majority of distributions appears approximately Gaussian. However, the skewness to the left was clearly evident for very lean operating conditions (e. g. in Figures E.1 and E.6 of Appendix E). More quantitatively, the RMS (root mean square), skewness and kurtosis of the identified parameters were evaluated for all data sets and are presented in Tables 8.2 and 8.3 for the crank angle of maximum burning rate, θ_{max}, and combustion duration, $\Delta\theta_c$, respectively. These values can be used to test if the corresponding distribution is significantly non-Gaussian, or if a Gaussian distribution is statistically justifiable. In particular, the standard deviation of the skewness estimated from N samples of a Gaussian population is approximately $\sqrt{15/N}$, and that of the kurtosis is $\sqrt{96/N}$ [114, 115]. In this case, using a set of 100 samples, a distribution should be considered significantly non-Gaussian if its skewness and kurtosis fall outside the 95% confidence limits of 0 ± 0.76 and 3 ± 1.92, respectively [114, 115, 164, 165]. As it can be seen that most of the distributions of the stochastic model parameters fall into the Gaussian distribution and are therefore relatively straightforward to characterize.

The analysis of the variance of the model parameters were presented in Table 8.4 for the crank angle at the maximum burning rate, θ_{max} and in Table 8.5 for the combustion duration, $\Delta\theta_c$. As stated earlier the distributions of the model parameters could be considered as approximately normal and different tests can be performed to investigate their variance. In this case, the Cochran's test and the F-distribution test were performed to check the equality of the several variances

Table 8.2: The Skewness and Kurtisos of Normalized Crank Angle of Maximum Burning Rate, θ_{max}, for Different Experimental Data Sets

Data Set No.	Mean Value	RMS σ	Skewness 0 ± 0.76	Kurtisos 3 ± 1.92
1	0.571	0.106	-0.5147	2.2702
2	0.689	0.022	0.1405	2.6107
3	0.715	0.019	-0.0006	2.6211
4	0.741	0.026	0.0856	2.4696
5	0.722	0.017	0.2693	2.6071
6	0.713	0.021	0.1052	2.5352
7	0.568	0.119	-0.5532	2.3698
8	0.701	0.023	-0.1987	2.6289
9	0.694	0.019	0.2085	2.7432
10	0.704	0.024	0.8651	3.1181

Table 8.3: The Skewness and Kurtisos of Combustion Duration, $\Delta\theta_c$, for Different Experimental Data Sets

Data Set No.	Mean Value	RMS σ	Skewness 0 ± 0.76	Kurtisos 3 ± 1.92
1	69.49	6.430	-0.5947	2.3849
2	43.85	2.774	0.0910	2.3281
3	40.87	2.490	-0.1909	2.6821
4	45.64	3.322	0.0797	2.5482
5	43.32	2.189	-0.0563	2.7527
6	36.81	2.355	-0.0458	2.9154
7	74.12	5.345	-0.4802	2.2425
8	44.38	2.693	-0.1266	2.5163
9	37.23	2.378	0.0774	2.6223
10	37.51	2.287	-0.2977	3.0637

[164, 166, 165]. Cochran's test is particularly useful in detecting if one variance is much larger than the others. The statistic that is used is given by:

$$G = \frac{largest \quad \sigma_i^2}{\sum_{i=1}^{k} \sigma_i^2} \tag{8.6}$$

and the hypothesis of equality of variances is rejected if $G > G_\alpha$, where the value of G_α with the 99% of the confidence limit is 0.1914 [164]. Therefore, Cochran's test-I in Tables 8.4 and 8.5 showed that the data set No. 1 and 7 did not pass. The data sets No. 1 and 7 represent the very lean operating conditions at compression ratios 8.5:1 and 10:1 respectively, where cyclic variations were found to be more severe than at other operating conditions (e.g. [30]). Once the data sets 1 and 7 were rejected on the ground that normal engine operation does not include such extremely lean operating conditions, the rest of the variances in Cochran's test II, indicates that the hypothesis of equality of variance does hold for all the cases considered except as can be seen in Table 8.5 for the data set No. 4 which represents the rich operating conditions. This is also expected since the cyclic variation at these rich mixture conditions was found also to be greater which is consistent with the result of other researchers [30].

As stated earlier, the F-distribution test was also evaluated and presented in Tables 8.4 and 8.5. The test statistic of the F-distribution for equal sample sizes is given by:

$$F = \frac{\sigma_i^2}{\overline{\sigma^2}} \tag{8.7}$$

Table 8.4: The Variance of the Normalized Crank Angle at Maximum Burning Rate, θ_{max}, for Different Experimental Data Sets

Data Set No.	Variance $\sigma^2 \times 10^3$	Cochran's Test I	Cochran's Test II	F-Distribution Test
1	11.2172	0.3839	-	-
2	0.4800	0.0164	0.1277	1.0217
3	0.3637	0.0124	0.0968	0.7741
4	0.7046	0.0241	0.1875	1.4997
5	0.3025	0.0104	0.0805	0.6438
6	0.4323	0.0148	0.1150	0.9201
7	14.2423	0.4874	-	-
8	0.5388	0.0202	0.1433	1.1468
9	0.3612	0.0124	0.0961	0.7688
10	0.5755	0.0197	0.1531	1.2249

Table 8.5: The Variance of the Combustion Duration, $\Delta\theta_c$, for Different Experimental Data Sets

Data Set No.	Variance $\sigma^2 \times 10^3$	Cochran's Test I	Cochran's Test II	F-Distribution Test
1	41.3498	0.3352	-	-
2	7.6979	0.0624	0.1441	1.1530
3	6.2018	0.0502	0.1161	0.9289
4	11.0347	0.0894	0.2066	1.6529
5	4.7917	0.0388	0.0897	0.7177
6	5.5463	0.0449	0.1038	0.8307
7	28.5718	0.2316	-	-
8	7.2498	0.0587	0.1357	1.0859
9	5.6549	0.0458	0.1058	0.8470
10	5.2303	0.0424	0.0979	0.7834

where $\overline{\sigma^2}$ is the average variance. The hypothesis of equality of variance is rejected if the value of "F" lies outside of the interval of the confidence limits. In this case, using confidence limits of 98% with 99 degrees of freedom, the upper and lower values of the confidence limit were 1.6431 and 0.6086 [166]. Again it seems that all data sets passed the test except the data set No. 4 in Table 8.5 by a small margin, as expected. Therefore, excluding the data set No. 4 from further consideration, the variance of the rest of the data sets could be treated as equal and the values were evaluated as their average for both stochastic parameters, i.e. the crank angle at the maximum burning rate, θ_{max} and the combustion duration, $\Delta\theta_c$.

To complete the characterization of Gaussian distribution parameters it is necessary to evaluate the normalized correlation between the various parameters according to:

$$\rho_c(x_1, x_2) = \frac{\sum_{i=1}^{n}(x_{1,i} - \overline{x}_1)(x_{2,i} - \overline{x}_2)}{\sqrt{[\sum_{i=1}^{n}(x_{1,i} - \overline{x}_1)^2]}\sqrt{[\sum_{i=1}^{n}(x_{2,i} - \overline{x}_2)^2]}} \tag{8.8}$$

where ρ_c is the correlation coefficient of variables x_1 and x_2 with the corresponding mean or average values of $\overline{x_1}$ and $\overline{x_2}$, respectively. If high values of one parameter were always associated with high values of another for example, then the correlation coefficient, ρ_c , would approach unity, while if there was no apparent correlation between the two, then ρ_c would be close to zero.

Accordingly, the evaluated values of correlation coefficient were presented in Table 8.6 and close to unity. It is expected because it is physically obvious that the values of combustion duration would be shorter when the maximum burning rate occurred earlier and vice versa. Cochran's test and F-distribution test performed showed

Table 8.6: The Correlation Coefficient of Stochastic Model Parameters for Different Experimental Data Sets

Data Set No.	Correlation Coefficient ρ_c	Covariance $(\rho_c \sigma_{x_1} \sigma_{x_2})$	Cochran's Test	F-Distribution Test
2	0.976	0.05933	0.1812	1.2688
3	0.948	0.04502	0.1375	0.9627
5	0.957	0.03643	0.1112	0.7790
6	0.904	0.04426	0.1352	0.9465
8	0.944	0.05901	0.1802	1.2619
9	0.939	0.04244	0.1296	0.9076
10	0.745	0.04087	0.1248	0.8740

clearly that the hypothesis of equality of covariances was acceptable as the values were within the confidence limits.

The statistical analysis, thus, showed that the distribution of the stochastic model parameters could be considered adequately as a Gaussian distribution. The results of the variance and covariance analysis showed that their values of the stochastic model parameters for the experimental data sets were of the same magnitude except for the cases of very lean and rich mixture operations of the engine. Therefore, the statistical description of the stochastic model parameters has been made and will provide the foundation for generating statistically similar random values of the stochastic model parameters and simulating the cyclic variations close to the real ones of the engine at any operating conditions.

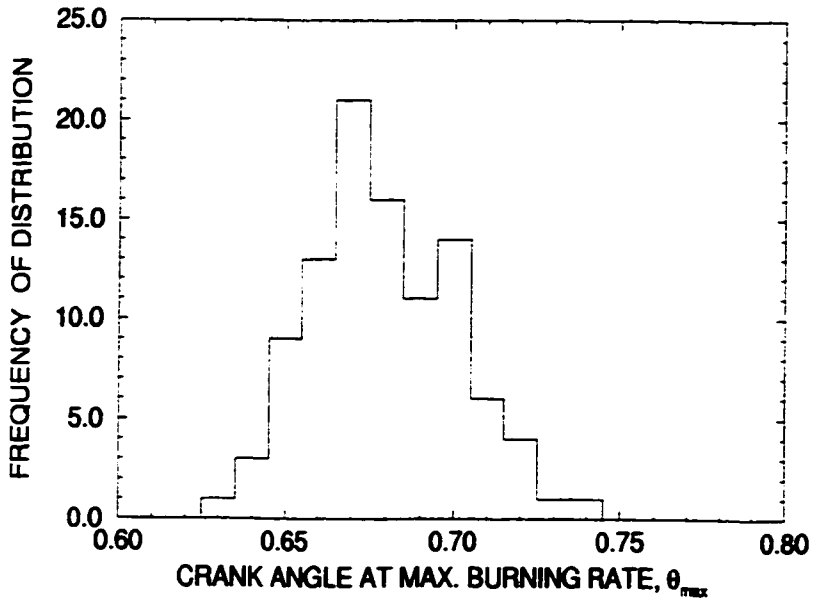

Figure 8.19: The Frequency of Distribution of the Normalized Crank Angle at Maximum Burning Rate, θ_{max}, for 100 Cycles at Equivalence Ratio of 0.80, Compression Ratio of 8.5:1, Spark Timing of 20 degrees BTC and Initial Temperature of 294 K (Data Set No. 2).

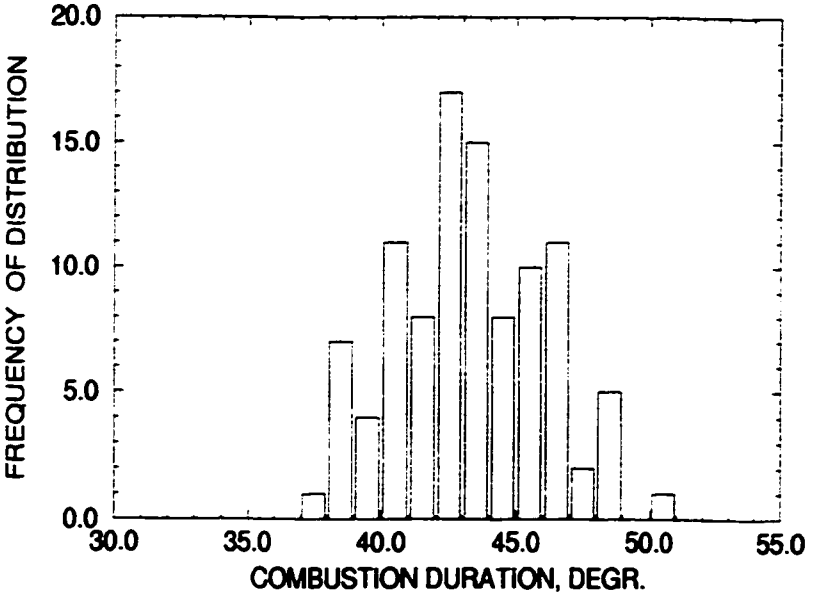

Figure 8.20: The Frequency of Distribution of the Combustion Duration, $\Delta\theta_c$, for 100 Cycles at Equivalence Ratio of 0.80, Compression Ratio of 8.5:1, Spark Timing of 20 degrees BTC and Initial Temperature of 294 K (Data Set No. 2).

8.3 Results and Discussion

The cyclic variations of the spark ignition engine were simulated using the stochastic approach described earlier for a number of operating conditions. The probability of incidence of knock were also investigated. Knock was assumed to take place when the estimated value of the knock parameter, K, as described in Section 3.2.3, was greater than or equal to the critical value. The probability of incidence of knock at a given operating conditions was evaluated as the number of cycles knocking in a hundred consecutive cycles simulated by the model. Some of the results of the simulation for an operating set of conditions are presented in Figures 8.21 to 8.24.

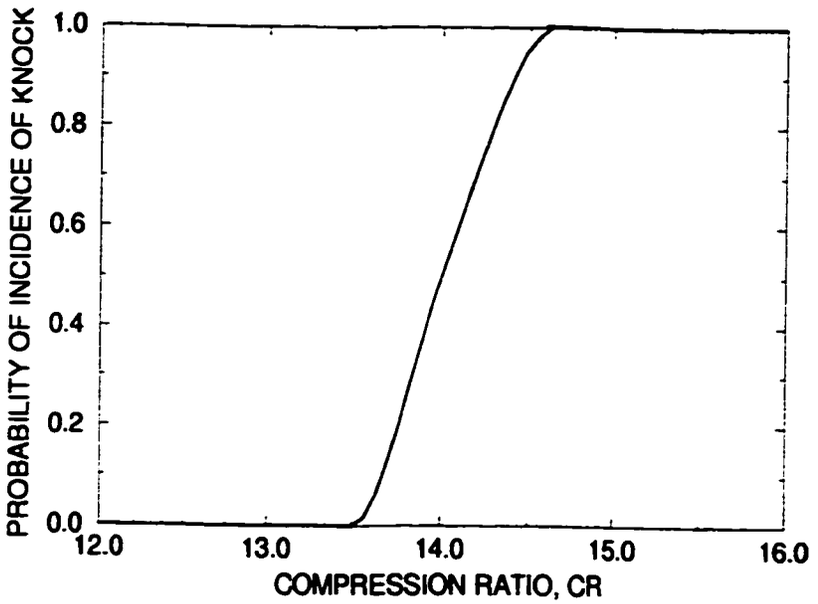

Figure 8.21: The Probability of Incidence of Knock Versus Compression Ratio at Equivalence Ratio of 0.90, Spark Timing of 20 degrees BTC and Initial Temperature of 294 K.

It can be seen in Figure 8.21 that the probability of the incidence of knock increased from zero to a hundred percent as the compression ratio was increased by about only unity [13]. This effect of increasing compression ratio on the incidence of

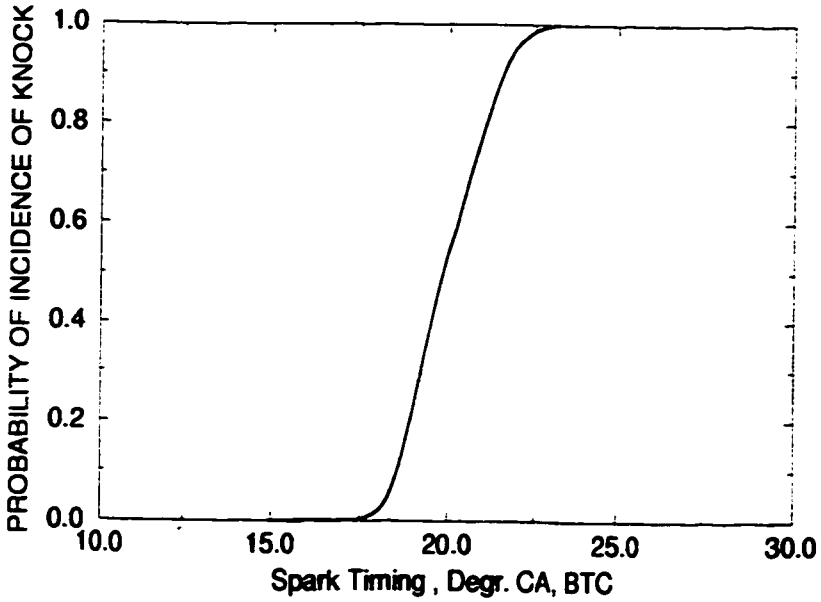

Figure 8.22: The Probability of Incidence of Knock Versus Spark Timing at Compression Ratio of 14:1, Equivalence Ratio of 0.90, and Initial Temperature of 294 K.

knock is somewhat obvious since it is associated with increased mixture temperature at around top dead centre which increased the reaction activity within the end gas region much more than the associated reduction in the combustion period leading to the more frequent occurrence of knock. Similarly, the probability of the incidence of knock versus the spark timing is presented in Figure 8.22. The steep dependence of the probability of incidence of knock on the spark timing is evident. In fact, the results of the simulation showed that the advancement of the spark timing by only about 4 degrees crank angle for these conditions turned a non-knocking condition into a cyclically repeatable knock [13]. The effect of the initial mixture temperature on the incidence of knock in spark ignition engine is shown in Figure 8.23. The high sensitivity of the autoignition reactions of the end gas region to increasing the initial mixture temperature was evident leading to the increased incidence of

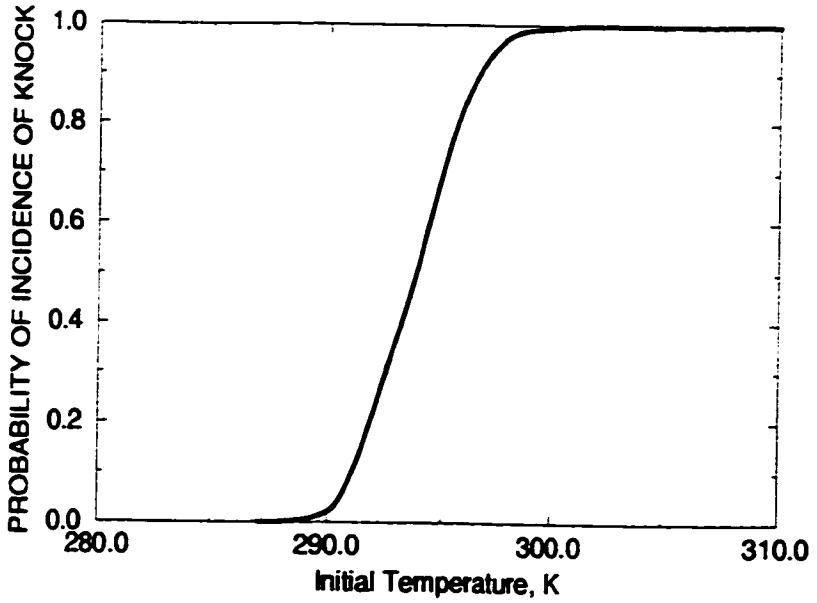

Figure 8.23: The Probability of Incidence of Knock Versus Initial Temperature at a Compression Ratio of 14:1, Equivalence Ratio of 0.90 and Spark Timing of 20 degrees BTC.

knock. Only an increase of 10 to 12 degrees in the initial mixture temperature produced a full knocking condition from a non-knocking state for the conditions shown. The probability of the incidence of knock in a spark ignition engine for different equivalence ratios was also simulated and is presented in Figure 8.24. It can be seen that as the equivalence ratio was changed towards the stoichiometric value the probability of the incidence of knock, as expected, was increased.

As mentioned earlier, the simulation of the cyclic variation of the spark ignition engine were conducted through the generation of the random values of the stochastic parameters at the given operating conditions employing the previously described model. These random values were generated about the simulated mean or average value of the corresponding stochastic parameters with the similar statistical characteristics as of the corresponding experimental data. Generally the deviation between

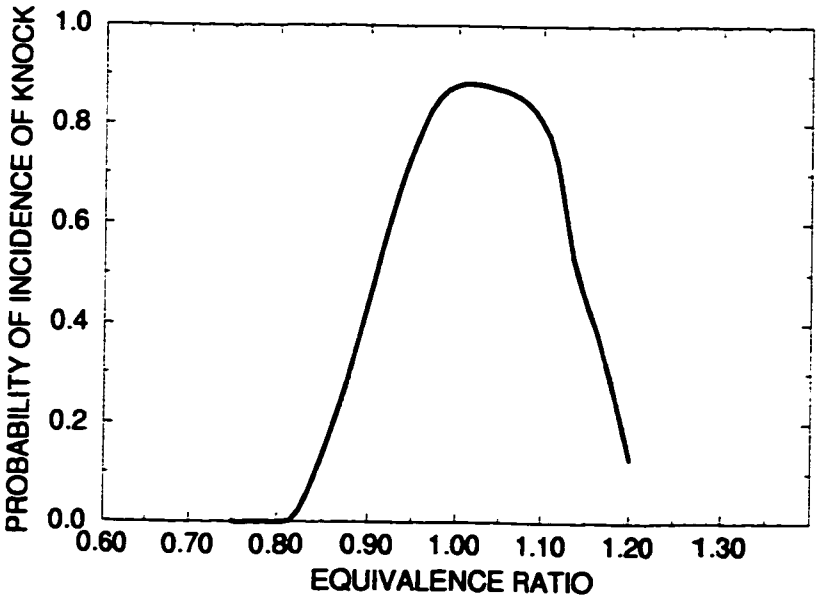

Figure 8.24: The Probability of Incidence of Knock Versus Equivalence Ratio at Spark Timing of 20 degrees BTC, Compression Ratio of 14:1 and Initial Temperature of 294 K.

the simulated mean or base values of the stochastic parameters, the crank angle of maximum burning rate, θ_{max}, and the combustion duration, $\Delta\theta_c$ and their corresponding experimental average values were within the experimental error (about within 10 percent).

Hence, to evaluate the consequences of such a deviation, the probability of incidence of knock in the spark ignition engine was investigated for the corresponding operating conditions that provide the range of conditions at the certain level of probability to knock. Such type of an investigational tool is important for the simulation modeling process where the exact value is varying. Accordingly, the simulation of the cycle to cycle variation using the prescribed approach was conducted through the generation of random values of the stochastic parameters as a typical example for 10 percent changes in their mean values (e. g. Figure 8.25). The results of such in-

vestigations were presented for different operating conditions in Figures 8.26 to 8.29. Accordingly, the better and worse values of the probability of incidence of knock in the spark ignition engine due to the possible error in experimental and/or the simulation were illustrated and the interval of possible fluctuations could be identified for the given operating conditions. The interval of such fluctuations of the probability of incidence of knock as shown in Figure 8.26 to 8.28 for the operating parameters compression ratio, spark timing and initial mixture temperature respectively was found to be narrower than other operating parameters considered.

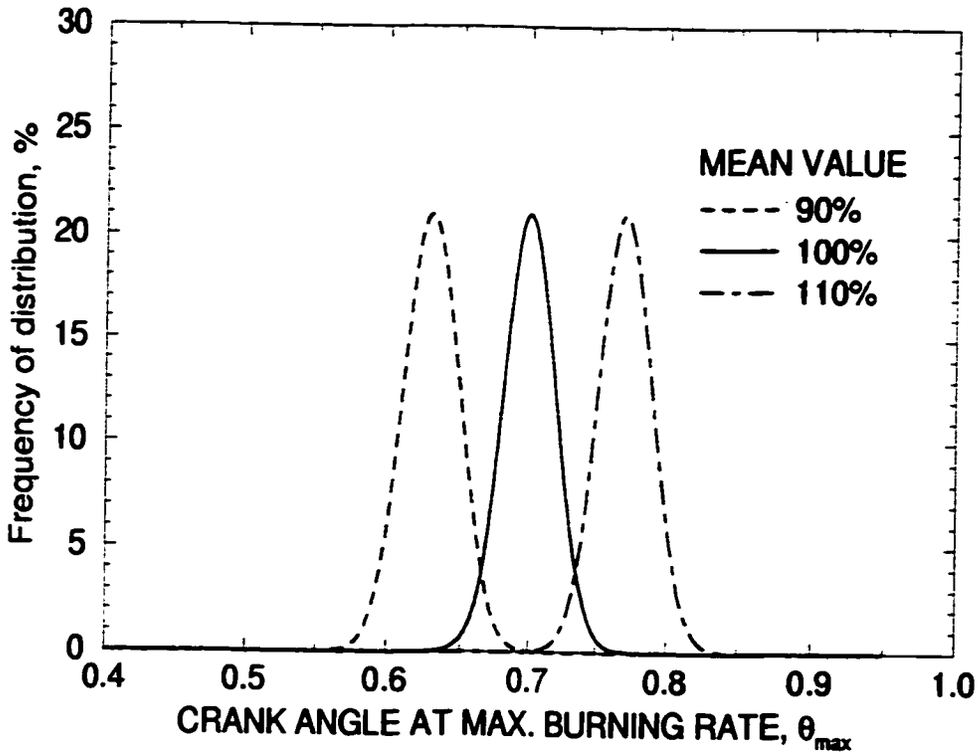

Figure 8.25: The Variation of Frequency Distributions of the Normalized Crank Angle at Maximum Burning Rate, θ_{max}, for different Mean/Average Values.

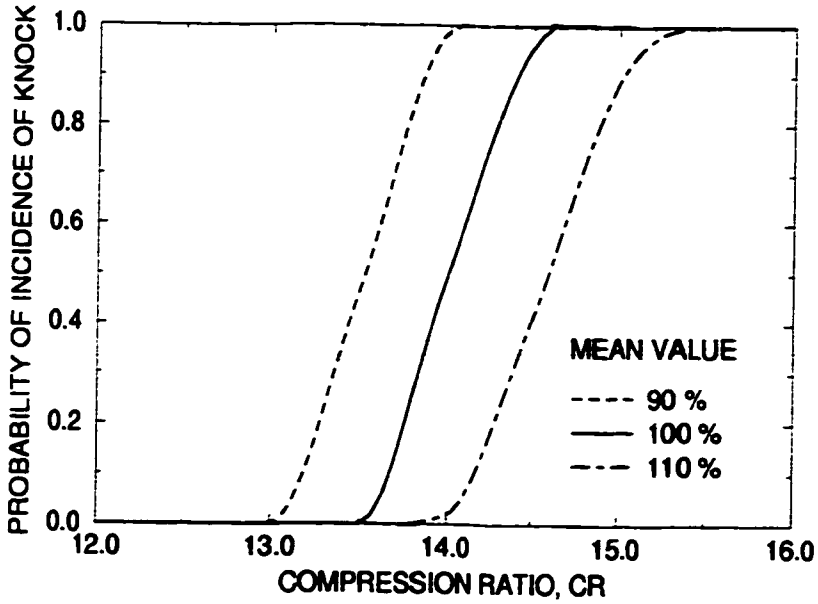

Figure 8.26: The Variation of Probability of Incidence of Knock Versus Different Compression Ratios at Equivalence Ratio of 0.90, Spark Timing of 20 degrees BTC and Initial Temperature of 294 K.

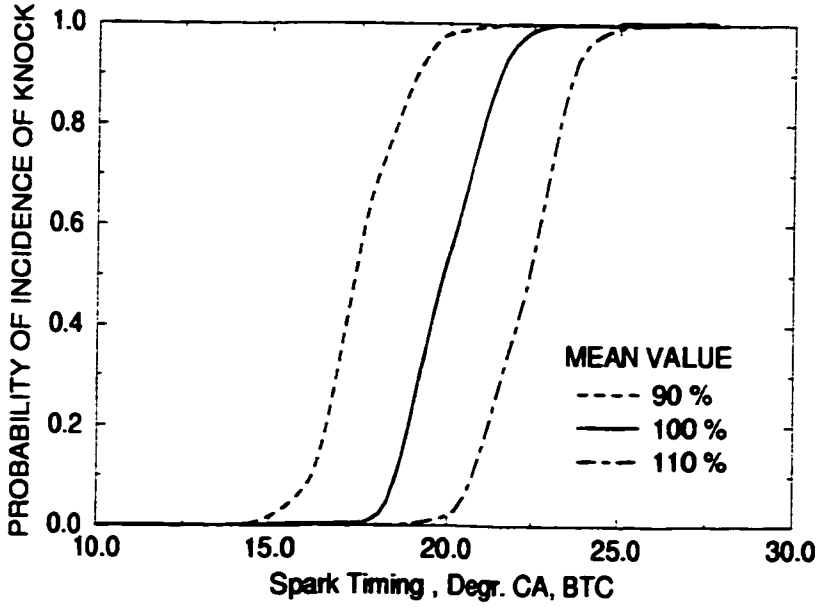

Figure 8.27: The Variation of Probability of Incidence of Knock Versus Different Spark Timing at a Compression Ratio of 14:1, Equivalence Ratio of 0.90 and Initial Temperature of 294 K.

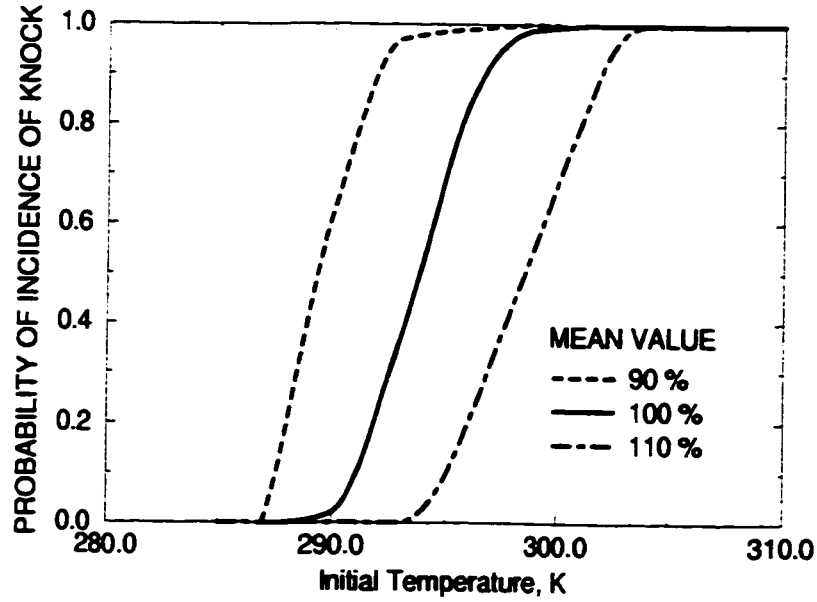

Figure 8.28: The Variation of Probability of Incidence of Knock Versus Different Initial Temperatures at a Compression Ratio of 14:1, Equivalence Ratio of 0.90 and Spark Timing of 20 degrees BTC.

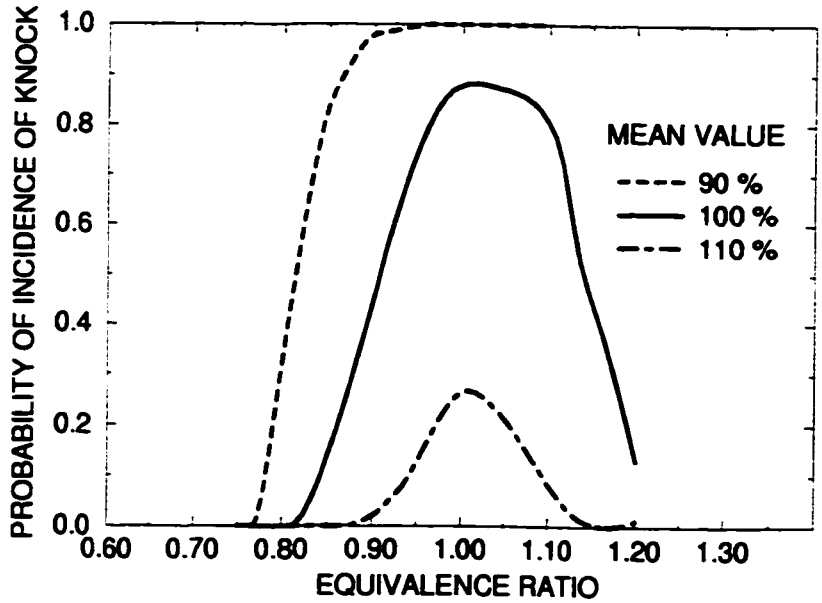

Figure 8.29: The Variation of Probability of Incidence of Knock Versus Different Equivalence Ratios at Spark Timing of 20 degrees BTC, Compression Ratio of 14:1 and Initial Temperature of 294 K.

8.4 Summary

A novel stochastic approach for modeling the cyclic variation in a spark ignition engine was developed and presented. In this stochastic approach, the cyclic variation was simulated cycle by cycle using the similar statistical parameters as of the corresponding experimental data. Hence, once the statistical characteristic of the stochastic parameters were established, the approach could provide not only simulation of cyclic variation of a specific parameter but also regeneration of the whole cycle without requiring to run the engine.

It was also demonstrated that the probability of incidence of knock in a spark ignition engine could be investigated using the described stochastic approach. Hence, this method could be used not only in simulating the cyclic variations of different parameters of interest but also in estimating analytically the possibility of encountering knock in a spark ignition engine at a given set of operating conditions.

Chapter 9

GENERAL SUMMARY, CONCLUSIONS AND RECOMMENDATIONS

9.1 General Summary and Conclusions

- A comprehensive simulation model of the main features of the combustion process for a spark ignition engine has been further developed and presented. This predictive model with little empirical input can generate important performance parameters, such as the temporal variations of cylinder pressure, the two zone mean temperatures, power output and efficiency for different values of intake temperature, intake pressure, spark timing and speed as well as the effects of changes in some design parameters such as compression ratio, bore diameter while operating on gaseous fuels such as methane, propane, ethane and hydrogen and their mixtures. The predicted values show good agreement with the corresponding experimental data.

- The model can also be used to test for the occurrence of knock for any operating conditions while employing detailed reaction kinetics (155 elementary reaction steps and 39 species) for the preignition reactions of the end gas region. When knocking is encountered the value of the knock criterion, "K", builds up to a sufficiently high value that exceeds an acceptable limit. However, under normal operating conditions, the value of K remains at comparatively low level throughout. Its corresponding calculated value can provide an indication of the intensity of the resulting knock

when it occurs.

- An approximate approach using the model has been developed to predict the operational limits of a spark ignition engine while operating on the gaseous fuels methane, propane and hydrogen. Predicted values of the limits were in good agreement with the corresponding experimental values for a wide range of operating conditions (e. g. compression ratios from 6:1 to 16:1 and initial temperatures from 300 to 450 K). Moreover, a second alternative approximate approach that is particularly useful when much of the corresponding experimental information is not available, is shown to produce reasonably good results. However, some caution is needed in its application especially for different engine speeds.

- A methodology has been developed to consider the presence of diluent gases such as carbon dioxide or nitrogen in the main fuel. Predicted values were in good agreement with the corresponding experimental data. The agreement was particularly good for low and moderate concentrations of the diluent (e. g. up to 50 percent) in the fuel-diluent mixtures. The inhibiting effects of diluents on knock in a spark ignition engine were also evaluated quantitatively. The superior capacity of carbon dioxide to suppress knock was evident.

- The effectiveness of an addition of a small quantity of hydrogen to methane was examined and shown to be attractive, especially for the lean fuel mixtures where the superior burning characteristics of hydrogen compared to methane enhanced the combustion rates and contributed towards increasing the indicated power output and efficiency of the engine. In general, the presence of hydrogen in the fuel mixture increases the tendency to knock but at the lean fuel-mixtures the effect was small.

- The effectiveness of the addition of a small quantity of the products of dissoci-

ation of water via electrolysis to the main fuel to enhance engine performance was examined. It was shown that the production of hydrogen on board an engine this way while consuming some of the engine output was not economically viable. The addition of a small amount of oxygen to the fuel-air mixtures produced negligible effect on engine performance particularly for lean mixture operation.

- A stochastic approach developed to simulate the cyclic variations phenomena commonly observed in engines, can provide not only an effective simulation of cyclic variations of a number of performance parameters but also can provide cyclically averaged predicted values. This stochastic approach was shown to be effective in establishing the probability of knock for any given set of operating conditions. The approach not only helps to maximise the power output and efficiency by providing the opportunity to operate the engine at or near borderline of knock conditions but also can enable engine operation within an allowable limit of knocking intensity to secure improvements in efficiency and power output.

9.2 Limitations

The comprehensive model developed has its limitations which arise mainly from the theoretical basis and the associated assumptions made. Some of the main limitations are the following:

- The model developed is based on dividing the combustion chamber into two zones, burned and unburned. Each has uniform temperature and pressure. This is an obvious departure from reality with its own limitations. The unburned zone chemical reaction activity was predicted while decoupling the unburned gas mean

temperature and pressure from the energy release due to chemical reactions. The assumption also ignores the turbulent nature of the flame front and the non-uniform nature of unburned gas temperature. Regions having higher temperatures will undergo autoignition earlier than when predicted on the basis of a uniform temperature assumption.

- An effective energy release pattern was used instead of calculating directly turbulent flame front propagation rates and the associated flame front area. This approximation of the real combustion process in a spark ignition engine, though facilitates the modeling process, has its own limitations.

- The assumptions of negligible flame front thickness with no heat transfer between the burned and unburned zones nor accounting for radiation heat transfer were necessary simplifications that should contribute errors to the predicted results.

- Due to the lack of a more realistic representation, the cylinder wall temperature was assumed to be constant, uniform and equal to the coolant temperature. In reality, the cylinder wall temperature is varying and differs from one location to another which affect the amount of heat transfer. Moreover, when engine starts to knock the excessive heat transfer to the wall in the region of the end-gas can not be modelled realistically.

- When the temperature rise due to the chemical reactivity of the end gas was significant in comparison to the normal combustion temperature rise, the end gas temperature was suitably modified while assuming such reactivity has no direct effect on the variation of cylinder pressure. Moreover, the normal combustion process was considered not to be affected directly by the end gas reaction activity. This approach brings some unknown errors in the predicted results, particularly when

knock is encountered because the combustion and autoignition processes are inevitably interactive in a real engine situation.

- The chemical reaction scheme used in the model to simulate the reaction activities in the end gas region has been assumed to be suitable to follow the reactions of the fuels methane, ethane, propane and hydrogen and their mixtures in engines while allowing for a very wide range of variations in temperature, pressure and equivalence ratio. However, further research is needed to develop and validate the chemical reaction scheme for engine like conditions while accounting for the presence of higher hydrocarbons.

- The simulation of the cyclic variations including knock and its probability in the model was carried out by the stochastic representation of only the energy released parameters. However, it is expected that in a real engine situation all parameters are varying throughout.

Despite these limitations, the model as developed, serves as a comprehensive and effective tool to investigate and analyse the various performance parameters including their possible cyclic variations in a spark ignition engine while operating on gaseous fuels and their mixtures including the presence of diluents. The model is particularly useful for predicting the onset of knock, its intensity and its probability in a spark ignition engine which would certainly provide better opportunities to design and operate engines more efficiently. The model has also shown to be a useful tool in the optimization of spark ignition engine performance in a wide range of applications.

9.3 Recommendation for Future Work

The present comprehensive model developed needs further improvement and upgrading to provide more accurate predictions and applicability over a wider range of operating conditions and in various types of engines. Some measures to be under taken are the following:

- The model developed was mainly validated with the experimental data obtained in a single cylinder, four stroke and constant speed spark ignition CFR engine. The model needs further experimental verifications beyond the CFR engine to consider a wider range of engines that would include various sizes and applications of both four and two stroke engines, as well as turbo-charged engines.

- The chemical kinetic scheme used in the model considers only the common gaseous fuels methane, ethane, propane and hydrogen and their mixtures. Further experimental validations and appropriate upgrading of the kinetic schemes and relevant data are needed to extend its applicability to higher hydrocarbon fuels.

- The effect of the end gas reactivity on the whole combustion process is not fully considered, although an account of the end gas temperature rise due to preignition reactions is taken into consideration. There is a need to consider the interaction between the end gas reaction activity and the normal combustion process in the cylinder and its effect on the cylinder pressure.

- The model does not consider in detail the intake and exhaust processes including the gas motion such as swirl and squish. Further work is needed to include a more comprehensive modeling of these processes including the effect of scavenging, turbocharging, intercooling, manifold mixture heating, mixture motion, exhaust gas

recirculation and others.

- The applicability of the model in simulating cyclic variations needs to be extended to consider a wider range of engines and operating conditions. There is also a need to apply the stochastic simulation model developed to different energy release patterns and parameters.

References

[1] Ang B. W. and Neoh K. G. An Energy and Environmental Assessment of Road Transport Fuels. *International Journal of Vehicle Design*, 15:58–70, 1994.

[2] Asit Das. *Optimization of a Natural Gas Spark Ignition Engine*. PhD thesis, Department of Mechanical and Manufacturing Engineering, University of Melbourne, September 1995.

[3] Gold T. *Earth Outgassing of Methane, Methane fuel for Future*. Plenum Press, 1982.

[4] Heywood J.B. *Internal Combustion Engine Fundamentals*. McGraw Hill Book Co., 1988.

[5] Somchai Chanchaona. *Cyclic Variability in a Natural Gas Fuelled Spark Ignition Engine*. PhD thesis, Department of Mechanical and Manufacturing Engineering, University of Auckland, September 1990.

[6] Weaver C.S. Natural Gas Vehicle- A Review of the State of Art. *SAE*, (892133), 1989.

[7] Dulger M. and Sher E. Experimental Study on Spark Ignition of Flowing Combustible Mixtures. *SAE*, (951004), 1995.

[8] Gatowski J.A. and Heywood J.B. Effects of Valve-Shrouding and Squish in Combustion in a Spark Ignition Engine. *SAE*, (852093), 1985.

[9] Seong-Soo Kim and Sung-Soo Kim. Effects of Swirl and Spark Plug Shape on Combustion Characteristic in a High Speed Single-Shot Visualized SI Engine. *SAE*, (951003), 1995.

[10] Kesler M. and Rychter T.J. A Jet Dispersed Combustion (JDC) Method to Stimulate Lean Burning in SI Piston Engines. *SAE*, (951006), 1995.

[11] Olsson K. and Johansson B. Combustion Chambers for Natural Gas SI Engines, Part 2: Combustion and Emissions. *SAE*, (950517), 1995.

[12] Milton B.G. and Keck J.C. Laminar Burning Velocity in Stoichiometric Hydrogen and Hydrogen-Hydrocarbon Gas Mixtures . *Comb. and Flame*, 58:13–22, 1984.

[13] Attar A. A. *Optimization and Knock Modelling of a Gas Fuelled Spark Ignition Engine.* PhD thesis, Department of Mechanical Engineering, University of Calgary, 1997.

[14] Bade Shrestha S. O. and Karim G. A. Hydrogen as an Additive to Methane for Spark Ignition Engine Applications. In *The Thirty Second Intersociety Energy Convention Engineering Conference Proceedings*, volume 2, pages 910–915, 1997.

[15] Daily J. W. Cycle-to-Cycle Variations: A Chaotic Process? *SAE*, (870165), 1987.

[16] Young M. B. Cyclic Dispersion in the Homogeneous-Charge Spark Ignition Engine - A Literature Survey. *SAE*, (810020), 1981.

[17] Hirshfeld C.F. and Barnard W.N. *Elements of Heat-Power Engineering.* John Wiley and Sons, 1915.

[18] Rassweiler G.M. and Withrow L. Motion Pictures of Engine Flames Correlated with Pressure Cards. *SAE Trans.*, 42:185–204, 1938.

[19] Woschni G. A Universally Applicable Equation for the Instantaneous Heat Transfer Coefficient in the Internal Combustion Engines. *SAE Trans.*, 76(670931):3065–3083, 1967.

[20] Warnatz J. and Stahl G. Numerical Investigation of Time-Dependent Properties and Extinction of Strained Methane and Propane-Air Flamelets. *Combustion and Flame*, 85:285–299, 1991.

[21] Westbrook C.K. and Pitz W.J. A Comprehensive Chemical Kinetics Reaction Mechanism for Oxidation and Pyrolysis of Propane . *Combustion Science and Technology*, 37:117–152, 1984.

[22] Westbrook C.K. and Pitz W.J. Detailed Kinetic Modeling of Autoignition Chemistry. *SAE*, (872107), 1987.

[23] Westbrook C.K., Wartnatz J., and Pitz W.J. A Detailed Chemical Kinetic Mechanism for the Oxidation of Iso-Octane and n-Heptane over an Extended Temperature Range and its application to Analysis of Engine Knock. In 22^{nd} *Symposium (Int.) on Combustion, The Combustion Institute*, pages 893–901, 1988.

[24] Westenberg A.A. and Fristrom R.M. H and O Atoms Profile Measure by ESR

in C_2 Hydrocarbon-O_2 Flames. In 20^{nd} *Symposium (Int.) on Combustion, The Combustion Institute*, page 473, 1985.

[25] Krieger R.B. and Borman G.L. The Computation of Apparent Heat Release for Internal Combustion Engines. *ASME*, (66-WA/DGP-4), 1966.

[26] Peters B.D. and Borman G.L. Cyclic Variations and Average Burning Rates in a SI Engine. *SAE*, (700064), 1970.

[27] Patterson D.J. and Van Wylen G. A Digital Computer Simulation for Spark Ignited Engine Cycles. *SAE*, (663F), 1963.

[28] Benson R.S., Annand W.J.D., and Baruah P.C. A Simulation Model Including Intake and Exhaust Systems for a Single Cylinder Four Stroke Spark Ignition Engine. *Int. J. Mech. Sci.*, 17:97–124, 1975.

[29] Hong C.W. A Combustion Correlation for Spark Ignition Engines Simulation Under Steady and Transient Conditions. *SAE*, (901602), 1990.

[30] Al-Alousi Y. *Examination of the Combustion Processes and the Performance of a Spark Ignition Engine, Using a Data-Acquisition System.* PhD thesis, Department of Mechanical Engineering, University of Calgary, 1982.

[31] Al-Himyary T.J. *A Diagnostic Two-Zone Combustion Model for Spark Ignition Engines Based on Pressure Time Data.* PhD thesis, Department of Mechanical Engineering, University of Calgary, 1988.

[32] Karim G.A. and Gao J. A Predictive Model for Knock in Gas Fueled Spark Ignition Engine. In *Proceeding of the International Congress on Computational*

Methods in Engineering (ICCME), volume 2, pages 429–437, May, Iran 1993.

[33] Sirignano W. A. One Dimensional Analysis of Combustion in a Spark-Ignition Engine. *Combustion Science and Technology*, 7:99, 1973.

[34] Hires S.D., Tabaczyinski R.J., and Novak J.M. The Prediction of Ignition Delay and Combustion Intervals for a Homogeneous Charge Spark Ignition Engine. *SAE*, (780232), 1978.

[35] Tabaczynski R.J., Ferguson C.R., and Radhakrishnar K. A Turbulent Entrainment Model for Spark Ignition Engine Combustion. *SAE*, (770647), 1977.

[36] Blumberg P.N. and Kummer J.T. Prediction of *NO* Formation in Spark Ignited Engines- An Analysis of Methods of Control. In *Combustion Sci. and Tech.*, volume 4, pages 73–95, 1971.

[37] Borgnakke C. and Arpaci V.S. A Model for the Instantaneous Heat Transfer and Turbulence in a Spark Ignition Engine. *SAE*, (800287), 1980.

[38] Davis G.C, Mikulec A., Kent J.C., and Tabaczynski R.J. Modeling the Effect of Swirl on Turbulence Intensity and Burn Rate in S.I. Engines and Comparison with Experiment. *SAE*, (860325), 1986.

[39] Checkel M.D. and Dale J.D. Testing a Third Derivative Indicator on a Production Engine. *SAE*, (861216), 1986.

[40] Checkel M.D. and Dale J.D. Computerized Knock Detection From Engine Pressure Records. *SAE*, (860028), 1986.

[41] Checkel M.D. and Dale J.D. Pressure Trace Knock Measurement in a Current SI Production Engine. *SAE*, (890243), 1989.

[42] Haghgooie M. Effects of Fuel Octane Number and Inlet Air Temperature on Knock Characteristics of a Single Cylinder Engine. *SAE*, (902134), 1990.

[43] Karim G.A. and Klat S.R. Knock and Autoignition Characteristics of Some Gaseous Fuels and Their Mixtures. *J. of the Institute of Fuel*, 39:109–119, March 1966.

[44] Lovell W.G. Knocking Characteristics of Hydrocarbons. In *Ind. Engng. Chem.*, volume 40, pages 2388–2438, 1948.

[45] Boyd T.A. Pathfinding in Fuels and Engines. *SAE Trans.*, 4:182, 1950.

[46] Annand W.J.D. and Sulaiman S.J. Knock Limits and Performance of Some Gaseous Fuels in a Supercharged Spark Ignition Engine. In *Proc. Instn. Mech. Enggrs*, volume 185-62/71, pages 857–867, 1970.

[47] Leiker M., Christoph K., Rankl M., Cartellieri W., and Pfeifer U. Evaluation of Anti-Knock Property of Gaseous Fuels by means of the Methane Number and its Practical Application to Gas Engines. *ASME*, (72-DGP-4):1–15, 1973.

[48] Ryan T.W., Callahan T.J., and King S.R. Engine Knock Rating of Natural Gases-Methane Number . *Transaction of ASME, J. of Engineering for Gas Turbines and Power*, 115:769, October 1993.

[49] Nakagawa Y., Takagi Y., Itoh T., and Iijima T. Laser Shadow graphic Analysis of Knocking in SI Engine. *SAE*, (845001), 1984.

[50] Nakajima Y., Nagai T., Iijima T., Yokoyama J., and Nakamura K. Analysis of Combustion Patterns Effective in Improving Anti-Knock Performance of a SI Engine. *JSAE Review*, 13:9–17, 1984.

[51] Konig G. and Sheppard C.G.W. End Gas Autoignition and Knock in a Spark Ignition Engine. *SAE*, (902135), 1990.

[52] Spicher U. and Kollmeier H.P. Detection of Flame Propagation During Knocking Combustion by Optical Fiber Diagnostics. *SAE*, (861532), 1986.

[53] Spicher U. and Krebs R. Optical Fiber Technique as a Tool to Improve Combustion Efficiency. *SAE*, (902138), 1990.

[54] Spicher U., Kroger H., and Ganser J. Detection of Knocking Combustion Using Simultaneously High-Speed Schlieren Cinematography and Multi Optical Fiber Technique. *SAE*, (912312), 1991.

[55] Cuttler D.H. and Girgis N.S. Photography of Combustion During Knocking Cycles in Disc and Compact Chambers. *SAE*, (880195), 1988.

[56] Karim G.A. An Analytical Approach to Auto-Ignition and Knock in Internal Combustion Engines. *J. Mech. Eng. Sci.*, 6(4):353, 1964.

[57] Livengood J.C. and Wu P.C. Correlation of Autoignition Phenomena in Internal Combustion Engines and Rapid Compression Machines. In *Fifth Symposium(International) on Combustion*, pages 347–356, 1955.

[58] Trumpy D. R., Uyehara O. A., and Myers P. S. The Preknock Kinetics of Ethane in a Spark Ignition Engine. *SAE*, (690518), 1969.

[59] Westbrook C.K., Creighton J., Lund C., and Dryer F.L. A Numerical Model of Chemical Kinetics of Combustion in a Turbulent Flow Reactor. *J. of Phys. Chem.*, 81:2542, 1977.

[60] Dimpelfeld P.M. and Foster D.E. The Prediction of Autoignition in a Spark Ignition Engine. *SAE*, (841337), 1984.

[61] Leppard W. R. A Detailed Chemical Kinetics Simulation of Engine Knock. *Combustion Science and Technology*, 43:1–20, 1985.

[62] Chun K. M., Heywood J. B., and Keck J.C. Prediction of Knock Occurrence in a Spark Ignition Engine. In *Twenty-Second Symposium (International) on Combustion*, pages 455–63, 1988.

[63] Hu H. and Kech J. Autoignition of Adiabatically Compressed Combustible Gas Mixture. *SAE*, (872110), 1987.

[64] Zhou G. and Karim G.A. The Uncatalyzed Partial Oxidation of Methane for the Production of Hydrogen with recirculation. In *Proc. of the ASME/ETCE Emerging Energy Technology Symposium , Houston, Tx*, volume 39,Fossil Fuel Combustion, pages 77–84, 1992.

[65] Karim G.A. and Liu Z. A prediction Model for Knock in Dual Fuel Engines. *SAE*, (921550), 1992.

[66] Karim G.A. and Gao J. Prediction of the Performance of Spark Ignition Engine Including Knock. *SAE*, (932823), 1993.

[67] Cowart J.S., Keck J.B., Heywood C.K., Westbrook, and Pitz W.J. Engine Knock Predictions Using a Fully-Detailed and Reduced Chemical Kinetic Mechanism. In *Twenty-Third Symposium(International) on Combustion*, page 1055, 1990.

[68] Schreiber M., Sadat Sakak A., Poppe C., Griffiths J.F., and Rose D.J. Spatial Structure in End-Gas Autoignition. *SAE*, (932758), 1993.

[69] Pan J. and Sheppard C.W. A Theoretical and Experimental Study of the Modes of End Gas Autoignition Leading to Knock in SI Engines. *SAE*, (942060), 1994.

[70] Blunsdon C.A. and Dent J.C. The Simulation of Autoignition and Knock in a Spark Ignition Engine with Disk Geometry. *SAE*, (940524), 1994.

[71] Karim G. A. An Examination of the Nature of the Random Cyclic Pressure Variations in a Spark Ignition Engine. *Journal of Institute of Petroleum*, 53(519), March 1967.

[72] Soltau J. P. Cylinder Pressure Variations in Petrol Engines. In *Proceedings of the Institute of Mechanical Engineers*, number 2, 1960-61.

[73] Patterson D. J. Pressure Variations, A Fundamental Combustion Problem. *SAE*, (660129), 1966.

[74] Harrow G. A. and Orman P. L. A Study of Flame Propagation and Cyclic Dispersion in a Spark Ignition Engine. In *Advanced School of Automotive*

Engineering (Part IV), Combustion Processes in the Spark Ignition Engine, Pergamon Press, July 1965.

[75] Warren J. A. and Hinkamp J. B. New Instrumentation for Engine Combustion Studies. *SAE Transactions*, 64, 1956.

[76] Kuroda K., Nakajima Y., Sugihara Y., Takagi Y., and Muranaka S. . The Fast Burn with Heavy EGR, New Approach for Low NOx and Improved Fuel Economy. *SAE*, (780006), 1978.

[77] Nakanishi K., Hirano T., and Inoue T. The Effect of Charge Dilution on Combustion and its Improvement - Flame Photograph Study. *SAE*, (750054), 1975.

[78] Kalghatgi G. T. Early Flame Development in a Spark Ignition Engine. *Combustion and Flame*, 60:299–308, 1985.

[79] Mattavi J. N., Groff E. G., and Matekunas M. A. Turbulence Flame Motion and Combustion Chamber Geometry - Their Interactions in a Lean Combustion Engine. In *Conference Proceedings on Fuel Economy and Emission of Lean Burn Engines, Institute of Mechanical Engineers*, number C100/79, June 12-14 1979.

[80] Pundir B. P., Zvonow V. A., and Gupta C. P. Effect of Charge Non-homogeneity on Cycle by Cycle variations in Combustion in SI Engines. *SAE*, (810774), 1981.

[81] Nakamura N., Baika T., and Shibata Y. Multipoint Spark Ignition for Lean Combustion. *SAE*, 852092, 1985.

[82] Hirao O. and Kim Y. Combustion Variation Analysis on Flame Propagation in 4 Cycle Gasoline Engines. In *Special Issue of JARI Technical Memorandum: Intermediate Reports of Combustion and Emission Researches*, pages 30–42, March 1970.

[83] Mayo J. The Effect of Engine Design Parameters on Combustion Rate in Spark Ignited Engines. *SAE*, (750355), 1975.

[84] Barton R. K., Kenemuth D. K., Lestz S. S., and Meyer W. E. Cycle by Cycle Variations of a Spark Ignition Engine - A Statistical Analysis. *SAE*, (700488), 1970.

[85] Fayette Taylor C. *The Internal Combustion Engine in Theory and Practice.* The M.I.T. Press, 1984.

[86] Vichnievsky R. Combustion in Petrol Engines. In *Proceedings on the Joint Conference on Combustion*, 1955.

[87] Mori T. and Yamazaki T. Variation in the Flame Propagation Time in Spark Ignition Engine. *Bulletin JSME*, 13(58), 1970.

[88] Winsor R. E. and Patterson D. E. Mixture Turbulence - A Key to Cyclic Combustion Variation. *SAE*, (730086), 1973.

[89] Lucas G. G. and Brunt. M. F. J. The Effect of Combustion Chamber Shape on the Rate of Combustion in a Spark Ignition Engine. *SAE*, (820165), 1982.

[90] Tuttle J. H. and Toepel R. R. Increased Burning Rates Offer Improved Fuel Economy - NOx Emission Trade-offs in Spark Ignition Engines. *SAE*, (790388), 1979.

[91] May M. G. Lower Specific Fuel Consumption with High Compression Lean Burn Spark Ignited 4-Stroke Engines. *SAE*, (790386), 1979.

[92] Young M. B. Cyclic Dispersion - Some Quantitative Cause-and-Effect Relationships. *SAE*, (800459), 1980.

[93] Matekunas F. A. Modes and Measures of Cyclic Combustion Variability. *SAE*, (830337), 1983.

[94] Namazian M., Hansen S., Lyford-Pike E., Sanchez-Barsse J., Heywood J., and Rife J. Schlieren Visualization of the Flow and Density Fields in the Cylinder of a Spark Ignition Engine. *SAE*, (800044), 1980.

[95] Rashidi M. The Nature of Cycle-to-Cycle Variation in the S. I. Engine from High Speed Photographs. *Combustion and Flame*, 42:111–122, 1981.

[96] Swords M. D., Kalghatgi G. T., and Watts A. J. An Experimental Study of Ignition and Flame Development in a Spark Ignition Engine. *SAE*, 821220, 1982.

[97] Hamai K., Kawajiri H., Ishizuka T., and Nakai M. Combustion Fluctuation Mechanism Involving Cycle-to-Cycle Spark Ignition Variation Due to Gas Flow Motion in SI Engine. In *Twenty-First Symposium (International) on Combustion*, pages 505–512, 1986.

[98] Urushihara T., Murayama T., Takagi Y., and Lee K. H. Turbulence and Cycle-by-Cycle Variation of Mean Velocity Generated by Swirl and Tumble Flow and Their Effects on Combustion. *SAE*, (950813), 1995.

[99] Hansel H. G. A Turbulent Combustion Model of Cycle-to-Cycle Combustion Variations in Spark-Ignition Engines. *Combustion Science and Technology*, 2, 1970.

[100] Quader A. A. Lean Combustion and the Misfire Limit in S. I. Engine. *SAE*, (741055), 1974.

[101] Matthes W. R. and McGill R. N. Effects of Degree of Fuel Atomisation on Single Cylinder Engine Performance. *SAE*, (760117), 1976.

[102] Peters B. D. and Quader A. A. Wetting the Appetite of Spark Ignition Engines for Lean Combustion. *SAE*, (780234), 1978.

[103] Lee K. H. and Foster D. E. Cycle-by-Cycle Variations in Combustion and Mixture Concentration in the Vicinity of Spark Plug Gap. *SAE*, (950814), 1995.

[104] Johansson B. Cycle to Cycle Variations in S. I. Engines - The Effects of Fluid Flow and Gas Compositions in the Vicinity of the Spark Plug on Early Combustion. *SAE*, (962084), 1996.

[105] Daw C. S., Finney C. E. A., Green J. B., Kennel M. B., Thomas J. F., and Connolly F. T. A Simple Model for Cyclic Variations in a Spark Ignition Engine. *SAE*, (962086), 1996.

[106] Barton R. K., Lestz S. S., and Meyer W. E. An Empirical Model for Correlating Cycle-by-Cycle Cylinder Gas Motion and Combustion Variations of a Spark Ignition Engine. *SAE*, (710163), 1971.

[107] Beretta G. P. andRashidi M. and Keck J. C. Turbulent Flame Propagation and Combustion in Spark Ignition Engines. ***Combustion and Flames***, 52:217–245, 1983.

[108] Bouloushos K., Steiner T., and Dimopoulos P. Investigation of Flame Speed Models for the Growth Period During Premixed Engine combustion. *SAE*, (940476), 1994.

[109] Ho C. M. and Santavicca D. A. Turbulence Effects on Early Flame Kernel Growth. *SAE*, (872100), 1987.

[110] Peters N. Laminar Flamelet Concepts in Turbulent Combustion. In ***Twenty-First Symposium(International) on Combustion***, page 1231, 1986.

[111] Pischinger S. and Heywood J. B. A Model for Flame Kernel Development in a Spark Ignition Engine. In ***Twenty-Third Symposium(International) on Combustion***, page 1033, 1990.

[112] Pischinger S. and Heywood J. B. How Heat Losses to the Spark Plug Electrodes Affect Flame Kernel Development in a S. I. Engine. *SAE*, (900021), 1990.

[113] Belmont M. R., Hancock M. S., and Buckingham D. J. Statistical Aspects of Cyclic Variability. *SAE*, (860324), 1986.

[114] Roberts J. B., Peyton Jones J. C., and Landsborough K. J. Cylinder Pressure Variations as a Stochastic Process. *SAE*, (970059), 1997.

[115] Peyton Jones J. C., Landsborough K. J., and Roberts J. B. Identification of Stochastic Models for Cyclic Variations from Measured Pressure Data. *SAE*, (970060), 1997.

[116] Jenkin R. J., James E. H., and Malalasekera W. Predicting the Onset of End Gas Autoignition with a Quasi-Dimensional Spark Ignition Engine Model. *SAE*, (972877), 1997.

[117] Soriano B. Turbulent Combustion. Master's thesis, Department of Mechanical Engineering, University of Calgary, Dec. 1990.

[118] Sarpal G. S. *The Non-Repeatability of Combustion Processes with Particular Reference to Cyclic Pressure Variations in Internal Combustion Piston Engines.* PhD thesis, Department of Mechanical Engineering, University of Calgary, 1974.

[119] Karim G.A., Gao J., and Attar A. A Predictive Approach to Spark Ignition Engine Performance Fueled with Common Gaseous Fuels and Their Mixtures. In *Proceeding of the* 17^{th} *Annual Fall Technical Conference of the ASME Internal Combustion Engine Division*, volume 25-2, pages 59–64, September 1995.

[120] Alizadeh Attar A. and Karim G.A. An Analytical Approach for the Optimization of a Gas Fueled SI Engine Performance Including the Consideration of Knock. In *Proc. of ASME, International Combustion Engine Division*, volume 28-2, pages 65–71, April 1997.

[121] Blizard N. C. and Keck J. C. Experimental and Theoretical Investigations of Turbulent Burning Model for Internal Combustion Engines. *SAE Trans.*, 83(740191), 1974.

[122] Zhou G. *Analytical Studies of Methane Combustion and the Production of Hydrogen and/or Synthesis Gas by the Uncatalyzed Partial Oxidation of Methane.* PhD thesis, Department of Mechanical Engineering, University of Calgary, 1993.

[123] Liu Z. *Combustion in Gas Fueled C.I. Engines.* PhD thesis, Department of Mechanical Engineering, University of Calgary, 1995.

[124] JANAF. *Thermochemical Tables.* National Bureau of Standards, Washington D.C., USA, 1985.

[125] Karim G.A. and Gao J. A Predictive Model for Knock in Spark Ignition Engines. *SAE*, (922366), 1992.

[126] Gao J. *Knock Modeling in S.I. Engines.* PhD thesis, Department of Mechanical Engineering, University of Calgary, 1993.

[127] Strehlow R. *Fundamentals of combustion.* McGraw Hill Co., 1988.

[128] Westbrook C.K. and Pitz W.J. *Complex Chemical Reaction Systems Mathematical Modeling and Simulation.* J. Warnatz and W. Jager(eds.) Springer-Verlag, Heidelberg,West Germany, 1986.

[129] Badr O., Elsayed N., and Karim G.A. An Investigation of the Lean Operational Limits of Gas Fueled Spark Ignition Engines. *Transactions of the ASME, J.*

of Energy Resources Technology, 118:159–163, 1996.

[130] Karim G.A and Wierzba I. Experimental and Analytical Studies of the Lean Operational Limits in Methane Fueled Spark Ignition and Compression Ignition Engines. *SAE*, (891637), 1989.

[131] Zabetakis M. Flammability Characteristics of Combustible Gases and Vapours. In *US Bureau of Mines, Dept. of Interior, Bulletin 627*, 1965.

[132] Al-Himyary T.J. ***Reseach Report.*** The University of Calgary, 1988.

[133] Hirst S.L. and Kirsch L.J. ***The Application of a Hydrocarbon Autoignition Model in Simulating Knock and other Engine Combustion Phenomena.*** Plenum Press, 1980.

[134] Kido H., Huang S., Tanoue K., and Nitta T. Improving the Combustion Performance of Lean Hydrocarbon Mixtures by Hydrogen Addition. *SAE of Japan*, (9430653), 1994.

[135] Karim G.A. and Al-Alousi Y.H. Some Considerations of Cyclic Variations in Spark Ignition Engines Fueled with Gaseous Fuels. *SAE*, (840232), 1984.

[136] Karim G.A. and Zhou G. An Analytical Examination of Various Criteria for Defining Autoignition within Heated Methane-Air Mixtures. In *Transactions of the ASME, J. of Energy Resources Technology*, volume 116-3, pages 175–180, September 1994.

[137] ASTM Committee D-2, editor. ***ASTM Manual for Rating Motor Fuels by Motor and Research Methods.*** American Society for Testing and Materials,

1916 Race St., Philadelphia, Pa. 19103, 1964.

[138] Anderson R. W. and Asik J. R. Ignibility Experiments in a Fast Burn, Lean Burn Engine. *SAE*, (830477), 1983.

[139] Durbin E. and Tsai K. Extending the Lean Limit Operation of a S. I. Engine with Multiple Electrode Spark Plug. *SAE*, (830476), 1983.

[140] Tanuma T., Sasaki K., Kaneko T. , and Kawasaki H. Ignition, Combustion and Exhaust Emission of Lean Mixtures in Automotive S. I. Engine. *SAE*, (710159), 1971.

[141] Ryan T. W. , Lestz S. S., and Meyer E. Extension of the Lean Misfire Limit and Reduction of Exhaust Emission of an S. I. Engine by Modification of Ignition and Intake Systems. *SAE*, (740105), 1974.

[142] Coward H. F. and Jones G. W. Limits of Flammability of Gases and Vapours. *Bulletin 503, Bureau of Mines (U. S.)*, 1952.

[143] Bade Shrestha S.O., Wierzba I. , and Karim G. A. A Thermodynamic Analysis of the Lean Flammability Limits of Fuel-Diluent Mixtures in Air. *J. of Energy Resources Technology*, 116(3):181–185, 1994.

[144] Bade Shrestha S. O., Wierzba I., and Karim G. A. An Approach for Predicting the Flammability Limits of Fuel-Diluent Mixtures in Air. *Journal of the Institute of Energy*, pages 122–130, September 1996.

[145] Karim G. A. and Wierzba I. Methane-Carbon Dioxide Mixtures as a Fuel. *SAE*, (921557), 1992.

[146] Karim G. A. and Wierzba I. Methane-Carbon Dioxide-Nitrogen Mixtures as a Fuel. In *Proc. of Emerging Energy Technology Symposium (ASME Conference)*, January 1996.

[147] Karim G. A., Hanafi A. S., and Zhou G. A Kinetic Investigation of the Oxidation of Low Heating Value Fuel Mixtures of Methane and Diluents. *Transactions of the ASME, Journal of Energy Resources Technology*, 115:301–306, December 1993.

[148] Glassman I. *Combustion*. Academic Press Inc., 1987.

[149] Lewis B. and von Elbe G. *Combustion, Flames and Explosions of Gases*. Academic Press Inc., 1982.

[150] Bade Shrestha S.O., Wierzba I. , and Karim G. A. A Thermodynamic Analysis of the Rich Flammability Limits of Fuel-Diluent Mixtures in Air. *J. of Energy Resources Technology*, 117:239–242, 1995.

[151] Karbassi Massoumeh. *Analytical and Experimental Studies of the Stability Limits of Nonpremixed Flames in Co-Flowing Stream*. PhD thesis, Department of Mechanical Engineering, University of Calgary, September 1997.

[152] Haniff M.S., Melvin A., Smith D.B., and Williams A. The Burning Velocities of Methane and SNG Mixtures with Air. *J. Inst. Energy*, LXII(435), 1987.

[153] Karim G.A. and Wierzba I. Comparative Studies of Methane and Propane as Fuels for Spark Ignition and Compression Ignition Engines. In *SAE Transaction*, volume 92, pages 3677–3688, 1984.

[154] Karim G.A., Wierzba I., and Al-Alousi Y. Methane-Hydrogen Mixtures as Fuels. *International Journal of Hydrogen Energy*, 21(17):625–631, 1996.

[155] Varde K. S. Combustion Characteristics of Small Spark Ignition Engines Using Hydrogen Supplemented Fuel Mixtures. *SAE*, (810921), 1981.

[156] Rosen M. A. and Scott D. S. Analysis of the Efficiencies of Several Hydrogen Production Process. *Hydrogen Energy Congress XI*, pages 479–488, 1996.

[157] Matsuoka S., Yamaguchi T., and Umemura Y. Factors Influencing the Cyclic Variations of Combustion of Spark Ignition Engine. *SAE*, (710586), 1971.

[158] Dye A. O. Turbulence Controlled Induction. *I. Mech. E. Automotive Engineer*, December 1976.

[159] Starkman E. S., Strange F. M., and Dahm T. J. Flame Speeds and Pressure Rise Rates in Spark Ignition Engines. *SAE*, (83V), 1959.

[160] Curry S. A Three-Dimension Study of Flame Propagation in a Spark Ignition Engine. *SAE Trans.*, 71, 1963.

[161] Ohigashi S. and Hamamoto Y. Study of Ignition Lag and Flame Propagation in Spark Ignition Engines. *Bulletin of JSME*, 13(64), 1970.

[162] Soriano B. P. Some Considerations of Fluid Mechanics on the Combustion of Homogeneous Stream of Fuel and Air. Master's thesis, Department of Mechanical Engineering, University of Calgary, 1982.

[163] Ledermann W. and Churchhouse R. F. *Hand Book of Applied Mathematics: Volume III Numerical Methods*. John Wiley and Sons Publications, 1981.

[164] Walpole R. E. and Myers R. H. *Probability and Statistics for Engineers and Scientists.* Macmillan Publishing Company, New York, 1989.

[165] Ledermann W. and LLoyd E. *Hand Book of Applied Mathematics: Volume II Probability.* John Wiley and Sons Publications, 1980.

[166] Dougherty E. D. *Probability and Statistics for the Engineering, Computing and Physical Sciences.* Prentice Hall Inc., New Jersey, 1990.

[167] Karim G.A. and Klat S.R. The Measurement of the Mass Flow Rate of Different Gases Using a Choked Nozzle. *Int. J. of Laboratory Practice*, 15:184, 1966.

Appendices

Appendix A

Multi-Species Equilibrium Calculations

It is consistent with experimental evidence to assume that over the entire possible ranges for operating variables, solids (such as soot) are not formed, while the products of combustion due to flame propagation are in equilibrium at the local flame zone temperature and pressure. The problem of calculating the products composition during combustion by flame propagation, then reduces to the calculation of the gas phase equilibrium composition of a general C-H-O-N-I system, where 'I' could be an inert and 'C', 'H', 'O' and 'N' are carbon, hydrogen, oxygen and nitrogen respectively. This approach was based on that suggested by Strehlow [127].

The species composition of the initial mixture allows the calculation of the atomic ratios $\overline{N}_{C/O}, \overline{N}_{H/O}, \overline{N}_{N/O}$, and $\overline{N}_{I/O}$. This information, the specified equilibrium pressure and temperature and the list of the species present at equilibrium plus the assumption that the gas is an ideal gas, are all that is required to perform equilibrium product composition calculations. A very general case is assumed in which the 14 species, oxygen, O_2, nitrogen, N_2, hydrogen, H_2, carbon dioxide, CO_2, carbon monoxide, CO, water vapour, H_2O, hydroxyl radical, OH, nitric oxide, NO, nitrogen dioxide, NO_2, oxygen atoms, O, nitrogen atoms, N, hydrogen atoms, H, methane, CH_4, and an inert, I, are present at equilibrium.

The atomic ratios which specify the fixed atomic composition can be written in

terms of partial pressures as follows:

$$\overline{N}_{C/O} = \frac{B_C}{B_O} \qquad \overline{N}_{H/O} = \frac{B_H}{B_O} \qquad \overline{N}_{N/O} = \frac{B_N}{B_O} \qquad \overline{N}_{I/O} = \frac{B_I}{B_O} \quad \text{(A.1)}$$

where

$$\begin{aligned} B_C &= P_{CO_2} + P_{CO} + P_{CH_4} \\ B_O &= 2P_{O_2} + 2P_{CO_2} + P_{CO} + P_{H_2O} + P_{OH} + P_{NO} + 2P_{NO_2} + P_O \\ B_H &= 2P_{H_2} + 2P_{H_2O} + P_{OH} + P_H + 4P_{CH_4} \\ B_N &= 2P_{N_2} + P_{NO} + P_{NO_2} + P_N \\ B_I &= P_I \end{aligned} \quad \text{(A.2)}$$

with the added equation that the specified pressure of the system is the sum of the partial pressures:

$$P = \sum_{i=1}^{i} P_i \quad \text{(A.3)}$$

At this point, there are 14 unknowns (the P_i's) and only five equations [Eqs. A.1 and A.3]. Thus additional nine independent equilibrium equations are needed to solve for the equilibrium composition. The choice is arbitrary and the following independent equations are used:

1. Carbon dioxide dissociation: $CO_2 \rightleftharpoons CO + \frac{1}{2}O_2$

$$K_{p1} = \frac{P_{CO} P_{O_2}{}^{\frac{1}{2}}}{P_{CO_2}} \quad \text{(A.4)}$$

2. The dissociation of water: $H_2O \rightleftharpoons H_2 + \frac{1}{2}O_2$

$$K_{p2} = \frac{P_{H_2} P_{O_2}{}^{\frac{1}{2}}}{P_{H_2O}} \tag{A.5}$$

3. The formation of hydroxyl radical: $H_2O \rightleftharpoons \frac{1}{2}H_2 + OH$

$$K_{p3} = \frac{P_{H_2}^{1/2} P_{OH}}{P_{H_2O}} \tag{A.6}$$

4. The dissociation of hydrogen: $\frac{1}{2}H_2 \rightleftharpoons H$

$$K_{p4} = \frac{P_H}{P_{H_2}^{1/2}} \tag{A.7}$$

5. The dissociation of oxygen: $\frac{1}{2}O_2 \rightleftharpoons O$

$$K_{p5} = \frac{P_O}{P_{O_2}^{1/2}} \tag{A.8}$$

6. The formation of methane: $4H_2 + CO_2 \rightleftharpoons CH_4 + 2H_2O$

$$K_{p6} = \frac{P_{CH_4} P^2{}_{H_2O}}{P_{H_2}{}^4 P_{CO_2}} \tag{A.9}$$

7. The formation of nitrogen atoms: $\frac{1}{2}N_2 \rightleftharpoons N$

$$K_{p7} = \frac{P_N}{P_{N_2}^{1/2}} \tag{A.10}$$

8. The formation of nitric oxide: $\frac{1}{2}N_2 + \frac{1}{2}O_2 \rightleftharpoons NO$

$$K_{p8} = \frac{P_{NO}}{P_{N_2}{}^{1/2} P_{O_2}{}^{1/2}} \tag{A.11}$$

9. The formation of nitrogen dioxide: $\frac{1}{2}N_2 + O_2 \rightleftharpoons NO_2$

$$K_{p9} = \frac{P_{NO_2}}{P_{N_2}{}^{1/2} P_{O_2}} \tag{A.12}$$

The solution of this set of equations can be reduced by noting that the partial pressures of the species N, NO and NO_2 will always be rather small and that they can be calculated by an ***add-on technique***. This reduces the main calculation to the determination of the composition of a system containing only the three active components 'C', 'H' and 'O'.

To do this, the only needed assumptions are the partial pressures of three species that independently contain the component elements. Any set that satisfies this requirement may be chosen, such as $P'_{CO_2}, P'_{O_2}, P'_{H_2}$ or $P'_{CO_2}, P'_{H_2O}, P'_{O_2}$, etc., where the primes indicate that the partial pressure is a guessed value. Using this guess the (incorrect) partial pressures of the remaining species, P'_i, may be calculated using the equilibrium constants. The three mass-conservation equations [from using Eqs. A.1, A.2, and A.3] are then written by substituting $P_i = P'_i + \delta_i$ where δ_i is the correction to the partial pressure which is unknown. However, the equilibrium relations written in terms of $P_i = P'_i + \delta_i$ can be differentiated to yield an expression for each of the remaining δ_i's in terms of the three guessed correction factors δ_i's for the three pre-selected species. When these are substituted into the mass-balance

set, three equations are obtained for the three unknown correction factors, one for each of the three guessed species. Since these equations are linear they are easily solved in determinant form. The calculation converges rapidly if the initial guesses of partial pressures are reasonable and if the guessed species have a relatively large pressure at equilibrium.

The nitrogen-containing species and the inert are included in the calculation as *add-on* species at each step by writing:

$$P_{calc} = P - P_{N} - P_{NO} - P_{NO_2} - P_{I} \tag{A.13}$$

where P_{I} is calculated from $\overline{N}_{I/O}$ and the properly weighted partial pressures of the oxygen containing species (Eq. A.2) and the P_{N}, P_{NO}, P_{NO_2} are calculated from the values of P_{N_2} and P_{O_2} and the appropriate equilibrium constants. The main calculation is then performed using P_{calc} as a fictitious total pressure for the C-H-O system.

Appendix B

The Physical Properties and the Chemical Kinetics Schemes

The predictive model described in Chapter 3 includes a chemical kinetics scheme of 155 reaction steps and 39 species to predict the reactivity of the end-gas mass. The physical properties of these 39 species considered are shown in Table B.1. Figure B.1 and Table B.2 show the flow chart and the relevant information of the chemical kinetic scheme [123, 13]. Reaction rates in Table B.2 are in $m^3 - mol - s - Joule$ units.

Table B.1: The Physical Properties of the Species in the Chemical Kinetic Scheme

No.	Species	Chemical Formula	Molecular Weight	Element Count			
				C	H	O	N
1	Methane	CH_4	16.0430	1	4	0	0
2	Ethynyl	C_2H	25.0303	2	1	0	0
3	Acetylene	C_2H_2	26.0382	2	2	0	0
4	Vinyl	C_2H_3	27.0462	2	3	0	0
5	Ethylene	C_2H_4	28.0542	2	4	0	0
6	Ethyl	C_2H_5	29.0622	2	5	0	0
7	Ethane	C_2H_6	30.0701	2	6	0	0
8	Methylidene	CH	13.0191	1	1	0	0
9	Methylene	CH_2	14.0270	1	2	0	0
10	Ketene	CH_2CO	42.0376	2	2	1	0
11	Formaldehyde	CH_2O	30.0265	1	2	1	0
12	Methyl	CH_3	15.0351	1	3	0	0
13	Acetaldehyde	CH_3CHO	44.0536	2	4	1	0
14	Acetyl	CH_3CO	43.0456	2	3	1	0
15	Methyloxide	CH_3O	31.0345	1	3	1	0
16	Ketyl	$CHCO$	41.0297	2	1	0	0
17	Carbon Monoxide	CO	28.0106	1	0	1	0
18	Carbon Dioxide	CO_2	44.0100	1	0	2	0
19	Hydrogen Atom	H	1.00797	0	1	0	0
20	Hydrogen Molecule	H_2	2.01594	0	2	0	0
21	Steam	H_2O	18.0153	0	2	1	0
22	Hydrogen Peroxide	H_2O_2	34.0147	0	2	2	0
23	Formyl	HCO	29.0185	1	1	1	0
24	Hydroperoxo	HO_2	33.0068	0	1	2	0
25	Oxygen	O_2	31.9988	0	0	2	0
26	Oxygen Atom	O	15.9994	0	0	1	0
27	Hydroxyl	OH	17.0074	0	1	1	0
28	Carbon	C	12.0110	1	0	0	0
29	Cyanogen	CN	26.0180	1	0	0	1
30	Nitrogen	N_2	28.0134	0	0	0	2
31	Nitrogen Atom	N	14.0067	0	0	0	1
32	Hydrogen Cyanide	HCN	27.0260	1	1	0	1
33	Hydrogen Isocyanate	$HCNO$	43.0250	1	1	1	1
34	Nitric Acid	HNO_3	63.0130	0	1	3	1
35	Imidogen	NH	15.0150	0	1	0	1
36	Nitrogen Oxide	NO	30.0060	0	0	1	1
37	Nitrogen Dioxide	NO_2	46.0060	0	0	2	1
38	Nitrous Oxide	N_2O	44.0130	0	0	1	2
39	Nitrogen Trioxide	NO_3	62.0050	0	0	3	1

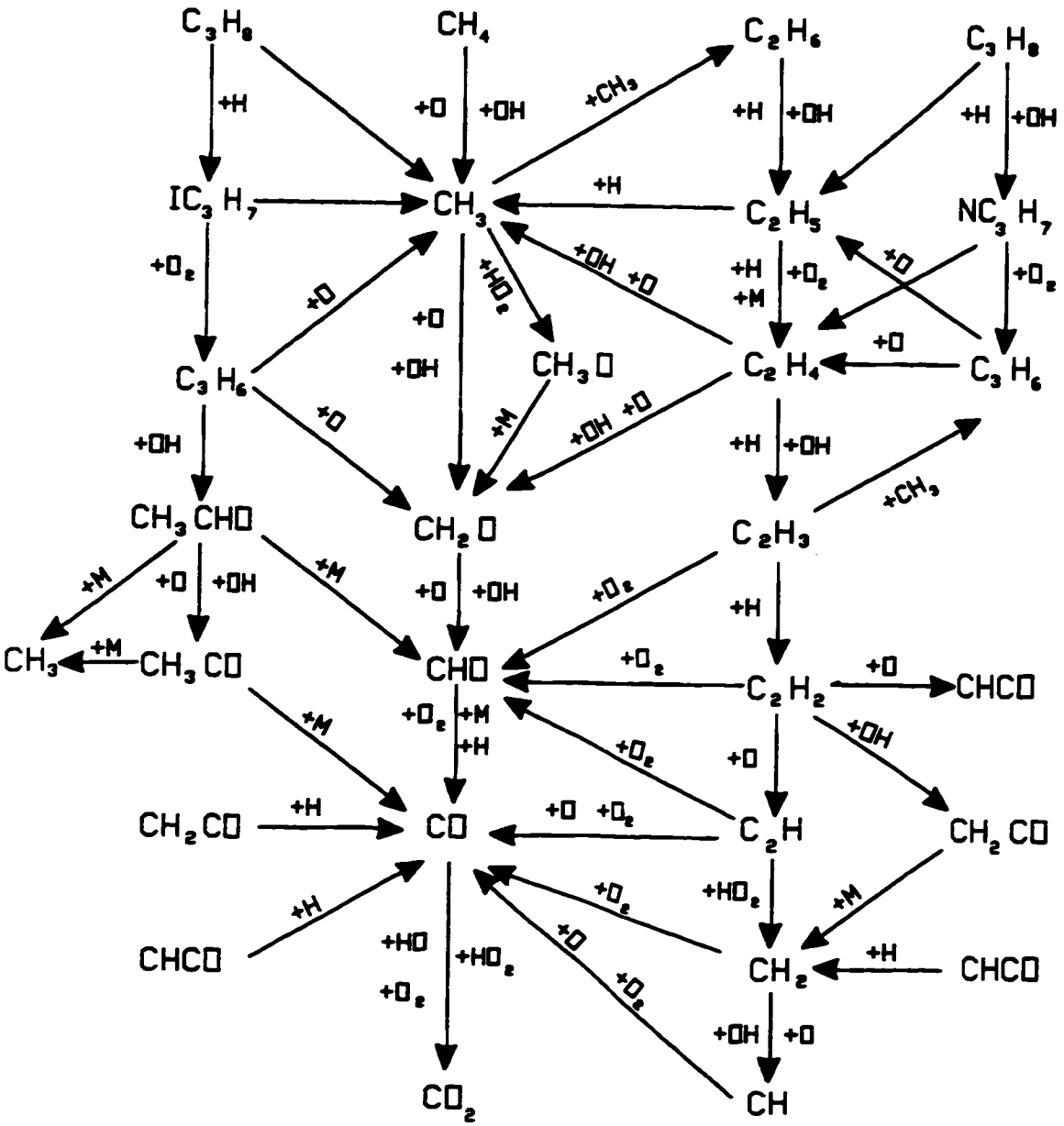

Figure B.1: The Flow Chart of the Chemical Kinetic Scheme.

Table B.2: The Chemical Kinetic Scheme

No.	Reactions	Forward Reaction Constants			Backward Reaction Constants		
		A_f	B_f	E_f	A_b	B_b	E_b
1	CH4 + OH ⇌ CH3 + H2O	3.460E-03	3.060	8.370E+03	2.990E+07	.000	8.940E+04
2	CH4 + H ⇌ CH3 + H2	2.200E-02	3.000	3.661E+04	8.330E-04	3.000	3.330E+04
3	CH4 + O ⇌ CH3 + OH	1.200E+01	2.100	3.190E+04	1.990E-01	2.100	2.050E+04
4	CH4 + HO2 ⇌ CH3 + H2O2	1.120E+07	.000	1.020E+05	7.470E+02	.000	5.350E+03
5	CH4 + O2 ⇌ CH3 + HO2	7.585E+07	.000	2.452E+05	1.000E+06	.000	1.675E+03
6	CH4 ⇌ CH3 + H	6.300E+14	.000	4.185E+05	1.279E+03	1.000	-1.300E+04
7	CH3 + O ⇌ CH2O + H	1.300E+03	.000	8.400E+03	1.590E+09	.000	2.925E+05
8	CH3 + HO2 ⇌ CH3O + OH	3.200E+07	.000	0.000E+00	2.000E+04	.000	1.070E+05
9	CH3 + O2 ⇌ CH2O + OH	1.000E+05	.000	0.000E+00	8.450E+04	.000	2.117E+05
10	CH2O + OH ⇌ H2O + HCO	7.590E+06	.000	7.100E+02	4.210E+04	.490	1.185E+05
11	CH2O + H ⇌ H2 + HCO	3.311E+08	.000	4.390E+04	2.630E+07	.000	1.053E+05
12	CH2O + O ⇌ HCO + OH	1.000E+08	.000	2.220E+04	1.000E+08	.000	1.460E+05
13	HCO + OH ⇌ CO + H2O	5.000E+07	.000	0.000E+00	1.170E+08	-.500	3.824E+05
14	HCO + O2 ⇌ CO + HO2	3.020E+06	.000	0.000E+00	6.760E+06	.000	1.351E+05
15	HCO + HO2 ⇌ CH2O + O2	1.000E+08	.000	1.250E+04	3.630E+09	.000	1.920E+05
16	CO + OH ⇌ CO2 + H	4.400E+00	1.500	-3.098E+03	1.600E+08	.000	1.100E+05
17	CO + O2 ⇌ CO2 + O	3.140E+05	.000	1.570E+05	2.780E+06	.000	1.830E+05
18	H2 + OH ⇌ H + H2O	2.200E+07	.000	2.155E+04	9.300E+07	.000	8.520E+04
19	H2 + O ⇌ H + OH	1.800E+04	1.000	3.711E+04	8.300E+03	1.000	2.900E+04
20	H2 + O2 ⇌ HO2 + H	5.000E+06	.460	2.240E+05	6.600E+07	.000	8.930E+03
21	H2 + HO2 ⇌ H + H2O2	7.240E+05	.000	7.820E+04	1.700E+06	.000	1.570E+04
22	H + HO2 ⇌ OH + OH	1.500E+08	.000	4.185E+03	1.530E+04	.840	1.416E+05
23	H + H + M ⇌ H2 + M	1.830E+06	-1.000	0.000E+00	6.280E+08	.000	4.010E+05
24	H + OH + M ⇌ H2O + M	3.600E+01	.000	0.000E+00	8.300E+11	.000	5.010E+05
25	H + O2 + M ⇌ HO2 + M	8.000E+05	-1.000	0.000E+00	2.400E+09	.000	1.900E+05
26	O + O + M ⇌ O2 + M	4.700E+03	-.280	0.000E+00	5.100E+09	.000	4.800E+05
27	OH + OH + M ⇌ H2O2 + M	3.200E+10	-2.000	0.000E+00	1.690E+18	-2.000	2.000E+05
28	HO2 + OH ⇌ H2O + O2	1.500E+07	.000	0.000E+00	1.410E+10	-.560	2.870E+05
29	H2O + O ⇌ OH + OH	1.500E+04	1.140	7.213E+04	1.500E+03	1.140	0.000E+00
30	H2O2 + O2 ⇌ HO2 + HO2	1.000E+06	.000	1.670E+05	2.500E+05	.000	-5.200E+03
31	H + H2O2 ⇌ H2O + OH	1.000E+07	.000	1.500E+04	3.340E+06	.000	3.121E+05
32	H + O2 ⇌ O + OH	5.130E+10	-.820	6.890E+04	1.300E+07	.000	0.000E+00
33	C2H6 + H ⇌ C2H5 + H2	5.370E-04	3.500	2.176E+04	9.700E-04	3.500	1.143E+05
34	C2H6 + OH ⇌ C2H5 + H2O	6.300E+00	2.000	2.700E+03	6.550E-01	2.000	1.000E+05
35	C2H6 + O ⇌ C2H5 + OH	3.000E+01	2.000	2.140E+04	3.140E-01	2.000	4.743E+04
36	C2H6 + O2 ⇌ C2H5 + HO2	4.070E+07	.000	2.120E+05	1.930E+03	.590	-2.140E+03
37	C2H6 + HO2 ⇌ H2O2 + C2H5	1.120E+07	.000	8.100E+04	6.500E+06	.000	4.300E+04
38	C2H5 + O2 ⇌ C2H4 + HO2	1.500E+05	.000	0.000E+00	1.330E+05	.000	5.730E+04
39	C2H5 + H ⇌ CH3 + CH3	3.160E+07	.000	0.000E+00	3.660E+06	.000	3.740E+04
40	C2H5 ⇌ C2H4 + H	2.340E+26	-4.240	1.810E+05	1.170E+08	-.620	7.240E+03
41	C2H5 + O ⇌ CH3CHO + H	5.000E+07	.000	0.000E+00	5.360E-01	2.540	2.900E+05
42	C2H4 + OH ⇌ C2H3 + H2O	7.000E+07	.000	1.255E+04	2.110E+30	-6.580	1.150E+05
43	C2H4 + H ⇌ C2H3 + H2	1.510E+08	.000	4.270E+04	9.220E+06	.000	5.845E+04
44	C2H4 + O2 ⇌ C2H3 + HO2	4.220E+07	.000	2.410E+05	7.760E+03	.540	-7.177E+03
45	C2H2 + H2 + M ⇌ C2H4 + M	4.600E+00	1.000	1.528E+05	2.600E+11	.000	3.198E+05
46	C2H3 + O2 ⇌ C2H2 + HO2	1.200E+05	.000	0.000E+00	1.420E+06	-.360	4.713E+04
47	C2H3 + H ⇌ C2H2 + H2	2.000E+07	.000	0.000E+00	3.850E-19	7.390	2.137E+05
48	C2H3 ⇌ C2H2 + H	1.600E+32	-5.500	1.935E+05	8.350E+25	-5.500	4.270E+03
49	C2H + H + M ⇌ C2H2 + M	1.090E-03	1.000	3.220E+03	1.000E+08	.000	4.770E+05
50	C2H2 + OH ⇌ CH2CO + H	3.230E+05	.000	8.370E+02	3.160E+06	.000	8.732E+04
51	C2H2 + O ⇌ CH2 + CO	6.760E+07	.000	1.674E+04	1.250E+07	.000	2.287E+05
52	C2H + O2 ⇌ CO + HCO	2.410E+06	.000	0.000E+00	2.180E+04	.540	6.257E+05

Table B.2: The Chemical Kinetic Scheme (Continued)

No.	Reactions	Forward Reaction Constants			Backward Reaction Constants		
		A_f	B_f	E_f	A_b	B_b	E_b
53	C2H + O ⇌ CH + CO	5.000E+07	.000	0.000E+00	3.160E+07	.000	2.457E+05
54	CH + O2 ⇌ HCO + O	3.300E+07	.000	0.000E+00	8.000E+07	-.070	3.013E+05
55	CH + O ⇌ CO + H	4.000E+07	.000	0.000E+00	5.490E+08	.150	7.343E+05
56	CH2 + O2 ⇌ HCO + OH	1.000E+08	.000	1.148E+04	4.070E+07	.000	3.204E+05
57	CH2 + O ⇌ CH + OH	1.900E+05	.680	1.046E+05	5.900E+04	.680	1.085E+05
58	CH2 + H ⇌ CH + H2	2.690E+05	.670	1.075E+05	1.900E+05	.670	1.201E+05
59	CH2 + OH ⇌ CH + H2O	2.690E+05	.670	1.075E+05	8.120E+05	.670	1.836E+05
60	CH3CHO + H ⇌ CH3CO + H2	4.000E+07	.000	1.757E+04	8.420E+10	-1.370	9.719E+04
61	CH3CHO + O ⇌ CH3CO + OH	5.000E+06	.000	7.489E+03	7.390E+09	-1.420	7.979E+04
62	CH3CHO + OH ⇌ CH3CO + H2O	1.000E+07	.000	0.000E+00	1.910E+07	.000	1.532E+05
63	CH3CHO ⇌ CH3 + HCO	7.000E+15	.000	3.410E+05	3.800E+03	1.000	0.000E+00
64	CH3CO ⇌ CH3 + CO	1.000E+10	.000	0.000E+00	0.000E+00	.000	0.000E+00
65	CH2CO + H ⇌ CH3 + CO	1.090E+07	.000	1.423E+04	2.310E+06	.000	1.682E+05
66	CH2CO + O ⇌ HCO + HCO	1.000E+07	.000	1.000E+04	3.470E+05	.000	1.400E+05
67	CH2CO + OH ⇌ CH2O + HCO	6.200E+07	.000	4.000E+03	2.750E+07	.000	7.740E+04
68	CH2 + CO + M ⇌ CH2CO + M	4.570E-02	.000	0.000E+00	1.990E+10	.000	2.510E+05
69	C3H8 ⇌ C2H5 + CH3	1.700E+16	.000	3.550E+05	1.500E+04	1.000	-1.340E+03
70	C3H8 + O ⇌ IC3H7 + OH	2.820E+07	.000	2.170E+04	1.870E+06	.000	4.050E+04
71	C3H8 + O ⇌ NC3H7 + OH	1.130E+08	.000	3.280E+04	7.500E+06	.000	5.130E+04
72	C3H8 + H ⇌ NC3H7 + H2	1.300E+00	2.400	1.870E+04	8.900E+03	.890	6.646E+04
73	C3H8 + H ⇌ IC3H7 + H2	1.320E+00	2.540	2.820E+04	9.120E+03	1.030	6.177E+04
74	C3H8 + OH ⇌ NC3H7 + H2O	5.800E+02	1.400	3.550E+03	1.003E+03	1.250	9.360E+04
75	C3H8 + OH ⇌ IC3H7 + H2O	4.670E+01	1.610	-1.460E+02	3.000E+01	1.610	9.050E+04
76	C3H8 + HO2 ⇌ NC3H7 + H2O2	6.300E+06	.000	7.400E+04	6.910E+05	.000	8.100E+04
77	C3H8 + HO2 ⇌ IC3H7 + H2O2	5.600E+06	.000	6.800E+04	4.160E+05	.000	7.100E+04
78	C3H8 + CH3 ⇌ NC3H7 + CH4	7.500E+06	.000	6.250E+04	3.980E+06	.000	8.350E+04
79	C3H8 + CH3 ⇌ IC3H7 + CH4	4.306E+06	.000	5.553E+04	5.830E+06	.000	8.840E+04
80	C3H8 + C2H5 ⇌ C2H6 + NC3H7	1.000E+05	.000	4.340E+04	3.630E+04	.000	4.157E+04
81	C3H8 + C2H5 ⇌ C2H6 + IC3H7	1.000E+05	.000	4.340E+04	3.630E+04	.000	4.157E+04
82	NC3H7 + O2 ⇌ C3H6 + HO2	0.000E+00	.000	0.000E+00	0.000E+00	.000	7.310E+04
83	IC3H7 + O2 ⇌ C3H6 + HO2	3.000E+06	.000	1.250E+04	4.141E+04	.000	5.190E+04
84	NC3H7 ⇌ C3H6 + H	1.250E+14	.000	1.540E+05	7.940E+06	.000	1.200E+04
85	IC3H7 ⇌ C3H6 + H	2.000E+14	.000	1.610E+05	2.890E+08	.000	1.660E+04
86	NC3H7 ⇌ C2H4 + CH3	9.549E+13	.000	1.290E+05	2.187E+02	1.000	2.400E+04
87	IC3H7 ⇌ C2H4 + CH3	2.000E+10	.000	1.230E+05	4.570E-02	1.000	1.800E+04
88	C3H6 + O ⇌ C2H4 + CH2O	6.800E-02	2.560	-4.720E+03	6.600E-02	2.560	3.370E+05
89	C3H6 ⇌ C2H3 + CH3	6.300E+15	.000	3.580E+05	1.000E+04	1.000	0.000E+00
90	C3H6 + OH ⇌ C2H5 + CH2O	3.000E+06	.000	0.000E+00	4.600E+07	.000	7.260E+04
91	CH3 + O2 ⇌ CH3O + O	4.800E+07	.000	1.210E+05	3.040E+08	.000	3.070E+03
92	CH2O + H + M ⇌ CH3O + M	7.700E+20	-6.650	4.050E+04	3.910E+31	-6.650	1.390E+05
93	CH3O + O2 ⇌ CH2O + HO2	6.000E+06	.000	2.210E+04	2.800E+05	.000	1.280E+05
94	O + C3H6 ⇌ HCO + C2H5	6.760E-02	2.560	-4.730E+03	1.360E-02	2.560	1.200E+05
95	C3H8 + O2 ⇌ NC3H7 + HO2	4.000E+07	.000	1.900E+05	2.080E+06	.000	0.000E+00
96	C3H8 + O2 ⇌ IC3H7 + HO2	4.000E+07	.000	1.900E+05	2.080E+06	.000	0.000E+00
97	CO + O + M ⇌ CO2 + M	5.900E+03	.000	1.715E+04	5.500E+15	-1.000	5.515E+05
98	CO + HO2 ⇌ CO2 + OH	5.800E+07	.000	9.581E+04	6.600E+08	.000	3.546E+05
99	CH3 + OH ⇌ CH2O + H2	4.000E+06	.000	0.000E+00	1.200E+08	.000	3.043E+05
100	CH2O + HO2 ⇌ H2O2 + HCO	1.000E+06	.000	3.340E+04	1.090E+05	.000	2.757E+04
101	CO + H + M ⇌ HCO + M	1.340E+05	-.930	8.430E+03	2.000E+11	-1.000	7.130E+04
102	C3H6 + OH ⇌ CH3 + CH3CHO	1.000E+05	.000	0.000E+00	2.800E+05	.000	8.537E+04
103	C3H6 + O ⇌ CH3 + CH3CO	6.761E-02	2.560	-4.729E+03	1.023E-02	2.560	1.533E+05
104	C3H8 ⇌ NC3H7 + H	4.010E+15	.000	4.190E+05	2.000E+07	.000	0.000E+00

Table B.2: The Chemical Kinetic Scheme (Contd.)

No.	Reactions	Forward Reaction Constants			Backward Reaction Constants		
		A_f	B_f	E_f	A_b	B_b	E_b
105	C3H8 ⇌ IC3H7 + H	1.570E+15	.000	4.070E+05	2.000E+07	.000	0.000E+00
106	C2H4 + O ⇌ CH3 + HCO	2.200E+03	1.200	3.096E+03	1.600E-03	2.370	1.062E+05
107	CH3O + H ⇌ CH3 + OH	4.750E+10	-.140	8.836E+04	4.500E+08	.000	6.485E+04
108	C2H5 + O ⇌ OH + C2H4	6.000E+07	.000	0.000E+00	6.900E+05	.000	2.680E+05
109	HCO + O ⇌ CO + OH	3.000E+07	.000	0.000E+00	2.880E+08	.000	3.678E+05
110	CH3O + OH ⇌ CH2O + H2O	1.810E+07	.000	0.000E+00	4.620E+03	.590	4.105E+05
111	C2H2 + O2 ⇌ HCO + HCO	3.980E+06	.000	1.172E+05	1.000E+05	.000	2.659E+05
112	C2H2 + O ⇌ C2H + OH	3.230E+09	-.600	7.113E+04	2.950E+08	-.600	3.810E+03
113	C2H4 + O ⇌ CH2 + CH2O	4.000E+07	.000	2.092E+04	3.020E+06	.000	6.561E+04
114	C2H6 ⇌ CH3 + CH3	6.310E+15	.000	3.560E+05	1.440E+01	.000	2.170E+04
115	CHCO + H ⇌ CH2 + CO	3.000E+07	.000	0.000E+00	6.380E-02	2.200	1.122E+05
116	CHCO + O ⇌ HCO + CO	3.388E+07	.000	8.370E+03	8.317E+07	.000	5.367E+05
117	C2H4 + OH ⇌ CH3 + CH2O	4.500E+06	.000	3.760E+03	1.400E+06	.000	7.300E+04
118	C2H3 + H + M ⇌ C2H4 + M	2.000E+05	.000	0.000E+00	6.800E+12	.000	4.200E+05
119	H2O2 + OH ⇌ H2O + HO2	1.000E+07	.000	7.500E+03	2.800E+07	.000	1.378E+05
120	C2H3 + O2 ⇌ CH2O + HCO	4.000E+06	.000	-1.045E+03	4.000E+06	.000	3.607E+05
121	C2H2 + O2 ⇌ CH2 + CO2	6.000E+07	.000	1.674E+05	4.830E-02	.000	3.753E+05
122	HCO + H + M ⇌ CH2O + M	6.300E-01	.000	-1.330E+04	5.000E+10	.000	3.000E+05
123	H + O + M ⇌ OH + M	1.000E+04	.000	0.000E+00	8.000E+13	-1.000	4.336E+05
124	HO2 + O ⇌ O2 + OH	2.000E+07	.000	0.000E+00	2.810E+08	-.330	2.141E+05
125	C2H6 + CH3 ⇌ C2H5 + CH4	5.500E-07	4.000	3.470E+04	2.290E+08	.000	1.001E+05
126	IC3H7 + C3H8 ⇌ C3H8 + NC3H7	3.020E+04	.000	5.400E+04	3.020E+04	.000	5.400E+04
127	H2 + O2 ⇌ OH + OH	2.500E+06	.000	1.630E+05	6.000E+04	.000	8.537E+04
128	C2H3 + C2H5 ⇌ C2H4 + C2H4	1.500E+08	.000	-1.100E+04	5.000E+08	.000	2.710E+05
129	CH3 + O ⇌ H2 + HCO	1.000E+08	.000	0.000E+00	9.372E+07	.000	3.943E+05
130	C2H4 + H2 ⇌ CH3 + CH3	1.540E+14	-.750	3.794E+05	5.000E+09	.000	1.339E+05
131	CH2O + CH3 ⇌ CH4 + HCO	1.000E+04	.500	2.512E+04	2.090E+04	.500	8.851E+04
132	CH3 + HCO ⇌ CH4 + CO	3.000E+05	.500	0.000E+00	5.140E+07	.500	3.787E+05
133	HCO + O ⇌ CO2 + H	3.000E+07	.000	0.000E+00	9.690E+09	.000	4.611E+05
134	H2O2 + O ⇌ HO2 + OH	2.800E+07	.000	2.681E+04	9.510E+06	.000	8.668E+04
135	CH2 + O2 ⇌ CO + H2O	1.870E+04	.000	-4.184E+03	3.070E+00	1.400	7.276E+05
136	H + HO2 ⇌ O + H2O	3.000E+07	.000	7.200E+03	2.950E+07	.000	2.445E+05
137	C2H6 + C2H4 ⇌ C2H5 + C2H5	5.000E+05	.000	2.500E+05	5.000E+05	.000	0.000E+00
138	C3H6 ⇌ C3H5 + H	1.000E+13	.000	3.260E+05	1.000E+05	.000	0.000E+00
139	C3H6 + HO2 ⇌ C3H5 + H2O2	3.240E+05	.000	6.220E+04	3.400E+04	.000	6.150E+04
140	C3H6 + OH ⇌ C3H5 + H2O	2.000E+07	.000	1.279E+04	3.800E+01	.000	3.044E+05
141	C3H6 + O2 ⇌ C3H5 + HO2	1.000E+08	.000	1.632E+05	1.000E+05	.000	0.000E+00
142	C3H5 ⇌ C3H4 + H	3.981E+13	.000	2.926E+05	1.000E+02	1.000	0.000E+00
143	C3H5 + O2 ⇌ C3H4 + HO2	6.020E+05	.000	4.180E+04	1.200E+05	.000	4.185E+04
144	C3H4 + OH ⇌ CH2O + C2H3	1.000E+06	.000	0.000E+00	8.490E+05	.000	1.410E+05
145	C3H4 + O ⇌ HCO + C2H3	1.000E+06	.000	0.000E+00	2.950E+04	.000	1.288E+05
146	C3H4 + OH ⇌ HCO + C2H4	1.000E+06	.000	0.000E+00	5.011E+05	.000	1.413E+05
147	NO + N ⇌ O + N2	3.270E+06	.300	0.000E+00	1.800E+06	.000	3.174E+05
148	N + O2 ⇌ O + NO	1.100E+07	.000	3.130E+04	2.100E+06	.000	1.666E+05
149	N + OH ⇌ H + NO	3.800E+07	.000	0.000E+00	1.200E+08	.000	2.024E+05
150	NO + HO2 ⇌ NO2 + OH	8.700E+05	.000	0.000E+00	6.000E+06	.000	3.350E+04
151	NO + O + M ⇌ NO2 + M	5.800E-02	1.000	-3.580E+04	1.100E+10	.000	2.720E+05
152	NO2 + O ⇌ NO + O2	1.000E+07	.000	2.510E+03	2.204E+06	.000	1.930E+05
153	NO2 + H ⇌ NO + OH	2.900E+07	.000	0.000E+00	3.500E+05	.000	1.230E+05
154	NO + NO ⇌ O2 + N2	1.410E+09	.000	3.600E+05	2.850E+10	.000	5.358E+05
155	NO + NO + O2 ⇌ NO2 + NO2	4.900E-06	1.000	2.512E+03	4.000E+06	.000	1.130E+05

Appendix C

Air and Fuel Metering Systems

(A) Laminar Flow Air Meter

A laminar flow meter, schematically shown in Figure C.1, was used for measurement of air flow rates into the engine. The two pressure taps were connected to an inclined manometer containing "Meriam Oil". The meter was calibrated as installed on the engine using the standard sharp edged orifice plate method. The calibration of the air meter was carried out in situ, i.e. as installed in the intake air ducting system. During the actual calibration of the meter, a large tank was attached upstream of it to dampen any pulsation arising from engine operation. The orifice installation was attached to the side of the tank and upstream of it.

During the experiment, the engine was running at a constant speed of 900 rev./min. and variations in air flow rates was achieved by feeding controlled amount of gaseous fuel/fuels fulfilling the breathing capacity of the engine partially.

The calibration curve for the air meter is plotted in Figure C.2.

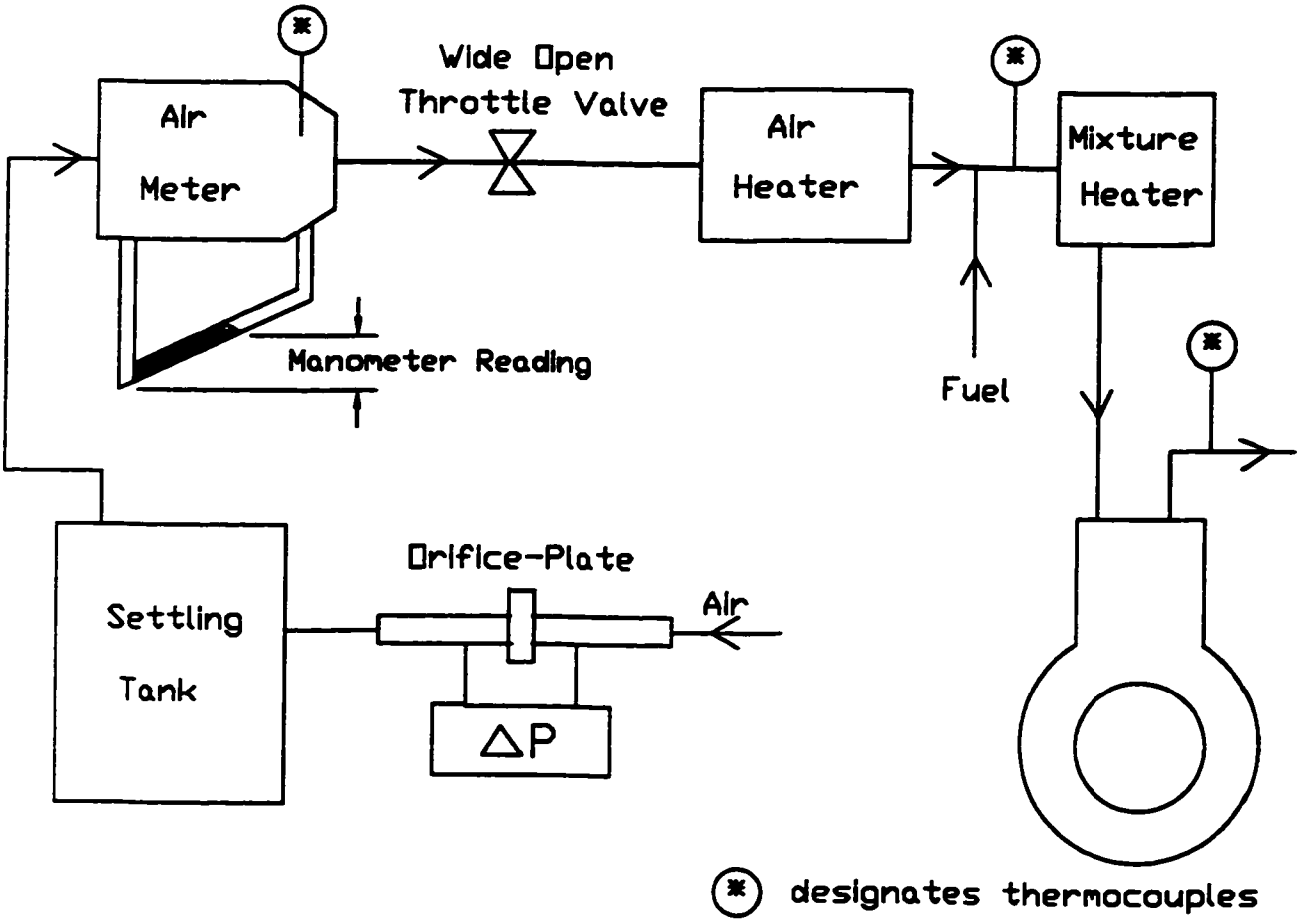

Figure C.1: A Schematic Diagram of Air Meter Calibration Set-up.

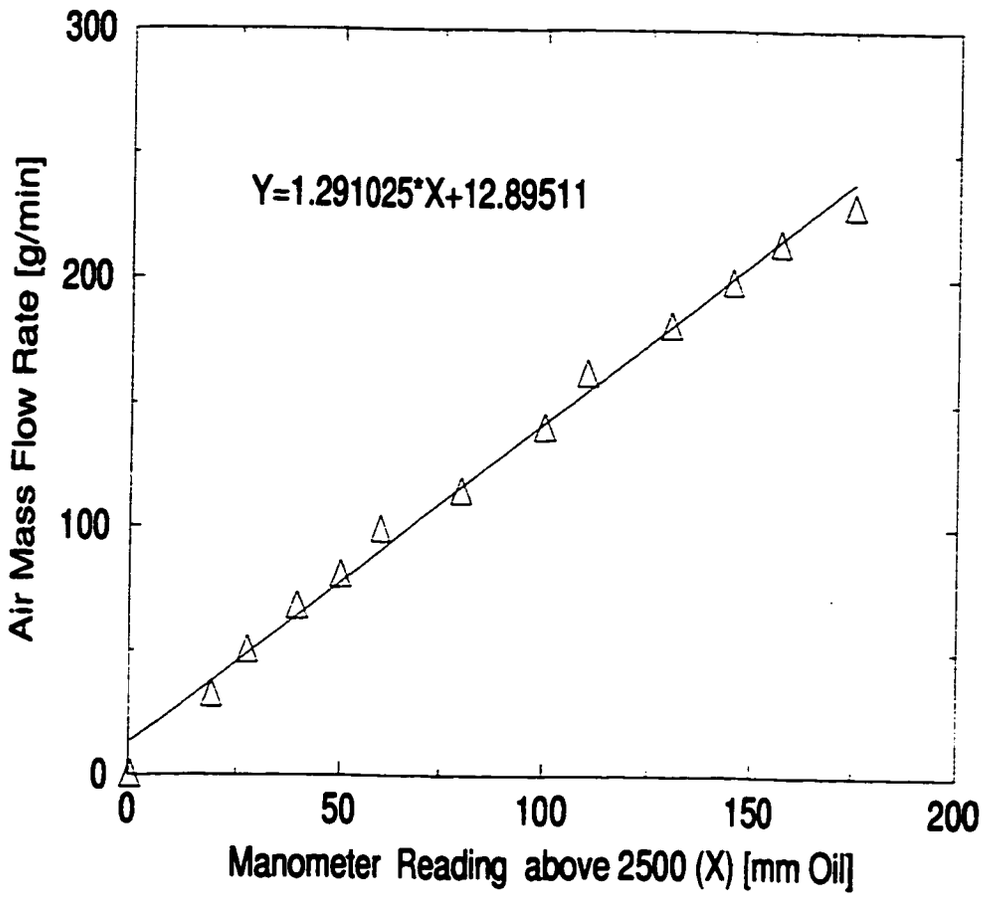

Figure C.2: Calibration Curve for Meriam Oil Manometer.

(B) Fuel and Oxygen Metering Systems

The engine was operated on processed natural gas as the main fuel. Its composition typically is shown in Appendix (D). The main fuel and other gaseous fuels were metered by the choked nozzles systems. These nozzles were calibrated with a wet test meter using air as the working fluid. These results were then converted to yield flow rates for the fuel using the equation suggested by Karim and Klat [167].

Oxygen was supplied through a rotameter mounted in the main fuel panel. The rotameter was also calibrated with a wet test meter using oxygen itself.

It should be noted that the calibration of all choked nozzles and the rotameter were done while they were mounted on the panel where they were eventually used. This assured consistency and eliminated the need to consider the accuracy of the pressure gauges or the effect of the panel piping geometry, etc. on the gas flow rate.

The calibration curve for the processed natural gas nozzle used in this research work is shown in Figure C.3. Figures C.4, C.5 and C.6 show the calibration curves and the corresponding linear curve fitting equations for the fuel lines. Figure C.7 shows the calibration curve with the curve fitting equation of the rotameter used to supply oxygen.

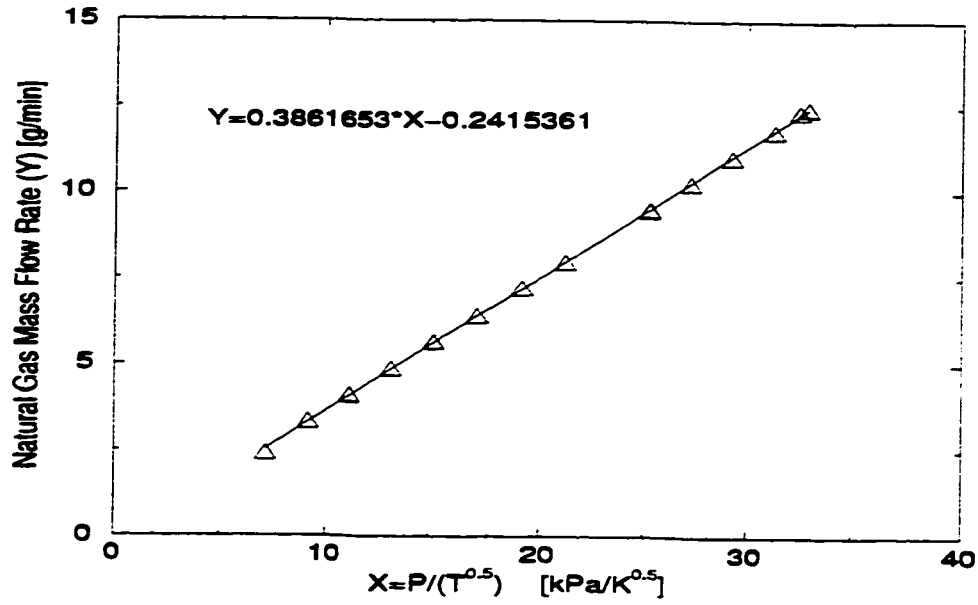

Figure C.3: Calibration Curve for Natural Gas Line.

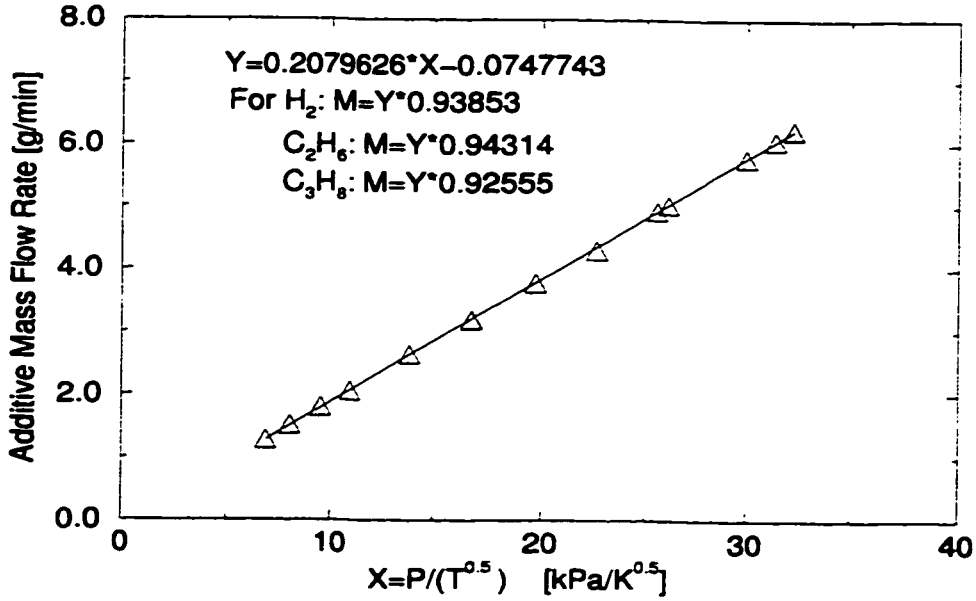

Figure C.4: Calibration Curve for Additives, Nozzle 1.

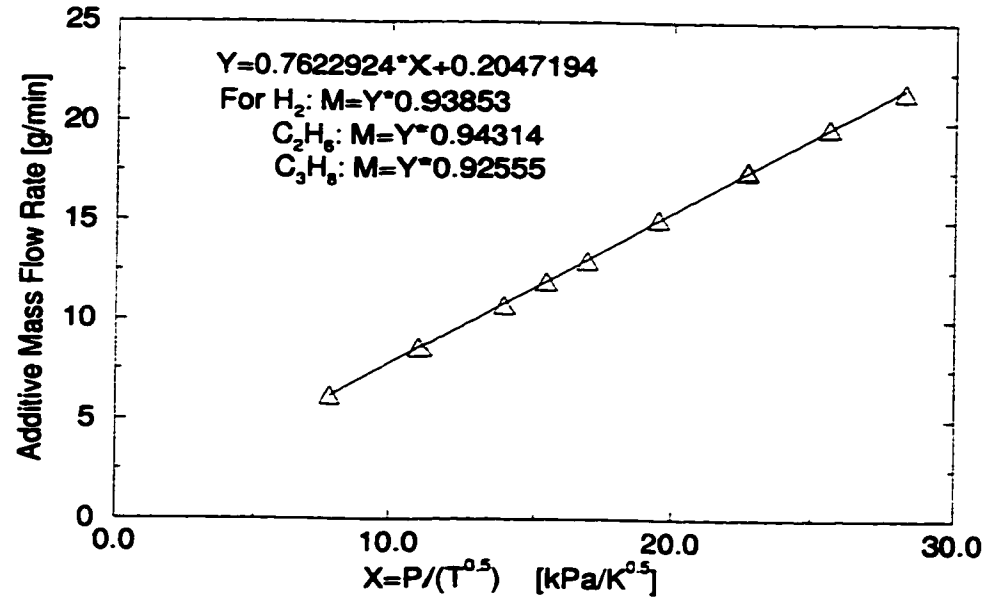

Figure C.5: Calibration Curve for Additives, Nozzle 2.

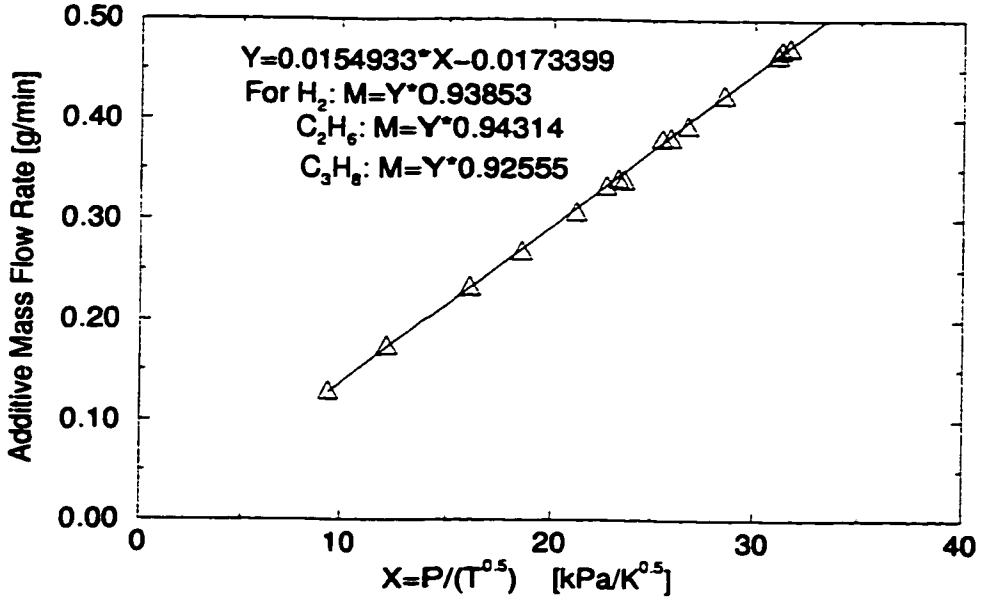

Figure C.6: Calibration Curve for Additives, Nozzle 3.

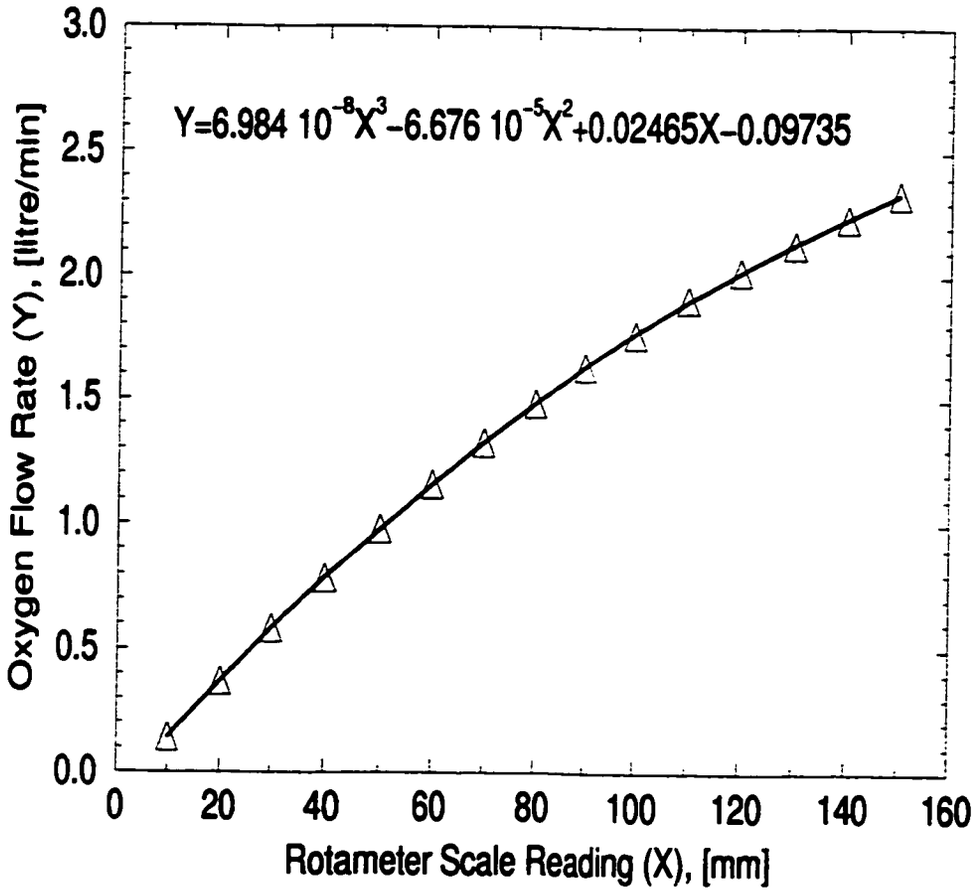

Figure C.7: Calibration Curve of Rotameter for Oxygen Line.

Appendix D

Fuel Composition

The gaseous fuels that were used in this investigation were processed natural gas, hydrogen, ethane and propane. The typical composition of the processed natural gas is listed in the following table. The other fuels were of more than 99% purity.

Composition of the Processed Natural Gas

Specie	Formula	Molar Concentration
Methane	CH_4	93.07%
Ethane	C_2H_6	5.74%
Carbon Dioxide	CO_2	0.16%
Nitrogen	N_2	1.03%

Appendix E

Histograms of Stochastic Parameters

The results of the statistical analysis of the stochastic parameters (i. e. the combustion duration, $\Delta\theta_c$, and the crank angle of maximum burning rate as normalized to the corresponding combustion duration, θ_{max}) for each experimental data set considered are included. The probability/frequency distributions of these parameters for each data sets are shown in Figures E.1 to E.9.

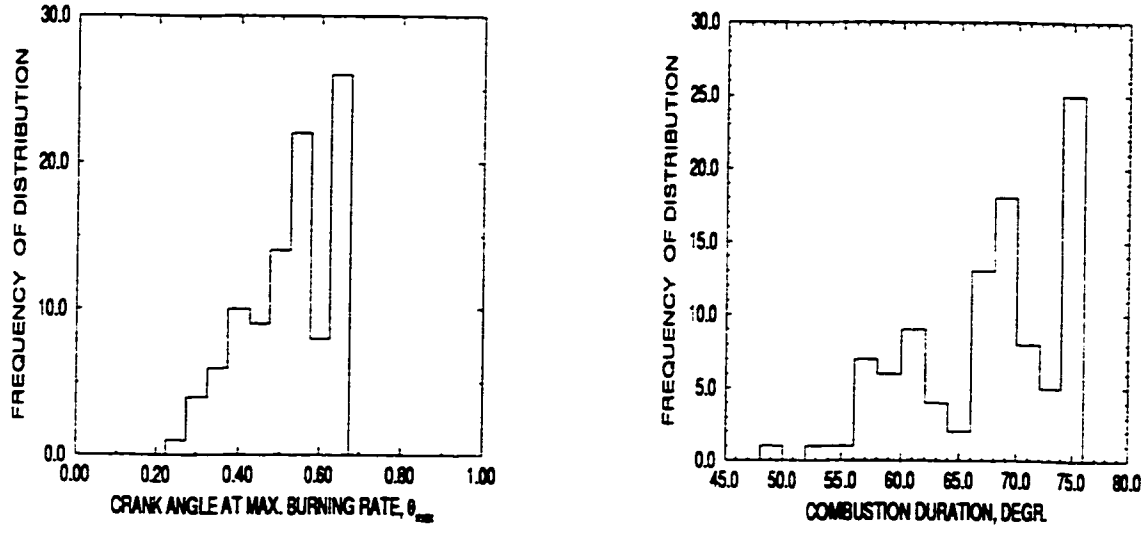

Figure E.1: The Frequencies of Distribution of the Normalized Crank Angle at Maximum Burning Rate, θ_{max}, and the Combustion Duration, $\Delta\theta_c$, for 100 Cycles at Equivalence Ratio of 0.66, Compression Ratio of 8.5:1, Spark Timing of 20 degrees BTC and Initial Temperature of 294 K (Data Set No. 1).

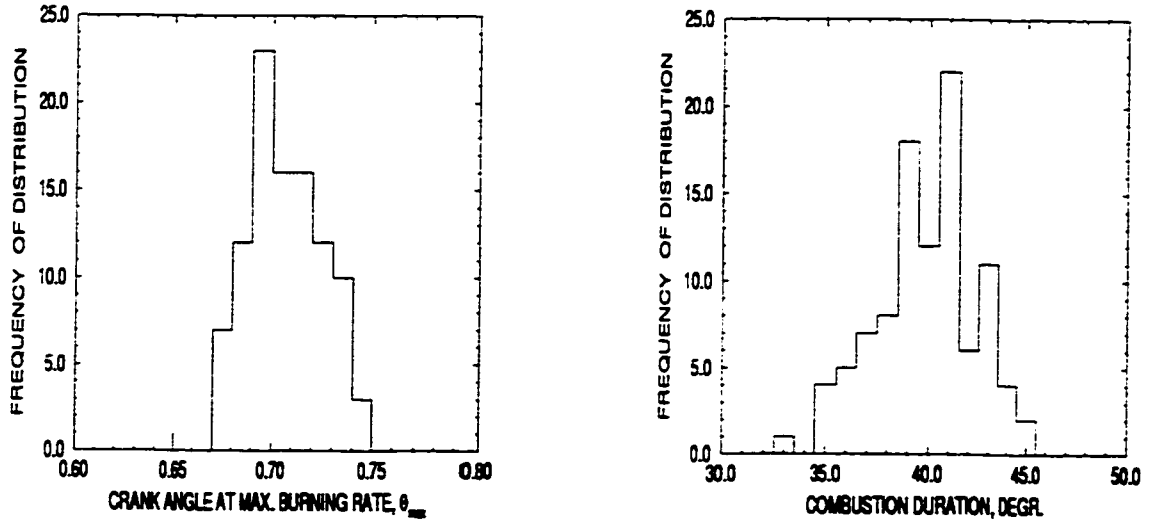

Figure E.2: The Frequencies of Distribution of the Normalized Crank Angle at Maximum Burning Rate, θ_{max}, and the Combustion Duration, $\Delta\theta_c$, for 100 Cycles at Equivalence Ratio of 0.99, Compression Ratio of 8.5:1, Spark Timing of 20 degrees BTC and Initial Temperature of 294 K (Data Set No. 3).

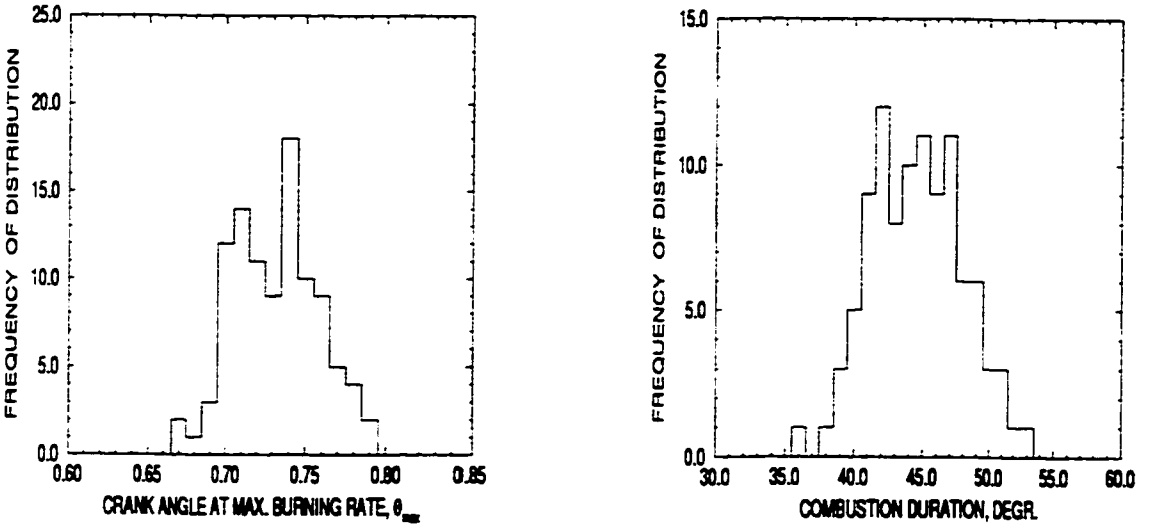

Figure E.3: The Frequencies of Distribution of the Normalized Crank Angle at Maximum Burning Rate, θ_{max}, and the Combustion Duration, $\Delta\theta_c$, for 100 Cycles at Equivalence Ratio of 1.10, Compression Ratio of 8.5:1, Spark Timing of 20 degrees BTC and Initial Temperature of 294 K (Data Set No. 4).

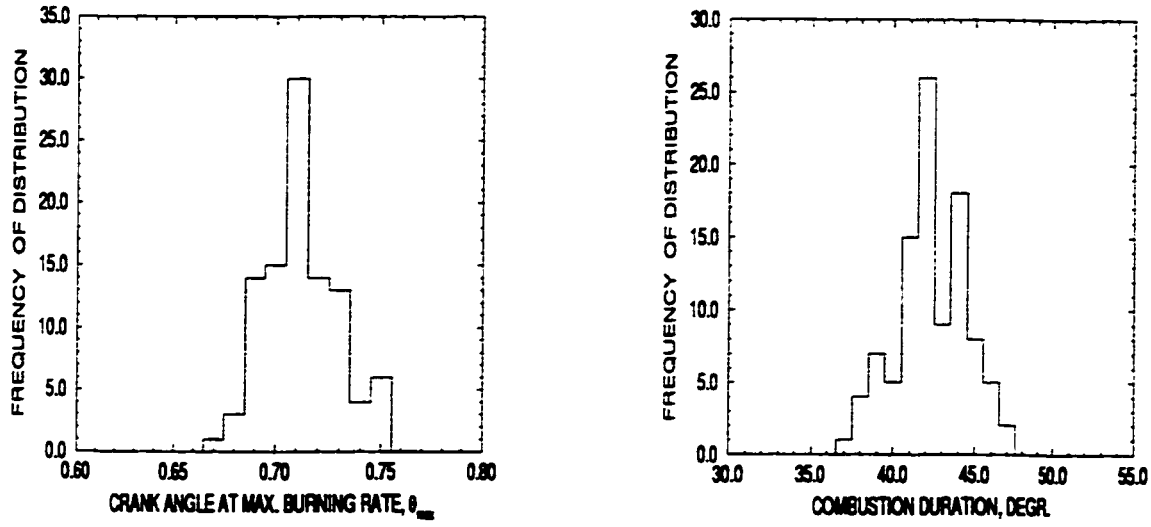

Figure E.4: The Frequencies of Distribution of the Normalized Crank Angle at Maximum Burning Rate, θ_{max}, and the Combustion Duration, $\Delta\theta_c$, for 100 Cycles at Equivalence Ratio of 0.99, Compression Ratio of 8.5:1, Spark Timing of 15 degrees BTC and Initial Temperature of 294 K (Data Set No. 5).

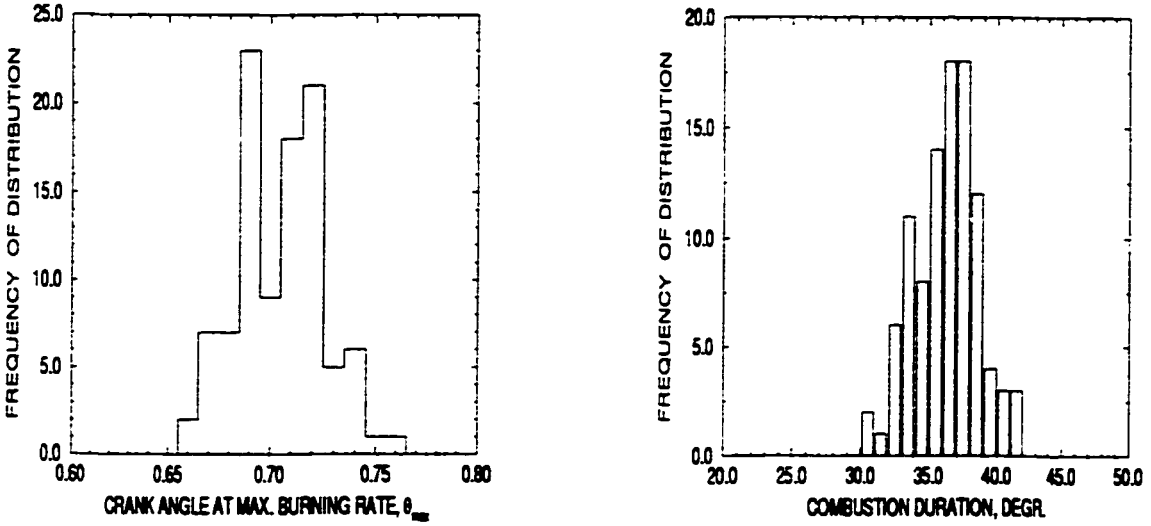

Figure E.5: The Frequencies of Distribution of the Normalized Crank Angle at Maximum Burning Rate, θ_{max}, and the Combustion Duration, $\Delta\theta_c$, for 100 Cycles at Equivalence Ratio of 0.99, Compression Ratio of 8.5:1, Spark Timing of 30 degrees BTC and Initial Temperature of 294 K (Data Set No. 6).

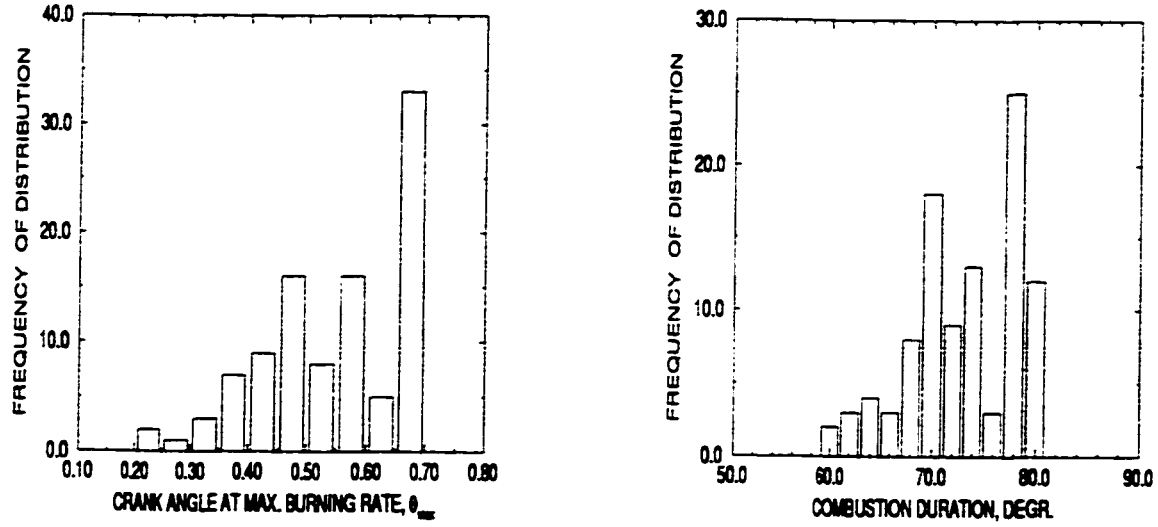

Figure E.6: The Frequencies of Distribution of the Normalized Crank Angle at Maximum Burning Rate, θ_{max}, and the Combustion Duration, $\Delta\theta_c$, for 100 Cycles at Equivalence Ratio of 0.65, Compression Ratio of 10:1, Spark Timing of 20 degrees BTC and Initial Temperature of 294 K (Data Set No. 7).

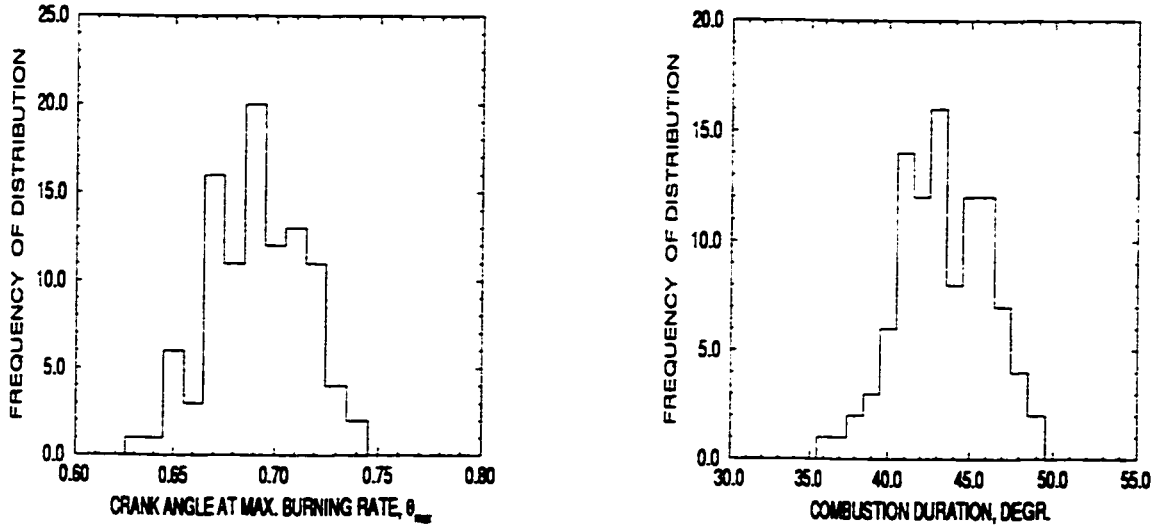

Figure E.7: The Frequencies of Distribution of the Normalized Crank Angle at Maximum Burning Rate, θ_{max}, and the Combustion Duration, $\Delta\theta_c$, for 100 Cycles at Equivalence Ratio of 0.80, Compression Ratio of 10:1, Spark Timing of 20 degrees BTC and Initial Temperature of 294 K (Data Set No. 8).

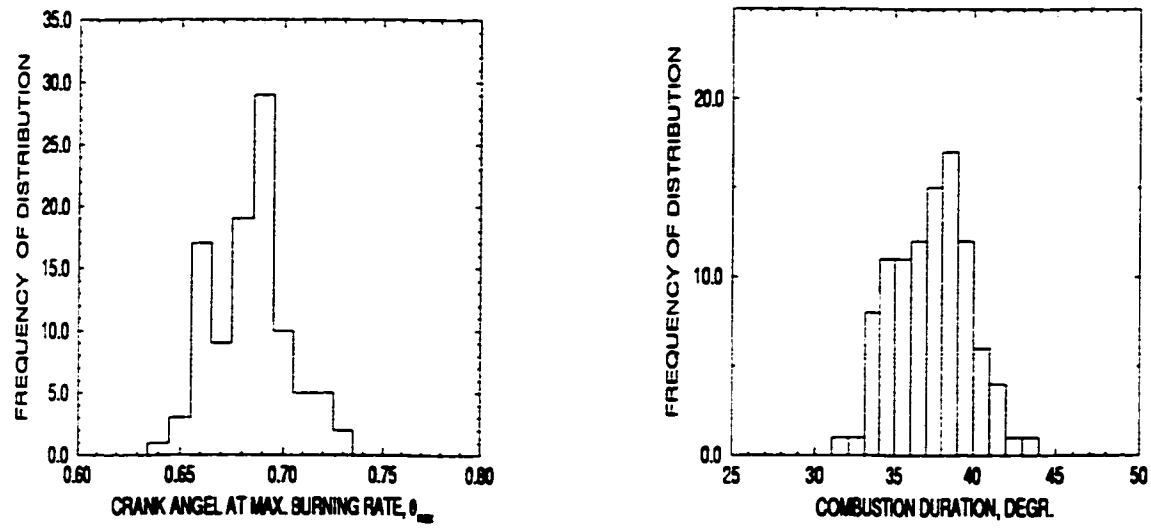

Figure E.8: The Frequencies of Distribution of the Normalized Crank Angle at Maximum Burning Rate, θ_{max}, and the Combustion Duration, $\Delta\theta_c$, for 100 Cycles at Equivalence Ratio of 0.99, Compression Ratio of 10:1, Spark Timing of 20 degrees BTC and Initial Temperature of 294 K (Data Set No. 9).

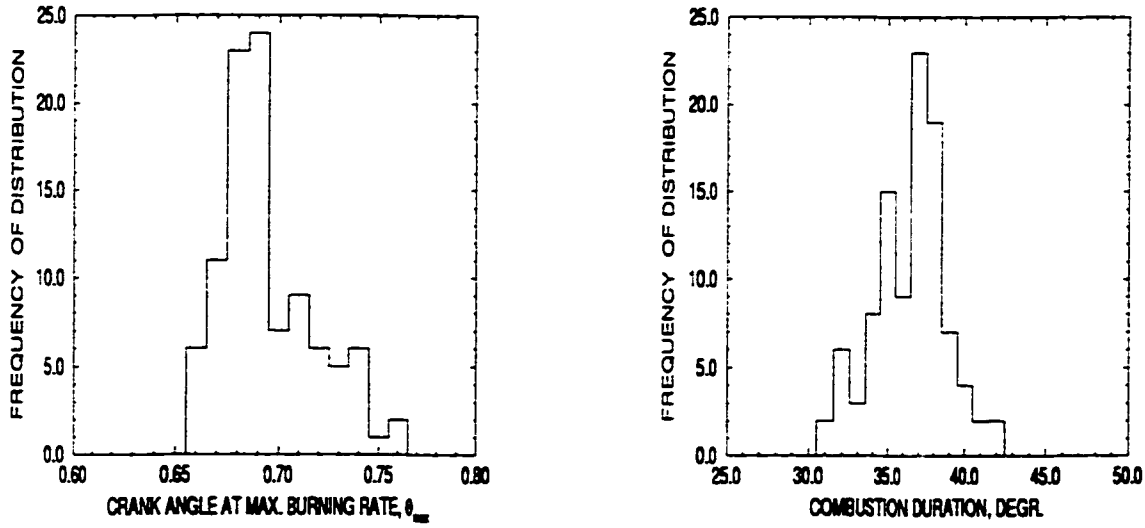

Figure E.9: The Frequencies of Distribution of the Normalized Crank Angle at Maximum Burning Rate, θ_{max}, and the Combustion Duration, $\Delta\theta_c$, for 100 Cycles at Equivalence Ratio of 0.99, Compression Ratio of 11:1, Spark Timing of 20 degrees BTC and Initial Temperature of 294 K (Data Set No. 10).